A Study of Bed Agglomeration in Biomass-Fired Fluidized Bed Combustor

Mr.Pawin Chaivatamaset M.Eng (Chemical Engineering)

A Thesis Submitted in Partial Fulfillment of the Requirement for
the Degree of Doctor of Engineering (Chemical Engineering)
Faculty of Engineering
King Mongkut's University of Technology Thonburi
2011

Thesis Committee

..... Chairman of Thesis Committee
(Assoc. Prof. Suvit Tia, D.Eng)

..... Member and Thesis Advisor
(Prof. Dr.-Ing. habil. Dr. h.c. Bernd Bilitewski, D.Eng)

..... Member and Thesis Co-Advisor
(Asst. Prof. Panchan Sricharoon, Ph.D.)

..... Member
(Assoc. Prof. Solot Suwanayuen, Ph.D.)

..... Member
(Assoc. Prof. Wittaya Teppaitoon, Ph.D.)

..... Member
(Assoc. Prof. Chaiyot Tangsathitkulchai, Ph.D.)

Thesis Title	A Study of Bed Agglomeration in Biomass-fired Fluidized Bed Combustor
Thesis Credits	36
Candidate	Mr. Pawin Chaivatamaset
Thesis Advisors	Assoc. Prof. Dr. Suvit Tia
	Prof. Dr. Bernd Bilitewski
	Asst. Prof. Dr. Panchan Sricharoon
Program	Doctor of Engineering
Field of Study	Chemical Engineering
Department	Chemical Engineering
Faculty	Engineering
B.E.	2554

Abstract

Bed agglomeration behaviors were investigated when palm shell, corncob, palm empty fruit brunch and rice straw as the representative biomass were combusted in the fluidized bed reactors. The focus of this study was the influences of biomass characteristics and the operating conditions of fluidized bed on the bed agglomeration tendency, and the behaviors of ash forming elements. The mathematical models to predict the bed agglomeration behaviors were also proposed. The bed agglomeration tendency was described by the defluidization time (t_{def}) and the extent of potassium into the bed as K/Bed. It was experimentally found that the defluidization caused by the agglomeration of bed particles can be observed by the abnormal decrease in bed pressure drop, more clearly than the deviation from relatively uniform bed temperature. The defluidization was developed steadily from partial to complete by an extension in an increase and growth of agglomerates. The bed defluidization increased as the increase of bed temperature, static bed height and bed particle size and the decrease of fluidized air velocity. The biomass fuel with relatively high alkali and chloride contents, as used in this study, was likely to increase the bed agglomeration problem. The SEM/EDS analysis on the features of the agglomerate samples indicated that the bed agglomeration is mainly attributed to the formation of the ash derived potassium silicate compounds as liquid phase during combustion. This was initiated by the burning char particles. The propagation of ash formed material inward the sand grains could be observed, which may cause by the gaseous/aerosol alkali species. In this study, the migration of ash forming elements from fuel particle to bed particle was likely dominated by the collision. The agglomeration process was the reactor scale independent. The plot of EDS data employing ternary phase diagram showed that the compositions of the coating and neck fused materials were mainly located in the low Ca and high Si region where the eutectic composition is nearby, and the relatively large amount of the melt (70-95%) in fused materials at relatively low temperature (740-800 °C) was estimated using lever bar rule for all biomass samples studied, which seemed likely that the melt formation controls the agglomeration. The order from high to low of the bed agglomeration tendency of the biomass samples were palm brunch, corncob, rice straw, and palm shell, respectively. The fairly well to good satisfactory in the model predictabilities were obtained.

Keywords : Bed Agglomeration / Fluidized Bed Combustion / Biomass Combustion / Palm Shell / Corncob / Palm Fruit Brunch / Straw

หัวข้อวิทยานิพนธ์	การศึกษาการเกาะตัวของเบดอนุภาคในเตาเผาฟลูอิดไดซ์เบดโดยใช้ชีวมวลเป็นเชื้อเพลิง
หน่วยกิต	36
ผู้เขียน	นายปวีณ ชัยวัฒมเสฏฐ์
อาจารย์ที่ปรึกษา	รศ.ดร.สุวิทย์ เตีย Prof. Dr. Bernd Bilitewski ผศ.ดร.ปานจันทร์ ศรีจรูญ
หลักสูตร	วิศวกรรมศาสตรดุษฎีบัณฑิต
สาขาวิชา	วิศวกรรมเคมี
ภาควิชา	วิศวกรรมเคมี
คณะ	วิศวกรรมศาสตร์
พ.ศ.	2554

บทคัดย่อ

งานวิจัยนี้ศึกษาพฤติกรรมการเกาะตัวของเบดอนุภาคที่เกิดจากการเผาไหม้ชีวมวลทางการเกษตร อันได้แก่ กะลาและทะลายปาล์ม ซังข้าวโพด และ ฟางข้าว ในเตาเผาฟลูอิดไดซ์เบดระดับห้องปฏิบัติการและระดับเครื่องต้นแบบ และสร้างแบบจำลองทางคณิตศาสตร์ที่ใช้ทำนายพฤติกรรมดังกล่าว โดยจะศึกษาถึงปัจจัยขององค์ประกอบทางอนินทรีย์ของชีวมวลและสภาวะของการเผาไหม้ ที่มีผลต่อความเป็นไปได้ของการเกาะตัวและการสูญเสียสภาพของไหลของเบดอนุภาค การสูญเสียสภาพของไหลของเบดอนุภาคระหว่างการเผาไหม้ถูกตรวจพบจากการลดลงของความดันสูญเสียของเบด โดยจะเปลี่ยนจากการสูญเสียสภาพบางส่วนไปเป็นการสูญเสียสภาพทั้งหมด ซึ่งเป็นการเปลี่ยนแปลงคุณสมบัติด้านอุทกพลศาสตร์ ที่เกิดจากการเพิ่มจำนวนและขนาดของกลุ่มอนุภาคเบดที่เกาะติดกัน การเพิ่มอุณหภูมิการเผาไหม้ ขนาดอนุภาคเบด และความสูงของเบด รวมถึงการลดความเร็วของอากาศ ทำให้การสูญเสียสภาพเร็วขึ้น ปริมาณของธาตุโพแตสเซียมและคลอรีนในชีวมวลที่สูงก็จะทำให้การสูญเสียสภาพเร็วขึ้น เช่นกัน การตรวจสอบอนุภาคเบดที่เกาะติดกันโดยใช้กล้องจุลทรรศน์อิเล็กตรอน พบว่า อนุภาคเบดเกาะติดกันด้วยเถ้าบางส่วนของชีวมวลที่กลายเป็นของเหลวระหว่างเผาไหม้อันเนื่องจากอุณหภูมิพื้นผิวของอนุภาคเชื้อเพลิงที่สูงกว่าอุณหภูมิการเผาไหม้ โดยเถ้าหลอมเหลวนี้มีส่วนประกอบของ ซิลิกอนและโพแตสเซียมเป็นหลัก เถ้าหลอมเหลวจะเคลือบที่ผิวของอนุภาคเบด ซึ่งจะทำหน้าที่เปรียบเสมือนกาวที่จะเชื่อมติดกับอนุภาคเบดอื่นๆ และพบว่ามีการแพร่ของเถ้าบางส่วนเข้าสู่ใจกลางของอนุภาคเบด โดยคาดว่ากลไกหลักที่เถ้าหลอมเหลวมาที่ผิวของอนุภาคเบดได้มาจากการชนปะทะระหว่างเบดอนุภาคและเถ้าหลอมเหลวที่อยู่บนผิวของอนุภาคเชื้อเพลิง การ

ตรวจสอบพฤติกรรมของธาตุอนินทรีย์ระหว่างการเผาไหม้ ตามหลักสมดุลของอุณหพลศาสตร์พบว่า เถ้าหลอมเหลวที่อยู่ในกลุ่มอนุภาคเบดที่เกาะตัวกัน จะเปลี่ยนสภาพเป็นของเหลวในสัดส่วนที่ร้อยละ 70 ถึง 90 ที่อุณหภูมิ 740 ถึง 800 องศาเซลเซียส และมีองค์ประกอบใกล้กับสารประกอบยูเทคติก โดยสัดส่วนของเถ้าหลอมเหลวจะขึ้นกับอุณหภูมิและองค์ประกอบเป็นสำคัญ แบบจำลองทางคณิตศาสตร์สำหรับการทำนายเวลาการเผาไหม้ที่ถูกพัฒนาขึ้นใหม่และปรับปรุงจากแบบจำลองทางคณิตศาสตร์เดิม สามารถทำนายเวลาการเผาไหม้ในเตาเผาระดับห้องปฏิบัติการและระดับเครื่องต้นแบบได้ดี

คำสำคัญ : การเกาะตัวของเบดอนุภาค / การเผาไหม้ชีวมวล / ฟลูอิดไดซ์เบด / กะลาปาล์ม / ทะลายปาล์ม / ซังข้าวโพด / ฟางข้าว

ACKNOWLEDGEMENTS

Financial support under a scholarship from the Royal Golden Jubilee Program, Thailand Research Fund (TRF) is gratefully acknowledged. I would like to pay my thanks my advisors, Assoc. Prof. Dr. Suvit Tia and Asst. Prof. Dr. Panchan Sricharoon, co-advisor, for their tireless helps and enthusiastic support on this thesis. Specially, my deeply gratitude is paid to my foreign co-advisor Prof. Bilitewski for enthusiastic support in the new experiences during the research in TÜ Dresden, Germany. I wish to thank my mom and my passed away dad for love and encouragement to my life.

Our team is also appreciative for the useful guidance and support offered by the staffs of National Metal and Materials Technology Center (MTEC), National Science and Technology Development Agency (NSTDA), Thailand, in performing the SEM specimen preparation; by the staffs of Scientific and Technology Research Equipment Center (STREC) of Chulalongkorn University for guidance in the SEM/EDS analysis; and, finally, by the staffs of Technical and Engineering System (TCS), Pilot plant Development and Training Institute (PDTI) of King Mongkut's University Technology Thonburi (KMUTT) for assisting in the pilot plant operations.

CONTENTS

LIST OF TABLES

LIST OF FIGURES

NOMENCLATURE

a, A	=	Constant
%ash	=	Weight percentage of ash in biomass
b	=	Radius of bonding neck
B, B0, B1, B2 B3, B4, B5	=	Constant
C	=	Constant
C_1, C_2, C_3, C_4	=	Constant
C_b	=	Bulk oxygen concentration
C_{new}	=	Constant
$C_{p,f}$	=	Fluid heat capacity
d_{ag}	=	Agglomerate diameter
d_b	=	Bubble diameter
d_p	=	Particle/Bed particle diameter
$d_{p,av}$	=	Average bed particle diameter
$d_{p,char}$	=	Char particle diameter
D	=	Particle separation distance
D_{AB}	=	Gas molecular diffusivity
D_b	=	Bed diameter
$D_{b,eq}$	=	Equivalent bed diameter
$D_{0,S}$	=	Pre-exponential factor for surface diffusion coefficient
E_S	=	Activation energy for surface diffusion
E_μ	=	Activation energy for viscosity
$E_{\mu,s}$	=	Activation energy for surface viscosity
f, f_1, f_2, f_3	=	Function
f_N	=	Existing ratio of alkali in bed material
F_{ad}	=	Adhesive force
$F_{ad,total}$	=	Total adhesive force
F_{br}	=	breaking-up force
$F_{LB,S}$	=	Static liquid bridge force
$F_{LB,V}$	=	Viscous force in liquid bridge
F_{seg}	=	Segregate force
F_{VW}	=	van der Waals force
g	=	Average gravity; 9.8 m/s^2
h	=	Heat transfer coefficient
H_b	=	Static bed height
H_{mf}	=	Bed height at minimum fluidization velocity
k	=	Boltzmann constant / constant
k(T)	=	Kinetic constant of devolatilization process
k_c	=	Combustion rate constant
k_f	=	Fluid conductivity
k_g	=	Gas conductivity
k_m	=	Mass transfer coefficient
K, K_2	=	Constant
m_{bed}	=	Bed inventory
m'_{fuel}	=	Fuel feed rate
m_p	=	Mass of a single particle/bed particle
M	=	Average convective sold mass flux
n	=	The number of particles/bed particles

p	=	Constant
P	=	Pressure in Pa
ΔP	=	Different pressure between in bridge and the surrounding Pressure
q	=	Heat of reaction at complete combustion ($C + O_2 \rightarrow CO_2$)
Q_{pp}	=	Polymer feed rate
r_p	=	Particle/Bed particle radius
r_a	=	Radius of curvature of asperities at a particle surface
$r_{LB,c}$	=	Liquid bridge meridional radius of curvature
$r_{LB,n}$	=	Liquid bridge neck radius
R	=	Gas constant
S	=	Adhesive stress / Bubble separation length
t	=	Time
t_{def}	=	Defluidization time
T	=	Operating temperature
T_{ag}	=	Agglomeration temperature
T_b	=	Bed (combustion) temperature
T_{char}	=	Char surface temperature
T_S	=	Sintering temperature
u_0	=	Absolute velocity of a solid/bed particle at initial conditions
u_b	=	Bubble velocity
u_p	=	Absolute velocity of a solid/bed particle
U	=	Superficial gas/air velocity
U_{BB}	=	Bed breaking fluidizing velocity
U_D	=	Defluidization velocity
U_f	=	Fluid velocity
U_{mf}	=	Minimum fluidization velocity under normal conditions
$U_{mf,S}$	=	Minimum fluidization velocity under sintering conditions
U_S	=	Limiting gas velocity
V	=	Particle-Particle relative velocity
W	=	Weight
W_{bed}	=	Weight of the bed particles in the bed
x_c	=	Critical sintering neck radius
X^2	=	Equivalent of neck contact area between particles
X_{ash}	=	Mass fraction of ash in the biomass
$X_{K\ in\ Ash}$	=	Mass fraction of potassium in the ash
$X_{K\text{-}Fuel}$	=	Mass fraction of potassium in the fuel
X_{melt}	=	Ash melt fraction based on the initial ash compositions

Greek letters

π	=	Pi constant
γ	=	Surface tension
φ	=	Three-phase contact angle
α	=	Half-filling bridge angle / ratio of volume of solids carried by bubble to bubble volume
μ_0	=	Pre-exponential factor for viscosity
μ_f	=	Fluid viscosity
μ_g	=	Gas/Air viscosity
μ_s	=	Surface viscosity
μ_{pp}	=	Polymer intrinsic viscosity

μ_l	=	Viscosity of molten material
ρ_{coat}	=	Density of coating material
ρ_f	=	Fluid density
ρ_g	=	Gas/Air density
ρ_p	=	Particle/Bed particle density
ρ_{pp}	=	Polymer particle density
ρ_s	=	Solid density
ε	=	Bed void fraction / Emissivity
ε_{mf}	=	Bed void fraction at minimum fluidization
ψ	=	Sintering force function / alkali feed rate
σ	=	Stefan-Boltzmann constant, 5.670×10^{-8} W/m^2 K^4
σ_S	=	Yield stress of neck
ϕ	=	Particle shape factor
η_0	=	Pre-exponential factor for surface viscosity
ζ	=	Specific surface free energy
δ	=	Lattice constant for a crystalline solid / Coating thickness
β	=	Magnitude of relative contribution in MLR analysis
υ_f	=	Fluid kinematic viscosity

Abbreviations

AI	=	Alkali Index
BAI	=	Bed Agglomeration Index
EARS	=	Early Agglomeration Recognition System
FBC	=	Fluidized Bed Combustion
FBG	=	Fluidized Bed Gasification
K/Bed	=	Potassium consumption to bed material weight ratio
M.P.	=	Melting temperature
RDF	=	Refuse Derived Fuel
$R_{b/a}$	=	Base to Acid ratio

Dimensionless group

Ar	=	Archimedes number; $\dfrac{\rho_f(\rho_s-\rho_f)d_p^3 g}{\mu_f^2}$
Co	=	Cohesive number; $\dfrac{6S}{(\rho_p-\rho_f)d_p g}$
Ga	=	Galileo number; $\dfrac{g d_p^3}{\upsilon_f^2}$
Nu	=	Nussult number; $\dfrac{h d_p}{k_f}$
Pr	=	Prandtl number; $\dfrac{c_{p,f}\mu_f}{k_f}$

Re_p = Reynolds number based on the particle; $\frac{\rho_f U_f d_p}{\mu_f}$

Sc = Schmidt number; $\frac{\mu_f}{\rho_f D_{AB}}$

Sh = Sherwood number; $\frac{k_m d_p}{D_{AB}}$

St = Stoke number; $\frac{2m_p u_0}{3\pi\mu_f r_p^2}$

CHAPTER 1 INTRODUCTION

1.1 Renewable energy overview

Climate change concerns, high oil prices, peak oil demand and increasing government support drive increasing renewable energy legislation, incentives and commercialization [1]. Renewable energy is an energy that is derived from naturally and constantly replenished resources. It includes electricity and heat generated directly or indirectly from sun, wind, tides, hydropower, biomass, geothermal resources and biofuels, as well as hydrogen derived from the renewable resources.

According to Figure 1.1, renewable energy supplied 18.9% of the global energy consumption of 474 EJ, counting traditional biomass, large hydropower (>10 MW production), and other renewable sources (small hydro (<10 MW), modern biomass, wind, solar, geothermal, and biofuels).

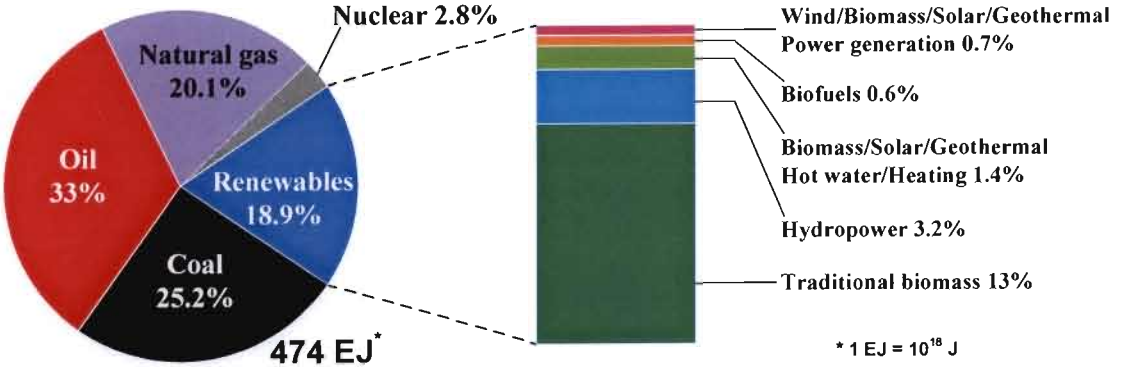

Figure 1.1 Share of renewable energy to global energy consumption in 2008 [2].

Of this 18.9%, traditional biomass which is used primarily for cooking and heating accounted for approximately 13%, and is growing slowly or even declining in some regions as biomass is used more efficiently or replaced by more modern energy forms. Hydropower at a large base (>10 MW) represented 3.2%, and is growing modestly. Other renewable sources accounted for 2.7% in total, and are increasing very rapidly in developed countries and in some developing countries. Renewable energy replaces the conventional fuels in four distinct markets: (i) power generation, (ii) hot water and space heating, (iii) transport fuels, and (iv) rural (off-grid) energy services. However, fossil fuels (coal, oil and natural gas) still dominated the consumption.

In Thailand, well-recognized as one of the top rank exporters of agricultural and food products, biomass has been the traditional renewable energy resource. As shown in Figure 1.2, about 24.4% of the total energy consumption of 2.37 EJ came from renewable energy, with 22% counted by traditional biomass, used mainly as cooking/heating, and 1.4% from biofuels (biodiesel and ethanol) including the garbage. Power from renewable energy represented approximately 0.9%, and is growing very rapidly by the government subsidies. However, the major contribution to the total consumption was fossil fuels, particularly oil for transportation.

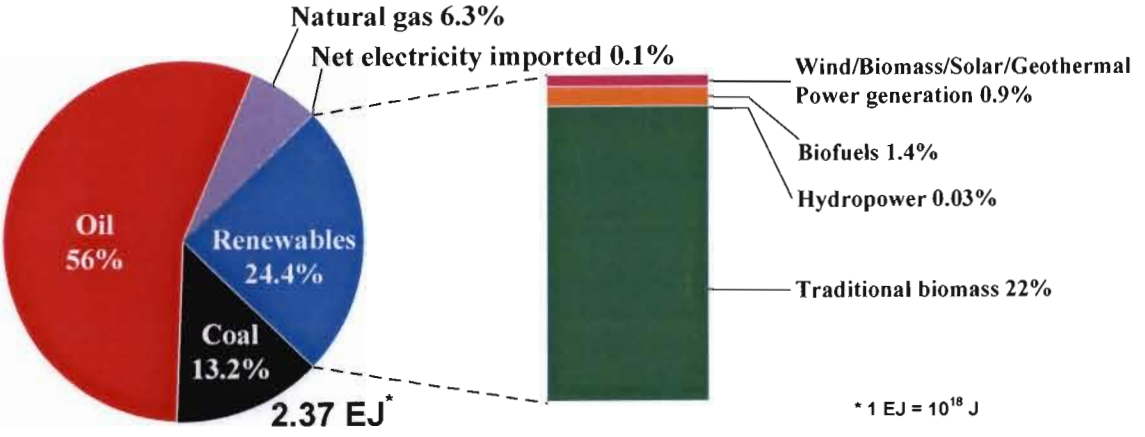

Figure 1.2 Contribution of renewable energy to total energy consumption of Thailand in 2009 [3,4].

Fossil fuels are not considered as biomass by the generally accepted definition [5], in spite of their origin in ancient biomass. Their production and use raise environmental concerns primarily caused by the CO_2 emission from the combustion. A global movement toward the generation of renewable energy is therefore under way to meet an increased energy needs and the attention to the biomass for the commercial power generation is also being paid increasingly.

1.2 Biomass overview

Biomass is biological material derived from living, or recently living organisms. Since the beginning of civilization, biomass has been a major source of energy throughout the world. Biomass, the fourth largest energy source after coal, oil and natural gas, is the largest and most important renewable energy option at present and can be used to produce different forms of energy [6]. In the developing world, wood biomass is a major renewable energy source, representing a significant proportion of the rural energy supply.

Biomass resources include primary, secondary, and tertiary sources [7]. Primary biomass resources are produced directly by photosynthesis and are taken directly from the land. They include perennial short-rotation woody crops and herbaceous crops, seeds of oil crops, and residues from the harvesting of agricultural crops and forest trees (e.g., wheat/rice straw, corn stover and the tops, limbs, and bark from trees). Secondary resources result from the processing of primary resources either physically (e.g., the production of sawdust in mills), chemically (e.g., black liquor from pulping processes), or biologically (e.g., manure produced by animals). Tertiary resources are post-consumer residues as biodegradable wastes including animal fats and greases, used vegetable oils, packaging wastes, and construction and demolition debris.

Using biomass represents an attractive way to environmental benefit by the decreasing CO_2 emission, because it is part of the short carbon cycle. Carbon from the atmosphere is converted into biological matters of plant by photosynthesis, building up lignin, hemicelluloses, cellulose, lipids and etc, as structure and non-structure carbohydrates [8]. On death of combustion, or decay, the carbon goes back into the atmosphere as carbon dioxide (CO_2). This happens over a relatively short timescale and plant matter

can be constantly replaced by planting for new growth. Though biomass is sometimes called a "carbon neutral" fuel since its use as a fuel reasonably stabilize the level of atmospheric carbon, its use can still contribute to global warming due to the processing of biomass, for instance the crops for biofuels are harvested and transported using machinery that burns fossil diesel.

Even though the annual global primary production of biomass was equivalent to 4,500 EJ [6], the biomass presence in the global energy consumption was only 62-66 EJ (13-14% according to Figure 1.1). In Thailand, only 0.53 EJ of biomass, referred to Figure 1.2, was utilized while the estimated biomass production was equivalent to 1.4 EJ [4]. These potentials are highly attractive for commercial power production and biomass contribution to power generation in Thailand has been promoted at present under the 15 Year Renewable Energy Development Plan [9], particularly focusing on the solid agricultural biomass.

1.3 Biomass conversion technology

There are a number of energy conversion technologies that can convert a variety of biomass into heat, power, and fuels as summarized in Figure 1.3.

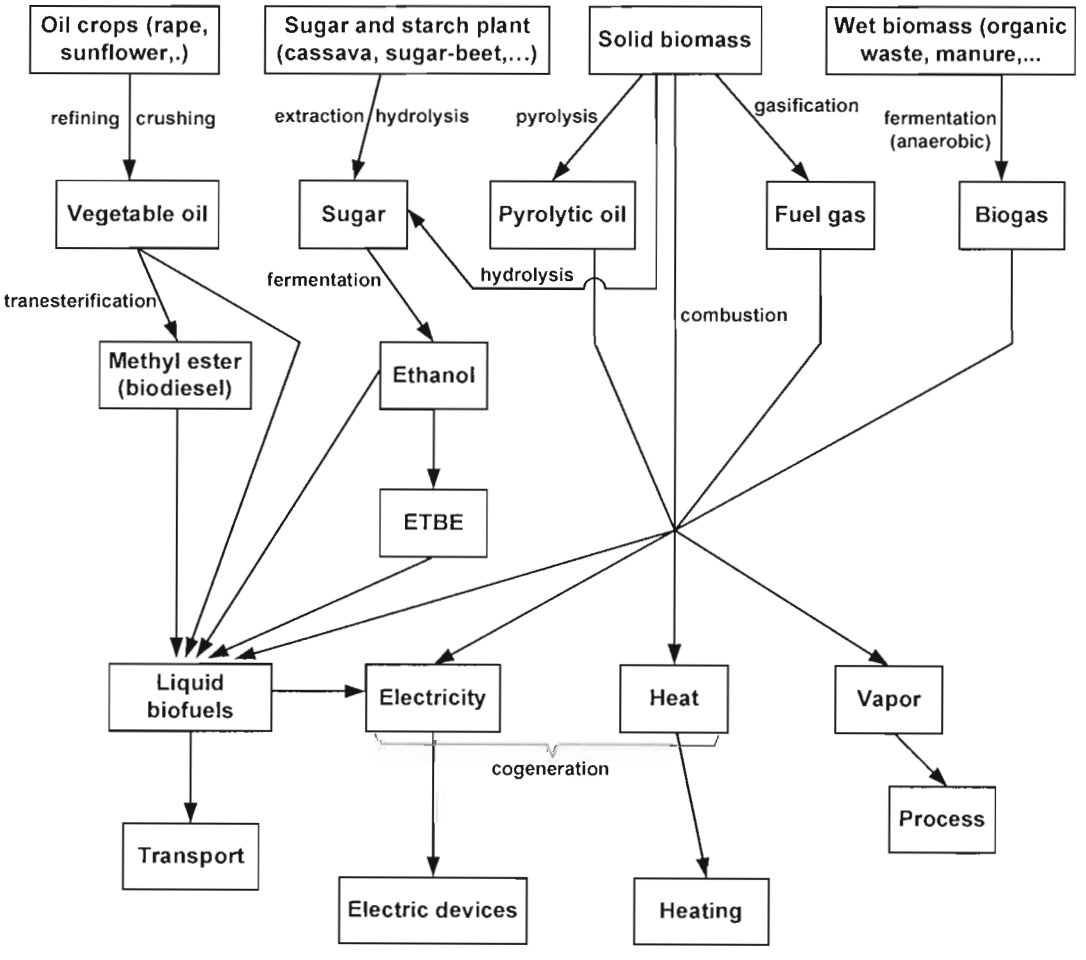

Figure 1.3 Biomass energy conversion overview [7].

Conversion technologies may release the energy directly, in the form of heat, or may convert to other forms, such as liquid biofuel or combustible biogas. While for some classes of biomass resource there may be a number of usage options, for others there may be only one appropriate technology. The most conventional way in which particularly solid biomass is used, however, still relies on the direct combustion.

The combustion is studied intensively over hundred years. The intimate understanding in the behaviors of solid combustion as well as the development in a number of techniques and implements have made it to utilize biomass in a more effective way, as the increasing heat/power productivity with the decreasing emission. Among them, one favorable technique built up is the fluidized bed combustion (FBC) technology.

1.4 Fluidization technology

1.4.1 Fluidization and Fluidized bed

Fluidization refers to the process by which a fluid-like is imparted to granular solid by the application of appropriate external forces [10]. The amount of solid particles is set into motion by blowing a fluid steam upward through a bed at sufficient velocity to locally suspend the particles, but yet not too great velocity to blow the particles out of bed. The bed appears like a boiling liquid and has other features of liquids such as exhibiting buoyancy and hydrostatic head, hence that it is called "fluidized bed". This behavior is characterized as shown in Figure 1.4.

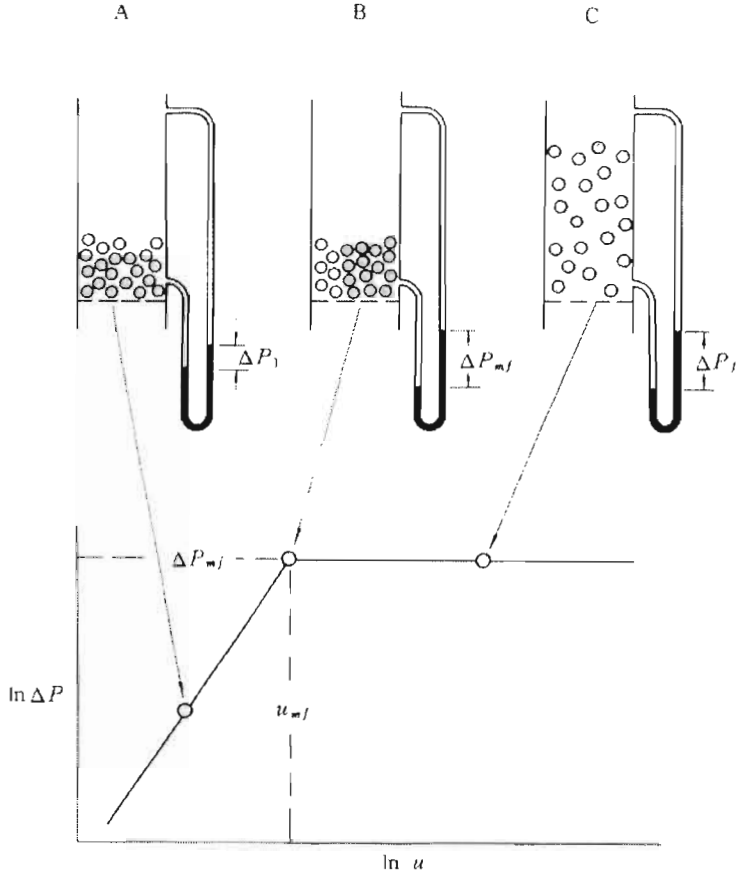

Figure 1.4 Characteristic of increasing fluid flow fluidization [10].

When fluid flow start at relatively low velocity through static bed of solid particles, the interstitial pores among the particles offer sufficient resistance to the fluid to create a corresponding drop in pressure in the flow direction. As the velocity increase, this pressure drop increases correspondingly until at some flow rate, this pressure drop equals the weight of this granular. At this point, the solid particles start to lose contact from their neighbors, which have up to this point offered mechanical support, and become buoyed up hydro-dynamically. As it increases further, the particles, which are now suspended, cannot offer greater resistance due to their limited masses. Instead, the flowing fluid pushes the particles further apart to make way for increased flow and the pressure drop remains constant at the same level corresponding to the solid weight.

1.4.2 Solid combustion application [11]

When fuel particles enter the hot bed of inert materials, such as sand, fluidized by the upward flowing air, their temperatures are raised to the point at which the moisture is vaporized and then are further increased to the point at which a certain part of the organic compounds is volatilized. Until reaching their self combustion temperatures, fuel char particles are burnt continually in the bed. A part of released heat is circulated to the recently fed fuel particles by the inert bed, acting as the heat reservoir, while the major one is utilized, for instance to boil water into steam. During combustion, fuel particles can be spread uniformly across the bed due to the chaotic bed mixing induced by the passing air bubble. The temperature field in a fluidized bed is rather uniform due to the intense in-bed heat transfer as a consequence of this bed mixing. This feature of fluidized bed combustor provides the advantages as summarized below:

- High fuel flexibility, both in size, rank and type.
- High combustion efficiency with low combustion temperature.
- High rate of heat transfer due to the turbulent mixing of bed.
- Effective emission control of SO_2 through removal by reaction with the poisonous gases capture additives.
- Expensive pretreatment and preparation of fuels are not needed.

By its prominent features, FBC is found suitable for a wide variety of fuels, especially the low grade fuels such as lignite and solid agricultural biomass. Presently this technique has been achieved to be the commercial scale power plants using biomass.

1.5 Problems of biomass firing in fluidized bed

Although FBC is a mature technique, many operational problems associated with the ash are frequently encountered in its application to biomass [12]. They are particularly connected with the unique alkali content. The relatively rich alkali of biomass cause the ash forming constituents to melt at relatively low temperature leading to a number of the critical ash-related operational problems [13] viz,

- The formation of fused or partly-fused ash agglomerates and slag deposits at high temperatures within furnaces and stoves.
- The formation of bonded ash deposits and accumulations of ash materials at lower temperatures on surfaces in the convective sections of boilers.
- The accelerated metal wastage of furnace and boiler components due to gas-side corrosion under ash deposits, and due to ash particle impact erosion or ash abrasion of boiler components and other equipment.
- The formation and emission of sub-micron aerosols and fumes.
- Biomass ash impacts on the performance of flue gas cleaning equipment.

- The handling and the utilization/disposal of ash residues from biomass combustion plants, and of the mixed ash residues from the co-firing of biomass in coal-fired boilers.
- Bed particle agglomeration caused by fused or partly-fused ash materials in the fluidized bed boiler.

Particularly, bed agglomeration is a common reason for decreased availability of the biomass fired fluidized bed boiler. It deteriorates the fluidization quality, which then disturbs the combustion process in the furnace. An increase in bed particle size, due to the agglomeration, is then translated into an increase in the minimum fluidization gas velocity. As a result, the superficial air/gas velocity must be increased in order to maintain the fluidization state. If it is not increased accordingly or the whole bed agglomerates in the extreme case, fluidization can no longer be maintained, namely defluidization, leading to an unscheduled shutdown with costly loss.

Defluidization by the bed particle agglomeration is one major challenge faced by the thermal based fluidized bed technologies for the power generation. The intimate insight to its behaviors concerning the fates of inorganic elements on the bed agglomeration and the contributions of the bed operating parameters on the defluidization is required to prediction and tackling, for the success of applying FBC to produce energy from the specific biomass.

1.6 Research objectives

This work aimed to find out the approach to predict the bed agglomeration behaviors during fluidized bed combustion of agricultural residues. The specific objectives were

1. To investigate the bed agglomeration tendency regarding to the biomass ash properties and the fluidized bed operating conditions.

2. To elucidate the plausible mechanisms of bed agglomeration and relevant inorganic behaviors.

3. To propose the developed mathematical models.

1.7 Scopes of work

1. Investigating experimentally by combustion of the representative agricultural residues as palm kernel shell, palm empty fruit brunch, corncob and rice straw in the laboratory and pilot scale bubbling fluidized bed facilities using only quartz sand as inert bed material at different bed (combustion) temperature, superficial air velocity, bed particle size and static bed height, of the operating conditions.

2. Developing the mathematical models to predict the bed agglomeration behaviors.

1.8 Research Methodology

To achieve this work, the study workflow was performed below:

1. Characterizing the materials.

Firstly, the physical and chemical properties as well as the ash compositions of selected biomass were necessary to be characterized intensively since they were handled in fuel

preparation and subsequently tested in fluidized bed. Similarly, the quartz sand was also characterized.

2. Performing the agglomeration test

The steady state combustion in fluidized bed reactors under the atmospheric condition was carried out to study the effects of biomass ash properties and operating conditions on the bed agglomeration tendency. The behaviors and states of bed during combustion were monitored until complete defluidization.

3. Characterizing the agglomerates

The morphology and chemistry of agglomerate samples from the bed at defluidization were studied in order to identify the inorganic behaviors and the interactions between the released ash constituents and bed particles responsible to the bed agglomeration.

4. Developing the mathematical models

The mathematical models were developed based on analyzing the laboratory scale experimental results.

5. Verifying the models.

The results of lab and pilot scale tests as well as the previously published data were used to verify these models.

CHAPTER 2 BED AGGLOMERATION

2.1 Introduction

Particle agglomeration was early recognized as critical factor for the operation of fluidized bed in fuel conversion, iron ore reduction and cement processes [14-16]. However, it became useful and common for food and pharmaceutical industries, the agglomerates of material grains are intentionally produced in order to improve the powder properties [17]. Bed particle agglomeration latterly was found to occur in likelihood by a mechanism of sintering in the presence of a liquid phase [18]. As the sintering process progressed, the coalescence and densification were evident.

The bed particle agglomeration was experienced during various fuel conversion processes such as fluidized bed combustion (FBC) and gasification (FBG) of coal, biomass and refuse derived fuels (RDF) [12,19-23]. It was mainly attributed to the chemistry of ash and bed material [24-28]. The interactions between the released ash species and bed particles under high temperature during the normal bed operating conditions resulted in the presence of the compounds with low melting temperatures on the surface of bed particle. At certain critical conditions, these compounds presenting as liquid phase induced the permanent bonds between bed particles to form agglomerates, and defluidization then began.

There are a large number of previously intensive studies toward the bed agglomeration, many investigations focused on the plausible and governing mechanisms, prediction or prevention. The following information on bed agglomeration is the comprehensive compilation and review of the research literatures.

2.2 Ash chemistry of biomass

A wide variety of solid and liquid biomass materials, and biomass materials as the components of mixed fuels, are combusted in a wide range of combustion devices, for heating and power generation purposes. The general types of installations [29] can be classified under the following broad categories, depending on the scale of operation:

- The very small stoves, fires and boilers employed for domestic cooking and heating.
- The small and medium scale boilers employed for commercial, process and district heat supply.
- The medium and large scale boilers employed for combined heat and power, or power-only applications.
- The co-firing of biomass materials with coal in large industrial and utility boilers.

For the case of solid fuel, biomass materials contain noncombustible constituents, and the nature and behavior of these constituents have a significant bearing on the design, operation and performance of the combustor and boiler.

2.2.1 Chemical compositions of biomass ash

Composition and other relevant data for a wide range of biomass, biomass ash and other relevant materials are available in a number of databases of biomass properties on the internet [30-33] and of previous literatures in the biomass related field study, including from presently reviewed literatures [8,12,29]. All of the biomass and biomass-based waste materials are distinguished to other industrial solid fuels by having relatively low

calorific values, high volatile matter contents and low bulk densities. They are the oxygen rich and carbon based fuel. Most of the biomass materials, in raw harvested form, also have very variable moisture contents, and it can be disadvantageous to dry and/or densify the biomass, prior to transportation, handling and storage as a fuel.

The reported ash data show fairly clear in some general trends of inorganic species, described below for woody fuels and agricultural residues. The wood materials, generally having very low ash contents (1-4 %), are particularly rich in calcium and very low in chlorine and sulfur. Some extraneous clay and quartz may be present from contamination with soil. The ash melting temperatures are generally very high. Agricultural residues have relatively higher ash content, ranging at a large variance from 2% to more than 20%. Their ash chemistry vary significantly but all are dominated by potassium, silicon and phosphorus compounds. Silicon is the abundant element. Their ash melting temperatures are therefore lower than those of wood, usually between 800-1000 °C. Some residues such as straws and grasses may also contain relatively high concentration of chlorine and sulfur.

Three different biomass ash systems have been generally described in terms of their ash chemical composition and their fusion behavior [34], viz:

- high silicon / high potassium / low calcium ashes with low fusion temperatures, in the agricultural residues.
- low silicon / low potassium / high calcium ashes with high fusion temperatures, found in woody materials.
- high calcium / high phosphorus ashes with low fusion temperatures, including manures, poultry litters and animal wastes.

The important inorganic elements in biomass from a view point of the bed agglomeration problems are the refractory silicon, the alkali potassium, the alkali earth calcium and the non-metallic chlorine, sulfur and phosphorus [12,24]. Potassium is well accepted by far as the most important element responsible for bed agglomeration and other ash-related problems in thermal treatments of biomass (given technical terms as combustion, pyrolysis and gasification).

2.2.2 Forms of inorganic in biomass

The form in which an inorganic element occurs in a solid fuel has a decisive influence on its reactivity and volatility in combustion and gasification. Inorganic material in low-rank solid fuels, including lignites and biomass, can be roughly divided into two broad fractions [35], viz:

1. Atomically dispersed inherent inorganic material

Inherent inorganic material exists as part of the organic structure of the biomass. It is most commonly and largely associated with the oxygen, sulfur and nitrogen-containing functional groups (carboxyl, hydroxyl, ketone or ether groups). The inorganic elements are associated chemically, in the form of cations or chelates (chelate; *a heterocyclic compound having a metal ion attached by coordinate bonds to at least two nonmetal ions*), with these organic functional groups in the suitable sites or are in the solution in inherent moisture as a soluble salt or are precipitated as a crystalline salt. It is also possible for some inorganic species to be present in a very fine particulate form within the organic structure.

2. Extraneous discrete mineral

This inorganic material is added to the fuel through geological processes, or during harvesting, handling and processing of the fuel. Biomass fuels are commonly contaminated with soil, sand, pebble, pieces of iron or tramp materials, which have become mixed with the fuel during collection, handling and storage.

The modes of occurrence and origins of the main inorganic elements in biomass based on the plant physiology [34] are summarized in Table 2.1, including the elements of interest, principal form of uptake, structural forms in plant, brief function description and main source of each element, and explain below viz;

- Silicon is taken up to plant by absorption of silicic acid from the soil and deposited as hydrated oxide ($SiO_2 \cdot nH_2O$) in plant structure usually in an amorphous form, but occasionally in a crystalline form [36].
- Aluminum is toxic occurring in small quantities and its presence is usually a marker of contamination via dust, dirt or other soil constituents.
- Calcium is essential for cell wall stiffening and forms exchangeable bonds with cell walls. Major sources of calcium are lime, dolomite or gypsum in the soil amendment.
- Magnesium is exclusively part of chlorophyll essential for photosynthesis [37]. Soil minerals, organic material, fertilizers, and dolomitic limestone are sources of magnesium for plants.
- Sodium is not an essential element to plant, but it is toxic at higher than 2 wt% in soil.
- Potassium occurs as the univalent ion with high mobility and has an important function in osmotic process and metabolism [38]. It is supplied to plants by soil minerals, organic materials and fertilizers.
- Phosphorus, noted especially for its role in converting the sun energy to useful compounds for plant, is a vital component of DNA *(*Deoxyribonucleic acid; *the genetic memory unit*), RNA (Ribonucleic acid; *the DNA decoder*) and ATP (Adenosine-5'-triphosphate; *the chemical energy unit*) of plants [39]. Its uptake is mostly as the primary orthophosphate ion ($H_2PO_4^-$) from mainly fertilizer, but some also absorbed as secondary orthophosphate (HPO_4^{2-}) as increasing soil pH [36,39].
- Iron has two principal forms; chelates and cations. It is involved in nitrogen fixation and photosynthesis. Soil mineral is its main source.
- Sulfur in plants is in the form of sulfates and organic sulfur. It can be incorporated into plants both by absorption and assimilation of the atmospheric SO_2 and by absorption of the sulfur dissolving water.
- Chlorine in biomass occurs as a chloride iron. Its concentration is closely related to the nutrient composition of the soils.

Table 2.1 Element structures in biomass

Element	Uptake form	Structural examples in plant	Function	Source
Silicon (Si)	H_2SiO_3, $Si(OH)_4$	$SiO_2 \cdot nH_2O$, usually in amorphous form and occasionally in crystalline form	- A structural component of some plant species - Play a role in disease resistance in crop plants	Soil
Aluminum (Al)	Al^{3+}	Al^{3+}	- Toxicity of Al decreases the uptake and distribution of other elements	Soil, Dirt
Calcium (Ca)	Ca^{2+}	Ca^{2+}, CaC_2O_4	- Essential for cell wall structure - Form exchangeable bonds with cell walls for osmotic and signaling purposes	Lime, Gypsum, Dolomite
Magnesium (Mg)	Mg^{2+}	Mg^{2+}	- Exclusive component of chlorophyll [37] - A cofactor for many enzymatic reactions	Soil, Fertilizer, Dolomite
Sodium (Na)	Na^+, NaCl	NaCl	- It is not an essential element for plant - Its high concentrations in soil are toxic	Intrusion of salt water or a process additive
Potassium (K)	KCl	K^+(univalent ion) or in the organic matrix [38]	- High mobility with little structural function in every living plant and animal cell - Aid in osmotic and ionic regulation - Function as a cofactor or activator of many enzymes of carbohydrate and protein metabolism	Fertilizer, Organic materials
Phosphorus (P)	$H_2PO_4^-$, HPO_4^{2-}	R-$(PO_4)_2$, a vital component of DNA, RNA, and ATP [39]	- Play central role in plants in energy transfer and protein metabolism - Energy used by an organism in its daily operations is released when ATP reduces to ADP (Adenosine diphosphate) - Essential for all plant growth	Fertilizer

Table 2.1 Element structures in biomass (Continue)

Element	Uptake form	Structural examples in plant	Function	Source
Iron (Fe)	Fe^{2+}, Fe^{3+}	Fe^{2+} in the form of chelates and ion	- Involved in N-fixation and photosynthesis - To be active a transport[1] - Essential for reversible oxidation/reduction reaction	Soil
Manganese (Mn)	Mn^{2+}	Mn^{2+}	- Involved in photosynthesis - A constituent of enzymes arginase[2] [40] and phosphotransferase[3] [41]	Soil, Fertilizer
Copper (Cu)	Cu^{2+}, $Cu(OH)_2$, $Cu(H_2O)_6^{2+}$	Cu^{2+}, $Cu(OH)_2$, $Cu(H_2O)_6^{2+}$	- Constituent of several enzymes - Relatively immobile element, associated in plant structure - Important trace in plants reproductive growth stage	Soil, Additive
Sulfur (S)	SO_4^{2-}, SO_2	SO_4^{2-}, organic-S	- Involved in plant cell energetics	Atmospheric SO_2, Sulfur dissolved in water
Chlorine (Cl)	KCl, Cl^-	Cl^-	- Essential for photosynthesis - Function in osmoregulation[4] [42] of plants growing on saline soils	Soil, Salt water

Remark

[1] an exchange of molecules (and their kinetic energy and momentum) across the boundary between adjacent layers of a fluid or across cell membranes

[2] a manganese-containing enzyme It is the final enzyme of the urea cycle.

[3] a category of enzymes that catalyze phosphorylation reactions (addition of a phosphate (PO_4^{3-}) group to a protein or other organic molecule)

[4] the active regulation of the osmotic pressure of an organism's fluids to maintain the homeostasis of the organism's water content; it keeps the organism's fluids from becoming too diluted or too concentrated.

The further investigations [36,43] of the major inherent inorganic species of biomass provide a roughly qualitative and quantitative data of the major inorganic element speciation in three categories, viz:

- Water soluble, i.e. in free ionic form
- Organically associated
- Precipitated as relatively pure compounds, in crystalline or amorphous forms

A listing of these major inorganic species is presented in Table 2.2.

Table 2.2 Speciation of inorganic materials [36,43]

Element	**Class 1 – water soluble (free ionic form)**		
	Compound	**Formula**	**Share of total element (%)**
Si	Silicon hydroxide	$Si(OH)_4$	<5
Ca	Calcium nitrate, chloride, phosphate	$Ca(NO_3)_2$, $CaCl_2$, $Ca_3(PO_4)_2$	20-60
Mg	Magnesium nitrate, chloride, phosphate	$Mg(NO_3)_2$, $MgCl_2$, $Mg_3(PO_4)_2$	60-90
Na	Sodium nitrate, chloride	$NaNO_3$, NaCl	>90
K	Potassium nitrate, chloride	KNO_3, KCl	>90
P	Phosphate ion	PO_4^{3-}	>80*
S	Sulfate ion	SO_4^{2-}	>90*
Cl	Chloride ion	Cl^-	>90*
	Class 2 – organically associated (covalent or ionic bonding with tissue)		
Ca	Calcium pectate	macromolecule	0.8-2.6
Mg	Chlorophyll, magnesium pectate	$C_{55}H_{72}MgN_4O_5$, macromolecule-	8-35
P	Nucleic acid	PO_4^{3-}	Not reported
Fe	Organic complex, organic sulfates	Fe^{3+}, Fe^{2+}	>80*
Mn	Various organic structures	Mn^{2+}, Mn^{3+}, Mn^{4+}	>90*
S	Sulfolipid, poteins, amino acids	SO_4^{2-}, S	Not reported
	Class 3 – precipitated (pure compound, amorphous, crystalline)		
Si	Phytolite	$SiO_2 \cdot nH_2O$	>90*
Ca	Calcium oxalate	$CaC_2O_4 \cdot nH_2O$	30-85
P	Phytates	Ca-Mg(-K)-salt of $C_6H_6[OPO(OH)_2]_6$	Up to 50-86% in seeds
Fe	Phytoferritin	$(FeO.OH)_8.(FeO.OPO_3H_2)$	Up to 50% in leaf tissue

* No exact quantities have been reported. The quoted value indicates that the speciation is the dominant one for that element.

The data in this table indicate clearly that the alkali, phosphorus, sulfur and chlorine in the inherent inorganic material tend to be present largely in the soluble form, as simple inorganic salts. Silicon is present predominantly as silica in the precipitated form. The alkaline earth metals are more complex and can occur in a number of forms. The extraneous inorganic material can also be present in many forms. It takes the form of contamination with sand, soil or other mineral materials, tramp metal components, etc.

The modes of occurrence of inorganic species are further discriminated according to their solubility in a sequence of increasingly aggressive chemical solvents, namely "the chemical fractionation" [44-45]. It is developed originally for the characterization of coals and later adapted to characterize a number of biofuels [24,46-47]. The leaching solvents employed for this purpose are commonly: Water ⇒ Ammonium acetate solution ⇒ Hydrochloric acid solution. The following four modes of occurrence distinguished by this analysis are listed in Table 2.3.

Table 2.3 Modes of chemical fractionation results

Solubility	Likely form in the fuel
soluble in water	principally the water soluble salts, sulfur and chlorine
soluble in ammonium acetate (ion-exchangeable)	organically bound as cations and chelates
soluble in hydrochloric acid	generally acid soluble salts as carbonates and sulfates
insoluble	principally mineral formed as oxides, silicates or sulfides

It is generally considered that the water and acetate-leachable elements are relatively reactive and are more readily released into the vapor phase and the submicron sized aerosol fraction of the ash generated from the biomass during elevated temperature processes. The elements in the acid soluble and residue fractions are more immobile and tend to release into the coarser ash fraction.

As result, the biomass materials, in general, have significantly and relatively higher levels of water and acetate soluble species, with the majority of the potassium and chloride, and some of the calcium and magnesium, compared with coals. The fractionation results in details of each element are provided in Table 2.4 and discuss, viz

Table 2.4 Fraction and form of elements in chemical fractionation of biomass

Element	Fraction	Likely form	Description
Refractory Si, Al, Ti	Insoluble mainly	Oxide, Silicate	- Al and Ti in trace concentration - Much less reactive in volatilization and chemical reaction
Alkali K, Na	>90% in water soluble or ion exchangeable	Chloride, Sulfate, Other salts, Cations, Chelates	- Na in trace concentration - Easily volatilized or easily available for chemical reaction
Alkali earth Ca, Mg	Largely in an ion exchangeable or acid soluble	Cations, Chelates, Carbonate, Sulfate	- Lesser volatile than alkali
Cl	Water soluble mainly	Salt, Anions	- Present in an easily vaporizable form
S	Variable	Variable	- Variable forms, ranging from completely water soluble to completely insoluble
P	Variable	Variable	-
Noble metals (Fe, Mn, etc)	Acid soluble or insoluble	Variable	- Trace elements in biomass

- All refractory elements (Si, Al and Ti) are insoluble and likely in the oxide and silicate as the major form. Al and Ti are present in trace concentrations. These refractory components are thus assumed to be much less reactive in volatilization and chemical reaction in a high temperature process.

- The alkali and alkali earth elements (K, Na, Ca and Mg), which mainly occur in plant organic structures or reactive mobile inorganic components, are predominantly in the soluble fractions.
- Over 90% of potassium in non-contaminated biomass (no soil) is in the water soluble and ion exchangeable form, hence it is believed to be easily volatilized or easily available for chemical reaction, probably leading to the ash-related problems. Sodium presents only in a trace element.
- Calcium is largely in an ion exchangeable or acid soluble form, thus it is lesser volatile than potassium. Magnesium also shows the same.
- Chlorine is supposed to be present in an easily vaporizable form, since almost all of it in biomass is in a water soluble form.
- Noticeably, sulfur occurs in variable forms, ranging from completely water soluble in wheat straw to completely insoluble in switchgrass. However, the volatility of sulfur is insubstantially depended on its form in fuel, as it is oxidized to SO_2 in combustion and released as H_2S in gasification and pyrolysis [48].
- Phosphorus and the noble metals also occur in variable forms.

It further seems that the chemical fractionation results are fairly consistent with the biological functions of inorganic elements. Clay contamination can give increasingly a fraction of insoluble.

The chemistry of biomass ash differs considerably with the biomass type, cultivated soil, fertilizers, climate, maturity, harvesting, handling, etc., and also with employed analytical techniques and ashing temperature [49-53]. The inorganic classes in biomass are early discriminated by the aforementioned analyses based on either the plant physiology or chemistry. They provide useful information to assist in the advance prediction about the potential behaviors of ashes in the thermal treatments of specified biomass fuels. However, the careful interpretation from these results is needed.

2.3 Inorganic behaviors and bed agglomeration process

Despite the result of the complex interactions in both physically and chemically, the bed agglomeration is likely treated as basically three sequential steps [24];

- Firstly, the ash forming elements in fuel are released during thermal treatments, as the inorganic transformation,
- Secondly, they are transported to the surface of bed particles forming the coating, namely the inorganic migration, and
- Thirdly, the coated bed particles stick their neighbors and then form the agglomerates, this is the sintering.

A review in this section is performed to identify the behaviors of inorganic elements during elevated temperature processes. Their interactions with the bed particle relevant to bed agglomeration and the sintering processes are focused and then summarized to the mechanistic information.

2.3.1 Inorganic transformations

The physical and chemical transformations of inorganic matter in biomass combustion are typically illustrated in Figure 2.1. The mechanisms for transformations in biomass-fired boilers are mainly based on analysis of deposits from different locations in large scale or commercial scale boilers, including travelling grates and fluidized beds.

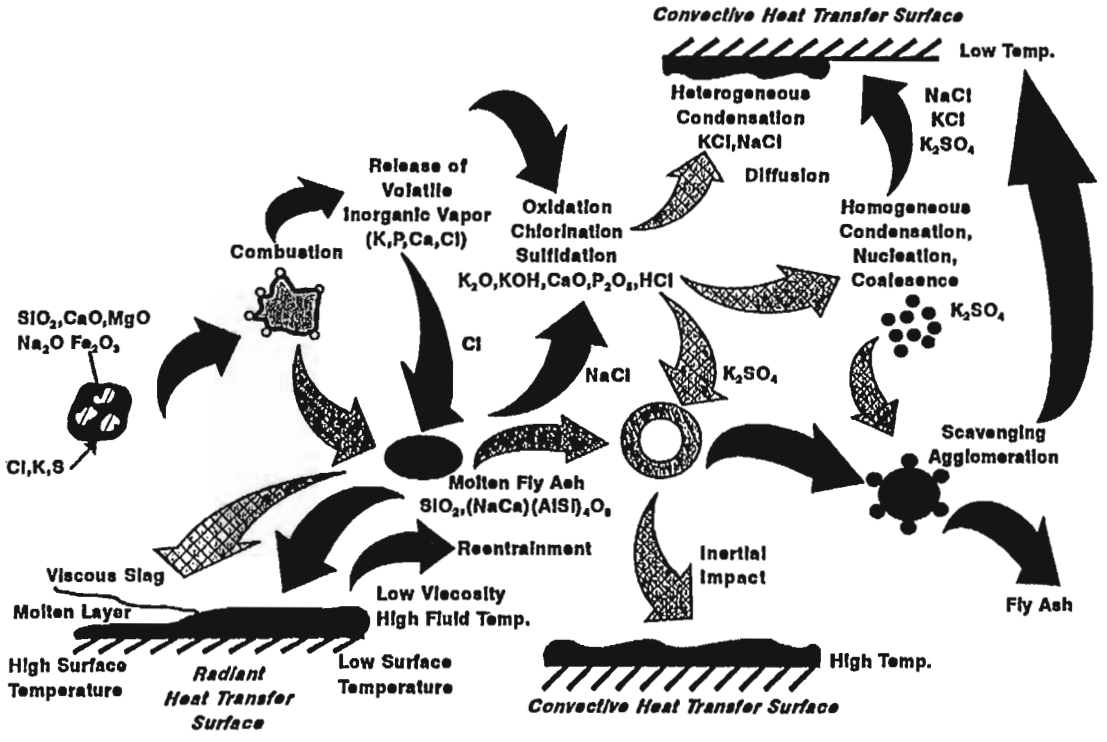

Figure 2.1 Transformation of mineral matters in biomass [54].

A certain part of the inorganic matters, derived supposedly from ionically or organically-bound inorganic, is released as a vapor phase. This volatilization of inorganic is a key role in fouling of biomass-fired boilers, (*fouling is defined as deposition in the heat-recovery section of the steam generator subjected to convective heat exchange by fly ash quenched to a temperature below its predicted melting point, condensation by volatiles, or sulfidation by SO_3*) [34]. The released ash constituents have else present in the fine liquid/solid of particulate matters (aerosols), coarse fly ash particles and sintered ash as bottom ash, which they can contribute to slagging and further to intensified fouling (*slagging is deposition of sintered ash on heat transfer surface and refractory in the furnace volume primarily subjected to radiant heat transfer*). However, there are some general agreements on the ash release behaviors and no exact ranges and temperature on the release quantities and the start of volatilization, respectively. These are obviously due to many factors affecting the release: the form of inorganic elements in biomass, heating rate and final temperature of fuel particle, presence of chlorine, sulfur and silica, ambient conditions (oxidizing: *combustion* or reducing: *pyrolysis, gasification*), etc [51].

Basically, most solid fuels exposed to a hot gas stream during combustion experience in three sequentially distinct stages of mass loss; (i) drying, (ii) devolatilization and volatile combustion, and (iii) char combustion. No release of inorganic species as well as chlorine and sulfur occurs in the drying step [55-68], indicating that they may not be associated with water in the fuel. Generally, a minor extent of inorganic elements starts to be released during devolatilization while the major releases part is in the char combustion phase. The transformation mechanisms of elements of interest, particularly of potassium that had been proposed specifically [69] as illustrated in Figure 2.2, can be summarized in Table 2.5 and explained; viz.

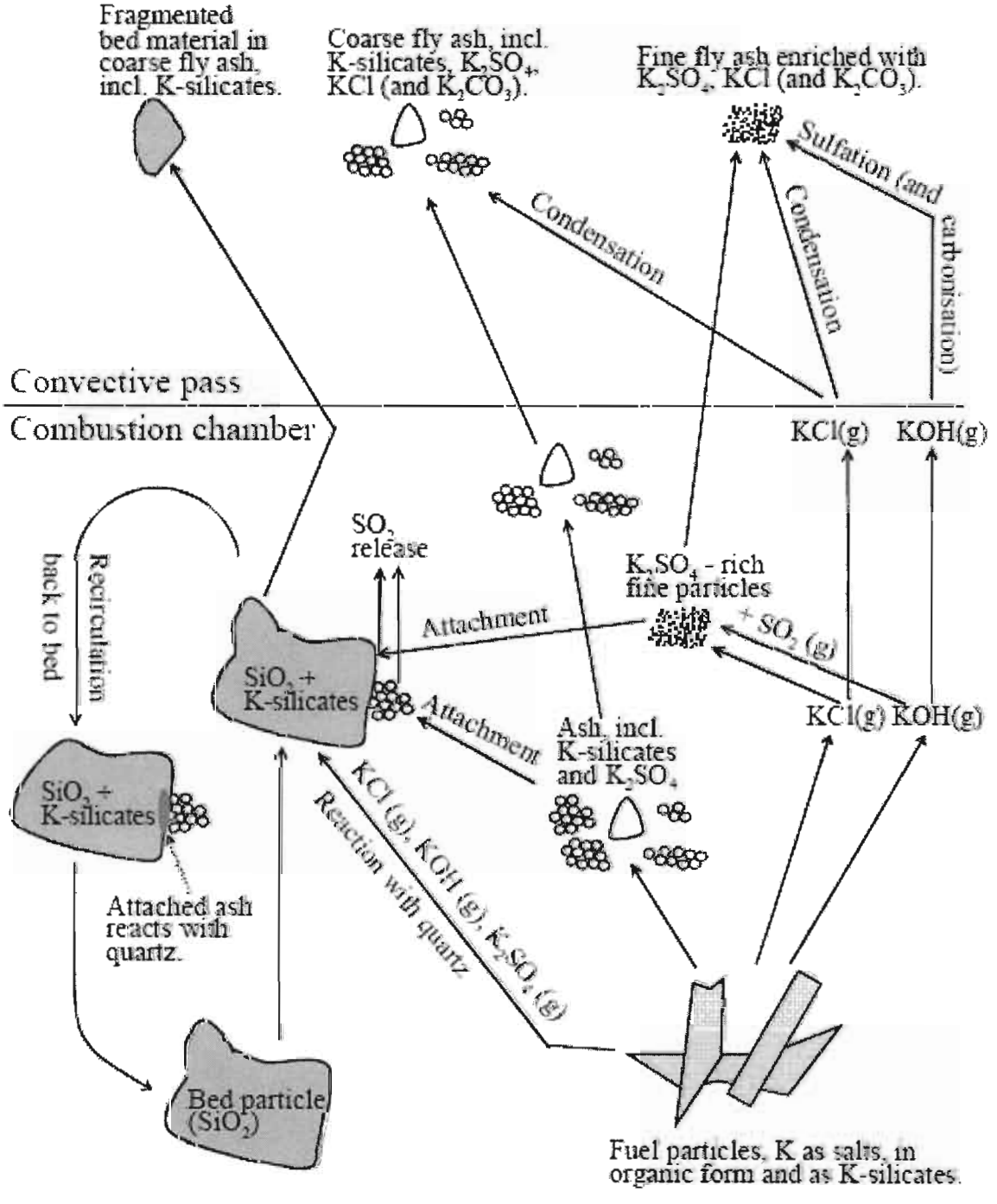

Figure 2.2 Behavior of potassium during biomass combustion [69].

Table 2.5 Fates of elements during heat treatment processes

Element	Transformation		Note
	Phase	Species	
Si	Molten	Silicates	-
	Solid	SiO_2 (Silica)	
Al	Solid	Al_2O_3, Silicates	-
Ca, Mg	Molten	Silicates	-
	Solid	Sulfate, Oxide and Chloride	
Na	-	-	Neglected in the account
K	Vapor	KCl, KOH, K_2SO_4	-
	Aerosol	K_2SO_4, K_2O, K_2CO_3	
	Molten	Silicates	
P	Solid	K_3PO_4, $K_4P_2O_7$, Silicates	-
Fe	Solid	Oxide form	-
S	Gas	SO_2, H_2S	-
	Aerosol	K_2SO_4	
	Solid	$CaSO_4$, $MgSO_4$	
Cl	Vapor	HCl, KCl	-
Trace	Variable	Variable	-

Potassium released from fuel particle includes (i) gaseous KCl, KOH and K_2SO_4, (ii) aerosol K_2SO_4, K_2CO_3 and K_2O, and (iii) K in the coarse particle mainly as silicates. If chlorine presents in biomass, especially the annual crop that has relatively large amount of potassium and chlorine, potassium will be released to the gas phase as KCl. This KCl is proved to be the major volatile K species and major volatile constituent [57,63]. The KCl release is initially in the devolatilization state and substantially on char combustion. The subsequent sulfation of KCl in both gas phase and condensed phase to form K_2SO_4 will be occurred, if SO_2 exists in the system [66]. The sulfation rate in the gas phase is significantly faster with occasionally up to complete conversion while that of the condensed phase is considerably slower with about 0.5-2% conversion. However, both rates are controlled by the availability of intermediate SO_3, depending on SO_2 and O_2 but not on H_2O concentration. A vapory K_2SO_4 is also directly released. As further suggested [66], the most in-flight KCl sulfation takes place in the gas phase while any sulfation of deposits likely occurs in the molten deposits. In the case of high water vapor concentration in the gas phase, KOH is formed and it is relatively stable [63]. KOH is yet still very reactive until it reacts to form the even more stable compounds by the reaction with vapor HCl to form gaseous KCl, the sulfation and carbonization to form aerosol K_2SO_4 and K_2CO_3 respectively or otherwise the absorption-reaction by some inorganic matters (chemisorption). The release of volatile alkali species out of fuel is however inhibited in consequence of the absorption onto the reactive char surface [60,61]. Solid K_2O is also an intermediate one among the released K species and it is unstable by thermal decomposition at temperature above 350 °C [70]. Since sodium is generally assumed to behave similarly with potassium and is further an insignificant content in biomass, the specific presence of sodium is always neglected in the account.

Chlorine is well already recognized as the facilitator of alkali volatilization, which can stabilize high temperature gaseous alkali species [59-62]. Its major amount in biomass is released to gas phase as HCl during devolatilization, this HCl is an important contributor to the high temperature corrosion in boiler [34]. Chlorine is hardly found in the non-volatile ash [24]. The KCl release to gas phase in char combustion is therefore determined by the existing chlorine in biomass char.

The main sulfur release in combustion is SO_2 [64]. In the devolatilization step, sulfur is released to gas phase from its primary binding sites in organic molecules, such as proteins or sulfolipids (a class of lipids which possess a sulfur-containing functional group), while sulfur in the form of inorganic sulfates may be partially reacted with char, and become attached to the char matrix or transformed to CaS/K_2S [61]. During char combustion phase, the inorganic sulfur bound to the char matrix is oxidized and released to gas phase as SO_2. However, the released gaseous sulfur species can be subsequently captured by reactive sites in the char, and become bound to the char. To the contrary in the reducing conditions, sulfur is largely converted to H_2S and the sulfation does not occur [51,64]. It was further suggested that the maximum achievable sulfur retention in fuel during heat treatments is largely determined by the content of silicate relative to calcium and potassium in biomass [64]. The interaction of gaseous sulfur species, as well as volatile alkali species, with char even inhibits their releases to gas phase.

The adsorption, mentioned above, and repeated desorption on the char surface allow resultantly the released alkali species to transform into thermally stable char-boned one and/or non-volatiles such as K-silicates, that is an important eutectics responsible for the bed agglomeration of biomass (Eutectics; *a mixture of substances having a minimum melting point*). Part of formed silicate fragments may partially or entirely be solidified in the deposition on convective surface as coarse fly ash from the entrainment of flue gas. In addition silica/silicate particles both from fuel as fly ash [34] and from silica sand (quartz sand); commonly used as the bed material, can absorb alkali hence creating the eutectics on their surfaces by the fluxing reaction [51].

Alkali earth elements, Ca and Mg, are hardly volatilized over the conventional temperature ranges of thermal treatments [51,61]. Therefore they are released mainly in char combustion and in association with the oxide and sulfate (by sulfation) groups, as the fine solid particle [46,53,69]. In some combustion cases of biomass rich in organically bound calcium [22,71-73] or co-combustion [74,75], calcium can cause problems by that it is involved to form the eutectics, while magnesium seems to be relatively more inert in eutectic formation. Calcium is an important bulk component in ash deposits of fouling but it is mostly not responsible for the initiation of deposits.

Phosphorus [76], aluminum [27], iron [12] and silicon [34,69] are mainly associated in oxide, silicate or potassium associated compounds as the fine solid particle with relatively high melting point, over than bed operating temperatures. The noble metals as the trace element in biomass have insignificant influences on the bed agglomeration [24,51], and there are a number of intensive studies on their behaviors and environmental impacts during combustion with a number of biomass [77-81].

The release behaviors of biomass ash forming elements during thermal conversions are influenced significantly by the chemical properties of biomass and operating temperature. The physical state (vapor, gas, molten or solid) and species of released ash have a remarkable effect on the form of ash deposition and on the physical and chemical interactions between the ash constituents and specific surface, for example the convective tube bank in fouling, the furnace wall for slagging and the surface of bed particle in bed agglomeration. Only extensive interactions between the ash forming constituents and bed particle are emphasized.

2.3.2 Inorganic migrations

The deposition mechanism of the ash forming elements from the burning fuel particle to the surface of bed particle to form the deposits as coating can be typically illustrated in Figure 2.3, including partly in Figure 2.1 and 2.2, and summarized: viz,

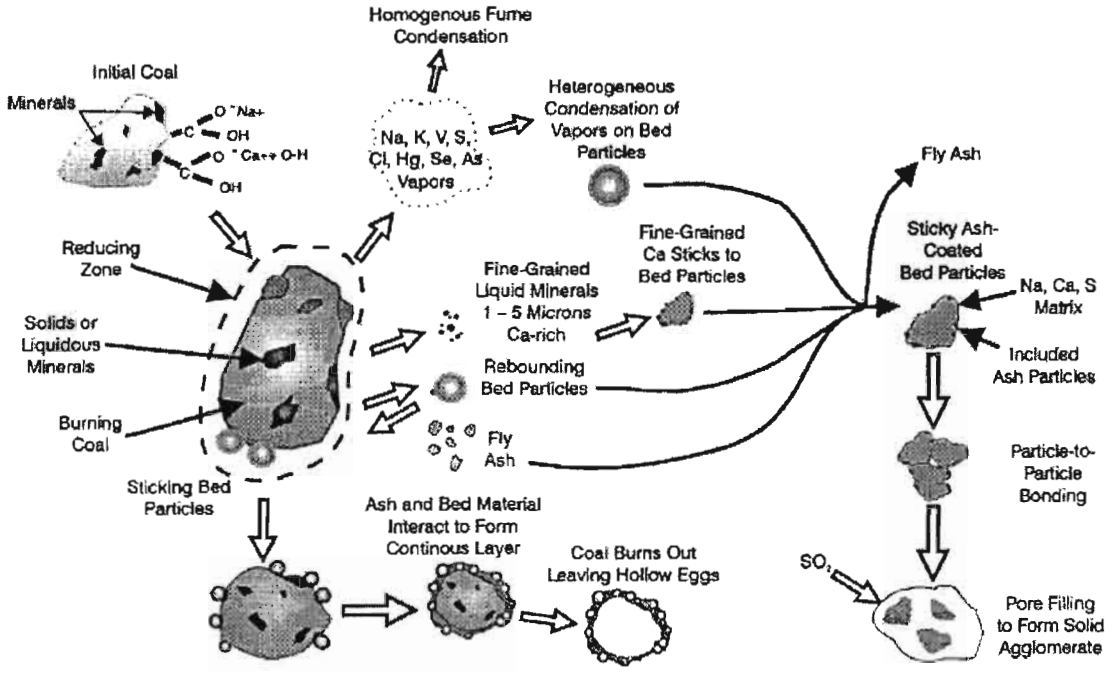

Figure 2.3 Mechanisms of ash-bed interaction [82].

1. Condensation

The submicron fly ash particles in size approximately between 0.02-0.8 μm had been identified in the elemental mass size distribution of K, S and Cl, of the ash matrix elements (Si, Ca, K, P, S and Cl), at downstream of cyclone during fluidized bed combustion of high alkali wood residues [69], and waste sludge mixtures [81]. This indicates that a certain part of the ash species is volatilized and these volatiles prefer nuclei condensation into submicron size as the homogeneous condensation, while the non volatile species remain mostly in the coarser particles (approximately 1-100 μm) [83]. Approximately half of gaseous KCl condenses into the aerosol particles, whereas the other half is found to condense on the coarser particle, or contact surface, as the heterogeneous condensation [69].

2. Adhesion

Aerosols that are originated from both non-volatile ash compounds (below 5 μm) and sublimed inorganic volatile compounds as freely fine particulate matter can be attached to bed particle surface, or relevant surface of constructions, via surface forces (the force that acts across an internal or external surface element in a material body) [84]. This attachment includes adhesion of the molten or solid ash on the surface of burning char particles with bed particle by the random collision, and the coagulation/fusion of coarse ash particles by sintering process.

Some certain compounds firstly formed or located in the proximity of the bed particle surface by above mechanisms can extend their transformation into the core of bed particle [28]. For instance [24,84], the possible decomposition of alkali sulfate in the

formed coating layer or diffusion of alkali compounds can be the source of free alkali metals that subsequently form the silicates extending inward the sand grain by the reaction with silicon of quart sand, as the sand particle residence time increases.

3. Chemical reaction

In some case, the gaseous inorganic species are absorbed on the surface of bed particle, or relevant silica/silicate particles of ash, by chemical reaction (chemisorption). The evidences of gas phase alkali reaction with silica sand have been revealed in a literature [85]. The chemical reactions of alkali with silica sand also include the decomposition of alkali sulfates, carbonates and chlorides by reaction with silicon of sand, forming K-silicates.

Building up the coating layer on bed particle, the ash forming elements released from the burning fuels migrates by the processes such as the condensation of volatile inorganic species, the adhesion by random collision of particulates either as freely or on the burning fuel surface, and chemical attack of gaseous ash species. The ash deposition on the bed particle is probably dominated by the combination of them. Subsequent chemical reactions within the coating layer or inward the bed particle may occur. As the continuous deposition on the bed particles proceeds under prolonged operation, the coating thickened up to certain critical conditions (e.g. viscosity or thickness) leads to the formation of permanent bonds between the bed grains, and then agglomerates are formed. The extensive particle bonding mechanisms are therefore mentioned as following, and the relevant sintering mechanisms to the bed agglomeration are focused.

2.3.3 Particle interactions

Interparticle forces (or intergranular force), well defined same as intermolecular forces [86], are the forces of attractions that exist between individual particles in a material. These cause the material to exist in a certain state of matter. Interparticle forces between particles can occur due to a variety of causes. In fluidized bed [87], they are mainly associated to van der Waals interaction, liquid bridge and sintering.

1. van der Waals forces

"van der Waals forces" is a collective term taken to include the dipole/dipole, dipole/non-polar and non-polar/non-polar (dispersion) bonding forces arising between atoms, ions or molecules [88]. As illustrated in Figure 2.4, they are defined for two spherical particles as;

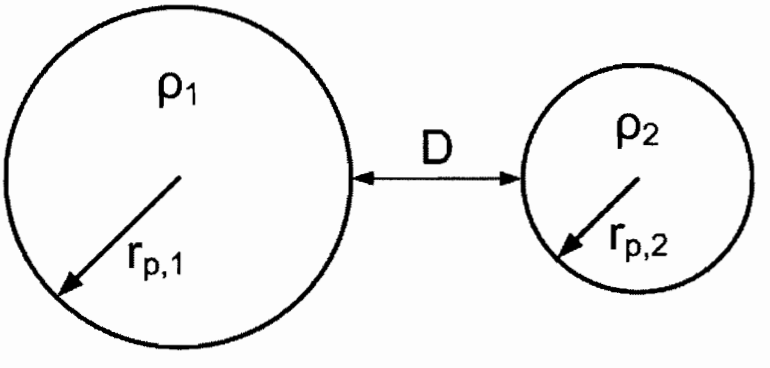

Figure 2.4 van der Waals interaction between two spheres [88].

$$F_{VW} = \frac{A}{6D}\frac{r_{p,1}.r_{p,2}}{(r_{p,1}+r_{p,2})} \qquad (2.1)$$

where A is the Hamaker constant (materials-dependent), r_p is particle radius and D is the surface separation between two particles, which takes a minimum value of the order of the intermolecular spacing. However, some confusion has risen between the expressions for intermolecular and interparticle van der Waals forces. To clarify, a previous study [88] showed the results that van der Waals forces increase in proportion to particle size, and are independent of it if asperity contact is assumed. They further revealed that the spherical particles with asperity contact in diameter of order 100 μm exhibit interparticle van der Waals forces to equal their single particle weight, while to much lesser for particles in diameter of order 1 mm. This is in accordance with common experience; dust particles of about 100 μm or below are commonly found adhering to all kinds of surface and resisting the gravity force, whereas particles of 1 mm or larger will only adhere to surface in the presence of some additional adhesives from the chemical reaction or sintering, for example.

2. Liquid bridges

If the surface of a particle has a film of mobile liquid at point of contact with other particles, or surfaces, liquid bridge will be formed, as shown in Figure 2.5. They are of practical importance in agglomeration processes, driers and in some types of reactors.

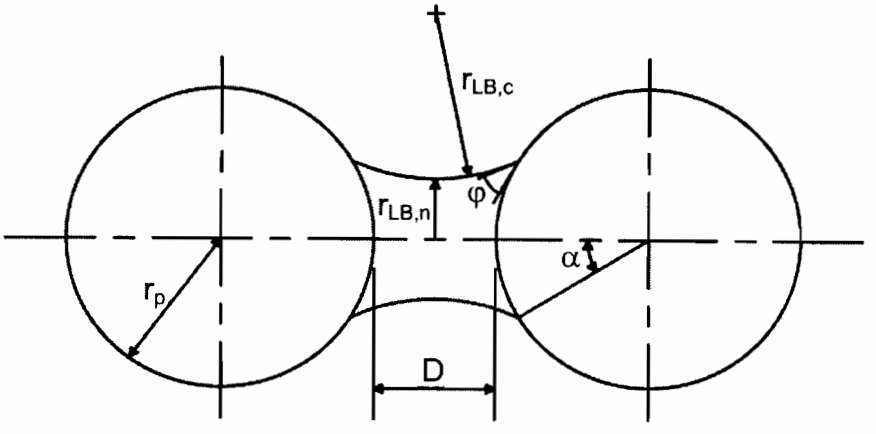

Figure 2.5 Liquid bridge between two equal spheres [88].

Liquid bridges are more complex than van der Waals forces in that they exhibit both static and dynamic forces, i.e. capillary and viscous forces, respectively, and are dissipative of energy [87]. Their magnitudes and forces can be varied by altering the amount of free liquid and its properties, particularly surface tension and viscosity. The static liquid bridge force (capillary force) arises from the sum of the surface tension force and the force arising from the pressure deficit in the liquid bridge.

$$F_{LB,S} = 2\pi r_{LB,n}\gamma + \pi r_{LB,n}^2 \Delta P \qquad (2.2)$$

where ΔP is the reduction of pressure within the bridge with respect to the surrounding pressure; γ is the surface tension. This reduced pressure is given by according to Laplace equation [89];

$$\Delta P = \gamma \left[\frac{1}{r_{LB,c}} - \frac{1}{r_{LB,n}} \right] \qquad (2.3)$$

The liquid bridges also dissipate energy by viscous force (dynamic liquid bridge force). This force always opposes to the relative movement, unlike the surface tension force, and it becomes appreciable if separation rates are high. The viscous force between two spheres being separated at a rate equal to the relative particle velocity can be determined, to a first approximation, by Reynolds' lubrication equation [90].

$$F_{LB,V} = 12\pi\mu_f r_p^2 V / D \qquad (2.4)$$

where μ is fluid dynamic viscosity, and V is particle-particle relative velocity. The comparison between capillary force and viscous force [88] indicated that viscous force can become significantly for separation rates (V) above approximately 1 cm s^{-1}, if particle separation (D) is small (around 2 μm). However, viscous force becomes comparable with capillary force for separation rates above 1 m s^{-1} at larger separation (above 10 μm) and increasing bridge angle (α).

3. Sintering

The forces arising from sintering are quite different in kind from two above mentioned mechanisms. Sintering is a time-dependent process in which material migrates, due to diffusion, viscous flow or combination of mechanism, to the region of contact to form a neck. That the bed particles are adhered to a sticky ash melt or bonded together by a molten ash layer, as a neck, on their surfaces is characteristic for the silicate and salt systems is described by this sintering mechanism.

In fluidized bed, sintering starts when a neck is formed between bed particles, resulting in the initially porous network in agglomerates. A sinter neck of sufficient size becomes permanent, resisting the breaking due to the movement of solids and gas, and eventually leads to defluidization. In general, the rate of adhesive material migration is a sensitive function of temperature [87]. In viscous sintering, the migration is driven by surface energy minimization (which is relatively independent of temperature) and opposed by viscosity (which is strong function to temperature) [87,91]. This indicates that sintering occurs much faster at higher temperature for high temperature sintering of ash in combustion and gasification. It may be noted that the effect of temperature on sintering is quite different from its effect on dynamic liquid bridge forces (viscous forces), where reduced viscosity by increasing temperature lead to decreasing forces (Eq. 2.4), decreasing energy disruption in collision and decreasing probabilities of agglomeration and growth (at which the fractional liquid loading remains constant).

In the previous studies on the sintering behaviors of ashes from coal, peat and biomass under FBC conditions [92-97], three mechanisms are considered to be significant viz;

- Partial melting
- Viscous flow
- Chemical reaction

They depend significantly on the ash chemical and mineralogical composition, the temperature history of the ash particles and gas components.

Partial melting sintering (Reactive liquid sintering or diffusion sintering)
It is a sintering in the presence of a reactive non-viscous liquid consisting of molten alkali salts, or other crystalline materials, where the solid phase is partly soluble in the liquid at the sintering temperature. The amount of liquid determines the neck formation. Decreasing temperature below their solidus temperatures (the temperature at which melting of a substance begins) gives crystallization of bonding agent and densification of agglomerates. It was suggested that this mechanism is likely predominant for fuels with high alkali, sulfur and chlorine ashes [51].

Viscous flow sintering (Viscous sintering or Vitrification)
It is sintering due to viscous flow of a vitreous silicate phase. When a silicate ash is heated above its solidus temperature, it becomes highly viscous liquid. Due to its high viscosity, the liquid remains viscous on rapid cooling below the solidus temperature [51]. The presence of silicate compounds in ash deposits on either bed particle or silicate/silica fly ash particle gives rise to the formation of the liquid layer of silicate eutectics on the surface of the particles under sintering temperature. Flowing of this viscous molten layer forms a neck between adjacent particles. Upon cooling, this neck is solidified to a glassy phase.

The dependence of this mechanism on properties of fly ash particle for typical fly ash agglomeration is given by Frenkel equation [98];

$$X^2 = \frac{3 \cdot r_p \cdot \gamma \cdot t}{2 \cdot \mu} \qquad (2.5)$$

where X^2 is equivalent neck contact area; γ is surface tension of the vitreous phase and t is time. Neck growth (X(t)) is controlled by time and viscosity, which is varied significantly with temperature and chemical composition of material. Sintering is inhibited by the crystallization on the surface [51].

Chemical reaction sintering
This is a sintering due to reaction between the particles or the particles and the gas, to form a third compound binding the particles together. This mechanism was found to be responsible for the sintering of coal and biomass ashes rich in calcium [23,50]. It is caused by the carbonation and sulfation of CaO with CO_2 and SO_2, respectively, resulting in the particle to particle bonding via thermodynamically stable $CaCO_3$ and $CaSO_4$ crystals, respectively. These mechanisms can be relevant to the deposit hardening and bond strengthening, where ash is firstly formed on/between particles and then reacts in the post combustion zone in CO_2/SO_2 rich environment. Sulfation of CaO is stable over a wider temperature range (carbonation: 600-800 °C, sulfation: above 500 °C). Calcium sulfate bonding was mentioned to be important in a deposit hardening mechanism when firing coals rich in organically bound calcium and sulfur or when adding finely ground limestone for sulfur capture [23,34]. Submicron CaO particles deposit on the surface via thermophoresis (the migration of a particle in response to a macroscopic temperature gradient) and then become sulfate by the reaction with SO_2 or SO_3. Locally low oxygen partial pressure can additionally give rise to the formation of $CaSO_4$/CaS eutectic (eutectic point 830 °C) [34].

2.3.4 Summary of mechanistic bed agglomeration

A summary of the mechanistic bed agglomeration processes including sub processes has been provided in the state-of-art [99] and pictorially illustrated only for the bed particle agglomeration in Figure 2.6.

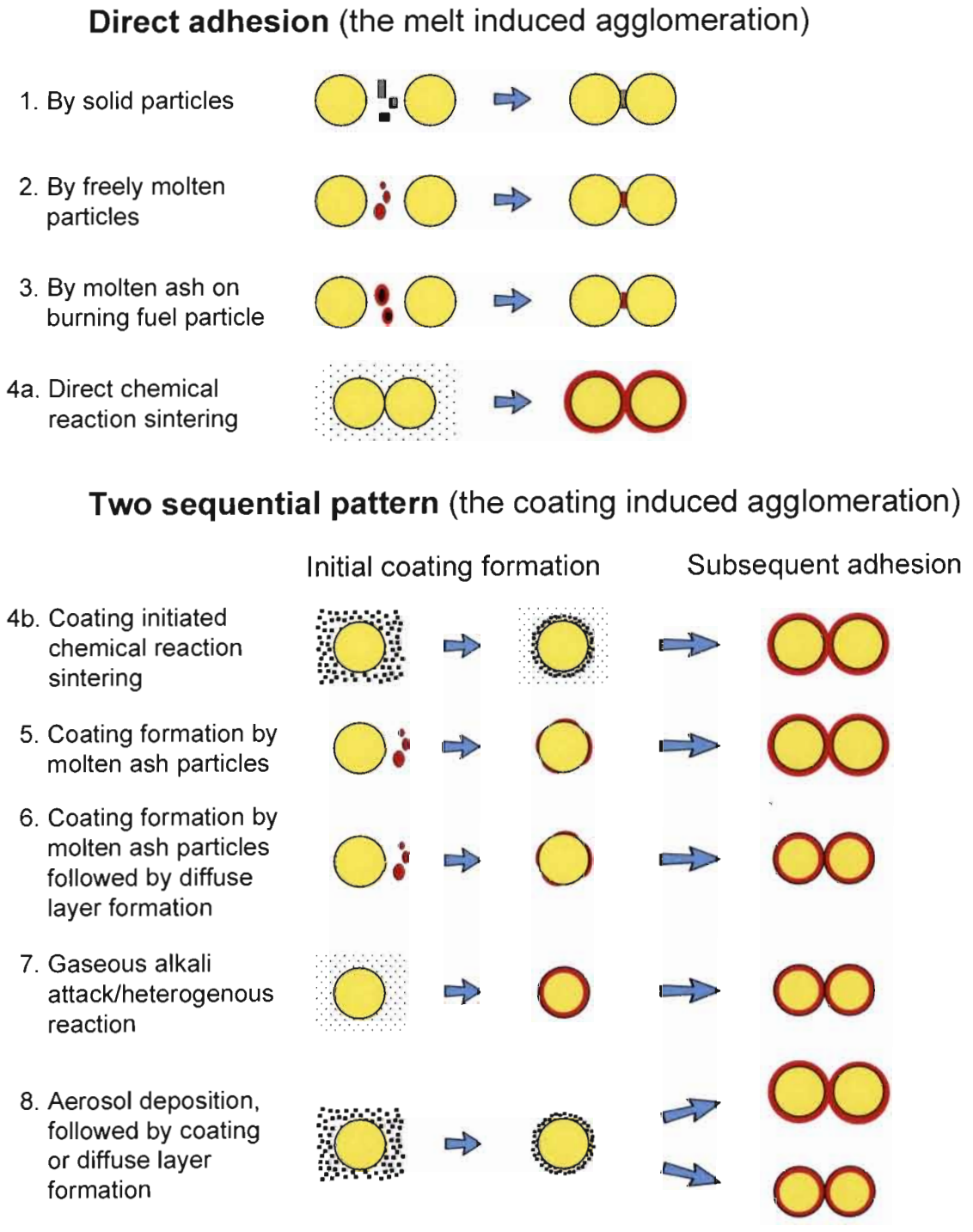

Figure 2.6 A summary of the different proposed bed agglomeration mechanisms [99].

The mechanisms can be divided into two main categories;

- Direct adhesion, as described in 1-4a
- Two sequential pattern initiated by the coating formation, as described in 4b-8.

The formation of coating layer can be initiated by: chemical reaction sintering; molten ash particle; chemical reaction with gas phase alkali species; and deposition of particulate matter followed by either coating formation or chemical reaction with bed particle. The molten ash fraction can be released in the form of the freely molten particle and the molten layer on fuel particle.

The two sequential processes, specifically named the coating induced agglomeration [72], including the direct chemical reaction sintering (4a) have been suggested to be dominating in the presently mechanistic bed agglomeration. Direct adhesion by the molten ash as freely and on burning fuel particle, dubbed as the melt induced agglomeration, have also been suggested and seem less likely, while the direct adhesion by solid ash particle is seemed unlikely.

Although the differently suggested mechanisms and sub processes (Fig. 2.6) may be dominating to bed agglomeration for different fuels and operating conditions, the molten phase formation seems to initiate the bed agglomeration and the coating induced agglomeration is likely dominating mechanism, particularly for biomass fuels. The formation of low melting point ash consisting mainly of alkali salts or alkali silicates is significantly dependent upon the ash chemistry and temperature. The gas phase reaction and/or aerosol deposition seem to be further important in some biomass for enhancing the melt formation and accelerating the defluidization [51,85].

2.4 Influence factors on bed agglomeration

2.4.1 Ash chemistry

It shows clearly that the ash chemistry plays an important role, as largely described in section 2.2. The most undesirable inorganic elements in biomass are alkalis in combination with sulfur, chlorine, phosphorus and silicon. Calcium causes problem in some cases of combustion of a fuel with a rich in organically bound calcium, or co-combustion of these fuels with a high sulfur fuel. The bed agglomeration is found to be a strong function of the level of these elements in fuel [19,69,82,100]. The large amount of these elements by either inherence in fuel, impregnation by additive impletion or fuel treatments can facilitate the bed agglomeration [20,24,101-102]. A high amount of volatile potassium in biomass also enhances the formation of melts due to the chemical reaction. Chlorine facilitates bed agglomeration due to the low melting point of chlorides and further provides the chemical reaction to form the eutectics. The same tread goes for sulfur. Sulfates originated from the reaction of alkali with SO_2 have very low vapor pressure and easily condense on surface, such as bed particles, to form the liquid layer. Both silica/silicate particles which absorb alkalis forming the low melting point compounds as coating layer and even originally released silicate particles are capable to sintering.

2.4.2 Bed material

The chemical reactions between bed material and ash are also an effect. It becomes clear from presently reviewed literatures that silica sand, commonly used, is not a suitable bed material in FBC and FBG of high alkali fuels, due to further formation of

eutectics on its surface by the chemical reaction of silica with alkali. Alumina sand does not react with the ash and make possible higher bed operating temperatures [27,103]. Pure hematite is reported as the most suitable bed material in combustion of high alkali biomass [104]. Dolomite and limestone seem to be also unsuitable [105] and limestone as bed materials shows a high tendency to bed agglomeration [19]. The extensive reviews of different bed material as a practical prevention option of bed agglomeration will be mentioned later.

2.4.3 Fluidization condition

Defluidization by bed agglomeration is widely accepted as a result of competition between the strengthening adhesion of bed particles by the molten ash formation and sintering process, and the breaking of agglomerates due to mechanical forces of collision induced by the fluidization [82]. The movement of bed particles is also important because of the corresponding transfer of heat, and it is significantly dependent upon the bed operating condition. An ineffective/obstructed bed particle movement can easily lead to local bed temperature derivations, resulting in a further and potentially self-enforcing obstruction of particle movement and subsequent hot spots in bed, that promote the local bed sintering. This is a good reason why the bed operating variables have an important role in the bed agglomeration process.

The contributions of the bed operating variables on the tendency of bed agglomeration have been studied in the controlled fluidized bed reactors and described in term of the agglomeration temperature (T_{ag}) [106-108] and the defluidization time (t_{def}) [108-111]. The temperature at the start of defluidization during an increase or step up of fluidized bed temperature by either external heat sources or conditions, in which a certain amount of ash is early contained in bed by combustion or gasification at a given ashing temperature, is termed the agglomeration temperature. The definitions of the defluidization time are variable. The time between the commencement of segregation-defluidization and agglomeration can be termed, and is normally represent the time available to restore the operating conditions, such that agglomeration is prevented [108]. The time interval between the start of fuel conversion processes and the complete defluidization is also termed. The contributions of operating variables can be summarized in Table 2.6.

Table 2.6 Contribution of operating variables to bed agglomeration tendency

Contribution	**Tendency; represented by**	
	T_{ag} (or T_S)	**t_{def}**
Temperature	- (Ashing)	+ (Combustion)
Heating rate	0	N.T.
Fluidizing air velocity	-	-
Bed particle size	+	+ and -
Fuel particle size	-	0
Static bed	+	N.T.
Ambient condition (Air to fuel ratio)	0	0

where the defludization by bed agglomeration is accelerated by an increased magnitude of a variable is described by the plus (+), the opposite trend is referred to the minus (-), 0 is a sign of unobtrusively effect and N.T. is no experimental investigation. The higher

tendency implied by lower bed agglomeration temperature and shorter defluidization time can be caused by lower ashing temperature, higher combustion temperature and lower fluidizing air velocity, for example. The major differences between combustion and gasification of fuel with high sulfur are that sulfates do not form in gasification and the much higher fuel particle temperature is in combustion. Sulfation, as well as carbonation, can facilitate the bed agglomeration. The air to fuel ratio which represents the effect of these ambient atmospheres, however, does not show clearly an influence.

The tendency for the colliding particles to stick together or the agglomerates to break apart is directly proportional to the particle adhesive properties and to the area of contact, and inversely proportional to particle momentum [15]. The formers are affected substantially by the chemistry and physic of particle, while the later is reflected to the bed hydrodynamics of fluidization.

2.5 Laboratory prediction

A number of laboratory methods are performed in order to assess the slagging, fouling and agglomeration propensity of a fuel. Some methods show low accuracy in their predictability and some give unclear support in the prediction, while some are not ever used to predict the bed agglomeration. They suffer from the fact that ash produced in laboratory is different substantially from actual ash generated in FBC and FBG. It is due to many influence factors in ash formation that can not be adequately simulated in the laboratory. These respect importantly to the ash partitioning, gas-solid reaction, and absorption and condensation of vapor alkalis. The predictive value of below mentioned laboratory methods is therefore hard to access.

2.5.1 Fuel analyses

Indices derived from the ash chemical composition

Several defined empirical indices are used commonly to assess the propensity of fireside ash-related problems during combustion of coal and biomass. They are formulated by only using the basic ash chemical composition derived from the standard methods of ash analyses. They include, for instance, Alkali index (AI) [112], Base-to-Acid ratio ($R_{b/a}$) [113] and Bed agglomeration index (BAI) [105]. These indices have correlated the ash composition to predict the standard deformation and fusion temperatures of coal ashes [114].

$$AI = \frac{kg(K_2O + Na_2O)}{GJ} \tag{2.6}$$

$$R_{b/a} = \frac{\%(Fe_2O_3 + CaO + MgO + K_2O + Na_2O)}{\%(SiO_2 + TiO_2 + Al_2O_3)} \tag{2.7}$$

$$BAI = \frac{\%Fe_2O_3}{\%(K_2O + Na_2O)} \tag{2.8}$$

Alkali index expresses the quantity of alkali oxides in the fuel per unit of fuel energy. The maximum alkali input, in kg/GJ, into the boiler is divided into: 0-0.17 does not give problems, 0.17-0.34 become problematic and need to frequent outages and lower furnace exit temperature, while >0.34 give certain to unmanageable problems. The label

for each compound in Base-to-acid ratio and Bed agglomeration index makes reference to its weight concentration in the ash. Of the fuel ash, the increasing $R_{b/a}$ values indicates the increasing fouling tendency while the decreasing BAI represents the increasing bed agglomeration problem. These indices are fuel specific and can not definitely take the effects of the boiler operating parameters and the complex behaviors of inorganic elements during conversion into consideration. Nevertheless, they can be the approximately secure basis for decision making.

Ash thermal behaviors based on chemical fractionation with TPEC

Based on the chemical fractionation analysis in section 2.2.2, the ash forming elements are divided into two parts, "a mobile part" and "an immobile part" [24]. The mobile part consisting of water and ammonium acetate leachable elements are supposedly in the form of volatile and submicron aerosol during heat treatments, while the immobile part comprising of acid leachable and residue elements are present as the coarse ash found in bed. Their individual contents of mobile and immobile parts give more information about the propensity of fouling and bed agglomeration, respectively, than total content. These chemical fractionation data are then used to establish the ash melting behaviors, as a function of temperature, based on the thermodynamic multi-component, multi-phase equilibrium calculations (TPEC) [24]. This procedure is based on Gibbs' free energy minimization on the database of elements and chemical reactions. The estimated initial melting temperatures of these melt profiles are marked and then verified with the agglomeration temperatures from actual fluidized bed experiments [115,116] and the evaluated melting temperatures based on SEM-EDS + phase diagram analyses of coating/neck materials in agglomerates [24]. Their predictability shows fairly in accuracy. It was further revealed that the chemical fractionation analysis can yield 5-15% higher total alkali concentrations than the analysis of ash prepared at 600 °C [51].

TPEC method is useful to enhance understanding of the complex ash behaviors. However, TPEC's small imperfection is thermodynamically based calculation procedure that assumes the system to be in equilibriums, while the real process may not reach [51] and, importantly, the better quality of database in chemistry and thermodynamics is required for the higher accuracy of prediction.

Agglomeration and deposition problems are sometimes reported even though the fuel analyses indicate an unproblematic fuel [51]. It may be that the fuel quality varies beyond what is indicated by even frequent fuel analyses. Therefore, the homogenization of the feedstock is needed and may be worthwhile in order to limit the risk of frequent agglomeration and deposition problems due to such fluctuation in fuel quality.

2.5.2 Static methods

The methods below are the conventional and developed laboratory procedures based on analyzing the laboratory ash in order to characterize the ash thermal behaviors.

ASTM standard ash fusion test

Standard ash fusion temperatures are determined according to ASTM-D1857. This well-known method is developed to access the slagging propensity of coal and coke in stoker type boilers. It is based on visual observation on the deformation of an ash cone during heat treatment. The characteristic temperatures include Initial deformation temperature (IDT), Softening temperature (ST), Hemispherical temperature (HT) and Fluid temperature (FT). However, bed agglomeration problems sill occur despite the

relatively low temperature in fluidized bed during conversion below the ASTM initial ash deformation temperature. The ashes substantially melt at 200-400 °C below the visually determined initial deformation temperature [117]. The melting process is not the shape phenomena, but the gradual process [114]. The characteristic temperatures of this method are affected by the size and geometry of ash cone, fineness of ash, heating rate and atmosphere.

Simultaneous thermal analysis (STA; TGA-DTA and TGA-DSC)
TGA, DTA and DSC are termed as Thermo gravimetric analysis, Differential thermal analysis and Differential scanning calorimetry, respectively. These methods are conventional analyses to study the ash thermal behaviors, such as the melting and volatilization behaviors of ashes, or to study in advanced applications such as characterizing the sorbents for alkali capture and the reactions between bed materials and alkali salts [118]. They are based on the simultaneous measurement of heat effects in ash samples (endothermic or exothermic processes) and weight loss. These methods can be useful to determine the initial melting temperature and to estimate the volatilization of elements. However, interpretation of the results without the knowledge of mineralogical composition of ash is a very difficult task due to many processes that can occur simultaneously in ash (decomposition, volatilization, evaporation, melting, and reaction with gas) and many disturbing effects (the combustion of residual carbon, absorption of gases and reaction of artefacts from low temperature ashing) [51]. Therefore, these methods do not clearly support the bed agglomeration.

Thermo-mechanical analysis (TMA, or shrinkage method)
This method is based on the measurement of volume changes and softening of ash samples during heat treatments to determine the sintering tendency, initial melting temperature and initial sintering temperature. It has been used to identify the initial sintering temperature of spent bed material and found well correlation between this temperature and temperature where agglomeration started in circulating fluidized bed (CFB) combustion of high sodium low rank coals [119]. The initial sintering temperature from TMA is the same as temperature where melting started in TGA-DTA, so that partial melting is probably the sintering mechanism, however it is substantially less than the ASTM initial deformation temperature. Additionally, the sintering rate of ash has been correlated to the decreasing rate of pressure drop across an ash pellet sample in a tube like holder for some certain time during heat treatments. The sintering changes the porosity of ash pellet by shrinkage [120-121]. This method has been applied for coal ashes only. The dilatometer is a scientific instrument that also employs this method.

Compressive strength measurement
This laboratory method is applied for determining the sintering tendency of ashes based on the compressive strength test on heat-treated ash pellets. The pellets of laboratory ash samples including the mix of ash with bed materials or additives [34,93-94,122] are heat treated at given temperatures and conditions. After cooling the crushing strength of pellets is measured. The temperature of treatments which the corresponding crushing strength deviates from the base line strength is then referred to the initial sintering temperature. This method is very useful for revealing the mechanism behind agglomeration and comparing different fuels for their sintering and agglomeration propensity, but it does not give absolute initial agglomeration temperature due to many other important factors beside ash chemistry.

High temperature light microscope (HTLM)
This advanced practical method is used to evaluate the melting quantification of biomass ash on the basic of the change in light transparency during melting [123]. As a part of the ash is molten, it becomes transparent. The transparency change on the plate area of spread ash is detected by the advanced image analyses and then converted to the melt fraction, relative to the area fraction. This method detects the onset of melting of ash samples significantly lower than STA and fusion test [124]. HTLM method is used to study the characteristics of ash fusion and deposit formation, but it is not ever applied to predict the bed agglomeration.

Heat treatment and subsequent SEM analysis
The common heat treatment of mixtures of ashes and bed materials is used to study their agglomeration characteristics in associate with Scanning electron microscope (SEM) [21,27,125-126]. The agglomeration temperatures determined correspond very well with experience in lab scale FBG [21,27]. This test can be used to obtain a first indication and comparison of the agglomeration propensities of the mixture of bed material and ash, but it does not give the absolute results of initial agglomeration temperature, again due to many other important factors beside ash chemistry.

Flow properties heat treated ash
A method is developed to evaluate the agglomeration propensity of ash from petroleum coke, based on the hot angels of repose and internal friction [127]. When desired temperature in a vertical stainless steel cylindrical heater is reached, the ash is allowed to flow from the cylinder through a small hole in the bottom. The repose and internal friction angel are then taken as an indication of the flow ease of ash at a given temperature. These results have been compared to the results from compressive strength method and SEM analysis of deposit from full-scale FBC to determine the sintering mechanisms. This allows determination of the ash agglomeration mechanism.

As mentioned, the ash prepared in laboratory by standard methods can not be representative in the attributes of actual ash formed in fluidized bed. Ashing temperature above 600 °C generally specified in the standard methods gives significant loss of alkali, artificially increasing the fusion temperature [51,53]. Although a study on ash behaviors has used ashing procedure at 350 °C [53], the low temperature ashing with long oxidation times gives rise to the formation of artifacts from organically bound inorganic elements which are not normally found in conventional biomass ash; e.g. potassium nitrate and perchlorates [34].

2.5.3 Dynamic methods

By the above reasons, the test in the controlled laboratory scale fluidized bed facilities seems to be the best laboratory method for the characterization and prediction of the bed agglomeration. From literatures, there are four methodologies to determine the tendency of bed agglomeration during FBC and FBG, which is reported in Table 2.6. The onset of defluidization and bed agglomeration is mainly detected by bed pressure monitoring.

- A certain amount of biomass is combusted at a fixed temperature (ashing), subsequently the biomass feeding is stopped and the bed temperature is increases by the external heat sources until the agglomeration occurs (sudden drop in pressure and sudden change in temperature) [22,106-107,128]. Bed agglomeration temperature, T_{ag}, is then recorded.

- Biomass is gasified in the bed at a fixed temperature for a certain time while the fuel feed rate and airflow are kept constantly. Subsequently the bed temperature is raised stepwise at certain temperature interval and time by the external heat sources until agglomeration occurs [51], and T_{ag}, is then recorded.
- A fixed amount of biomass is combusted batchwise at a constant temperature with the bed containing a fixed weight of bed material. After the fuel batch is depleted eventually, the test ends, the spent bed is then discharged and the reactor is emptied. A new experiment is then carried with the fresh bed material at a stepwise higher temperature. These procedures are repeated until the sign of defluidization is observed [51], and T_{ag}, is then recorded.
- At fixed operating conditions (temperature, airflow, bed particles size, mass of bed material, air to fuel ratio, etc), the steady state combustion of biomass is carried out until the signs of beginning defluidization are observed or complete defluidization is reached [109-111]. Defluidization time, t_{def}, is then recorded.

All above laboratory methods, mentioned in this section, for the prediction of bed agglomeration and their predictabilities are then summarized in Table 2.7.

Table 2.7 Summary of the laboratory prediction methods

Method	Method description	Predictability	Reference
Fuel analysis			
Indices	Chemical compositions of biomass ashes are determined by standard methods and then are correlated into the empirical indices.	- It is used mainly as the criteria for decision making	[34,72,112-113]
Chemical fractionation with TPEC	Increasingly aggressive solvents leach the same sample in a series of three sequential leaching, producing four samples for characterization. TPEC is used to estimate the ash behavior by which the leached compositions are the input data.	- Predictability is moderate.	[24,47,115-116]
Static methods			
ASTM standard ash fusion test	Four characteristic temperatures are identified according to standardized description (Visual observation of ash cone during heat treatment in electrical furnace).	- It predicts too high agglomeration temperature and the predicted trends are false as well.	[34,46,50,114]
STA	The heat effects and the weight loss of the ash samples are measured simultaneously. Detectable processes are melting, decomposition and chemical reactions.	- The STA measurements do not clearly support the melt formation and the bed agglomeration.	[50-51,118,124]
TMA	The change in volume or length of a pulverized ash sample pellet is measured during heating. Shrinkage indicates sintering or melting.	- This method is superior to the ash fusion test and shows fairly well agreements in the prediction for coal ashes.	[102,119-121]
Compressive strength	The ash sample is pulverized and palletized to the cylindrical pellet and then heated in a control condition. After cooling, the ash pellets are crushed in standard compression-testing equipment and the compressive strength is taken as a measure of the degree of sintering.	- This test is good for predicting the agglomeration trends except for the case at which interaction between ash and bed material takes place. - It is very useful to reveal the mechanism behind agglomeration.	[34,92-93,122]
HTLM	The ash sample spread over the flat plate is heated at a specific condition. The melted fraction is relative to the area fraction that becomes transparent.	- To ever compare the onset of melting temperature with STA and standard fusion test, but not used to predict the bed agglomeration temperature.	[123-124]

Table 2.7 Summary of the laboratory prediction methods (Continue)

Method	Model description	Predictability	References
Heat treatment and subsequent SEM analysis	Mixtures of ashes and bed materials are heated in an oven for a certain condition and period. The heat treated ash samples are then analyzed chemically and morphologically by SEM.	- Not used to predict bed agglomeration temperature. - Good to reveal the mechanisms behind agglomeration/sintering.	[21,27,125-126]
Flow properties heat treated ash	Ash is heat treated in vertical cylinder. When desired temperature is reached, the ash is flowed to the small hole at bottom. The repose and internal friction angels are measured as an indication of the flow ease of ash.	- No temperature is predicted and the predictability of this method is not very promising.	[127]
Dynamic methods			
Bubbling Fluidized bed combustion facilities	Combust a certain amount of fuel at a fixed temperature (ashing) and subsequently stop fuel feeding and rise the bed temperature externally until bed defluidization occurs, referring to the bed agglomeration temperature.	- This method includes interactions between ash and bed materials. - Bed agglomeration temperature is determined.	[22,106-107,128]
Bubbling Fluidized bed gasification facilities	Biomass is converted to ash at low bed temperature in gasification. Subsequently bed temperature is raised stepwise by external heater until bed defluidization occurs. The fuel feed rate and air flow rate are kept constantly.	- This method includes interactions between ash and bed materials. - Bed agglomeration temperature is determined.	[51]
Bubbling Fluidized bed combustion facilities	A fixed amount of fuel is combusted in a fixed mass of bed material at a constant temperature. After fuel batch is depleted, the bed is discharged and the reactor is emptied. A new experiment is then carried with the fresh bed material at a stepwise higher temperature. The procedures are repeated until sign of bed agglomeration is observed.	- Bed agglomeration temperature is determined.	[51]
Bubbling Fluidized bed combustion facilities	Steady state combustion at constant bed condition (air velocity and bed temperature) is proceeded until eventually bed is defluidized.	- Defluidization time and fuel consumption are determined.	[109-111]

2.6 Bed diagnostic tool

The conventional monitoring in thermal based fluidized bed applications or otherwise is principally based on the bed pressure, either local or different, and temperature measurements. In normal operation, bed pressure drop which directly related to the mass of bed can be described by the balance between the net gravitational force and the friction force exerted by fluid, as mentioned in Chapter 1, while in abnormal condition of bed during agglomeration, the adhesive force between bed particles is taken into consideration in the above force balance [18]. The isothermal condition inside fluidized bed is due to the intense in-bed heat transfer as a consequence of turbulent bed mixing. It seems clearly that the bed pressure indicates the better perception to any abnormal bed conditions [82,129]. An analysis method developed uses the short term predictability of time series of local bed pressure fluctuations to detect early changes in the hydrodynamic states of bed, named EARS (Early Agglomeration Recognition System) [130-131]. The incipient bed particle agglomeration causes changes in the hydrodynamics. This analysis gives the time period between the detection of a significant change in the hydrodynamics and the moment when the bed is defluidized, sufficiently large to take preventive measures, i.e. increasing gas velocity. This method has been further evaluated into the industrial scale fluidized bed boilers [132].

2.7 Measures for prevention

Some measures to prevent or delay bed agglomeration, and other ash-related problems, for an existing installation include viz:

- Alternative bed material,
- Chemical additive,
- Co-firing, with coal or forest wood residue,
- Fuel pre-treatment,
- Fluidized bed operation control,
- Bed management,
- Other measures

2.7.1 Alternative bed material

According to section 2.4.2, a number of alternative bed materials have been studied their bed agglomeration characteristics to serve as a practical option of the bed agglomeration prevention. Some less Si and Si free bed materials show inapplicable or the promotion on bed agglomeration, while many can reduce evidently the bed agglomeration problems. They include alumina, granite, gabbro, corundum, mullite, hematite ore, pure hematite, feldspar, magnesite, dolomite, limestone, bauxite, calcined sillimanite, calcite, ceramsite, GR GRANULE, lignite ash with high Al_2O_3 content, pure CaO, $CaSO_4$ and $CaCO_3$, blast-furnace slag and patented AGGLOSTOP^{TM} [19,25-28,51,73,100,103-105, 122,133-136].

The Al species bed materials for instance alumina, bauxite, corundum and ceramsite (a clay mineral rich in Al_2O_3) delay evidently the bed agglomeration since they do not interact chemically with biomass ash to further form the eutectic compounds. However, the coatings of silicate compounds on the surface of bed particles, as an evidence of the ash deposition, is still existed in the previous illustrative results [27,103], and possibly leads to defluidization. The lignite ash with high Al_2O_3 content is also inert to bed agglomeration. The use of alumina and mullite (aluminosilicates clay) in stead of silica sand has once been found that it does not change the agglomeration temperature [51].

The Fe species bed materials as hematite ore, pure hematite and blast-furnace slag show the potential mechanism of prevention. If sufficient Fe_2O_3 is present in the bed material, or otherwise in the ash of residues burnt, the agglomeration rate may be reduced since Fe_2O_3 may react preferentially with the alkali and present in bed as the fine particle of the eutectic mixtures with relatively high melting temperatures, in occasionally excess of 1135 °C [104-105].

The different effects of alkali earth based bed materials, such as magnesite, dolomite and limestone, on bed agglomeration are reported, but they are all unsuitable to be the bed particle [105]. Their high attrition rates which are several times higher than that of silica sand do not make possible to maintain sufficient bed inventory. Limestone particle show a high tendency to agglomeration due to a decrease of ash deformation temperature [114], while dolomite can extends the operation by several hours, due to the formation of high melting point Mg rich mineral phase in ash.

As mentioned above, the bed agglomeration is determined by the two competitive processes i.e. physical and chemical. Although the uses of different bed materials in stead of silica sand can inhibit efficiently the chemical reaction of ash with bed material, the physical transformations of ash (condensation or melt adhesion) are an influence and become dominating the bed agglomeration process. FBC or FBG with some bed materials is still eventually ended at defludization, or even increase other ash related problems.

2.7.2 Chemical Additive

The identified mechanisms of additives to reduce or delay bed agglomeration in FBC and FBG are revealed viz [51];

- Physical absorption: the molten phases are absorbed within porosity of additive particles.
- Chemical absorption: the problematic elements are absorbed chemically into the stable compounds with high melting point. This effect includes the absorption of the molten phases, fixation of volatile alkali species and the removal of sulfur prior to reaction with ash to form the compounds with low melting points.
- Powdering: the additives generate the molten phases which act less sticky to surface of bed and ash particles in order to reduce the rate of bed agglomeration.

The additives that at least in some cases offer the above positive effects are listed in Table 2.8, including the principal components.

Table 2.8 List of additives preventing bed agglomeration

Effect	Additive	Principal component	Reference
Physical absorption	Gibbsite	$Al(OH)_3$	[51,137]
	Calcined dolomite	CaO.MgO	[138]
	Sintered magnesite and Periclase	MgO	[51]
	Calcined alumina	Al_2O_3	[139]
Chemical absorption	Coal ash	Fe, Ca rich	[51,134]
	Aluminosilicates (Clay minerals)	$Al_xSI_yO_z$ (Al_2SiO_5 for Sillimanite)	[51,119,137]
	Bauxite	Rich Al_2O_3 + less SiO_2	[25]
	Kaolinite,Kaolin	$Al_2O_3.(SiO_2)_2.(H_2O)_2$	[82,137-138,140]
	Dolomite	$CaMg(CO_3)_2$	[51,137-139]
	Emathlite		[141]
	Diatomaceous earth (Diatomite)	SiO_2	[142]
	Limestone, Calcite	$CaCO_3$	[25,138]
	Magnesite	$MgCO_3$	[25]
Powdering	Coal fly ash	Ca, Mg rich	[139]
	Dolomite	$CaMg(CO_3)_2$	[143]
	Aluminosilicates	$Al_xSI_yO_z$	[51,140]
	Pure magnesium oxide	MgO	[114]
	Pure calcium oxide and carbonate	CaO, $CaCO_3$	[114]
	Calcined dolomite	CaO.MgO	[51]

It has been suggested that bauxite, kaolinite, kaolin (the rock that is rich in kaolinite) and emathlite (a rich Al additive) are promising alkali vapor sorbents. Aluminosilicates as clay minerals including kaolin seem to be preferable for the reaction with the molten phases. Gibbsite and porous calcined alumina reduce the available melt by soaking the molten species. Limestone and dolomite are the common commercial sulfur capture additives. Noticeably, dolomite can further affect the combustion of some biomass to form Ca-Mg rich layers with high melting points and these layers protect the bed particles from agglomeration [143]. In contrary, limestone can have the adverse effects in that it facilitate the bed agglomeration and increase problems of fouling and erosion in biomass fired fluidized beds by decreasing the ash deformation temperature [114]. The use of additive to reduce the bed agglomeration problem is considered primarily a selective prevention method since it is a conventional chemical treatment for FBC and FBG of coal and biomass [11-12].

2.7.3 Co-firing

Co-firing to achieve a higher ash melting temperature or lower alkali input into the system is to blend a problematic biomass with coal, forest wood residue or waste sludge. It includes co-combustion and co-gasification. This prevention method is considered as a good alternative to using additives. The mechanism primarily considered to be responsible for the positive effect of co-firing is that a major part of alkali from biomass is bound chemically into the high melting compounds found in co-fuels, such as aluminum silicates, magnesium aluminum silicates or iron species of coal and wood [12,113,144]. In addition, the low content of alkali and chlorine in coal gives the dilution effect so that the volatile alkali and chloride species may not condense due to resultantly very low vapor pressure.

The general criteria for the pairing of biomass-biomass, biomass-coal or biomass-waste fuel (sludge) in co-firing are given below [51],

- Co-firing of fuels having alkali and high chlorine concentrations should be avoided. Chlorine causes the high mobility of alkali during fuel conversions.
- Co-firing of fuels rich in KCl and high sulfur (some coals) should be avoided. Sulfation of KCl in gas or molten phase is the main reason.
- Co-firing of high alkali and high silica fuels should be avoided. The alternative bed material (not silica) is preferred as an optional solution.
- Co-firing of high alkali fuels with high magnesium or iron fuels should be considered.

The examples of successful co-firing experiences include; (i) the combustion of lucerne-coal and olive flesh-coal provided the stable operation possible for entire duration of experiments (10 hrs), instead of less than 30 min for their own biomass combustion [144]. Blending these fuels with coal also increased significantly their initial bed agglomeration temperatures, and further obtained 80% of sulfur retention in the bottom ash; (ii) Wood and rice straw were blended during combustion and this mixed fuel could delay bed defluidization by at least 50% fraction of wood [113]; (iii) The bed agglomeration risk seemed low, indicated by the increase of bed agglomeration temperatures, when straw was co-combusted with sewage sludge [51].

The ash characteristics of biomass and co-fuels, as another biomass, wood, coal or waste sludge, indicate a first sign for co-firing that cause more or less trouble than either of biomass used separately. The thermal behaviors of mixed ash analyzed by laboratory methods may provide the further possibilities of co-firing. However, the possible and appropriate combination of biomass with co-fuels needs further intensive experimental investigations in fluidized bed furnaces.

2.7.4 Fuel pre-treatment

The removal of problematic inorganic materials described largely in section 2.2.2 is an effective option of prevention [51,58]. The different inorganic materials provide the different effects on fluidization. Too large fraction of coarse particle impacts negatively to the quality of fluidization. The inert extraneous discrete particles such as soil, sand, pebble, pieces of iron or tramp materials, including coarse char particles under slow reaction conditions, can accumulate in bed to a concentration that limits the local bed circulation and subsequent heat transport and eventually destabilize the fluidization properties. Such destabilization easily leads to hot spots in bed that promotes the local sintering due to the obstructed heat transport. The major part of the whole bed may be involved in this irreversible process within a short time. These extraneous particles can also have the participation in sintering [51]. Mechanical breaking, crushing, washing, sieving, magnetic separation or fluid dynamic separation may be the solutions of separating out of fuel and bed material. The attached sand and soil can be removed more easily by sieving, if fuel is dry.

The inherent inorganic material being the main cause of bed agglomeration can be extracted out of biomass by leaching [24,45,58]. The biomass fuels leached by hot water show clearly the less problem of bed agglomeration, while the extensive bed agglomeration is observed for the untreated biomass [71,145-146]. The loss of alkali and other problematic elements, particularly chlorine and sulfur, in biomass by leaching is the main reason for this treatment.

Fuel pre-treatments particularly the leaching can reduce efficiently the risk of bed agglomeration because it eliminates the large fraction of alkali and chlorine elements as well as sulfur of inherent inorganic material before they are transformed to the problematic compounds during FBC/FBG. However, the excessive water content more hinders the combustion process and limits the availability of the fuel fired FBC/FBG. Otherwise, the removal of sand, soil and other inert contaminate materials can prevent the deterioration of fluidization quality only in a minor extent.

2.7.5 Fluidized bed operation control

As mentioned in section 2.4.3., defluidization is described as a part of the formation of stable bond between bed particles and the breaking of agglomerates. The breaking is significantly dependent upon the bed operations, particularly fluidizing air/gas velocity and operating temperature.

Velocity control

High fluidization velocities lower the tendency for bed agglomeration and deposition problems due to an increasing breaking force, and enhancing ash entrainment [147-148]. In some occasions, agglomerates already formed are disintegrated by temporarily increasing the gas velocity, which may mainly work on weakly bonded agglomerates that typically formed rather fast at relatively high temperatures [149]. However, increasing the gas velocity may also show a negative result when the agglomerates are bound with the stronger bond and settled on the base of bed. These agglomerates with slowly settling are more typically formed in the lower bed temperature ranges. Increasing the gas velocity in the primary zone (bed zone that is closely above the air/gas distributor) may even provide a worse situation by reducing the bulk density in the still fluidized areas adjacent to the agglomerates and thereby reducing the buoyancy forces acting on the agglomerates [51,149]. A suitable way in this case is to frequently or occasionally drain the bed, even if the boiler has to be shutdown. A sudden increase of air flow during combustion at an inappropriate stoichiometric ratio may also result in an overshoot of temperature, which is the worsen situation. However, simply increasing the fluidizing gas velocity does also result in the increasing loss of heat by flue gas and entrained unburned carbon.

Temperature control

Agglomeration is in most case caused by the melt formation of ash forming constituents at particle surface, which then glue particles together. It is therefore a straightforwardly logical measure to avoid agglomeration by combustion/gasification at a sufficiently low temperature below the initial agglomeration (sintering) temperature, or initial melting temperature [150]. However, there are several temperature related effects to be concerned.

Lowering bed temperature of FBG by decreasing air-fuel ratio is undesirable, as this generally gives a lower carbon conversion and higher tar concentration in the gas [51]. Increasing the excess air ratio in FBC is also difficult, as it can cause extinction of the flame at the bottom of the bed. Furthermore, a low bed temperature may cause a high CO emission [104]. Increasing air flow to lowering the bed temperature can result in the unacceptable carbon losses due to a high elutriation. A better way to achieve a lower bed temperature for a given air-fuel ratio is therefore the addition of steam, flue gas or nitrogen to the fluidizing gas [114], or otherwise additional heat transfer area in bed or

freeboard. Freeboard temperatures in biomass combustion are generally 100-200 °C higher than bed temperatures due to the volatile combustion [34].

Temperature overshooting during start up in combustion and gasification (start up and shut down usually in "combustion mode") is also a serious problem [51]. A delayed reaching the set point temperature often results in a major increase of a fuel feed rate, due to the natural impatience of operators. It results to an unrecognized excessive amount of fuel in bed. This fuel starts to react at a much faster rate shortly before reaching the set point of operation temperature, and thus gives overshoot bed temperature. A similar risk exists when changing to a less reactive fuel [11]. A good procedure during start up is to observe the temperature response on a short feeding stop, before an assigned operation temperature is reached. It is also a good start up not to exceed a previously experienced or calculated feed rate. To avoid temperature excursions during start up and shut down, it is simply patient and careful [51,82].

In addition, the local temperature peaks established by the locally poor bed circulation from the large bed area or inappropriate design of furnace chamber or fluidizing gas distributor should be avoided. Several measures are mentioned [51];

- improving the distribution of fuel and oxygen,
- better mixing by providing a more aggressive stage of fluidization in critical areas,
- moderating the temperature near gas nozzles e.g. adding steam in gasification or circulating flue gas in combustion,
- inducing further upwards streams through critical in-bed areas,
- allowing a higher particle flux, through critical part of a CFB reactor.

Fluidized bed reactors used for energy production are operated at specifically designed load conditions, e.g. steam or gas capacity. Increasing the fluidizing gas velocity by raising the gas flow merely delays the defludization state, due to the limited capacity of the designed air/gas flowing devices (blower or compressor). The temperature of burning char particle, especially in the high oxygen concentration zone inside the bed, is considerably higher than the mean temperature of the surrounding bed particles [51,96]. This high surface temperature of char particle can enhance the melt formation of eutectics on the char surface. Measures such as improved distribution of combustion or gasification agent (e.g. improved nozzle design) may be a solution, in order to avoid high concentration of oxygen in areas with high concentration of char. Oxidation or gasification at low (average) temperature also limit this problem due to the generally slowed reaction kinetics and higher margin from bed temperature to initial temperatures of melting and eutectic formation, resulting in a lesser formation of the melts [107,109].

Temperature control and velocity control are relevant operation. The operation controls as increasing gas velocity or decreasing bed operation temperature are an urgent prevention that delays the bed agglomeration. The furnace/nozzle designs and operations resulting to reduce effectively the poor bed circulation and poor fuel distribution is a solution to achieve this measure. However, the above operations out of the design conditions increase directly the losses of heat and carbon conversion of fuel, leading to the loss of boiler efficiency and the high emission. It is therefore seen to be a less extractive measure of bed agglomeration prevention.

2.7.6 Bed management

The bed properties on a continuous FBC/FBG after considerably long operating hours are largely different from the original properties of initially loaded bed particles. It includes a change in bed particle size, both larger and smaller than the initially loaded bed particle, as well as a change in chemical compositions of bed material. It is mainly due to the substantial contamination of the inorganic constituents from fuels and inherent fluidized bed behaviors [34,54]. The regular sampling and analysis of the bed material during operation and periodical refreshing the bed inventory, before a critical alkali concentration [104] or critical bed defluidization level is reached, is a necessary measure. The refreshment of bed inventory is a discharge of old bed material in the reactor and an addition of the new one.

In cases where some oversize particles are not possible to be removed by the fuel preparation, the fluidized bed chamber should be designed in such a way that the worst possible type of tramp material; passing through the preparation and feed system, and the agglomerates; formed in bed, can be efficiently drained out. The suggested design means for effective draining are mentioned viz; [51]

- designing for a light state of fluidization in the bed bottom (bed regime below the air/gas distributor), in order to loose the bed lock up,
- keeping the flow high enough to the vigorous and stable fluidization at the reactor bottom, at all times,
- inclining the bed bottom against draining opening/means,
- using directional air/gas distributor,
- using nozzle shaped in order not to hold up the irregular bed components,
- providing an open type of bed drain [151], instead of a base plate with nozzles.

A periodical addition of the fresh bed material keeps the bed sufficiently well sized and chemically corrected. The addition is considered in term of the mass ratio of batch fed fuel to bed particle. The potential needs for the bed refreshment is partly or fully covered by adding the chemically active particles to absorb sulfur, chlorine and alkali components.

2.7.7 Other measures

Carbonation and sulfation of CaO are a main agglomeration mechanisms based on chemical reaction (in section 2.3.3), according to below reactions.

Carbonation:	$CaO + CO_2 \rightarrow CaCO_3$	(exothermic)
Sulfation:	$CaO + SO_2 + \frac{1}{2}O_2 \rightarrow CaSO_4$	(exothermic)
	$CaCO_3 + SO_3 \rightarrow CaSO_4 + CO_2$	(exothermic)

The potential of these reactions to be taken place is increased by [34,51,66] viz,

- the presence of a high CaO concentration,
- a high partial pressure of CO_2 and SO_2/SO_3,
- decreasing bed temperature

An extension of the agglomeration due to carbonation and sulfation is particularly presented, when the high Ca fuels, bed materials or additives are used and temperature of local bed is decreased to form the thermodynamically stable Ca compounds. The particle stagnation is also a further effect, as badly fluidized zone in bed [51]. The possible preventions are suggested as;

- avoid stagnant zones such as the area near gas distributor grids, in particle return duct and particle coolers.
- limit the CO_2 or SO_X concentration in critical areas, e.g. (i) limiting the char concentration; (ii) adding steam, circulated flue gas or nitrogen; (iii) designing the chamber in such a way that liberate of SO_X out of bed as well as its subsequent absorption are primarily taking place , e.g., in the vigorously fluidized main reactor chamber,
- choose proper bed materials/additives,
- provide sufficient clearance and cleaning in hear absorption surfaces
- precautions in design of the flue gas and product gas coolers against deposition,
- avoid the combination of pressure and temperature that enhance the tendency for Ca compounds to alternate between calcinating and re-carbonating/re-sulfating conditions.

The formation of agglomerates/deposits based on condensation of vapor KCl on the particle surface/heat absorption surface and the subsequent sulfation forming K_2SO_4 is a risk, according to reaction;

$$2KCl + SO_2 + 2H_2O \rightarrow K_2SO_4 + 2HCl$$

It is a severe problem when high alkali and chlorine fuel is co-combusted with a high sulfur coal, for example. Some possible solutions are viz;

- avoid the combination of inputs of K/Na, chlorine and sulfur (e.g. co-firing straws/grasses and a high sulfur coal),
- limit the release of alkali to gas phase and/or promote its rebinding into non-sticky solid phase (e.g. using additive or free Si bed materials),
- provide sufficient clearance and cleaning in hear absorption surfaces,
- provide some rows of so called screening tubes in front of superheater surfaces in the convective pass, deposits will form on the screening tubes but tend to peel off due to thermal stress induced by a relatively low surface temperature.

Depending on the application and choice of fuel, an option of prevention or the combination of these can be the effective measure to reduce the bed agglomeration problem. The prevention methods to be success need the intensive experimental and practical experiences.

In above reviews including the further reviews of mathematical prediction in Chapter 4, despite the substantial efforts toward the bed agglomeration, the intimate understanding in its phenomena is still far from being complete. The several significant inconsistencies and uncertainties are shown in the present literatures. It is due to the fact that the bed agglomeration is a consequence of physically and chemically complex interactions in micro level between many different compounds. The intensive chemistry of bed agglomeration is hence important and needs to be studied in greater detail, in order to obtain more effective prediction and tackling for the success of applying FBC to produce energy from the specific biomass.

CHAPTER 3 EXPERIMENTAL

This chapter described the material, equipment, and experimental procedures of the study which covered both lab scale and pilot scale test rigs. All the instruments used for chemical analyses were also shown.

3.1 Material

3.1.1 Biomass

The biomass fuels selected for their bed agglomeration study were based on the agriculture residues. They included oil palm kernel shell (palm shell) and empty fruit bunch, corncob of feedstuff corn and rice straw from harvested paddy fields; all are the promising biomass fuel for heat/power generation in Thailand.

Palm shell and palm empty fruit bunch are the main residues of palm oil mill. In 2009 the domestic availability of palm shell and empty fruit brunch had been estimated to be 0.04 and 1.02 million tons equivalent to 17.02 and 433.29 ktoe (kilo ton oil equivalent), respectively [152]. As the consumption of bio-diesel which is mainly produced from palm oil continuously increases, there will be more residues to be used for energy generation. Palm shell is considered suitable for use as a solid fuel to generate heat and/or power due to its relatively high bulk density and uniform shape and size. It is presently a commercial solid fuel, and a good quality raw material for the activated charcoal. Empty fruit bunch that is fibrous material is mainly used in agricultural sector, for instance the fertilizer and culture media of mushrooms. However, its quantity in applications as a fuel for heat/power generation is being increased. These residues obtained from the mill were shown in Figure 3.1.

(a) (b)

Figure 3.1 Oil palm residues; (a) smashed palm shell, (b) empty fruit bunch.

In Figure 3.2, corncob is the dry stalk (core) of maize and has widely application. It is used as a fuel to mainly produce steam (heat) in the feedstuff mill or auxiliary fuel for neighbouring factories. It is also a raw material of briquette. Additionally, it is also a raw material for the furfural (a liquid aldehyde with a penetrating odour used in making furan; *raw material of nylon fiber synthesis*, and as a solvent) and ruminant fodder production. Approximately, 0.58 million tons equivalent to 249 ktoe of its leftover quantity was estimated in 2009 [152]. The commercial power plant using corncob as a fuel is being initiated.

Figure 3.2 Corncob in original shape.

Rice straw, the dry stalk of the plant, is an agricultural residue after the rice grain has been harvested on fields, and it was selected in this work for bed agglomeration study. In Thailand, rice is a domestic cereal staple and an important export product. It had been evaluated that about 25.6 million tons of straw, or 6,217 ktoe equivalent, is produced as the available potential in 2009 [152]. The use of straw in commercial-scale biomass power plants becomes a mainstream in the European Union [12] but in Thailand straw is mainly used as roughage animal feed, mainly for the cattle, and in agricultural sector as the culture media for mushrooms and mulch. Due to its relatively low bulk density, the densification of straw is needed for effective handlings and transportation, as shown in Figure 3.3.

Figure 3.3 Cubic bale of rice straw.

3.1.2 Bed particle

In this work only quartz sand, four different size ranges, was used as the bed particle to study their agglomeration by burning with the above mentioned biomass at given experimental conditions in fluidized bed reactors.

3.2 Material characterizations and instruments

Biomass is a very heterogeneous and physically/chemically complex renewable resource. Understanding this natural variability and range of properties is essential for conducting research and developing energy technologies using biomass resources. Physical property of biomass plays an important role particularly in sizing of the reactor/fuel handling equipments, such as conveyor, hopper or shredder, and in extent of co-firing [12], while chemical property describes its potential to undergo some chemical change or reaction by virtue of its composition. The former includes the material strength, particle and bulk densities and size, while the later is importantly the organic and ash compositions, and the energy value.

Basically, biomass fuels are characterized chemically by the standard methods of Proximate and Ultimate analyses, heating value determination and the ash composition analyses. The proximate analysis is a technique that separates and identifies categories of compounds in a sample and reports the contents of moisture, volatile, fixed carbon and ash in the sample. The ultimate analysis is also similar technique giving the contents of carbon, oxygen, hydrogen, sulfur, and nitrogen elements. The energy value of fuel substances analyzed in laboratory is reported generally in term of the high heating value (HHV) based on the complete combustion of the sample to carbon dioxide and liquid water (The low heating value, LHV, gives the heat released when the hydrogen is burned to gaseous water). The analysis of fuel ashes gives the composition of inorganic elements in the ash. The results of these analyses are so important for fuel handling, combustion/gasification system design, operation, and emission control [12].

Comparison of fresh and used bed materials based on their chemical and morphological characteristic are also necessarily.

The standard analytical methods used in this study were mainly based on ASTM (American Standard of Testing Materials). The analysis items, ASTM codes and the further advance analyses including laboratory instruments, used in this study, were listed in Table 3.1.

Table 3.1 Methods and instruments for characterization

Item	Code/Analysis	Instrument	Note/Description
Biomass			
Bulk density	E873-82 (1998)		- As fired basis
Size distribution	E828-81 (2004)		- As fired basis
Char particle density	D167-93 (2004)e1		
Fuel preparation	D2013-11		- As received and fired basis - Treating biomass before intensive characterization
Proximate analysis - Moisture - Volatile - Ash - Fixed carbon	E870-82 (2006) - E871 - E872 - D1102		- As received and fired basis - Fixed carbon is determined by difference
Ultimate analysis - C, H - N - S - O	E870-82 (2006) - E777 - E788 - E775	- CHN elementary Analyzer (Fig. 3.4a, **LECO; CHN-2000**) - S Analyzer (Fig. 3.4b, **LECO; S-144DR**)	- As dry basis - Oxygen is determined by difference
Chlorine	E776-87 (2004)		- As dry basis
Heat calorific value	E711-87 (2004)	- Bomb Calorimeter (Fig. 3.4c, **LECO; AC-350**)	- As dry basis
Ash composition (Si, Al, Ca, Mg, Na, K, Fe, P, Cl, S)	- D1102-84 (2007) - a digestion method [153]	- Microwave oven (Fig. 3.4d, **Anton Paar; Multiwave 3000**) - Inductively Coupled Plasma Atomic Emission Spectrometry (*ICP-AES*, Fig. 3.4e, **Perkin Elmer; OPTIMA 3000**)	- Dry ash - Ash sample is prepared according to ASTM and then digested into solution state in the microwave oven.
Thermal behavior		- Thermal Gravimetric Analysis (*TGA*, Fig. 3.4f, **Mettler Toledo; TGA/SDTA 851e**)	- Pulverized biomass as fired basis - Tested environment is air - Amount and rate of weight loss is determined as function of temperature

Table 3.1 Methods and instruments for characterization (Continue)

Item	Code/Analysis	Instrument	Description
Quartz sand (fresh and spent)			
Size distribution	sieve analysis (gradation test)	- A set of standard sieves - A mechanical shaker	
Chemical composition		- X-Ray Fluorescent (*XRF*, Fig. 3.5a, **Philips; PW2400**)	
Crystalline structure		- X-Ray Diffraction (*XRD*, Fig. 3.5b, **Bruker AXS; D8 DISCOVER**)	
Agglomerate sample			
Structure and composition of coating and neck		- Scanning Electron Microscope with Energy Dispersive X-ray Spectrometer (*SEM-EDS*, Fig. 3.5c, **JEOL; JSM-6400**) - X-Ray Diffraction	- Specimen preparation of agglomerate sample is needed, prior to SEM analysis.

The brand and model of instruments in bold are referred

(a)

(d)

(b)

(e)

(c)

(f)

Figure 3.4 Biomass characterization instruments, (a) CHN elementary analyzer; (b) S analyzer; (c) Bomb calorimeter; (d) Microwave oven; (e) Inductively Coupled Plasma Atomic Emission Spectrometry (ICP-AES); (f) Thermal Gravimetric Analyzer (TGA).

(a)

(b)

(c)

Figure 3.5 Characterization instruments for bed material, (a) X-Ray Fluorescent (XRF); (b) X-Ray Diffraction (XRD); (c) Scanning Electron Microscope equipped with Energy Dispersive X-ray Spectrometer (SEM-EDS).

3.2.1 Biomass

Prior to intensive chemical characterization, a number of samples of each biomass were taken and then pulverized separately to be in powder form of up to 250 μm grain size, according to ASTM D2013-11. The analyses of proximate and ultimate, heating value and chlorine content of these samples were then carried out. Additionally the amount and rate of mass loss of biomass samples during combustion in air ambient were also measured via TGA.

The quantitative analysis of the inorganic elements in biomass ash samples was carried out by using ICP-AES. As this technique requires the liquid form of the sample, the ash samples of biomass prepared according to ASTM D1102-84 (2007) were digested with the mixture of concentrated acids ($HF+HNO_3+H_2O_2$) in a microwave oven into solution state, according to the methods in a literature [153]. These ash solutions were then introduced to ICP to measure the concentrations of the required ash forming elements.

3.2.2 Bed material

Firstly, fresh quartz sand obtained was analyzed for the size distribution and then sorted out the size range for lab and pilot scale experiments. The ranges of 300-355 μm ($d_{p,av}$:323 μm) and 425-500 μm (459 μm) of sand sizes were used for lab scale experiments, as the controlled conditions, while 150-600 μm (354 μm) and 150-1180 μm (573 μm) in the original size ranges were tested in pilot scale, for verification. Secondly, the chemical properties of this sand were analyzed by using XRF and XRD to determine the composition and identify the crystalline structure, respectively.

3.2.3 Spent bed and agglomerate samples

The exhausted bed samples from FBC experiments were sized by a set of standard sieves to analyze their size distributions, and to separate the agglomerates. Prior to SEM-EDS analysis, the agglomerates samples had been prepared to be the specific specimen as follows:

- embedding by the slow curing epoxy resin (Fig. 3.6a, Struers; EpoFix) in a vacuum chamber (Fig. 3.6b, Mega advance; VEGA 5).
- cross-sectional cutting by the diamond saw of a precious cutting machine (Fig. 3.6c, Struers; Accutom-5).
- grinding (Fig. 3.6d, Buehler; Phoenix Beta) the prepared surface with the silicon carbide abrasive paper No.240 (Fig. 3.6e, Buehler).
- polishing with the 9 μm diamond suspension (Fig. 3.6f, Buehler; MetaDi).
- finishing the surface of agglomerate specimen by carbon sputtering to make specimen electrically conductive during SEM examination.

The SEM analysis was operated at the backscatter mode to characterize the appearance and EDS analysis was performed to determine the elemental distribution of the coating and neck in agglomerates.

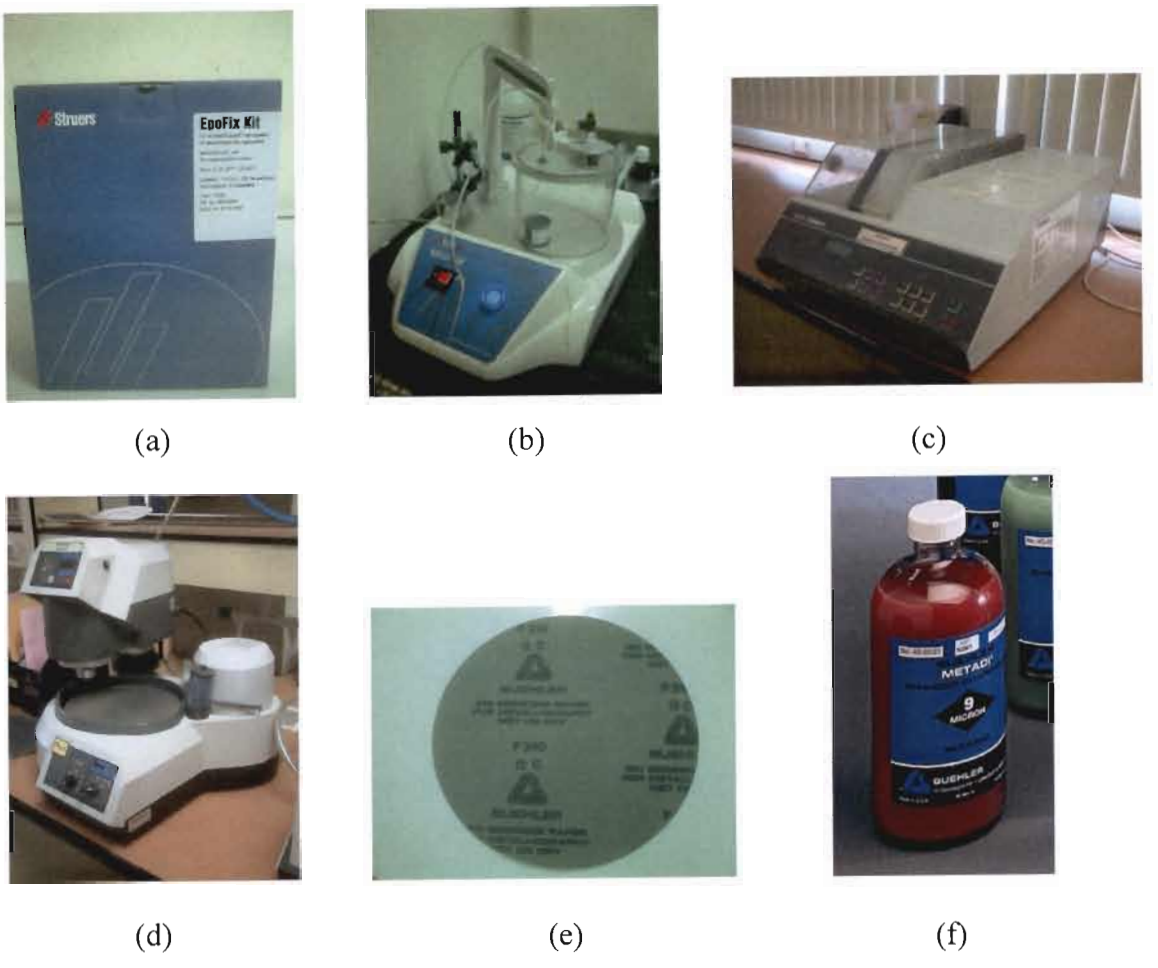

(a) (b) (c)

(d) (e) (f)

Figure 3.6 Materials and instruments of SEM specimen preparation, (a) epoxy resin; (b) vacuum chamber; (c) precious cutting machine; (d) grinder; (e) Si-C abrasive paper; (f) diamond suspension.

3.3 Fuel preparation for FBC experiments

Fuel preparation was required to treat the variable particle size and inappropriate properties of the fresh biomass samples, in order to feed uninterruptedly by existing fuel feeders and be efficiently the combustion process. The preparation was biomass specifics and described in details below. The controlled size range of biomass fuels in the present laboratory scale experiments was 0.8-1.0 cm.

3.3.1 Palm shell and fruit bunch

The mature fruit bunches cropped are steamed for a certain time, as the initial step of kernel separation process. They are then threshed to separate palm seeds by gravity. Only palm seeds are steamed once again to make the fiber to be easily peeled, while sodden empty bunches are sent off. The peeled palm seed are cracked by mechanical press to separate their kernels, as the final step. As a result, palm shell and empty bunch have substantially high moisture contents. They lead to poor combustion and subsequent increased stack emissions, and maintenance and operational problems [12]. Reducing these excessive moistures was necessary, as a fuel preparation.

The size range of 0.3-1.3 cm of actual shell as received from the mill was suitable to the present combustion experiments, and sufficiently amount was separated for lab scale tests (Fig. 3.7).

Figure 3.7 Size of palm shell particles for lab scale experiments.

Palm fruit bunch is the drop-like shaped bundle of natural long thread-like fibers (Fig. 3.1b), and the more steps in preparation were required. Initially, sodden bunches were ripped away and then introduced into a small agricultural shredder. Subsequently, the intermediate (Fig. 3.8a), which was still too large to be fed, were cut into the adopted size (Fig. 3.8b), and was employed in both lab and pilot scale tests.

Finally, both palm residues fuels were dried in the open air to remove the excess water.

(a) (b)

Figure 3.8 Treated palm bunch; (a) shredded by an agricultural shredder and (b) cut to end-used sample.

3.3.2 Corncob

Corncob from silo of the mill which had been dried naturally during storage was smashed by a laboratory hammer crusher generating the corncob flakes for the pilot scale experiments (Fig. 3.9a). The adopted size of lab scale tests was then separated out (Fig. 3.9b).

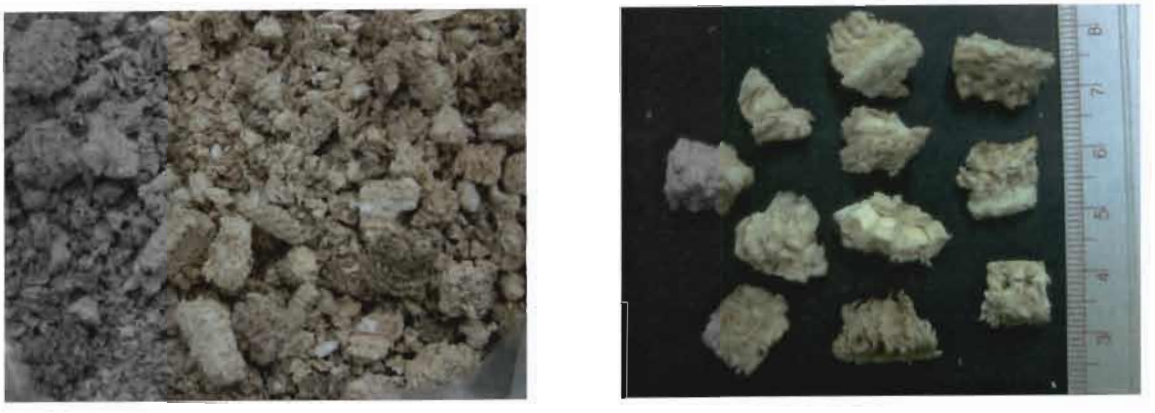

(a) (b)

Figure 3.9 Corncob samples; (a) crushed by a hammer mill and (b) end-used sample of lab scale test.

3.3.3 Rice straw

The bales of rice straw that had been dried by exposing to the sun at field for a certain time, after the grains were harvested, were unfolded and fed into a small shredder. The straw was then taken to further cut into internodes within the sizes for lab scale tests. For pilot scale tests, these internodes were bunched to form the cylindrical bale. The two treated straw samples were shown in Figures 3.10a and 3.10b, respectively.

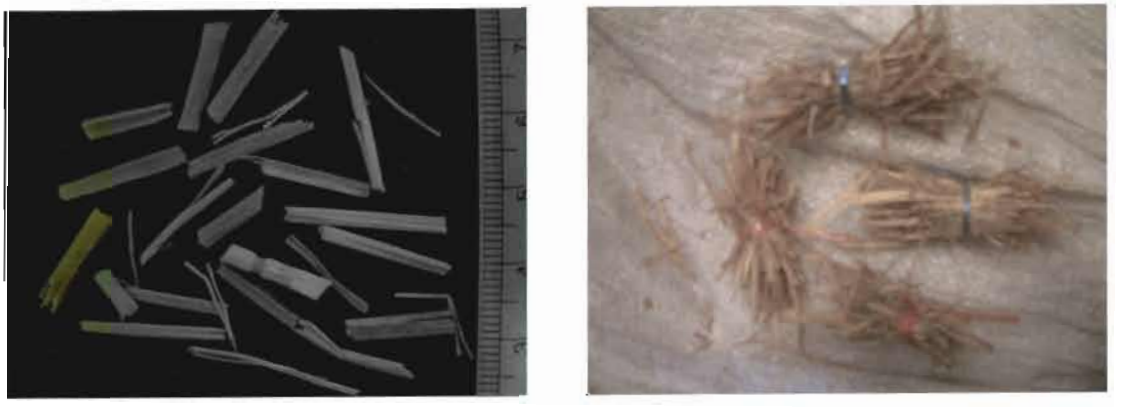

(a) (b)

Figure 3.10 Straw samples; (a) for lab scale test and (b) for pilot scale test.

3.4 Bubbling fluidized bed facilities

The bed agglomeration behaviors were investigated in the laboratory and pilot scales of bubbling fluidized bed apparatuses. The schematics and details of both facilities were illustrated in Figures 3.11-3.13.

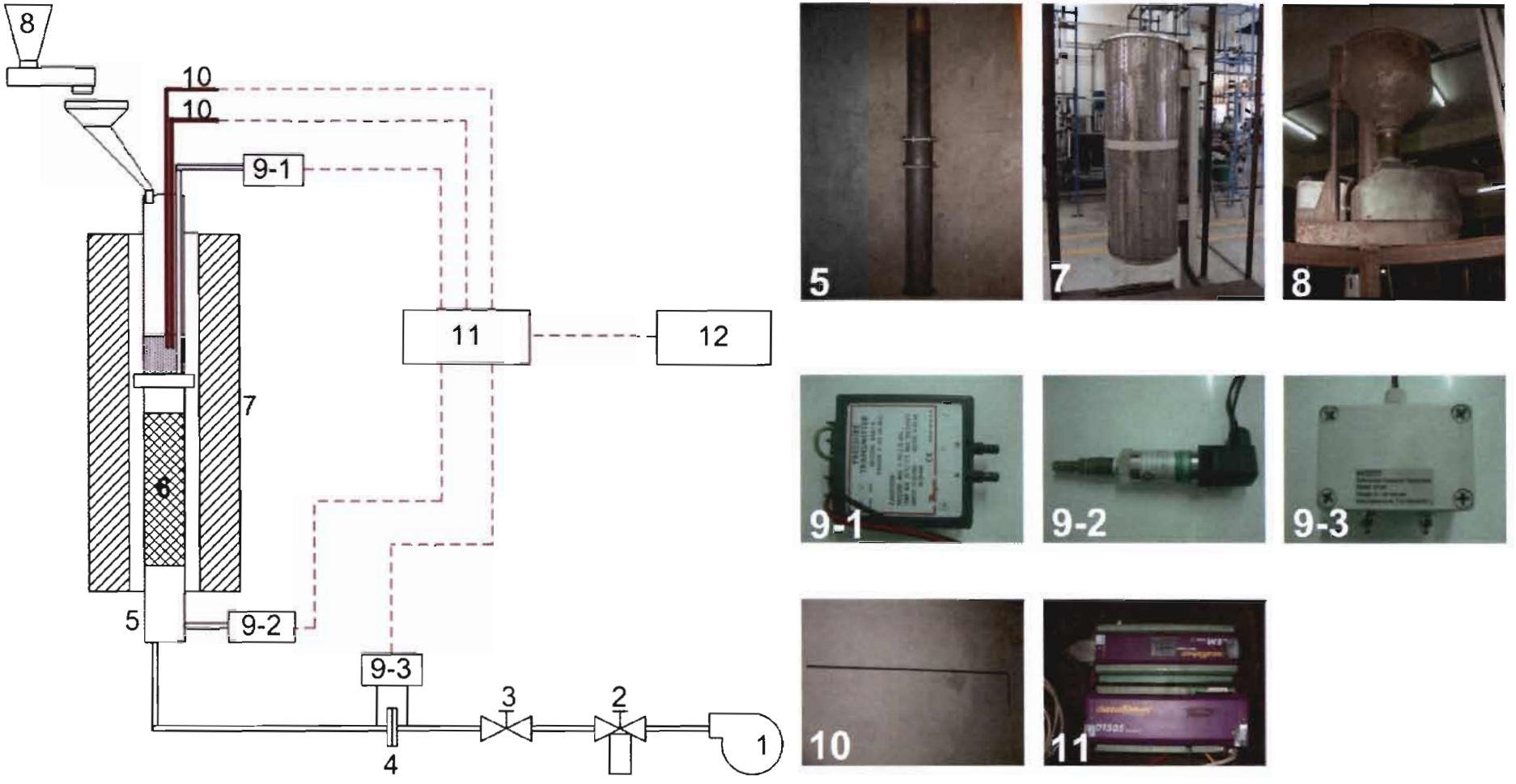

Figure 3.11 Laboratory scale fluidized bed apparatus: (1) air compressor; (2) pressure regulator with water/oil trap; (3) air control valve; (4) calibrated orifice; (5) a fluidized bed reactor; (6) air pre-heater; (7) electrical furnace; (8) fuel feeding device; (9) pressure transmitters; (10) K-type thermocouple; (11) data logger; (12) computer (PC).

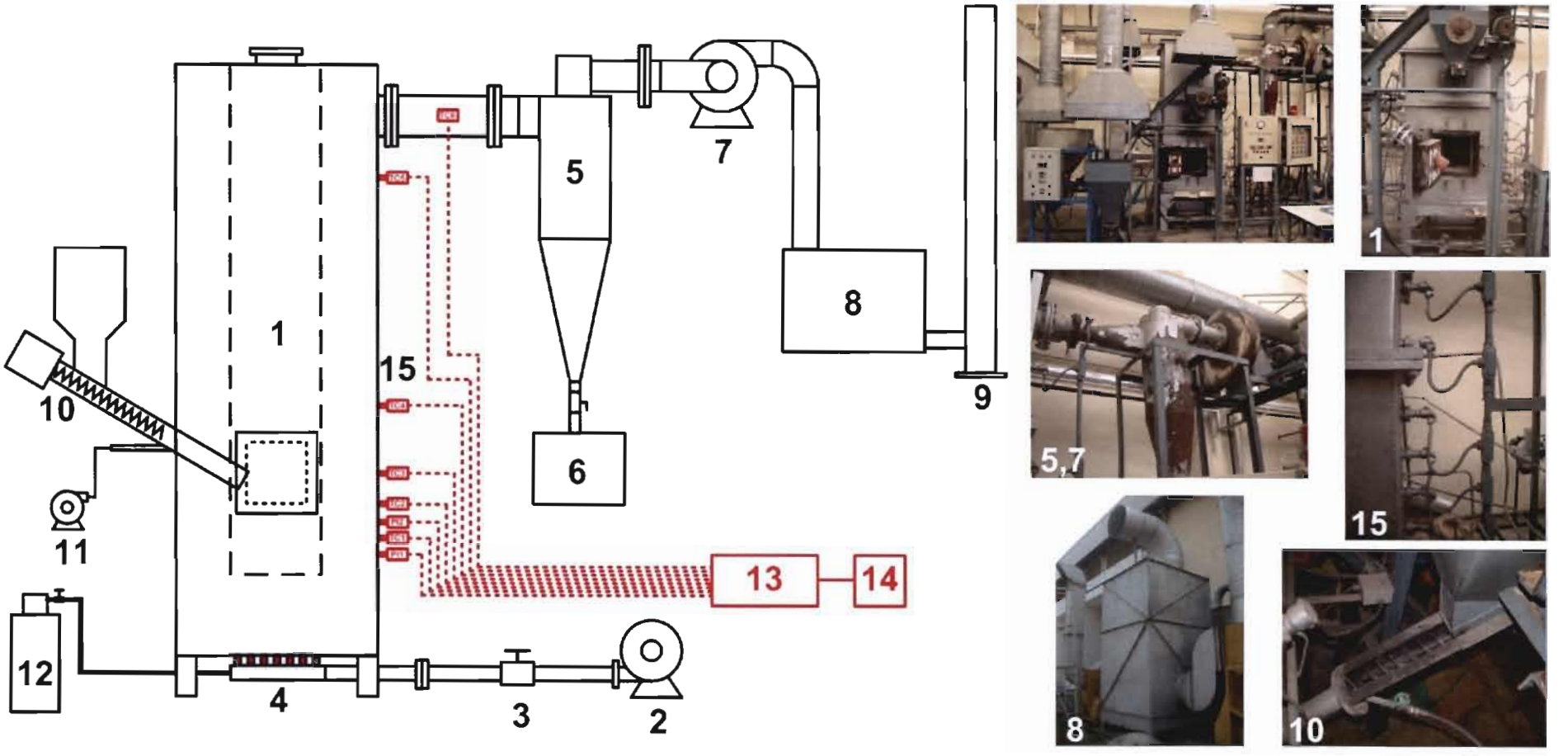

Figure 3.12 Pilot scale fluidized bed apparatus: (1) chamber; (2) force draft centrifugal fan; (3) air flow control valve; (4) air box with tuyeres; (5) cyclone separator; (6) fly ash receiver; (7) induced draft centrifugal fan; (8) wet scrubber; (9) chimney; (10) screw feeder with hopper; (11) air compressor; (12) LPG tank; (13) data logger;(14) computer (PC); (15) measuring devices.

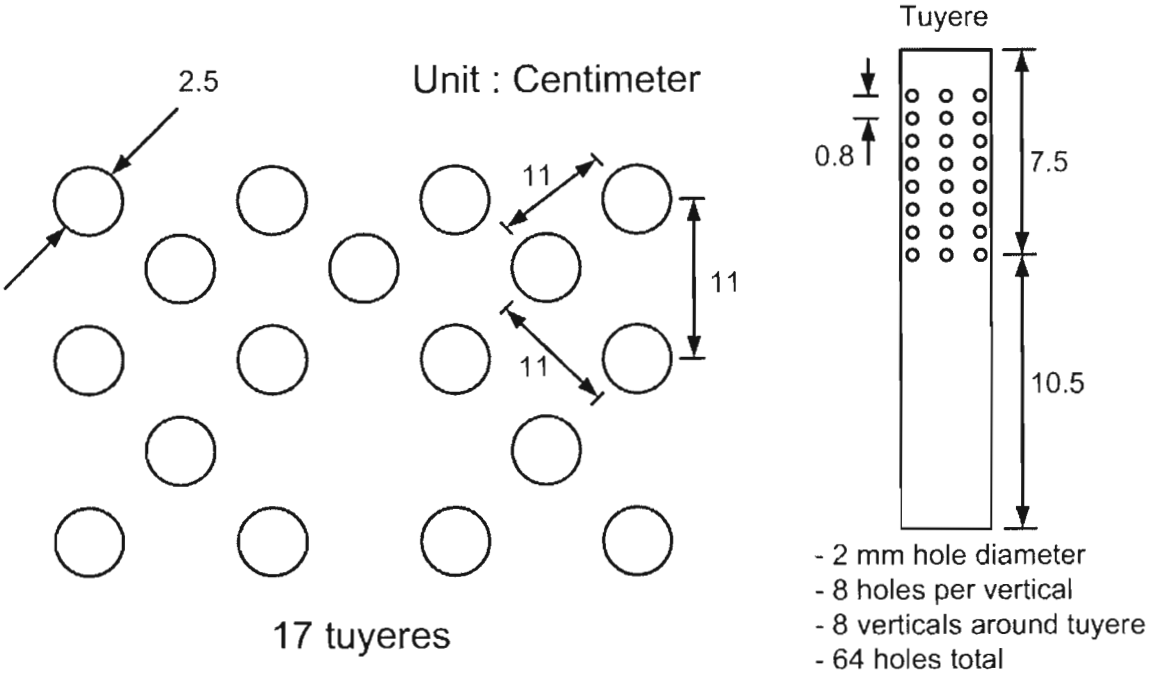

(a)

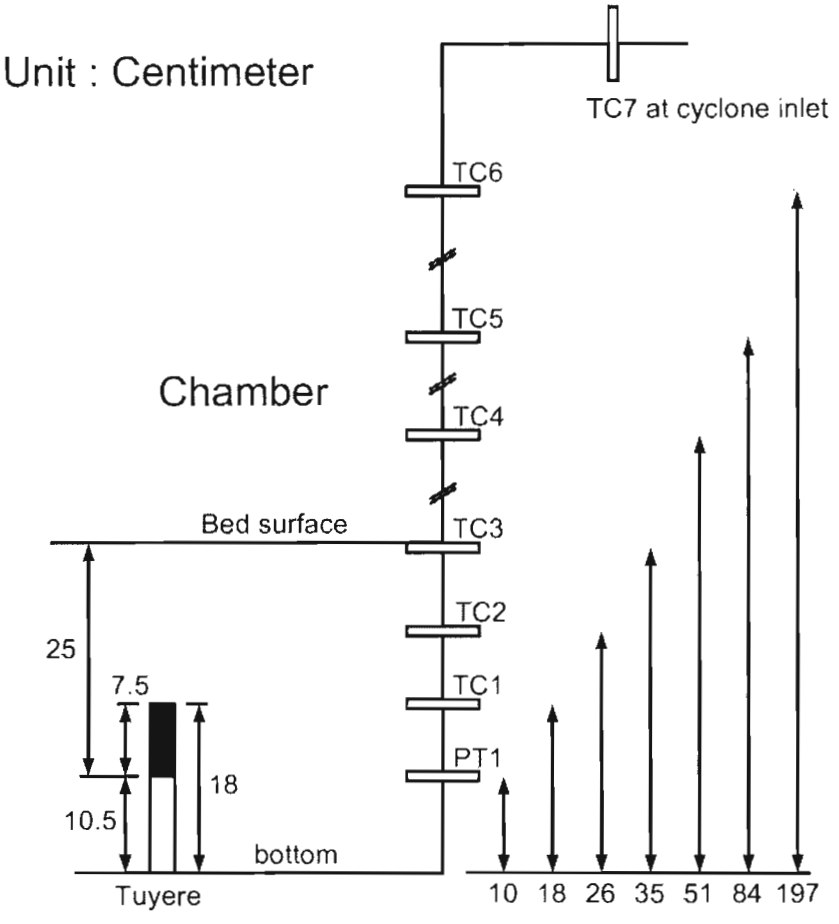

(b)

Figure 3.13 Layouts/Specifications of (a) tuyeres and (b) measuring devices (TC=thermocouple, PT=pressure transmitter).

3.4.1 Laboratory scale facilities

A laboratory scale unit sketched in Figure 3.11 consisted mainly of a cylindrical fluidized bed reactor, a fuel feeding unit, a set of devices and a data acquisition system. The reactor was made of a 316L-cylindrical stainless steel tube with 1.8 m-length, 9 cm-ID and 4 mm-thickness. A stainless perforated air distributor plate with 85 holes of 0.6 mm. diameter in equilateral triangular array was fitted to the chamber, approximately 1% opening area. The start up was accomplished electrically by a cylindrical tube furnace (Carbolite; STF), preheating the bed and fluidizing air. In a wind-box, the twisted stainless steel strips were packed to serve as an air pre-heater. The fluidized bed section was located near the middle of the furnace. An over bed fuel feeding unit was a frequency adjustable shaker mounted with a fuel hopper. The volumetric flow rate of fluidizing air supplied from an air compressor was measured by a calibrated orifice.

Three pressure transmitters were fitted at a calibrated orifice, an air-box and above an air distributor to measure the air flow rate, the air-box pressure and the whole bed pressure drop, respectively. Two K-type thermocouples for the bed temperature measurements were located along the vertical axis at 2 and 6 cm-heights above an air distributor. All devices were connected to a data acquisition instrument (data logger) to online record and display via PC in order to observe the bed pressure and temperature profiles.

3.4.2 Pilot scale facilities

A schematic diagram of a pilot scale unit was shown in Figure 3.12. A cubic and tall furnace chamber with the inner lining of refractory bricks had 45 x 45 cm^2 of bed cross-sectional area and 2.5 m of height. The plenum air box was connected with 17 tuyeres serving as the air distributor, which was detailed in Figure 3.13a, and to an access port of liquefied petroleum gas (LPG) tank for preheating. Biomass fuel was fed over the bed by a speed adjustable screw feeder mounted with a fuel hopper, and was spread onto the bed surface by the air jet produced by an air compressor. Dusty flue gas was treated in 2 sequential steps of a hot gas cyclone and then a water wet scrubber before emission. Several ports were fitted along the hot path for the pressure transmitters and K-type thermocouples, positioning in Figure 3.13b. Similarly the bed pressure and temperature profiles were monitored and logged on a PC via a data acquisition unit (data logger).

The bed pressure and temperature profiles were observed in both facilities in order to observe the changes in bed hydrodynamics and mark the onset and completion of bed defludization.

3.5 Experimental procedures

The bed agglomeration experiments were carried out under the atmospheric condition and steady state combustion at constant bed temperature and fluidizing air velocity. The influences of bed temperature (T_b), superficial air velocity (U), bed particle size (d_p) and static bed height (as H_b/D_b) on the bed agglomeration tendency was investigated.

3.5.1 Pre test

Prior to the bed agglomeration testes, these experiments were formerly carried out only in the lab scale unit to determine the significant characteristics of bed, viz;

1. Minimum fluidization velocity

In order to transition from a packed bed to a fluidized condition, the velocity of gas that passes over it is continually raised. A free-standing bed will reach to an incipient fluidization point, whereby the bed mass is suspended directly by the flow of gas stream. The corresponding gas velocity is termed the minimum fluidization velocity (U_{mf}). The transition boundaries between various fluidization regimes (i.e., bubbling to turbulent, and turbulent to fast fluidization) are affected by gas and solid properties and gas superficial velocity [148]. The regime of bubbling bed for the particle in Geldart group B, such as sand, is generally 3-5 of U/U_{mf}.

To investigate U_{mf}, a certain amount of quartz sand at given sizes (in section 3.2.2) in the lab scale reactor was heated up electrically to a given bed temperature without fluidizing air flow. Until reach, the gas flow was raised gradually and simultaneously the bed pressure and temperatures were recorded, until obtained the complete fluidization.

2. Reference profiles

As mentioned, the changes in bed hydrodynamics by bed defluidization were observed by monitoring the bed pressure and temperature. Their reference profiles would be formerly done by fluidizing the given sand at high temperature, derived from the electrical furnace, without fuel feeding. During a trial, the ongoing fluidized bed initially set at 0.5 of static bed height to bed diameter ratio (H_b/D_b) was doubled by immediately adding an identical amount and size of sand particle. The used bed samples would be sieved to find the abnormal sized particles at the end of tests, after cooling.

3.5.2 Agglomeration test

To start up, the bed was heated up by the external heat sources (the electrical furnace and burning LPG) from ambient to a certain temperature and then fluidized at a required air velocity. A required bed temperature was reached by subsequent combustion with biomass, and the external heat sources were then shut off. The recorded time started as the fuel feeding began. In the course of lab scale trials, regularly sampling the bed particles in reactor and visual observing (recorded by digital VDO camera) the fluidization were carried out. The trial completed when the bed was completely defluidized. The fuel consumption of each trial was estimated from the measured initial and final weights of biomass. The bed samples taken during the trial and discharged after defluidization were further characterized, as mentioned in section 3.2.3. All conditions were repeated twice to establish reproducibility.

In the next chapter, additional literature reviews on the theoretical prediction of bed agglomeration and the development of the present mathematical models will be mentioned and discussed in details.

CHAPTER 4 MODEL DEVELOPMENT

4.1 Introduction and reviews

As mentioned in Chapter 2, the tendency of bed particles to agglomerate is influenced by several factors such as their physical and chemical characteristics, the characteristics of the ash, the reaction mechanisms and the collision among particles. It is directly proportional to the particle adhesive properties and to the area of contact and inversely proportional to the particle momentum [15]. Interparticle forces which associate to the particle agglomeration of fluidized bed include van der Waals force, liquid bridge force and viscous force [87]. The formed liquid/molten phase existing on the surface of the moving bed particles makes them to be more deformable and inertia, so the agglomeration is easily taken place during FBC/FBG as described by the viscous sintering. Agglomerate is formed as the momentum of the colliding bed particles, induced by the kinetic energy of fluidizing gas, is dissipated by the interparticle forces [82,109]. The agglomerates can meanwhile suffer the breaking when these forces inside agglomerate are defeated by the segregated force such as the gravitational force or collision force. Some solutions involve changing the operating conditions in the bed to avoid the adhesion together or using alternative inert bed material and adding additives to reduce the tendency.

The mathematical models have been developed to predict particle/bed agglomeration characteristics, such as the minimum fluidization velocity, the minimum sintering temperature, the defluidization time and the agglomeration size and growth, based on the different approaches. Several models employ the mass balance and force balance combined with the statistical regression analysis to complexly formulate, or are the simple empirical model. The formulas of agglomeration and defluidization are summarized in Table 4.1, viz;

Gluckman et al. [18] performed defluidization experiments using a number of bed materials and correlated the fluidizing gas velocities as a linear function of temperature above the initial sintering temperature (T_S). Below T_S, the bed can always be fluidized at minimum fluidization velocity, while above T_S, a correspondingly higher fluidization velocity was needed to fluidize the bed. The minimum fluidization velocity was no longer determined only by a balance of gravity, buoyant and drag force but the interparticle cohesiveness and particle kinetic energy had to be taken into consideration, when particles were fluidized at temperature above T_S. The bed height was an influence on the tendency.

Siegell [154] correlated the fluidization velocity data in term of the excess velocity needed to keep the bed fluidized at high temperature to the excess temperature relative to T_S in high temperature defluidization experiments with several particle materials. The linear relationship between these two parameters was found.

Compo et al. [155] measured the fluidizing air velocity during high temperature defluidization experiments with a wide range of materials. The dimensionless excess velocity was correlated with the dimensionless excess temperature relative to T_S observing both linear and non-linear relations, and classified these according to whether the solid was amorphous or crystalline.

Table 4.1 Models of agglomeration/defluidization

Author	Calculation object	Model	Description/Note
Gluckman et al. [18]	Minimum fluidization velocity at sintering conditions	$U_{mf,S} = B + AT$, at $T \geq T_S$	- Particle material dependent - T_S is defined as the temperature at intersection between the experimental U - T curve result and traditional U_{mf} - The linear relationship
Siegell [154]	Minimum fluidization velocity at sintering conditions	$U_{mf,S} - U_{mf} = f(T - T_S)$	- Particle material dependent - T_S is determined by dilatometry technique - The linear relationship
Compo et al. [155]	Minimum defluidization velocity[1]	$\frac{U_D - U_{mf,S}}{U_{mf,S}} = f(\frac{T - T_S}{T_S})$	- T_S is determined by dilatometer - Linear and non-linear behaviors were observed which was classified by amorphous or crystalline material - $U_{mf,S}$ was obtained by correcting measured U_{mf} at ambient for gas property changes
Basu [156]	The limiting velocity for defluidization (Dubbed as minimum fluidization velocity at sintering conditions)	$U_{mf,S} = \frac{1}{1650}\frac{d_p^2 g}{\mu_g}\left(\rho_p - \rho_g + \frac{\psi(T,H_b,d_p)}{1-\varepsilon}\right)$ $\psi(T,H_b,d_p) = K(T - T_S)f_1(d_p)f_2(H_b)$ where $T_s=f_3(d_p,H_b)$ and $f_3(d_p,H_b)$ $\Psi(T,H_b,d_p) = 0$ at $T \leq T_S$	- Adhesive force is included to **Ergan's equation** [148], as ψ force function - T_S of particle is determined by dilatometry experiments - Verified with the results of coal ash agglomeration experiment
Liss et al. [157]	Minimum fluidization velocity at sintering conditions	$Ga(1+Co) = 150\left[\frac{(1-\varepsilon_{mf})}{\varepsilon_{mf}^3}\right]\mathrm{Re}_p + \frac{1.75}{\varepsilon_{mf}^3}\mathrm{Re}_p$ $Co = f((T - T_S)/T_S),.....)$	- Adhesive force is included to **Ergan's equation** - A non dimensional function of Co was used to be established by the results of copper bead sintering [154]
Seville et al. [158]	Minimum fluidization velocity at sintering conditions	$\ln(U_{mf,S} - U_{mf})/H_{mf} = \ln(K_2/\alpha\eta_0) - \frac{E_{\mu,s}}{RT}$	- Based on visco-plastic sintering - Based on a comparison of characteristic times for quiescent motion of particle in bed and for the growth of sinter necks

Table 4.1 Models of agglomeration/defluidization (Continue)

Author	Calculation object	Model	Description/Note
Knight et al. [159]	Minimum bed breaking fluidizing velocity under sintering condition[2]	$U_{BB} - U_{mf} = \frac{r_a^3}{x_c^7} K_1 K_2(T) D_{0,S} \exp\left(\frac{E_S}{RT}\right)$ K_1 = either H_{mf}/α or $2d_b/3$ and $K_2(T) = 56\zeta\delta^4/kT$	- Based on diffusion sintering - Based on a comparison of characteristic times for quiescent motion of particle in bed and for the growth of sinter necks
Tardos et al. [160,161]	Limiting gas velocity[3]	$\frac{U_S - U_{mf}}{U_{mf}} = K\left[\frac{1-\varepsilon}{\varepsilon^2}\right]\left(\frac{d_{ag}^{7/4} d_b^{1/2}}{D_b^{1/2} d_p^{3/2}}\right)\left(\frac{\rho_g \sigma_S}{\phi \rho_s \mu_s g^{1/2}}\right)^{1/2}$	- Based on the force balance approach between the strength of agglomerates and forces resulting from bubble motion - Predicting in both low temperature condition by the presence of sticky liquid and high temperature sintering
Moseley et al. [162]	Minimum defluidization velocity[1]	$U_D = C_0 + C_3 \frac{((T/T_S)-1)^{5p}}{\left[1 - a(T-273)^b\right]^{2p}}$	- Employ a two particle collision model and a model for granular energy of the bed - T_S is determined by dilatometry technique
Yang et al. [163]	Agglomerate size distribution	$W(d_p,t) = W(d_p,t)\big\|_{t=0} + \frac{(Volume\_of\_agglomeration\_zone)}{(total\_weight\_of\_bed)} x \int_0^t Rate(d_p)dt$ $Rate(d_p) = \left\{ \sum_{\substack{d',d'' \\ d'+d''\to d_p}} f_{agg}(d',d'') - \sum_{\substack{d \\ d_p+d\to d'}} f_{agg}(d_p,d) \right\} x \left(\frac{\pi}{6} d_p^3 \rho_p\right)$	- In a cone shaped fluidized bed with a central gas jet - Based on the multi-phase hydrodynamic and heat transfer principles - Defluidization behaviors were excluded in the model.

Table 4.1 Models of agglomeration/defluidization (Continue)

Author	Calculation object	Model	Description/Note
Arena et al. [164]	Defluidization time	$t_{def} = \frac{1}{k(T)} \ln\left\{1 - \frac{\left\{\left[\left[0.5\exp\left(\frac{m_p u_0}{\mu_{pp}\pi r_p^2}\right) - 1\right] + 1\right\}^3 - 1}{\frac{Q_{pp}\rho_p / W_{bed}\rho_{pp}}{k(T)}}\right\}$	- The time is that the coating layer on bed particle reach to a critical thickness which dissipate the momentum of bed particle - Viscous flow sintering - Critical thickness is described by a critical stoke number (St) [165]
Lin et al. [109]	Defluidization time	$t_{def} = C\left(\frac{U - U_{mf}}{d_p}\right)^{1/2} \exp\left(\frac{E_\mu}{2RT}\right)$	- The time is that the coating layer on bed particle give adhesive force equal to breaking force induced by the passing bubble - Based on the coating induced agglomeration of K-silicates system and the viscous flow sintering
Lin et al. [166]	Defluidization time	$t_{def} = C\left(\frac{1}{f_N \psi}\right)\left(\frac{M^k}{d_p}\right)^{1/a} \exp\left(\frac{E_\mu}{RT}\right)$ $M = 0.67(1-\varepsilon_{mf})\rho_p\left(\frac{1}{\phi_b} - 1\right)(U - U_{mf})$ $\phi_b = \{1 - 0.3\exp[-8(U - U_{mf})]\}\exp(-\beta H_b)$ $\beta = 7.2(U - U_{mf})\exp[-4.1(U - U_{mf})]$	- Similar approaches with Lin et al [109] - The model of average convective solid mass flux [167] is employed as an expression of breaking force - Viscous sintering under Na species system

[1] Minimum superficial velocity is required avoiding defluidization under sintering conditions

[2] Dubbed alternatively, the minimum fluidization velocity is required preventing defluidization under sintering conditions

[3] Velocity is necessary to break the large agglomerates and to keep a bed of sticky particles fluidized at temperature exceeding T_S and/or if the bed contain a sticky material

Basu [156] and Liss et al. [157] modified Ergun's equation by including the adhesive force in the force balance. The expressions of minimum fluidization velocity under sintering conditions were derived as the adhesive force was correlated with the excess temperature with T_S. The models of Basu had been verified by the experimental results of the coal ash thermal sintering.

Seville et al. [158] compared two characteristic times to predict the defluidization velocity as the function of bed temperature, based on plastic viscous sintering; i) a time for which particles in the quiescent zone of fluidized bed remain in contact with others, and ii) a time for the growth of a neck between particles of sufficient size, and hence strength, to withstand the breaking force imposed by the movement of gas bubbles. Knight et al. [159] also employed this approach to develop a model based on the diffusion sintering.

A model of Tardos et al. [160,161] was developed to predict the limiting velocity to defluidize, based on the approaches viz; (i) the comparison between the breaking force acting on agglomerates and the agglomerate strength and; (ii) the equilibrium in the dynamic formation and break of agglomerates. In this model, the cohesive forces between granular was described by the presence of sticky liquids in both high and low temperature conditions and the bonding mechanisms between particles was associated to the liquid bridge, viscous sintering and high temperature sintering. The theoretical prediction and their results of experiments showed an exponential relationship between the dimensionless excess velocity and the dimensionless excess temperature, which was in an agreement with the data of Liss et al. [157] and Compo et al. [155].

Moseley et al. [162] proposed a kinetic model for calculation of defluidization velocity as dependence of temperature. It was suitable to viscous plastic sintering. The kinetic energy was taken to be dissipated in doing against an adhesive force on rebound. Two collision models and a model for the granular energy of the bed were used to formulate. They introduced a surface adhesiveness coefficient, which was early used by Liss et al. [157] as Cohesive number (Co), to account for the temperature effect.

Yang el al. [163] developed a model to predict the extent of agglomeration in a fluidized bed with a central jet. The model included mass and momentum balance to describe the fluid dynamics, and collision number and adhesive probability to describe the agglomerate rate. The defluidization phenomena were, however, excluded from the model.

Arena et al [164] calculated the predictive time at which defluidization occurred in plastic waste combustion. It was the time at which the viscous coating layer formed and extended by continuous plastic feeding reached to the critical thickness that had viscous resistance to bind together the two colliding particles within initial particle velocity. The condition for this defluidization limit, rebound occurs, could be described in term of a critical stoke number (St) [165].

In wheat straw combustion, Lin et al. [109] proposed a simple model of the breaking force, induced by bubbles, in linear function of the excess air velocity and an expression of the coating thickness relative to the combustion time and potassium content in linear function. The model was then developed based on the regression analysis to describe the defluidization time as a dependence of temperature, fluidizing velocity and bed

particle size, in an approach of the force balance between the strengthening adhesive by viscous sintering in the potassium silicate system and the breaking of fluidization.

Similarly, Lin et al. [166] also developed a predictive model of the defluidization time based on an approach of the adhesive-breaking force balance under the viscous plastic sintering of the sodium species system. A new expression of coating thickness relative to fuel properties and time was further applied and the model of average convective solid mass flux [167] was accounted as the expression of breaking force.

4.2 Modeling the bed agglomeration in FBC

In this work, the defluidization time of FBC defined as the predictive time at which the bed at specific operation conditions is reached to the complete defluidization state would be described by two present mathematical models. One was newly developed and another was a modified model based on the study of Lin et al. [109].

4.2.1 A presently developed model

1. Approach

The bed particles in the fluidized bed system keep moving, colliding, coalescing and breaking. After coalescence, agglomerates may also experience the strengthening or breaking. Based on these considerations as well as the present experimental results and discussion, which have been reported in the next chapter, the following assumptions were made:

- Defluidization is a result of competition between the total adhesive force in bed and the segregated force on agglomerates.
- Bed will be in the complete defluidization state when the total adhesive force equals, or exceeds, the segregated force.
- The segregated force on agglomerates is induced by the gas bubble.
- Bed agglomeration is caused by the formed melt fraction in the dominant potassium silicate system under the collision of melt transfer mechanism.
- Agglomerate is formed by the neck whose adhesive strength develops according to the viscous sintering mechanism and the melt induced agglomeration.
- Particles of bed material are sphere with uniform size.
- The ash content in bed increases linearly with combustion time.

2. Formulation

According to section 2.3.3, the size of the neck developed by the sintering therefore increases with time. In fluidized bed, the adhesion of two moving bed particles at u_p of each particles caused by a bonding neck of molten material at sufficient size was illustrated in Figure 4.1. Based on the information of sintering in Chapter 2, and applying a modified Reynolds lubrication equation [168] (Eq. 4.1) and Frenkel equation of viscous sintering [98] (Eq. 2.5), which described the viscous force of liquid bridge between two moving spheres,

$$F_{ad} = \frac{3}{2}\pi\mu_l r_p^2 \frac{1}{D} 2u_p \tag{4.1}$$

$$X^2 = \frac{3 \cdot r_p \cdot \gamma \cdot t}{2 \cdot \mu_l} \tag{2.5}$$

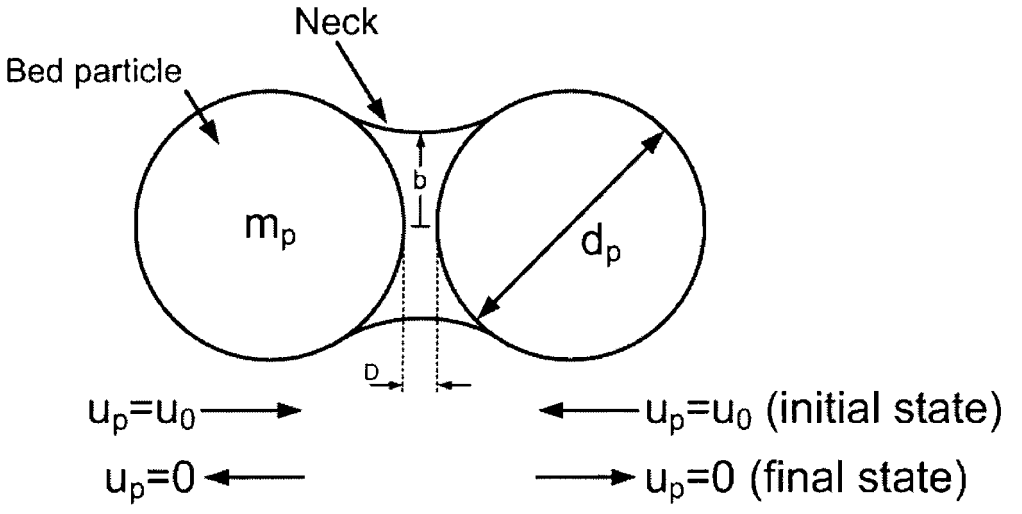

Figure 4.1 Illustration of adhesive force development by neck.

the adhesive force was herein simplified as;

$$F_{ad} = f(\mu_l, d_p, D, u_p, t) \tag{4.2}$$

where μ_l is viscosity of molten neck, d_p is particle diameter, D is particle separation distance, u_p is particle velocity and t is force developing time. The separation distance could be calculated from the kinematic law of Newton [169], also it was depended on;

$$D = f(\mu_l, d_p, m_p, u_p) \tag{4.3}$$

where m_p is the mass of a single particle. An average particle velocity (u_p) which represents the bed hydrodynamics depended substantially upon the bubble properties and was associated into the fundamental operating variables [148] viz;

$$u_p = f(d_b, d_p, S, u_b) \tag{4.4}$$

$$u_b = f(d_b, D_b, U) \tag{4.5}$$

$$d_b = f(\mu_g, \rho_g, \rho_p, D_b, H_b, U, U_{mf}) \tag{4.6}$$

$$S = f(d_b, u_b, U) \tag{4.7}$$

where ρ_g is the air density, ρ_p is the bed particle density, μ_g is the viscosity of air, d_b is the bubble diameter, D_b is the bed column diameter, H_b is the static bed height, S is the bubble separation length, u_b is the air bubble velocity, U is the superficial air velocity and U_{mf} is the minimum fluidization velocity.

In combination of Equation 4.2-4.7, the adhesive force per neck (F_{ad}) could be associated resultantly with the basic variables;

$$F_{ad} = f(\mu_g, \mu_l, \rho_g, \rho_p, d_p, D_b, H_b, m_p, U, U_{mf}, t) \tag{4.8}$$

The bed of inert particles at a specific experimental condition was partially and progressively defluidized by the thermally generated molten fraction of the inorganic constituents in biomass fuels, continuously fed during the steady state combustion. The complete defluidization was reached at the defluidization time (t_{def}), at which the adhesive force of a number of necks in bed was overcome by breaking force. Therefore, the total adhesive force ($F_{ad,total}$) at complete defluidization state was established;

$$F_{ad,total} = f(\mu_g, \mu_l, \rho_g, \rho_p, d_p, D_b, H_b, m_{bed}, m'_{fuel}, U, U_{mf}, X_{melt}, \%ash, t_{def}) \quad (4.9)$$

where X_{melt} is the melt fraction of ash in bed. It could be estimated from the phase diagram of involved ash elements in agglomeration by applying the "Lever rule" analysis [24], as mentioned in Appendix A, on the simplified initial fuel ash compositions at the surface temperature of the burning char particle. The char surface temperature was calculated according to the procedures in Appendix B. %ash is the percentage by weight of ash in biomass fuel on "as fired" basis. m_{bed} and m'_{fuel} are the bed inventory and fuel feed rate, respectively. X_{melt} and char temperature herein described an adhesive property of ash constituents.

Unfortunately, no exact mathematical model was published to describe the segregated force in fluidized bed. However, several pervious studies [108-109,164,170] suggested that the segregated force was defined from the behaviors of gas bubble in fluidized bed. Therefore, the segregated force of the present model was also correlated to the bubble properties in fluidized bed;

$$F_{seg} = f(d_b, S, u_b) \quad (4.10)$$

similarly simplified as;

$$F_{seg} = f(\mu_g, \rho_g, \rho_p, D_b, H_b, U, U_{mf}) \quad (4.11)$$

Defluidization time (t_{def}) was obtained by the setup in equality of Equation 4.9 and 4.11 as shown in Equation 4.12.

$$t_{def} = f(\mu_g, \mu_l, \rho_g, \rho_p, d_p, D_b, H_b, m_{bed}, m'_{fuel}, U, U_{mf}, X_{melt}, \%ash) \quad (4.12)$$

By mean of the dimensionless analysis, Buckingham-π theory [171], the variables in Equation 4.12 were grouped into the dimensionless terms;

$$\frac{m'_{fuel} \cdot t_{def}}{m_{bed}} = f\left(\frac{\mu_l}{\mu_g}, \frac{U}{U_{mf}}, \frac{d_p}{D_b}, \frac{H_b}{D_b}, (\%ash * X_{melt})\right) \quad (4.13)$$

The analysis of Multiple Linear Regression (MLR) on the lab scale experimental results was carried out in order to complete Equation 4.13 into general form of MLR model

(Equation 4.14), where B0 to B5 were the proportional constant, and to obtain the contribution of each independent dimensionless variable.

$$\left(\frac{m'_{fuel}.t_{def}}{m_{bed}}\right) = B0 * \left(\frac{\mu_l}{\mu_g}\right)^{B1}\left(\frac{U}{U_{mf}}\right)^{B2}\left(\frac{d_p}{D_b}\right)^{B3}\left(\frac{H_b}{D_b}\right)^{B4}\left(X_{melt}\%ash\right)^{B5} \tag{4.14}$$

Equation 4.14 was a purely statistical model. The viscosity ratio and melt fraction group represented the influence of fuel ash compositions and temperature on bed defluidization while the effect of bed hydrodynamics was described by the dimensionless velocity, particle size and static bed height. In this model, the viscosity of the molten ash (μ_l) was easily calculated from the practical viscosity model of the silicate glass melt [172] at the fuel ash composition and bed temperature. The gas properties were based on the physical properties of the air. It should be noted that although the present experiment was carried out with only quartz bed material, the effect of bed materials could have been physically taken into account in U_{mf} determined by Ergan's equation, as the bed particle density (ρ_p).

4.2.2 A modified model

A second model proposed in this work was modified from the model of Lin et al. [109] in order to probably correct the accuracy in the predication. The fully understanding of the model formulation and application in origin was thus necessarily.

1. Original assumption

Repeatedly, an original model [109] was early developed on the approach of the adhesive-breaking force balance. The adhesive force was well defined from the bonding stress on the neck cross sectional area as shown in Figure 4.2, while the breaking force was defined in the linear dependence with the excess velocity ($U-U_{mf}$). A linear extension of the coating thickness relative to the combustion time and potassium content in biomass was established and included in the model formulation. The assumptions of this formulation were as followed;

- The agglomeration tendency is caused by the formation of a coating layer composed of potassium silicates.
- Particles of bed material are spheres with uniform size.
- The coating is equally distributed on each sphere.
- The ash content in the bed increases linearly with time.
- Agglomerates are formed by necks, whose strength develops, according to the visco-plastic sintering mechanism.
- Defluidization is a result of competition between the adhesive force and the breaking force on agglomerates.
- The segregated force on agglomerates is induced by bubbles and is proportional to the excess fluidization velocity.
- If the adhesive force is equal to or higher than the breaking force, the bed will defluidize.

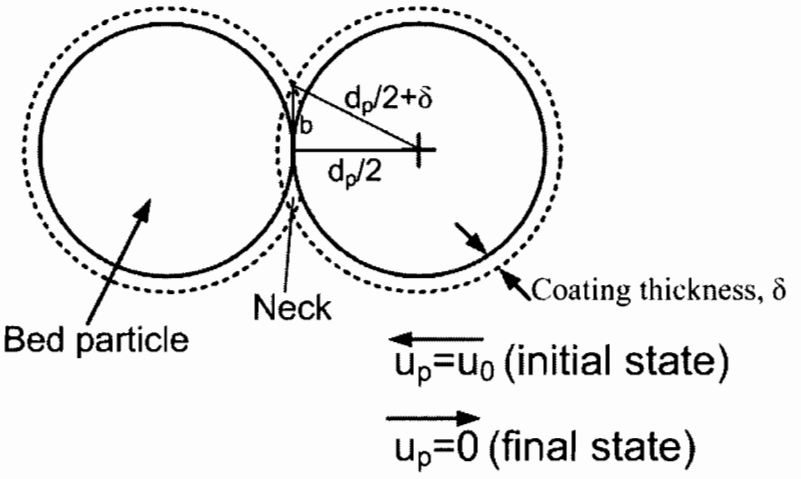

Figure 4.2 The development of adhesive force by bonding neck of coating [109].

2. Early formulation

The adhesive force between two particles caused by bonding, as illustrated in Figure 4.2, was described by

$$F_{ad} = \pi b^2 \sigma_S \tag{4.15}$$

where σ_s is the bonding stress. The accumulation of ash in the bed contributed to the build up of the coating and neck. According to mass balance and assumption, the thickness of coating layer on the bed particle as a function of time was expressed as;

$$n\rho_{coat}\pi d_p^2 \delta = C_1 m'_{fuel} X_{K-Fuel} t \tag{4.16}$$

where n is the number of bed particles, ρ_{coat} is the density of coating material, δ is the thickness of coating, $X_{K\text{-}Fuel}$ is weight fraction of potassium in the fuel and C_1 is the proportional constant. From Figure 4.2 and Equation 4.16, the growth of neck radius (b(t)) with the substitution for n was expressed as;

$$b^2 = d_p \delta = \frac{C_1 m'_{fuel} X_{K-Fuel} d_p^2 \rho_p t}{6 m_{bed} \rho_{coat}} \tag{4.17}$$

The strength development is proportional to the time and inversely proportional to viscosity of the coating due to the viscous sintering mechanism. The tensile stress of agglomerate (σ_S) was thus defined by [123];

$$\sigma_S = \frac{C_2 t}{\mu_l d_p} \tag{4.18}$$

where μ_l is the viscosity of coatings. Substitution of Equations 4.17 and 4.18 into 4.15, the adhesive force could be express as;

$$F_{ad} = \frac{C_3 d_p t}{\mu_l} \tag{4.19}$$

where

$$C_3 = C_1 C_2 \frac{\pi m'_{fuel} X_{K-Fuel} \rho_p}{6 m_{bed} \rho_{coat}} \tag{4.20}$$

The viscosity is dependent upon the composition and temperature in a K-Si system and the viscosity model applied was estimated by an Arrhenius's expression [158] as shown in Equation 4.21.

$$\mu_l = \mu_0 . \exp\left(\frac{E_\mu}{RT}\right) \tag{4.21}$$

where E_μ is activation energy of surface viscosity and μ_0 is pre-exponential factor for viscosity. The breaking force was assumed to be induced by bubbles and was proportional to the excess air as;

$$F_{br} = C_4 (U - U_{mf}) \tag{4.22}$$

When adhesive force (F_{ad}) is equal to the separating force (F_{br}), the bed is defuidized. Equations 4.19-4.22 were applied to obtain the defluidization time viz;

$$t_{def} = C\left(\frac{U - U_{mf}}{d_p}\right)^{1/2} \exp\left(\frac{E_\mu}{2RT}\right) \tag{4.23}$$

where

$$C = \sqrt{\frac{\mu_0 C_4}{C_3}} \tag{4.24}$$

3. Present modification

It had been noticed in Equation 4.24 that the fuel feed rate (m'_{fuel}), bed inventory (m_{bed}) and potassium mass fraction in fuel ($X_{K\text{-}Fuel}$) were considered to be the constant, and included in C constant. In present work, the effect of different biomass and bed conditions with one bed material were studied experimentally on the bed agglomeration tendency. The bed inventory, fuel feed rate and potassium content were therefore considered to be the variable, while the bed particle density (ρ_p) was considered to be the constant.

To obtain more generalized expression, the fuel feed rate, potassium content and bed inventory involved in C constant were separated out of Equation 4.24 and the equations were rewritten as,

$$t_{def} = C_{new}\left(\frac{m_{bed}}{m'_{fuel}\, X_{ash} X_{K.in.Ash}}\right)^{A}\left(\frac{U - U_{mf}}{d_p}\right)^{1/2} \exp\left(\frac{E_\mu}{2RT_b}\right) \quad (4.25)$$

where

$$C_{new} = \sqrt{\frac{6C_4\mu_0\rho_{coat}}{\pi C_1 C_2 \rho_p}} \quad (4.26)$$

where C_{new} and A were the presently defined constants. The original value of A was 0.5 [109] (Eqs. 4.20 and 4.24), while it expects to be 1 in this work. $X_{K\text{-}Fuel}$ was presented in the form of mass fraction of ash in the fuel (X_{ash}) and mass fraction of potassium in the ash ($X_{K\ in\ Ash}$). C_{new}, A, and E_μ would be calculated by the regression analysis on a set of present lab scale experimental data at constant air velocity and particle size. It was further noticed that the density of molten coating (ρ_{coat}) which was included in C_{new} (Eq. 4.26) was particularly depended upon the chemistry of coating material and the temperature, in a minor extent [173]. E_μ was also a function of the chemical composition of coating.

$$C_{news} = f(\rho_{coating}) \quad (4.27)$$

$$\rho_{coating}, E_\mu = f(the\_coating\_compositio n) \quad (4.28)$$

Therefore, these two parameters (C_{new}, and E_μ) could be possibly correlated as a function of the initial fuel ash composition, to which the coating composition was directly related.

Finally, the proposed models in Equations 4.14 and 4.25 were verified, in term of the defluidization time, with the present laboratory scale and pilot scale experimental results as well as the previous published experimental data.

CHAPTER 5 RESULTS AND DISCUSSIONS

This chapter presents and explains all the experimental results with the corresponding discussions.

5.1 Materials characterization

5.1.1 Bed material

The characterizations of quartz sand provided the important physical and chemical properties.

1. Chemical composition and crystalline structure

The detailed characteristics the chemical composition and crystalline structure of quartz sand were given in Table 5.1 and Figure 5.1.

Table 5.1 Quartz sand properties

Item	
Particle density (kg/m^3)	2,510
Bulk density (kg/m^3)	1,851
Fixed bed void fraction	0.351
Elemental composition (wt%)	
SiO_2	99.55
MgO	0.008
CaO	0.02
Al_2O_3	0.16
Fe_2O_3	0.05
Other	0.212

The chemical compositions, analyzed by XRF, which were reported as the oxide form in Table 5.1 revealed that this sand is almost pure of Si. The XRD spectrum illustrated in Figure 5.1 showed that the peak positions of this sand were perfectly matched with the standard material. This bed material was assertive SiO_2 compound in Hexagonal crystalline structure of quartz. Generally, the amplitudes of peaks in the XRD pattern are directly related to the atomic distances [174].

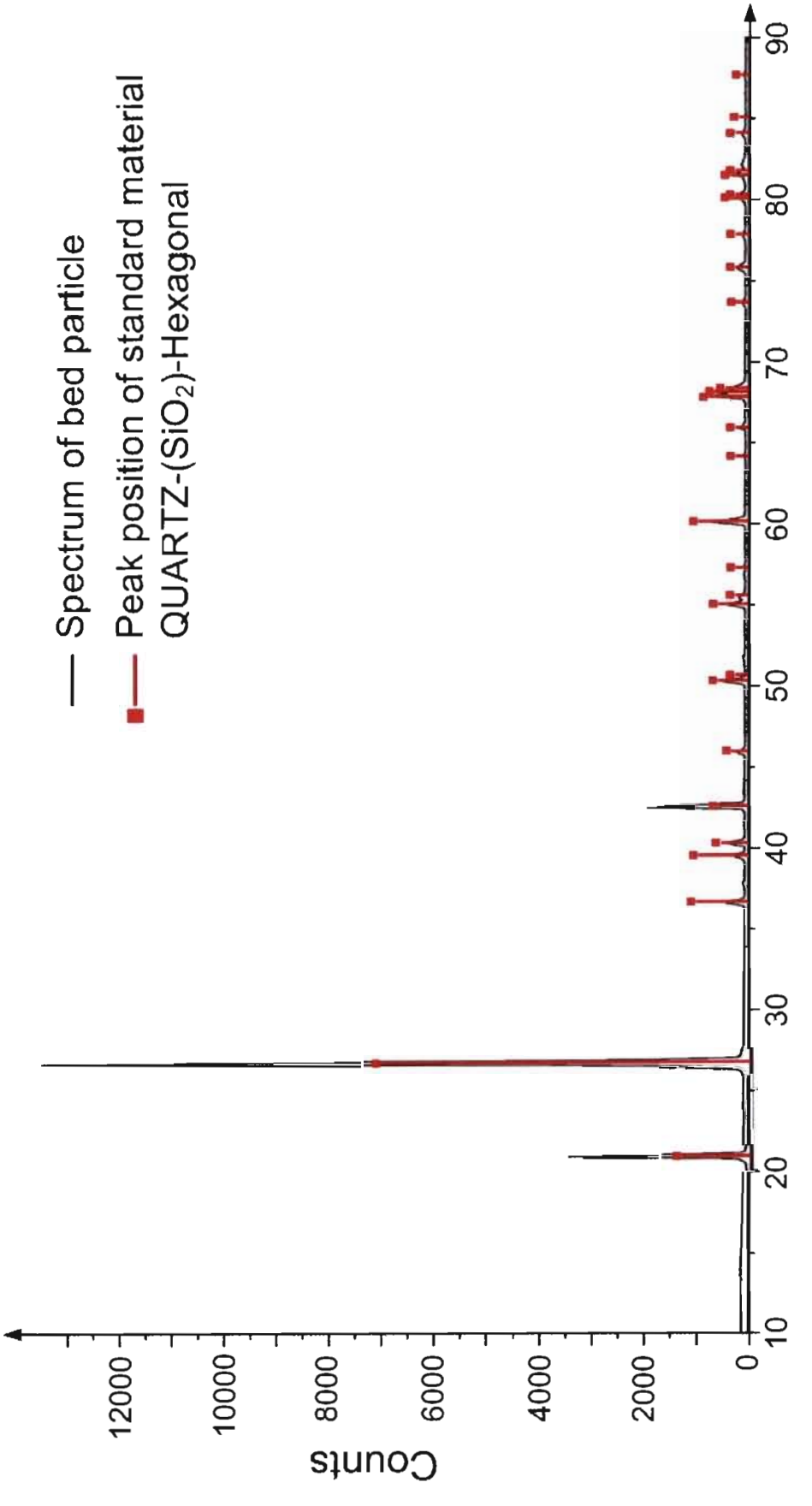

Figure 5.1 XRD analysis of quartz sand particles.

2. Size distribution

The screen analyses of quartz sand used specifically in the present experimental conditions were reported in Figure 5.2.

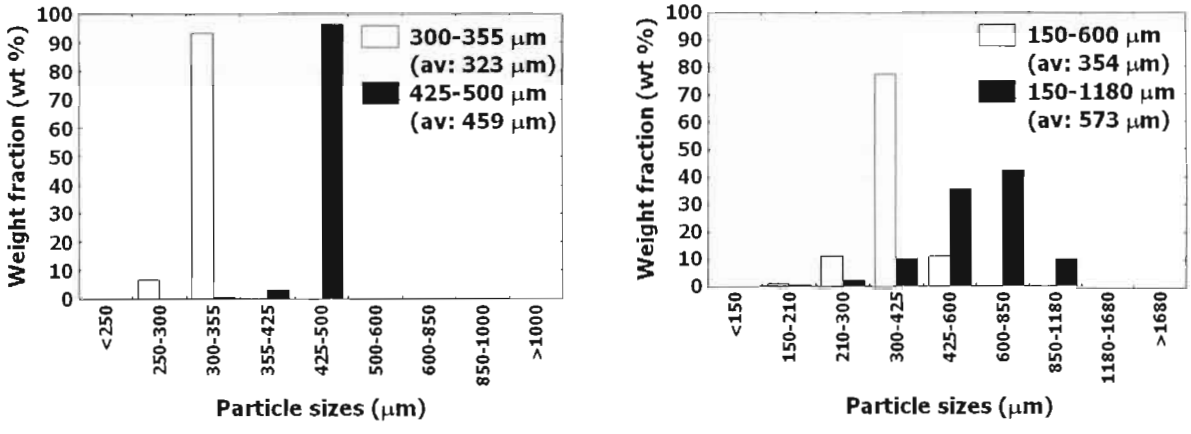

Figure 5.2 Size distributions of fresh sand particle for (a) lab scale and (b) pilot scale experiments.

Since the lab scale agglomeration test was to be the controlled condition, the adopted sizes ranges of sand were intentionally fixed in the relatively narrow distribution (Fig. 5.2a). The size ranges of 300-355 μm (average size, $d_{p,av}$:323 μm) and 425-500 μm (459 μm) were used for lab scale experiments, while those of 150-600 μm (354 μm) and 150-1180 μm (573 μm) (Fig. 5.2b) were used in pilot scale experiments. The diminutive fractions of undesirable size ranges for lab scale tests, however, were still found in bed samples, due to an imperfect separation and cracking.

5.1.2 Biomass

The properties of selected biomass samples were intensively characterized as shown below.

1. Biomass characteristics

The physical, chemical and combustion properties of biomass samples were reported in Table 5.2. They were analyzed based on "as fired basis" and "dry basis".

Table 5.2 Biomass properties

Description	Palm shell	Corncob	Palm bunch	Rice straw
Physical property				
Bulk density (Kg/m^3) [b]	500.04	124.06	28.69	42.56
Chemical property				
Proximate analysis (wt%) [b]				
Moisture	(17.36 [a]) 9.79	10.37	(63.44 [a]) 9.23	10.09
Volatile matter	68.35	72.01	74.48	69.49
Fixed carbon [d]	19.28	16.13	19.29	16.38
Ash	2.58	1.48	6.22	14.13
Ultimate analysis (wt%) [c]				
C	49.30	44.86	34.71	28.62
H	5.88	6.30	4.47	3.76
O [d]	41.52	46.39	53.79	52.49
N	0.40	0.66	0.64	0.89
S	0.019	0.049	0.05	0.09
Cl	0.02	0.06	0.16	0.02
HHV (kJ/kg) [c]	19,030	17,600	17,530	15,215

[a] As received basis; [b] As fired basis; [c] As dry basis; and [d] by subtraction.

Palm shell, the hard and dense shell of palm seed, had relatively high bulk density while corncob, which is the porous cylindrical stalk, showed lower. In contrary, palm bunch and rice straw, both were the fibrous matter, had relatively low bulk density. Due to steaming, palm shell and bunch had considerably high water concentration. Rice straw was a relatively high ash biomass. Sulfur content in these biomass differed only slightly while chlorine content in palm bunch was relatively high, 8 times higher than that of palm shell and rice straw.

2. Ash characteristics

The elements in biomass ash, presented as the oxide form, were reported in Table 5.3. It revealed that silicon proved evidently to be the dominant and abundant element in these ashes. Potassium and magnesium were the major alkali and alkali earth elements presented, respectively. The relatively high content of phosphorus and potassium could be noticed in corncob. From these information, the fluidization during combustion was expected to be problematic in some extent from the influences of the high potassium and chlorine content in these representative biomass fuels.

Table 5.3 Biomass ash compositions (wt% in ash)

Element	Palm shell	Corncob	Palm bunch	Rice straw
SiO_2	61.48	36.60	51.80	60.10
Al_2O_3	2.39	0.56	0.47	0.0
CaO	2.51	0.91	0.95	0.80
MgO	12.95	9.23	18.06	21.97
Na_2O	0.21	0.23	0.33	0.80
K_2O	5.78	33.08	21.39	10.57
P_2O_5	3.96	12.41	4.06	2.45
Fe_2O_3	5.56	5.08	0.72	0.20
Other	5.16	1.9	2.22	3.11

3. Thermal behaviors

The qualitative and quantitative measurement of mass change of the biomass samples associated with thermal degradation was provided by TGA. The amount and rate of change in weight of biomass as a function of temperature in air environment was illustrated in Figure 5.3.

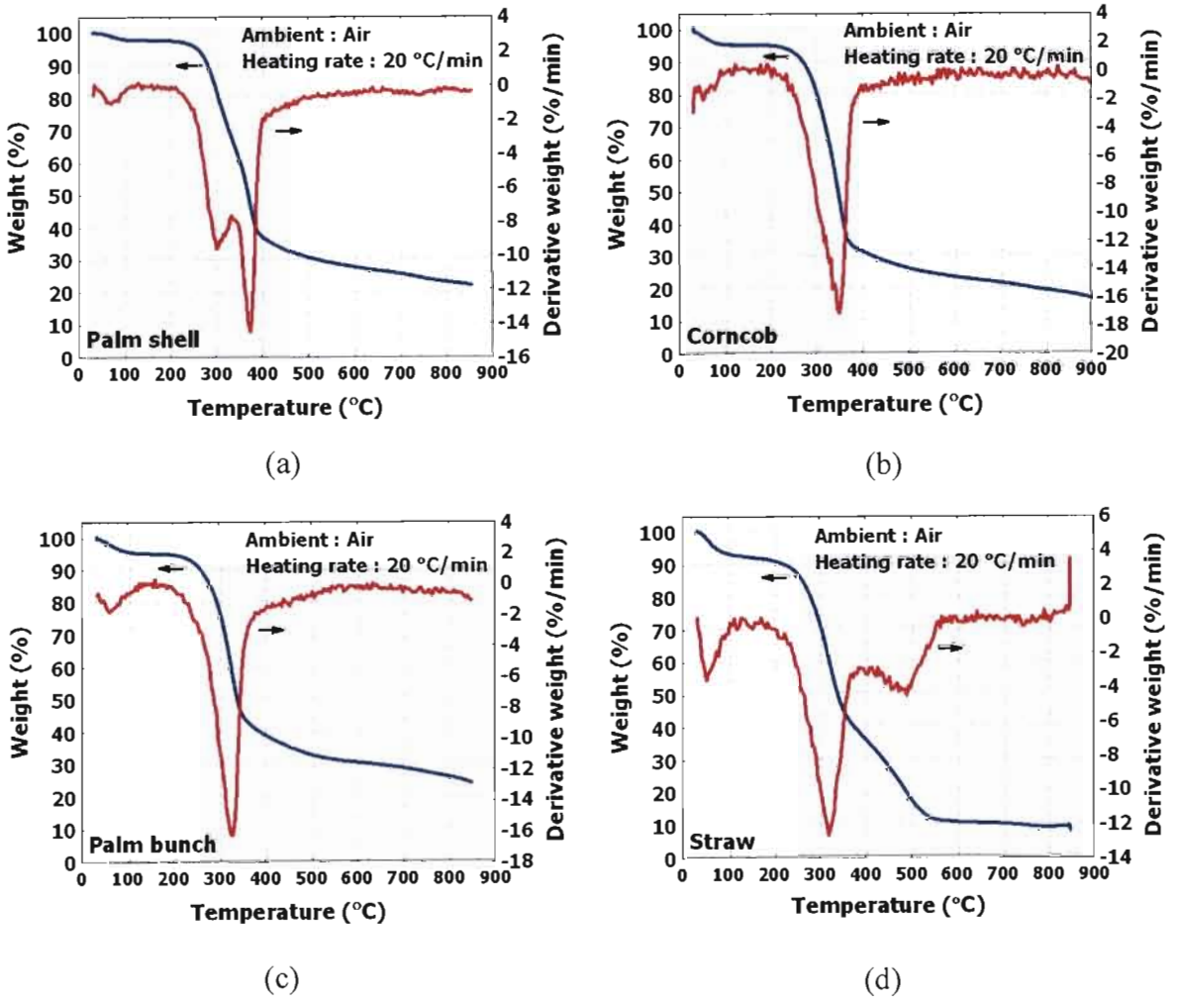

Figure 5.3 TGA weight loss profiles of (a) palm shell, (b) corncob, (c) palm bunch and (d) straw. Noted that all samples were tested based on "as fired basis" in air.

Three distinguishable ranges of the decreasing weight were observed in the relatively similar weight loss profiles. They could be interpreted as the following;

- Moisture in biomass samples began evaporating at about 50 °C until it was depleted at about 100 °C.
- Volatile components then started to release at around 200-230 °C.
- The biomass fuel accessed to the char combustion phase when the temperature reached to about 350-380 °C.

The characteristics of biomass and quartz sand provided the reference data and would be employed in the comparative description with the further results of agglomeration experiments reported below.

5.2 Agglomeration test

The agglomeration tests in both lab and pilot scale fluidized bed combustors were performed under an atmospheric condition and steady state combustion at constant bed temperatures and fluidizing air velocity. The influences of bed temperature (T_b), superficial air velocity (U), bed particle size (d_p), and static bed height (as H_b/D_b) on the bed agglomeration tendency were investigated.

5.2.1 Pre-test

1. Minimum fluidization velocity

The experimental minimum fluidization velocities (U_{mf}) of quartz sand at the given sizes associated to the given temperature ranges of the agglomeration tests were reported in Table 5.4, including the calculated U_{mf} values from Ergan's equation.

Table 5.4 Minimum fluidization velocity data

Size range (μm)	Average size (μm)	Experimental U_{mf} (m/s)	Calculated U_{mf} (m/s)
Lab scale experiment (Temperature range : 750-900 °C)			
300-355	323	0.048-0.051	0.048-0.053
425-500	459	0.078-0.084	0.083-0.091
Pilot scale experiment (Temperature range : 800-900 °C)			
150-600	354	0.055-0.058	0.055-0.060
150-1180	573	0.148-0.152	0.151-0.160

It can be seen that the predicted U_{mf} showed relatively good agreement with the observed values. In this study, 3 to 5 times of these experimental U_{mf} were set as the certain designed experimental conditions to study the air velocity effect.

2. Reference profiles

The bed defluidization which is directly associated to the change in bed hydrodynamics were observed and marked by monitoring the bed pressure and temperature. Therefore, their reference profiles were done before the agglomeration tests by fluidizing the given sand at high temperature without fuel feeding. The typical reference profiles at a specific condition were illustrated in Figure 5.4. It included the typical bed pressure loss and temperature profiles (Fig. 5.4a), and the superficial air velocity (Fig. 5.4b) for 425-500 μm sand size as a function of time in the case of without fuel feeding. Two bed temperatures, T1 and T2, were measured, along the vertical axis, at 2 and 6 cm. height above an air distributor, respectively.

The sand bed early heated up by an electrical heater began to be fluidized at about 600°C. As the temperatures of fluidized bed were increased to about 700 °C, the observed operating parameters began to be logged. The thermal steady state was reached at about 880°C. Adding the cold bed particles into the hot fluidizing bed resulted in a sharp fall about 200°C of bed temperatures, a sudden and double rise in whole bed pressure drop, and a marked increase in amplitude of fluctuation in pressure profiles. The conditions of bed, however, could recover rapidly from this serious disturbance. The isothermal bed temperatures as well as the persistent fluctuation of bed pressure at relatively uniform amplitude and constant baseline were clearly observed in both experimental conditions (H_b/D_b= 0.5 and 1). The changes in amplitude and

baseline of bed pressure relative to the different air velocity were not clearly observed. After 8 hour of trial, no agglomerate was found in the cold spent bed samples.

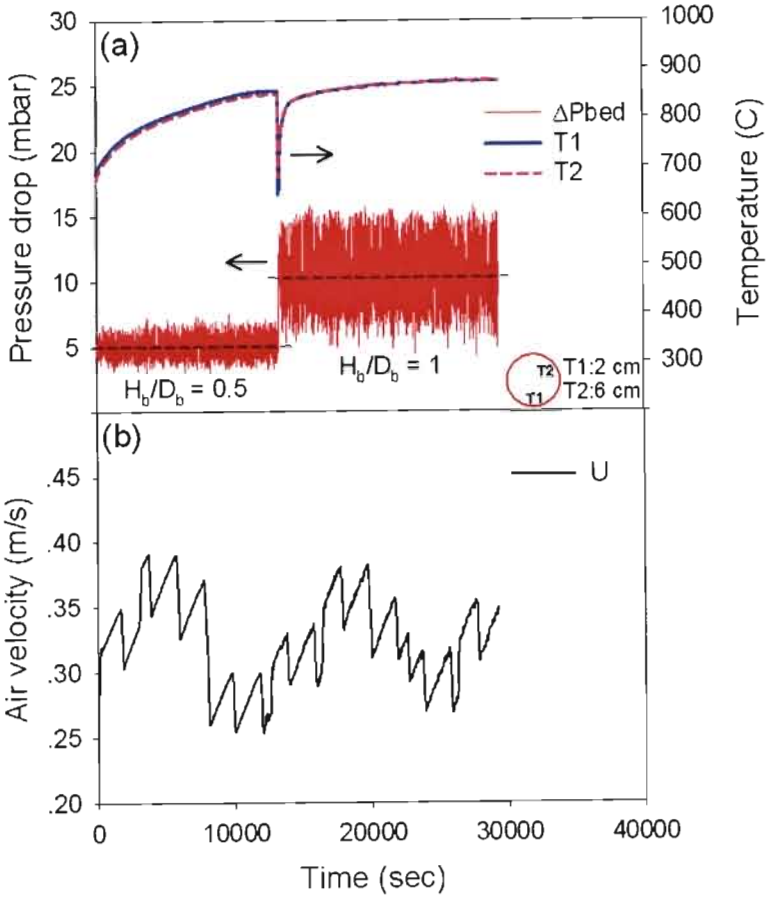

Figure 5.4 Typical bed pressure drop and temperature profiles of the pre-test for d_p=425-500 μm (a) pressure and temperature profile and (b) air velocity.

The isothermal condition inside the fluidized bed was unique due to the intense in-bed heat transfer as a consequence of turbulent bed mixing. Bed pressure drop was directly related to the mass of bed as described by the balance between the net gravitational force and the friction force exerted by fluid in Ergan's equation [148]. The fluctuation in bed pressure originated from the passage of bubbles between the pressure probe and the downwards propagating pressure wave formed by erupting bubbles at the bed surface [148,175]. The increased amplitude as a result of increasing bed height was assumed to be connected to a larger bubble size at the bed surface of higher bed height [175-176], where as an effect of the air velocity on the bed pressure was also in accordance with a previous experimental result [176].

5.2.2 Lab scale agglomeration test

The controlled operating conditions and the main results of lab scale test in term of defluidization time (t_{def}) and potassium consumption to bed mass ratio (K/Bed) were summarized in Table 5.5.

Table 5.5 Summary of operating conditions and main results of lab scale agglomeration test

Run	T_b (°C)	U (m/s)	d_p (µm)	H_b/D_b	K/Bed (x1000)				Defluidization time (t_{def},sec)			
					Palm shell	Corncob	Palm bunch	Straw	Palm shell	Corncob	Palm bunch	Straw
1	700	0.25	300-355	0.5	-	-	1.39	-	-	-	7,061	-
2	800	0.15	300-355	0.5	-	-	0.32	1.16	-	-	1,357	2,326
3	800	0.25	300-355	0.5	-	-	0.43	2.17	-	-	2,262	4,586
4	750	0.15	300-355	1.0	-	-	0.38	1.47	-	-	4,011	5,611
5	800	0.15	300-355	1.0	-	-	0.25	1.02	-	-	2,231	5,201
6	800	0.20	300-355	1.0	-	-	0.28	1.30	-	-	3,286	5,516
7	800	0.25	300-355	1.0	-	-	0.38	2.08	-	-	4,221	6,951
8	850	0.15	300-355	1.0	-	-	0.22	0.88	-	-	1,981	3,516
9	850	0.25	300-355	1.0	2.25	1.39	0.32	1.77	42,353	11,377	2,893	4,473
10	900	0.15	300-355	1.0	-	-	0.20	0.79	-	-	861	2,001
11	800	0.25	425-500	1.0	2.86	1.30	0.28	1.29	55,321	15,793	1,296	3,481
12	850	0.25	425-500	1.0	1.29	0.97	0.24	1.08	26,033	5,793	1,216	2,721
13	900	0.25	425-500	1.0	0.83	0.79	-	-	14,545	5,401	-	-
14	850	0.32	425-500	1.0	2.80	1.10	-	-	42,657	8,681	-	-
15	850	0.40	425-500	1.0	3.53	1.33	-	-	54,281	10,461	-	-
16	900	0.40	425-500	1.0	3.02	1.26	-	-	39,169	8,601	-	-
17	900	0.25	300-355	1.0	2.24	1.10	-	-	26,009	8,553	-	-
18	850	0.25	425-500	0.5	2.22	1.15	-	-	24,081	3,729	-	-
19	850	0.32	425-500	0.5	3.07	1.21	-	-	33,977	4,185	-	-
20	850	0.25	300-355	0.5	3.84	1.51	-	-	40,529	5,425	-	-

1. Bed behaviors

The behaviors of bed during agglomeration were illustrated in Figures 5.5-5.6.

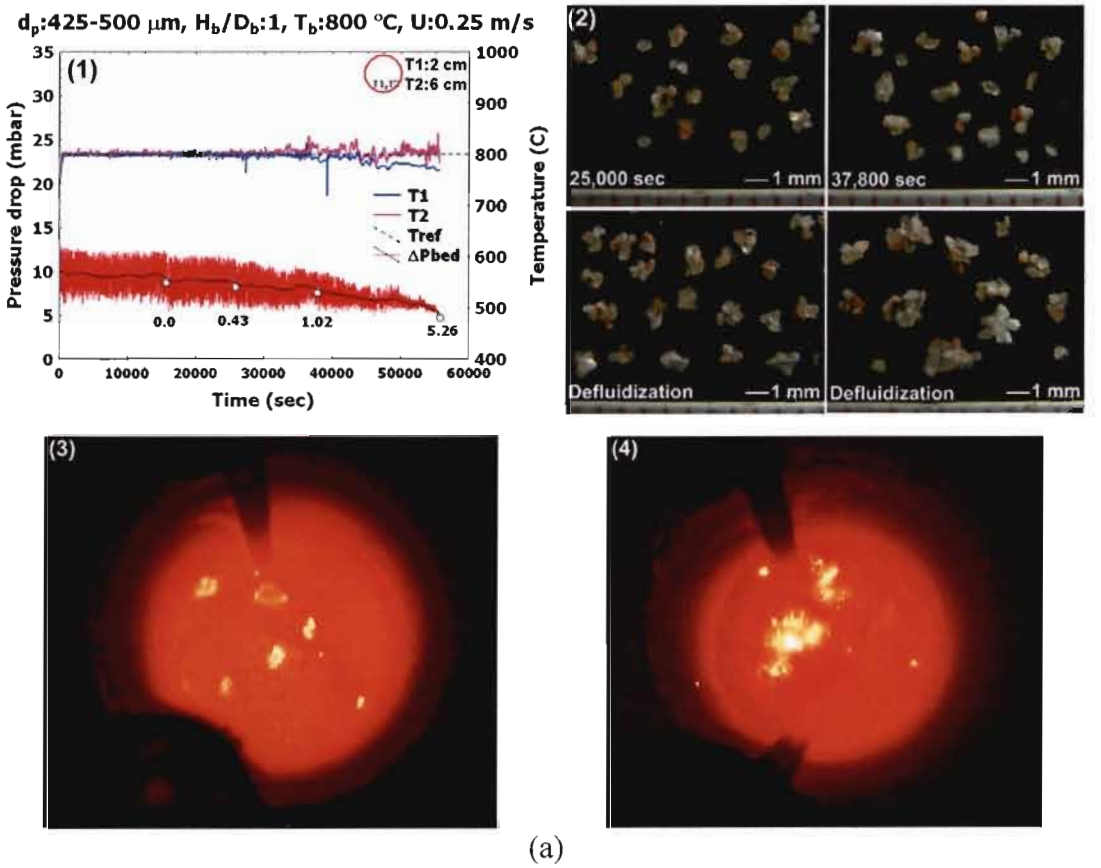

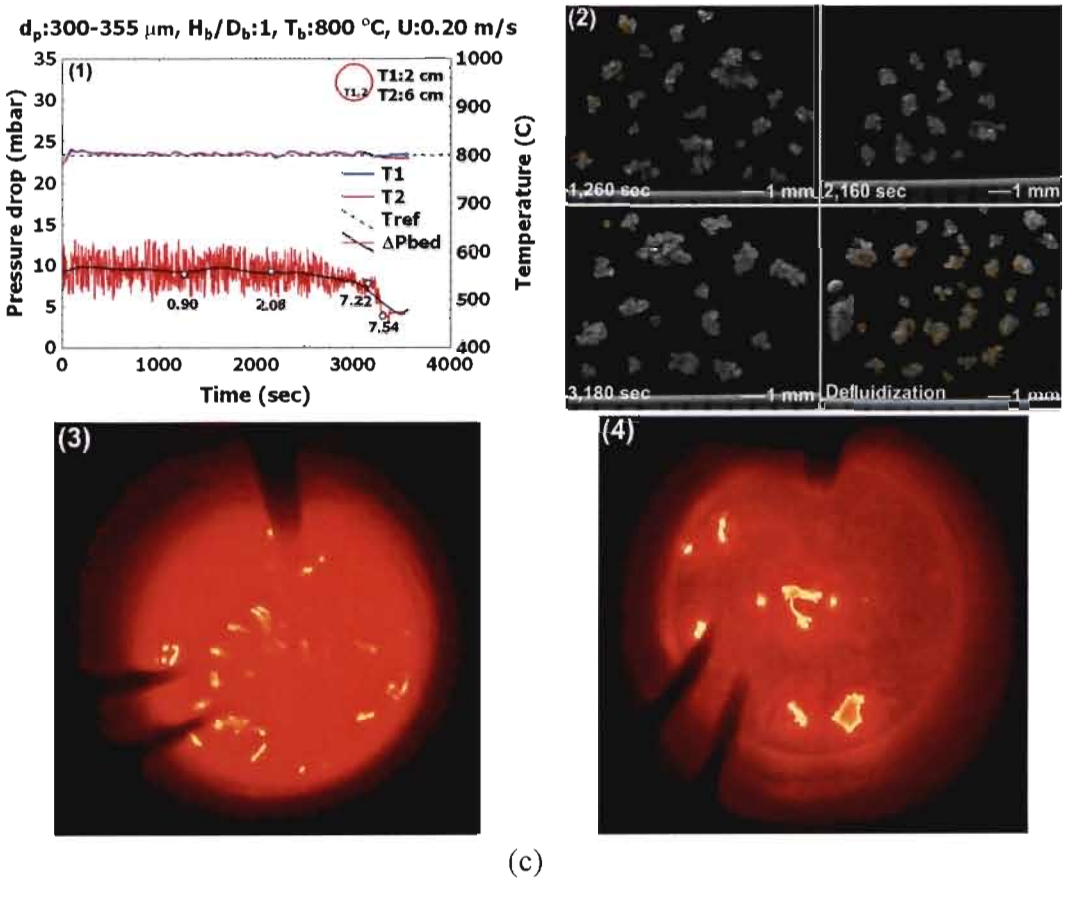

(c)

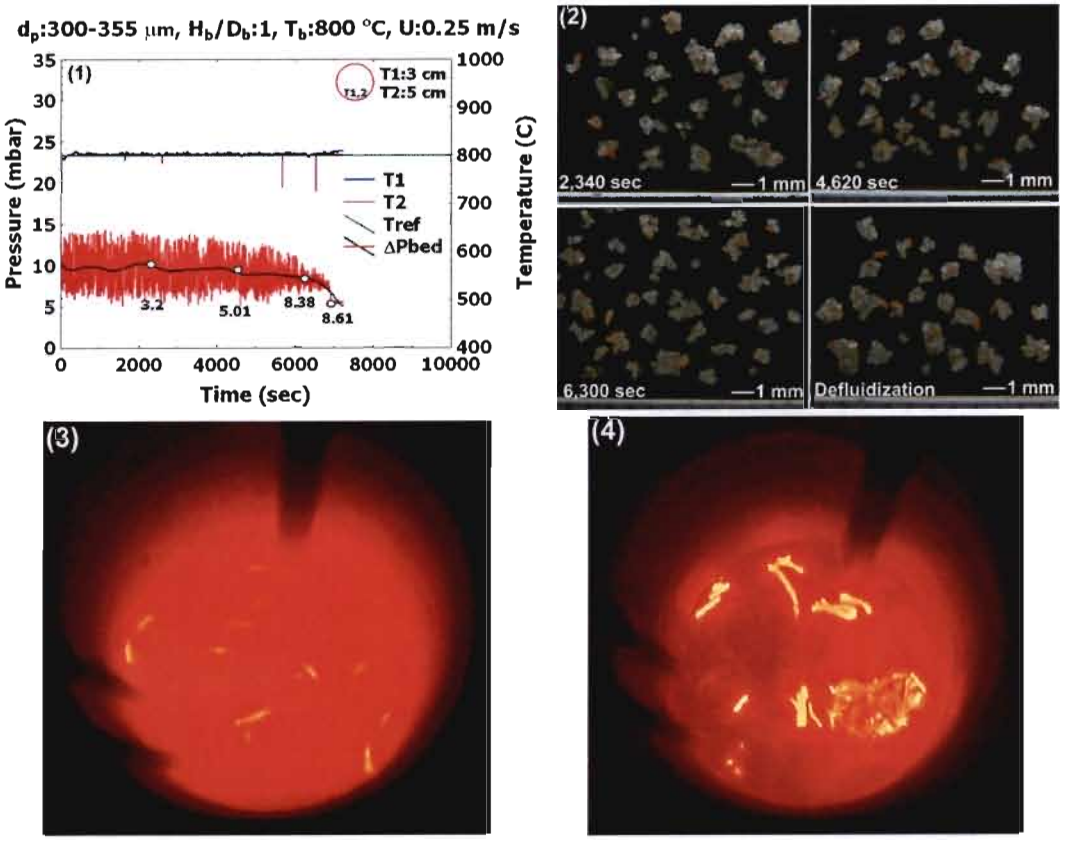

(d)

Figure 5.5 Typical bed behaviors during combustion of (a) palm shell, (b) corncob, (c) palm bunch, and (d) rice straw in lab scale fluidized bed combustor.

The behaviors of bed, as well as the agglomerate samples, at specific conditions during combustion of biomass in a lab scale fluidized bed from start until defluidization were reported typically in Figure 5.5. All biomass samples showed similar behaviors that bed pressure base line and its magnitude of fluctuation upon defluidization decreased steadily during combustion until complete defluidization (Sub-fig. 1), while the non-uniform bed temperatures occurred but it was not clearly observed in a number of trials. The agglomerates accumulated in the bed as the trials progressed. This was indicated by the exponentially increasing percentages of agglomerates in the drawn bed samples at different lengths of operating time, as reported beneath the pressure line. However, the agglomerate fractions were lesser than 10 wt% in all bed samples at complete defluidization. Agglomerates found were formed in various sizes and easily breakable (Sub-fig. 2). Channeling flow of air through the bed at defluidization (Sub-fig. 4), compared with the bed at beginning (Sub-fig. 3), can be observed visually. The higher temperature of fuel particle than bed temperature was noticed by its glowing combustion.

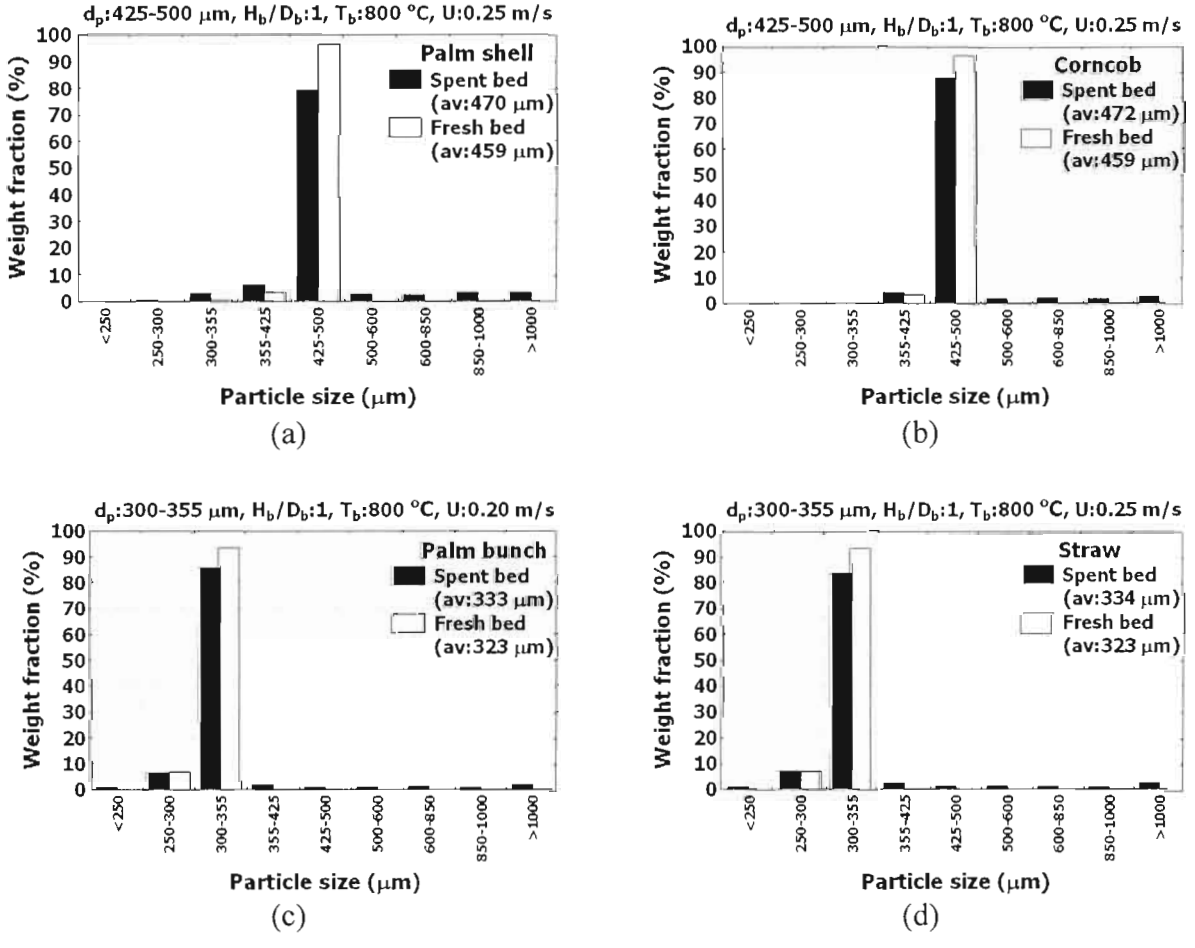

Figure 5.6 Typical particle size distributions of completely defluidized bed compared with fresh bed at specific conditions when burning (a) palm shell, (b) corncob, (c) palm bunch, and (d) rice straw in a lab scale fluidized bed.

An increase in bed particle size was evident from the size analyses of spent bed against fresh bed as shown in Figure 5.6, even though it was affected by partial breaking of agglomerates during discharge and sieving.

An increase in the number and growth of agglomerates inside the bed had established the more multi-size particles in bed. This essentially induced (i) an increased bed void fraction; channeling and decreasing pressure were as a result; the decreasing amplitude was also reflected to the decreasing size of flowing air bubble [176], (ii) a poor bed mixing that caused consequently a segregate combustion zone and local hot spots in bed. The occurrence of bed defluidization that directly affected the bed hydrodynamics was more clearly detectable from the pressure measurement. The bed started to be defluidized as the agglomerates began to be formed, and defluidization was progressively developed from being partial to completion.

To verify the decrease in experimental bed pressure drop, which is caused mainly by the bed agglomeration but can not be affected by the amount of samples taken out for analyses, the bed pressure drop of each trial was therefore estimated by Ergan's equation using initial particle size, and from the retained mass of bed material upon defluidization, and was found to be considerably higher (96-97% of initial bed pressure drop) than that of observed experimental values (60-75% of initial bed pressure drop upon defluidization). This clearly indicated that the decrease of bed pressure drop during the trial is certainly caused by bed agglomeration.

2. Bed agglomeration tendency

The main results of the lab scale agglomeration test in Table 5.5 were reported in terms of the defluidization time (t_{def}) and potassium to bed ratio (K/Bed). t_{def} was the time interval from the start of fuel feeding to the complete defluidization. The defluidization rate, or the formation rate of agglomeration, was inversely proportional to t_{def}; the lower the t_{def}, the higher this rate. K/Bed was well-defined as the maximum of potassium consumed by bed until complete defluidization. It was calculated as the total potassium input from fuel consumption divided by the initial bed inventory, which referred to the quantity of K consumed to completely defluidize the bed. The influences of the bed operating variables on the bed agglomeration tendency were described allegorically by t_{def} and K/Bed. In order to elucidate easily on the bed agglomeration tendency, the results in Table 5.5 were repeated graphically into Figures 5.7-5.11 viz.

It was noticed in Table 5.5 that, entirely, FBC of all given biomass fuels at given operating conditions suffered eventually the defluidization.

- **Effect of fuel inorganic composition**

In Figures 5.7a and 5.7b with the same operating conditions on Run No.9, 11 and 12, the effect of ash composition showed very significant on the bed agglomeration. The outstandingly larger t_{def} and K/Bed of palm shell indicated to its lower bed agglomeration tendency, while palm bunch also showed the markedly opposite results. This could be attributed to the comparatively low K content of palm shell. The higher K content can lead to the larger amount of formed eutectic melts serving as an adhesive material in agglomerates [51]. However, this reason was evidently uncertain. Palm bunch combustion showed the relatively higher tendency in all cases over than corncob combustion, as indicated by lower t_{def} and K/Bed, despite its significantly lower K content (Fig. 5.7c). It might be caused by the relatively high Cl content of palm bunch, which could facilitate the release of inorganic species and enhance the formation of molten K-derived compounds [62,69,85]. The evidences to this effect would be shown and discussed later, elsewhere. The agglomeration tendency of corncob against with rice straw could not be given clearly in comparison.

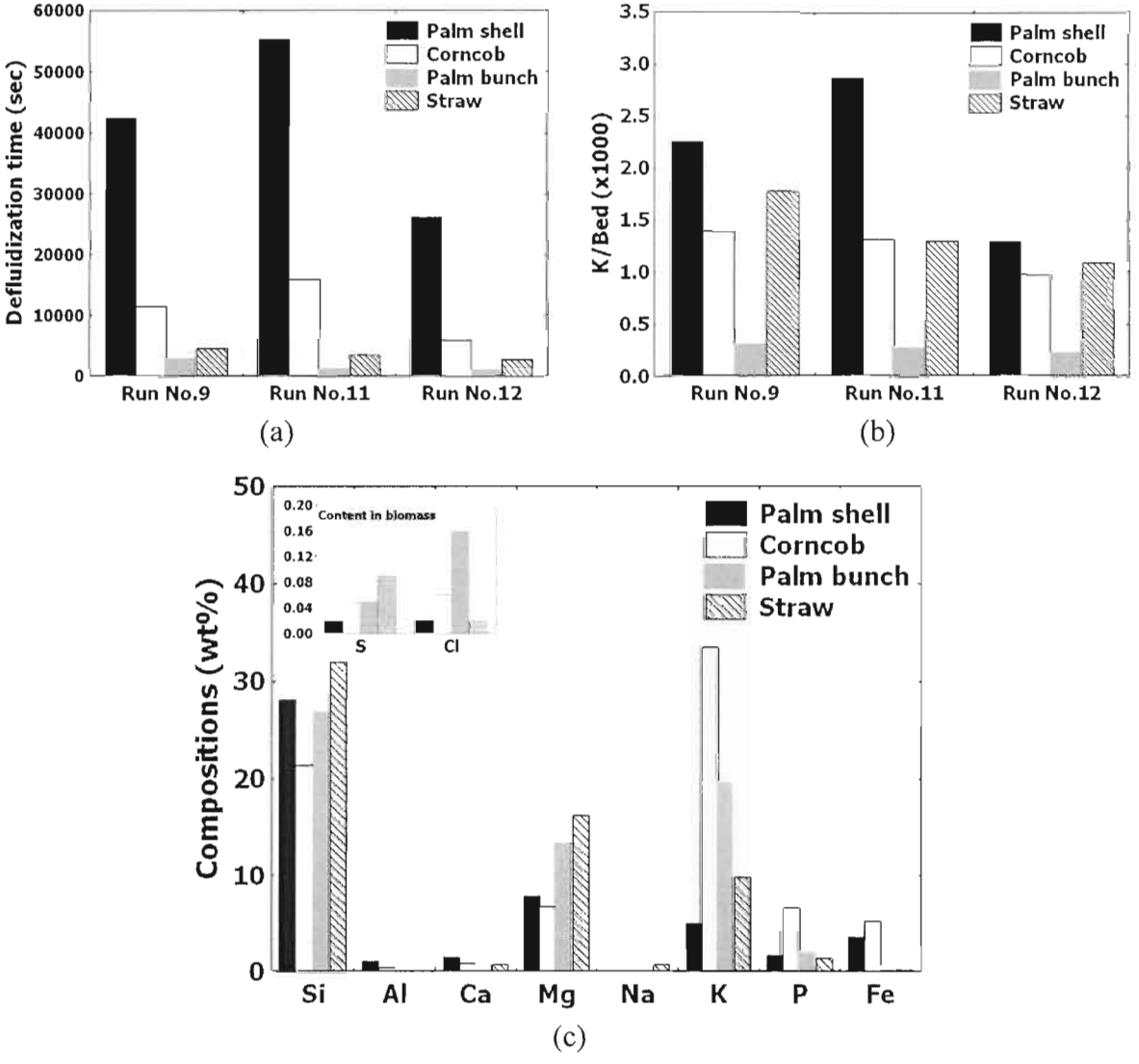

Figure 5.7 Bed agglomeration tendencies on fuel ash compositions described by (a) t_{def} (b) K/Bed, and(c) summary of biomass inorganic content.

- **Effect of bed (combustion) temperature**

t_{def} and K/Bed as a function of bed temperature were illustrated in Figure 5.8 and these results indicated that the bed temperature showed a significant effect. They both decreased exponentially as the bed temperature increased. The lower t_{def} at higher bed temperature came about the lesser K fed into bed, at relatively close fuel feed rate. As the temperature that exceeds the initial melting point of the ash-forming compounds in bed increases, the melt fraction increases [24] and viscosity of the melts decreases resulting to increase the adhesion efficiency [91]. Both factors may result in an increase of the amount and stickiness of coated bed particles by the melt. This in turn accelerates the defluidization process.

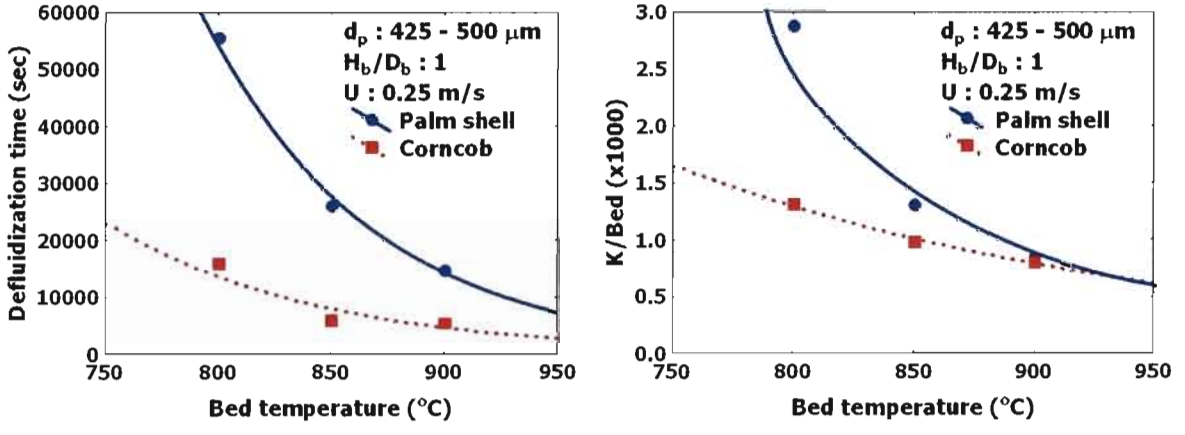

(a)

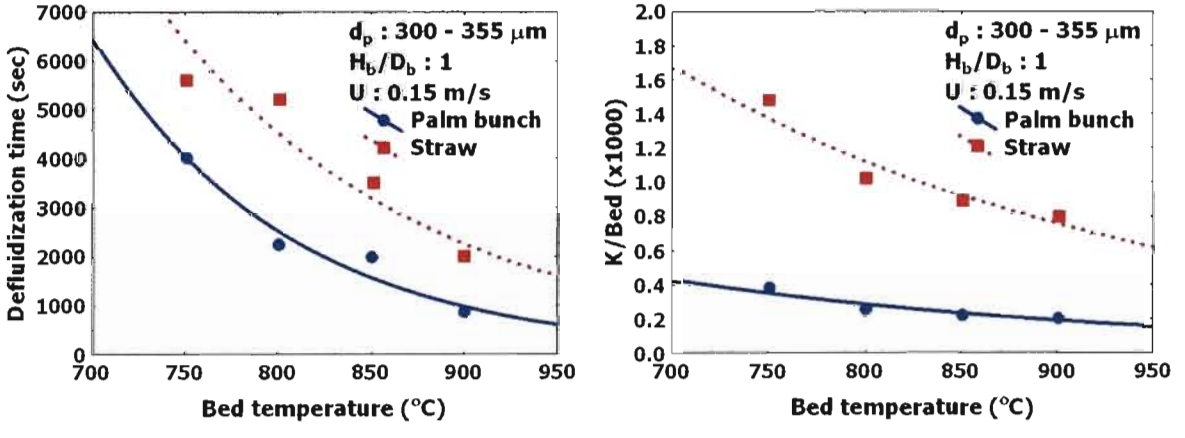

(b)

Figure 5.8 The effects of controlled bed temperature on the bed agglomeration tendency when burning (a) palm shell and corncob, and (b) palm bunch and rice straw in a lab scale fluidized bed.

- **Effect of superficial air velocity**

As shown in Figure 5.9, t_{def} and K/Bed for all biomass increased as the air velocity increased. The higher fluidizing air velocity increases the mobility of bed particles and the resultant force acting on the bed particles, induced by the gas bubbles [147-148]. This causes an increase in the attrition rate of coating, the elutriation rate of fine ash particles and the breaking rate of agglomerates via collision. These phenomena delay the defluidization, and the agglomerates needs more the ash melt to consolidate in order to reach the defluidization state.

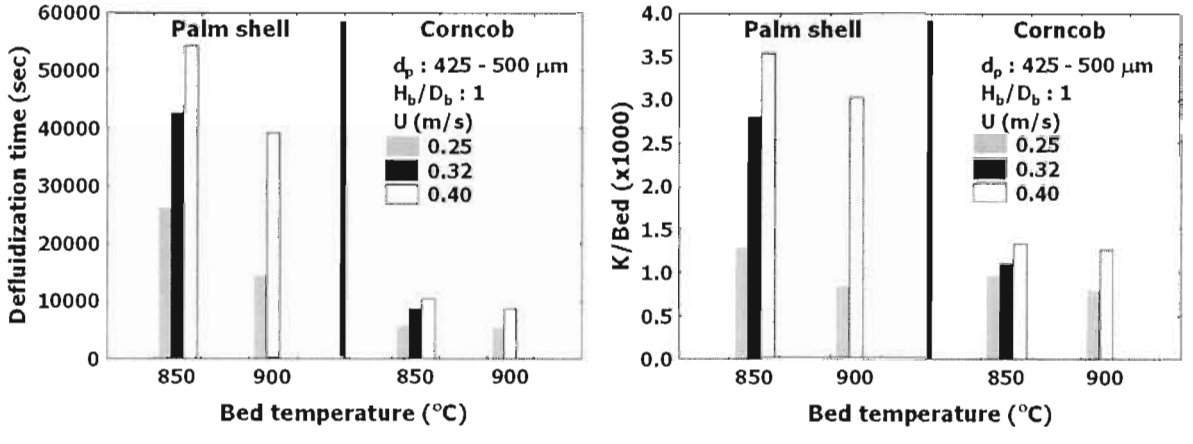

(a)

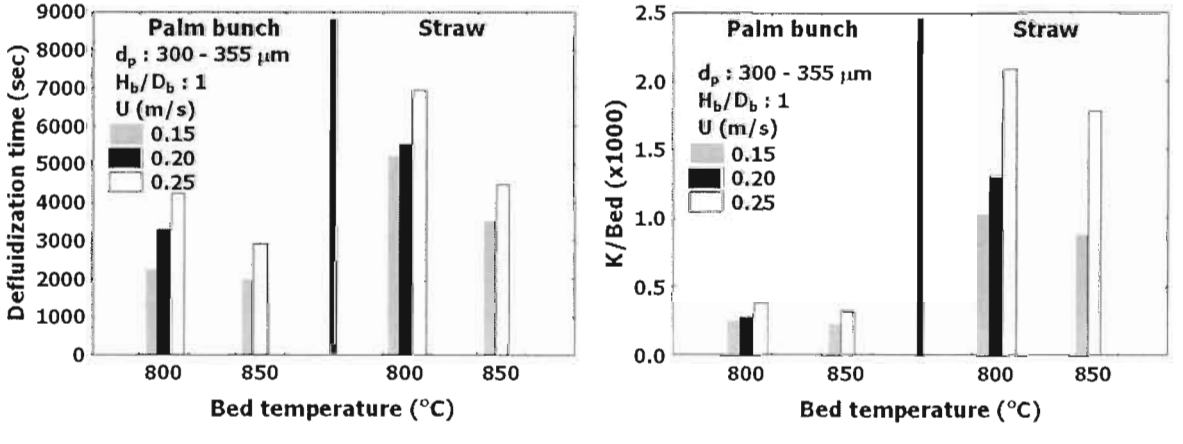

(b)

Figure 5.9 The effects of controlled fluidizing air velocity on the bed agglomeration tendency when burning (a) palm shell and corncob, and (b) palm bunch and rice straw in a lab scale fluidized bed.

- **Effect of bed particle size**

In the set of trials carried out with two different bed particle sizes, it was shown in Figure 5.10 that an increase of bed particle size clearly resulted in the lower t_{def} and K/Bed. A bed with the larger particle size has lower outer specific surface area, so it needs less the ash melts to form coating layers and necks. In additions, the bed mixing of larger bed grain is poorer at the same air velocity as the ratio of U/U_{mf} is lower, due to the higher U_{mf} for larger particles. This feature easily causes hot spots in bed, which enhances the formation of ash melt and the vaporization of ash constituents [51,110]. These two factors facilitate agglomeration and then accelerate defluidization.

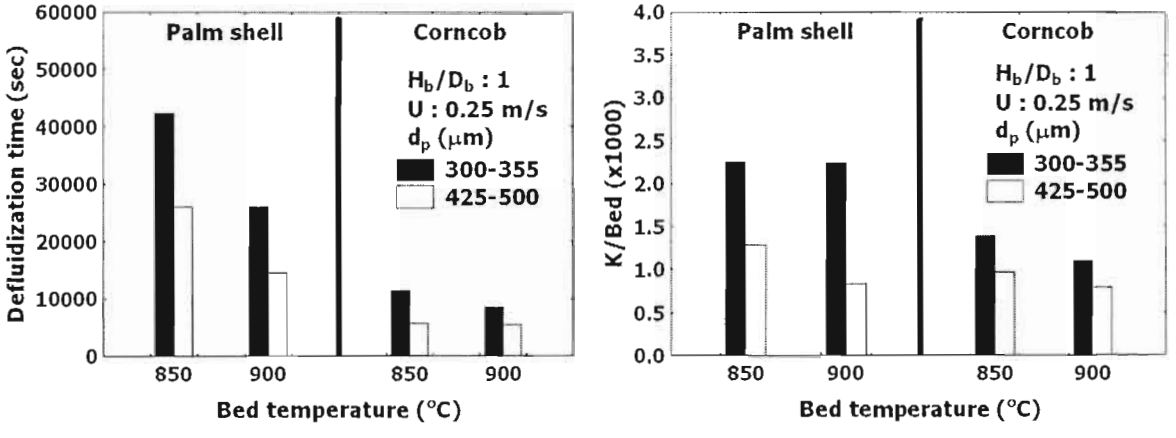

(a)

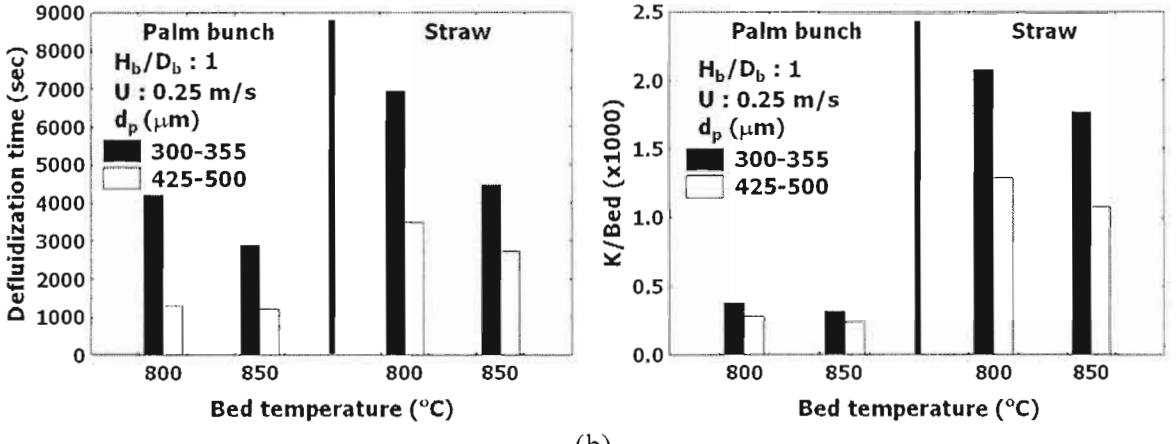

(b)

Figure 5.10 The effects of controlled sand size on the bed agglomeration tendency when burning (a) palm shell and corncob, and (b) palm bunch and rice straw in a lab scale fluidized bed.

In case of the same U/U_{mf} ratio at which the bed mixing behavior is supposed to be similar (Run No. 5 vs. 11 and 8 vs. 12 in Table 5.5), the increase of bed particle size showed the higher K/Bed. It is due to that larger particle has more inertia which consequently related to the higher energetic collision. Therefore, the adhesion to form agglomerates should be more difficult [51] and require the more amount of ash melt to form agglomerate. t_{def} may can not provide well suitable description in bed agglomeration tendency in this case, due to the difference in fuel feed rate as a consequence of the enhanced in-bed heat transfer and heat loss by flue gas from increasing air flow rate.

- **Effect of static bed height**

A set of the results for the effect of static bed height at different biomass was showed in Figure 5.11. The bed height was increased doubly as the mass of bed increased twice accordingly. The biomass consumption relative to K consumption in most trials increased less than twice and K/Bed for higher static bed height is resultantly lower. The increasing static bed height yields more surface area of bed particles, hence needing more amounts of ash melt, while the bed mixing is poorer and the ash melt in smaller fraction can stick easily to particles to form agglomerates. For this reason, the K/Bed of higher H_b/D_b showed lower while t_{def} showed an increasing trend, due to the poorer bed mixing. In this study, the effect of poor bed mixing was clearly seen from the reasonable decrease of K/Bed which otherwise would be relatively constant in value when the static bed height was doubled.

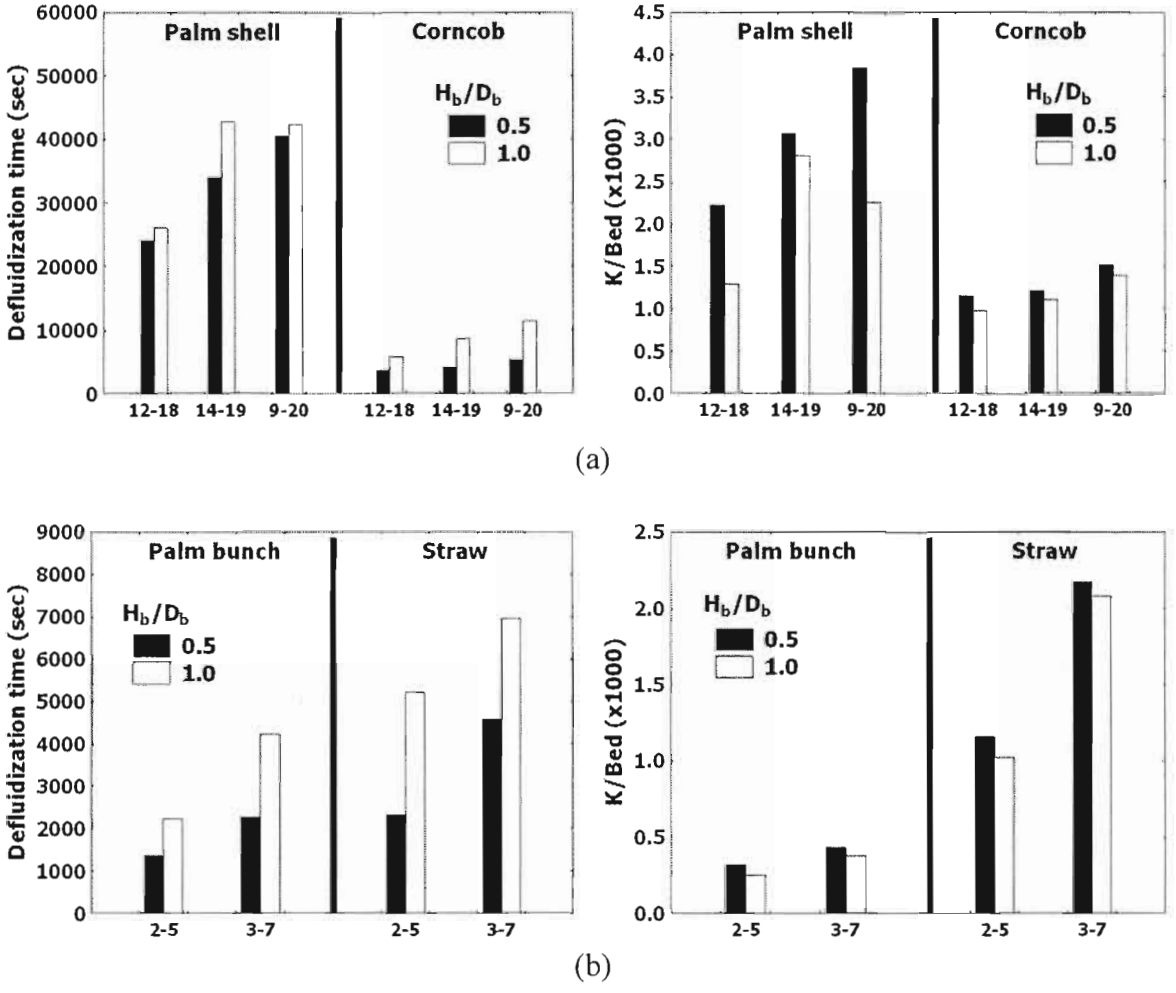

Figure 5.11 The effects of controlled static bed height on the bed agglomeration tendency when burning (a) palm shell and corncob, and (b) palm bunch and rice straw in a lab scale fluidized bed (No. in x-axis represent No. of Run in Table 5.5).

The influences of bed temperature, air velocity, particle size and static bed height on the bed agglomeration tendency in the present work were consistent with the experimental results reported in previous literatures [18,51,108-111,154].

The contributions of operating variables on the tendency of bed agglomeration in present work could be summarized in Table 5.6.

Table 5.6 Present summaries of bed variable contributions

Variable	Tendency
Alkali content	+
Bed temperature	+
Fluidizing gas velocity	-
Bed particle size	+
Static bed height	+

where the defludization by bed agglomeration was accelerated by an increased magnitude of a variable is described by the plus (+) and the opposite trend was referred as the minus (-).

t_{def} and K/Bed in this work showed good consistency and could be well for comparative characterization toward the bed agglomeration tendency. However, it must be noted that the elutriation loss of ash was not taken into account in K/Bed. t_{def} is also relative to the fuel feed rate It had been suggested that the rate of defluidization is considered to be the competition between the formation rate of stable bond and the breaking rate of agglomerated particles [109]. The former is a result of melt formation while the latter is significantly dependent upon the fluidization characteristics. Defluidization can take place rapidly if the former process is enhanced by the accumulation of K in bed and/or the increasing bed temperature; and the latter process is worsened by some certain conditions leading to the poor bed mixing.

5.2.3 Pilot scale agglomeration test

The conditions and results of pilot scale experiment similarly reported in term of t_{def} and K/Bed were shown in Table 5.7.

Table 5.7 Summary of pilot sale results

Run	Biomass	T_b (°C)	U (m/s)	$d_{p,av}$ (μm)	$H_b/D_{b,eq}$	Result	
						K/Bed (x1000)	t_{def} (sec)
1	Corncob	850	0.59	573	0.5	1.12	5,797
2	Palm shell	860	0.59	573	0.5	2.99	14,711
3	Palm shell	900	0.61	573	0.5	2.81	13,426
4	Palm bunch	810	0.35	354	0.5	1.02	2,376
5	Palm bunch	850	0.37	354	0.5	0.63	1,331
6	Rice straw	820	0.35	354	0.5	2.42	4,031

1. Bed behaviors

The behaviors of bed in pilot scale fluidized bed during agglomeration were illustrated in Figures 5.12-5.13.

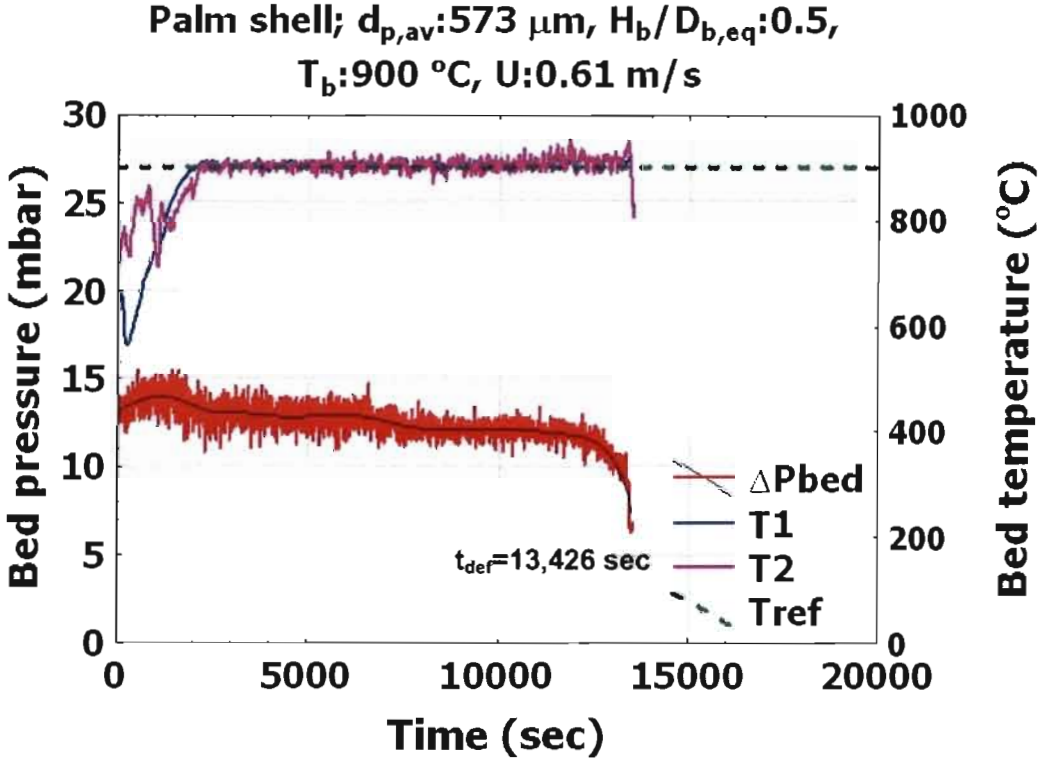

(a)

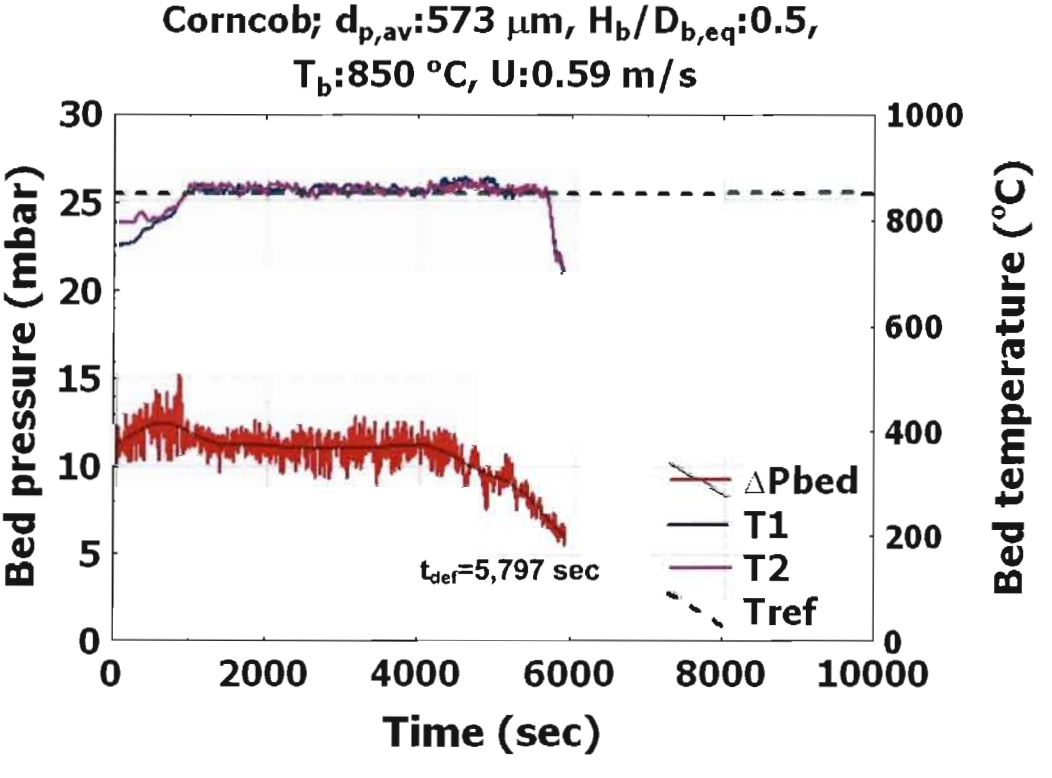

(b)

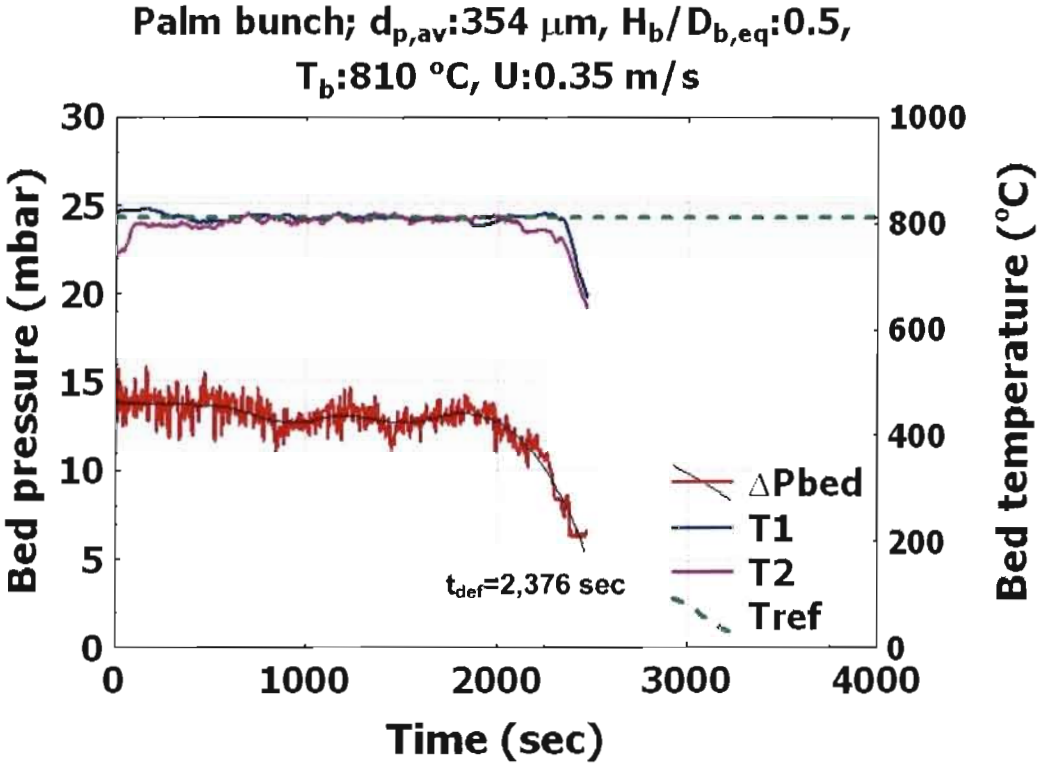

(c)

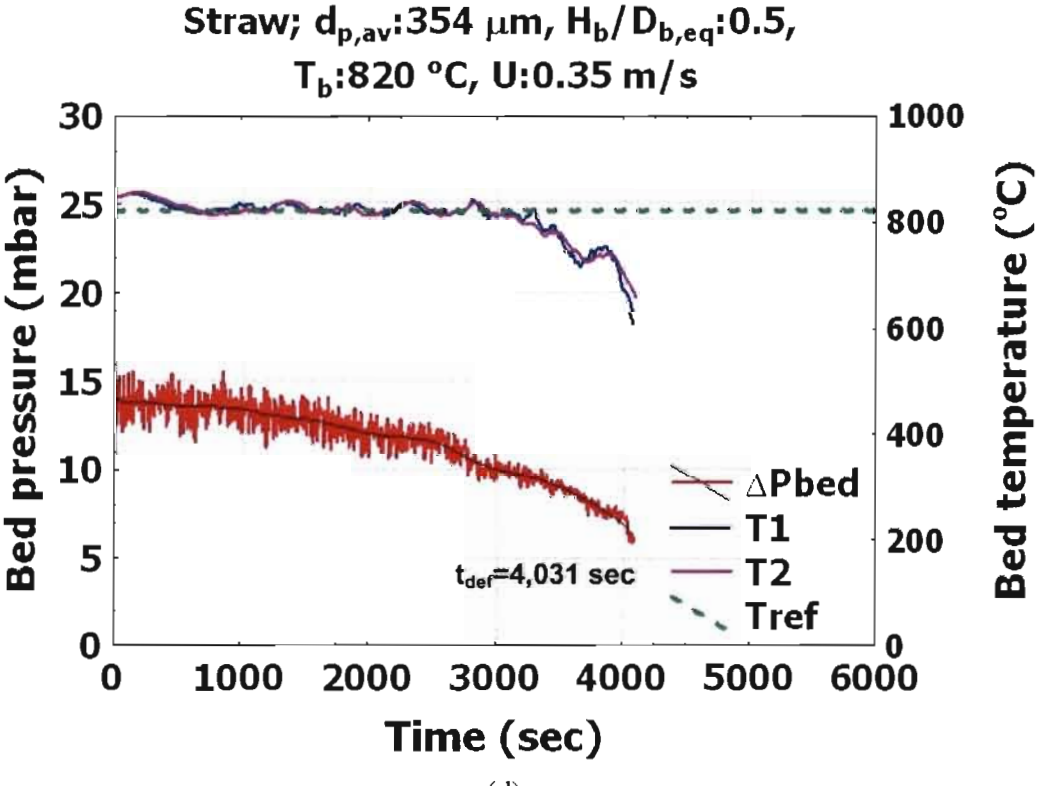

(d)

Figure 5.12 Typical bed pressure loss and bed temperature profiles during agglomeration in a pilot scale fluidized bed burning (a) palm shell, (b) corncob, (c) palm bunch and (d) rice straw.

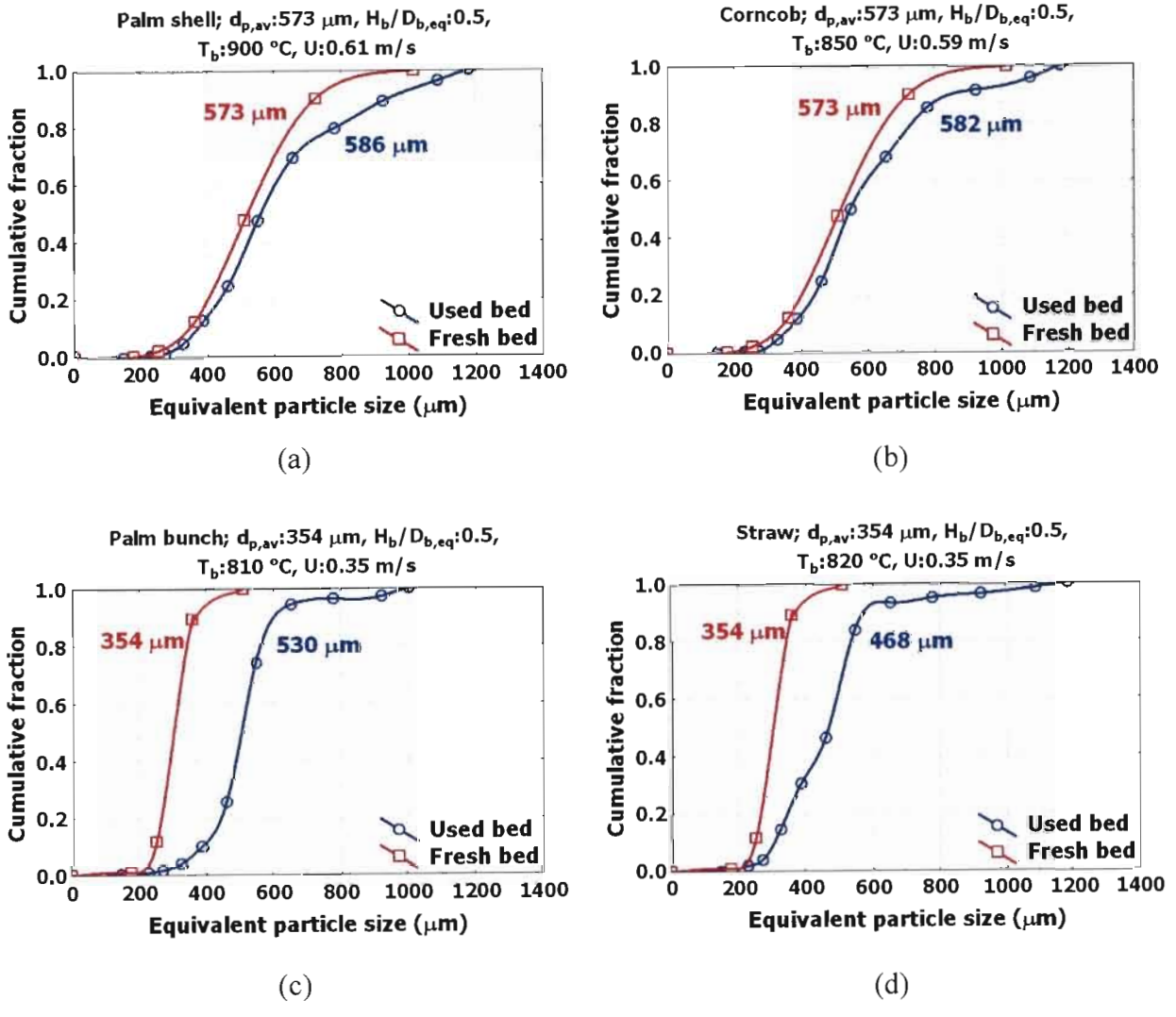

Figure 5.13 Typical size distribution of bed particle in a pilot scale fluidized bed burning (a) palm shell, (b) corncob, (c) palm bunch and (d) rice straw compared with the fresh bed.

The illustrations of typical bed pressure drop and temperature profiles during combustion in pilot scale FBC were shown in Figure 5.12. The similarity in bed behaviors relative to the lab scale test could be observed. As defluidization started, the pressure baseline and magnitude of fluctuation decreased until complete defluidization. Inhomogeneous bed temperatures were clearly observed. After the test, the bed particles had larger mean size, as depicted in Figure 5.13. The extension of bed agglomeration induced the increasing voidage inside bed as indicated by descending bed pressure and the decreasing amplitude, which was connected to the decreasing size of flowing air bubble through the bed. The subsequent result of poor bed mixing occurred and caused the segregated combustion zone in bed, and was shown by the inhomogeneous bed temperatures.

2. Bed agglomeration tendency

As reported in Table 5.7, the comparative degree of bed agglomeration affected by operating parameters also showed an agreement to some results of lab scale test. Corncob and palm bunch showed the higher bed agglomeration tendency than palm shell and rice straw, respectively, as indicated by their entirely lower in t_{def} and K/Bed. The higher content of problematic K and Cl elements is the main reason. The higher combustion temperature can accelerate the defluidization (Run No. 2 vs 3 and 4 vs 5).

5.3 Agglomerate characterizations

In order to investigate the interactions of the ash forming constituents with the bed particles, SEM-EDS analyses were carried out. A set of typical SEM images on the cross-sectioned agglomerates obtained from the bed at defludization state of some conditions were shown below. The EDS spot compositions given in the accompanying multiple bar graphs corresponded to the numbering.

5.3.1 Lab scale agglomerates

Figures 5.14 to 5.17 showed the SEM micrographs in backscatter mode of agglomerate samples at defluidization during combustion of palm shell, corncob, palm bunch, and rice straw, respectively, in lab scale fluidized bed.

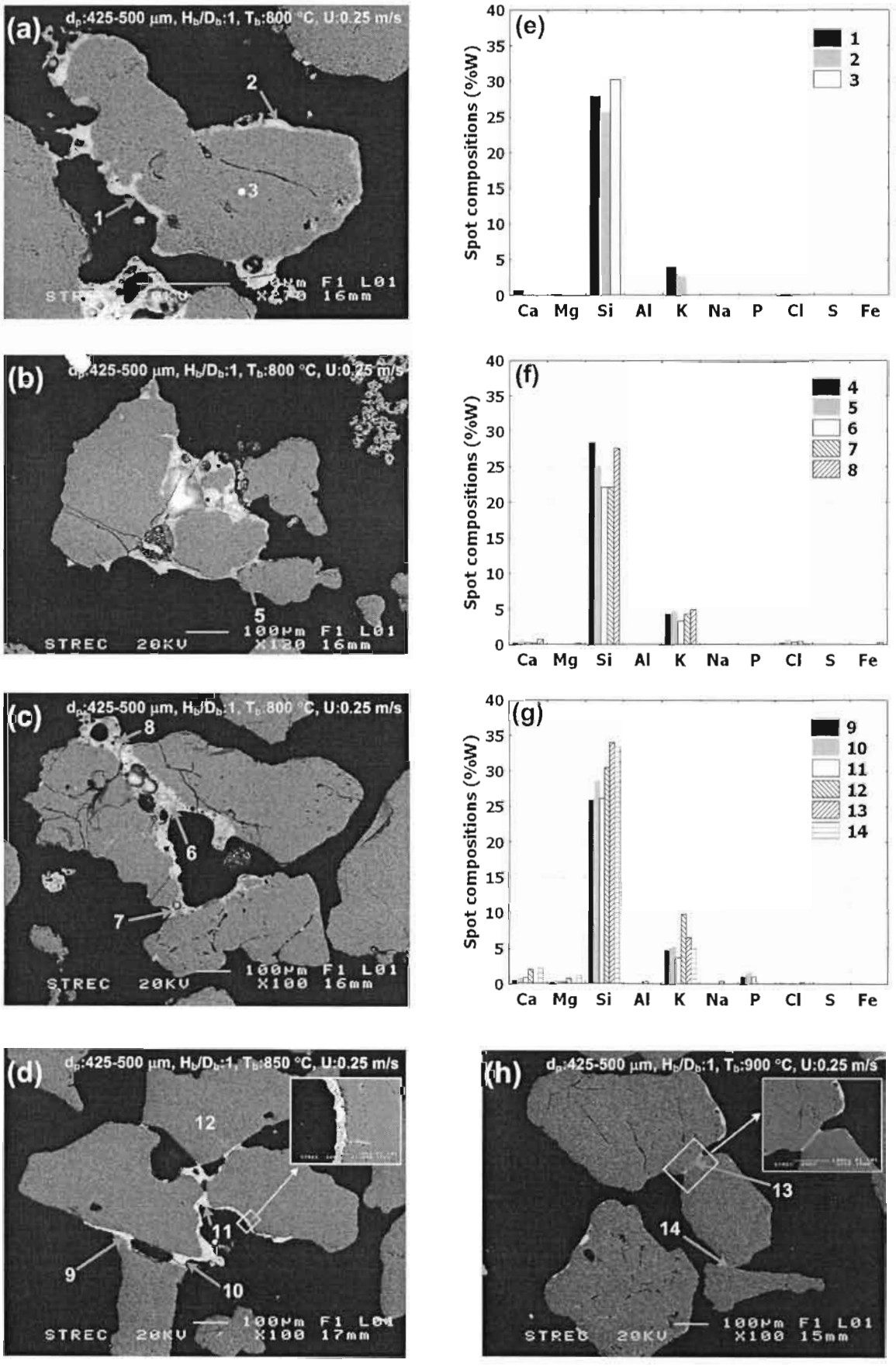

Figure 5.14 Typical SEM images and Spot EDS compositions of palm shell agglomerates from lab scale FBC tests.

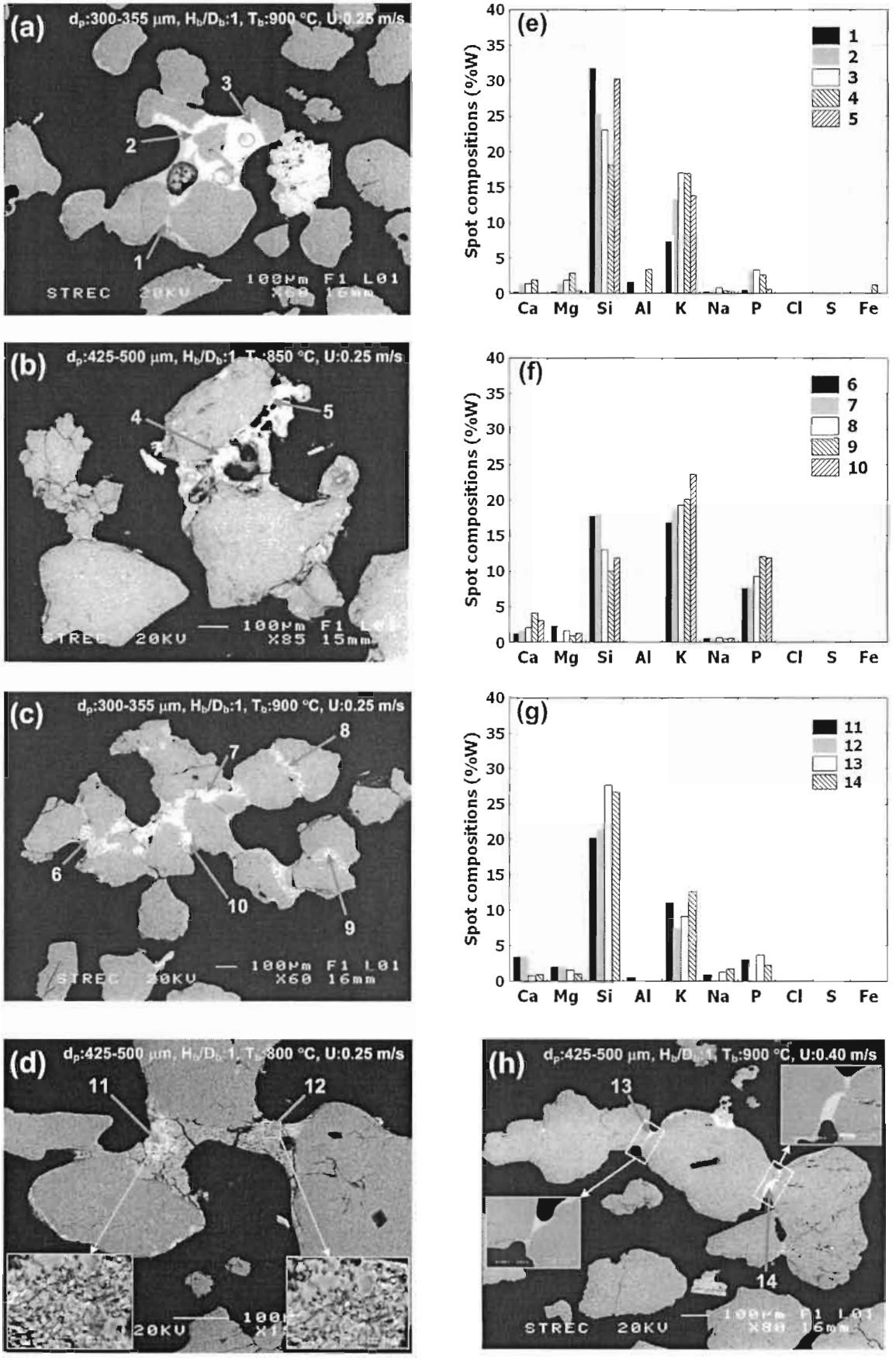

Figure 5.15 Typical SEM images and Spot EDS compositions of corncob agglomerates from lab scale FBC tests.

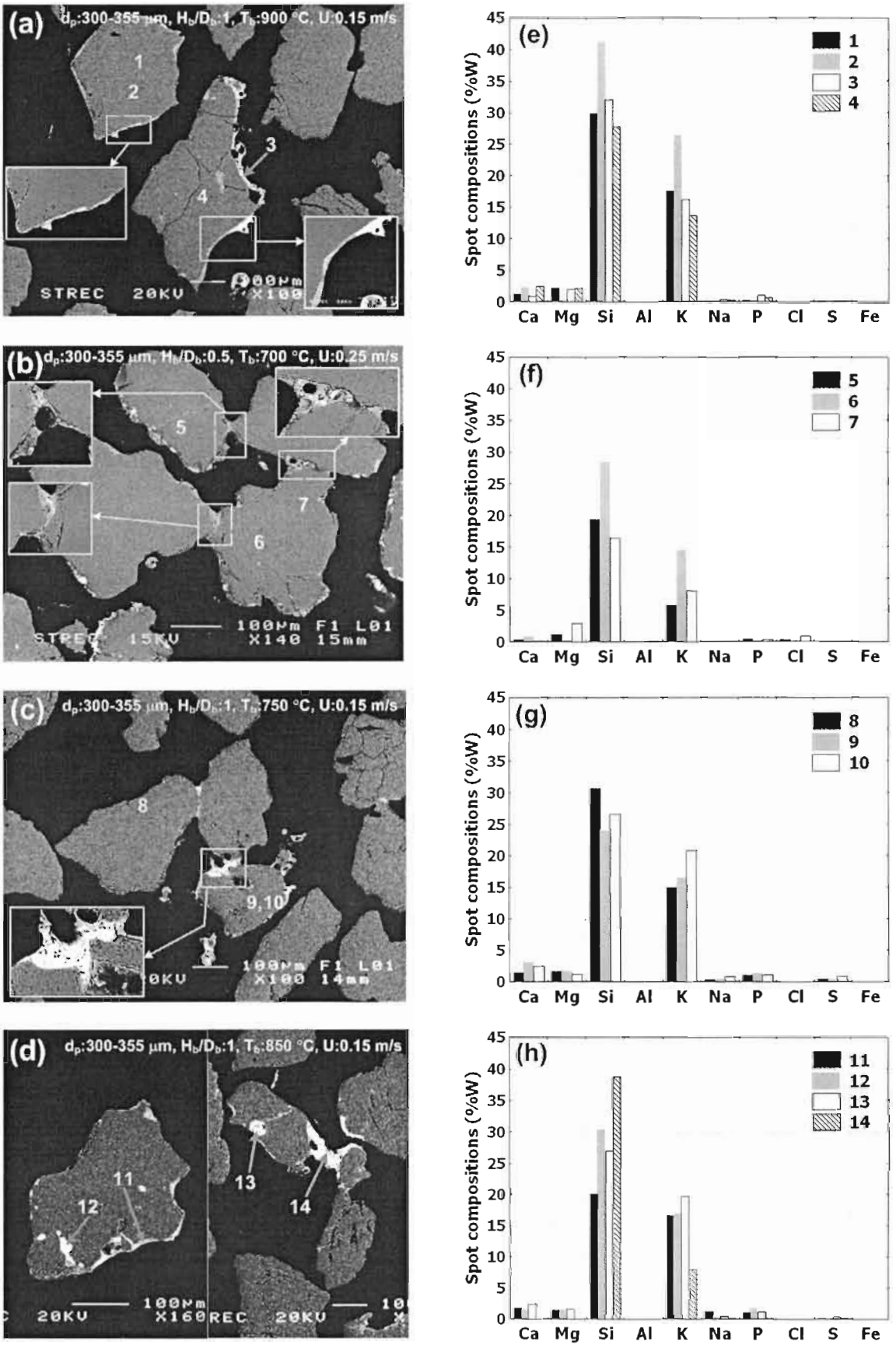

Figure 5.16 Typical SEM images and Spot EDS compositions of palm bunch agglomerates from lab scale FBC tests.

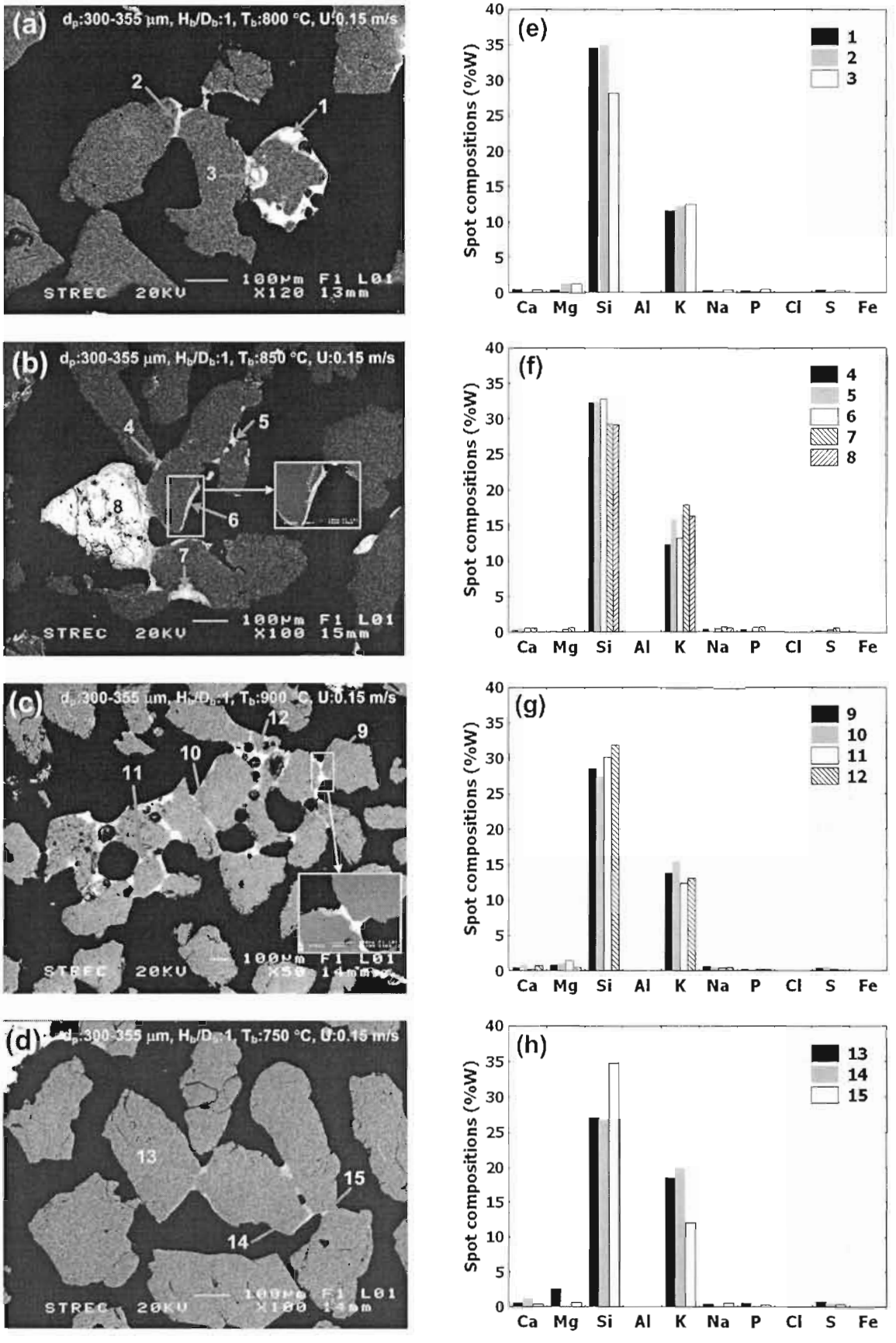

Figure 5.17 Typical SEM images and Spot EDS compositions of rice straw agglomerates from lab scale FBC tests.

In Figures 5.14-5.17, they revealed that sand particles (gray) in agglomerates were covered and cohered together by the fused materials (white) rich in Si and K, and Na, Ca, Mg and P to a lesser extent. Relatively, the rich P in the corncob agglomerates was noticed. S in diminutive fraction was detected while it seemed that Cl vanished in agglomerates.

Sand grains captured in agglomerates were attached together by either neck of material (Fig. 5.14h) or bonded layer (Fig. 5.14c). Both the total (Fig. 5.14b, 5.15a and 5.17a) and partial (Fig. 5.14d and 5.16a) coatings on bed particles could be observed. Concave and convex edges in the features of coating and neck appeared on the polygon shaped sand. The hollow structure had been found on bed particle surfaces (Fig. 5.14a and 5.16a) or located between the sand particles (Fig. 5.14c, 5.15b, 5.16c and 5.17c). The porous coating layers and necks were observed (Figure 5.14d, 5.15d and 5.16a). These non-homogeneous structures were commonly found while thin necks of relatively homogeneous matter were found in a specific contact point between particles (Figure 5.14h, 5.15h and 5.17d). The attack propagating inwards sand grain (in cracks or surface diffusion) was noticed in some palm bunch agglomerates (Fig 5.16d).

The above results gave clear evidence that the formation of biomass ash derived molten compounds, which presented likely as Potassium Silicates, was the main reason for the bed agglomeration in this study. The hollow structures indicated that the burning char particle was previously located inside. So it is likely that the agglomerates start to be formed near the burning char where the formation of molten ash on the char surface is enhanced by high surface temperature of char particle; about 50-200 °C significantly higher than bed temperature, based on calculation. This molten ash on char surfaces causes char particle becoming sticky. As sand grains collide with the burning char particles, they may adhere to the char surface. Collision from bed mixing, however, can break this coherence and the remnant melt is left on sand surface. This is an important way of inorganic migration, namely the collision mechanism. If no breaking due to a local poor bed mixing, the formed hollow structure as the remaining ash skeleton from burnt out char would appear.

The melts migrating from the high temperature of char surface to the lower temperature of sand surface may be partly solidified; hence the partially molten coating layer occurs. Bed particles having the liquid phase presents on their surfaces has more inertia and tend to get close to the larger fuel char particles, and resultantly the continuous deposition of the additional melt on the limited sand surface extend the porous coating and finally the agglomerates are developed by the porous bonding necks with certain thickness. The agglomerate supported by thin necks may be formed by the rapid formation of the melt and the sudden adhesion. Other possible migration ways of inorganic elements to bed grain are condensation/deposition of inorganic gases/aerosol [69, 81], of which the evidences were given in Figure 5.16d. The diffusion of K in existing cracks or from surface of sand particle results in the formation of K-silicates toward the core of sand grains, as the compounds with higher thermochemical stability [69]. This material may partially be solidified at typical bed temperature and thus allows the additional K to diffuse through the early formed high porous silicate layer, accelerating a continuous widening of the attacking silicates formation. It should be noted that the diffusion of potassium is the rate determining step in the K-Silicates formation rate. This mechanism enhances the formation of the silicate melt and may be further responsible for the relatively high agglomeration tendency of palm bunch.

Two kinds of agglomerates could be observed in the same spent bed samples (Figs. 5.14b and 5.14c). Agglomerate with thin neck was composed to a great extent of two to four particles while agglomerate of a larger number of sand grains was supported by the larger amount of the melt, by the thicker layer or larger number of neck. Previous studies suggested that the adhesive force by the melt ash is strongly dependent on the amount and stickiness [109,160]. Agglomerate formed by large amount of the melt may require some certain resident time to develop the coating layer and neck while agglomerate supported by thin necks is suddenly formed by rapid formation of the melt [72]. The former agglomerate may thus appear in the bed at the early combustion stage while the latter, having a weaker structure, may dominate in the bed upon defluidization or otherwise in a local poor bed circulation zone, such as the corner of furnace chamber.

5.3.2 Pilot scale agglomerates

Typical agglomerate samples obtained from pilot scale experiments, including EDS analyses, were shown in Figures 5.18-5.22 during palm shell, corncob, palm bunch and rice straw combustion, respectively, in a pilot scale fluidized bed.

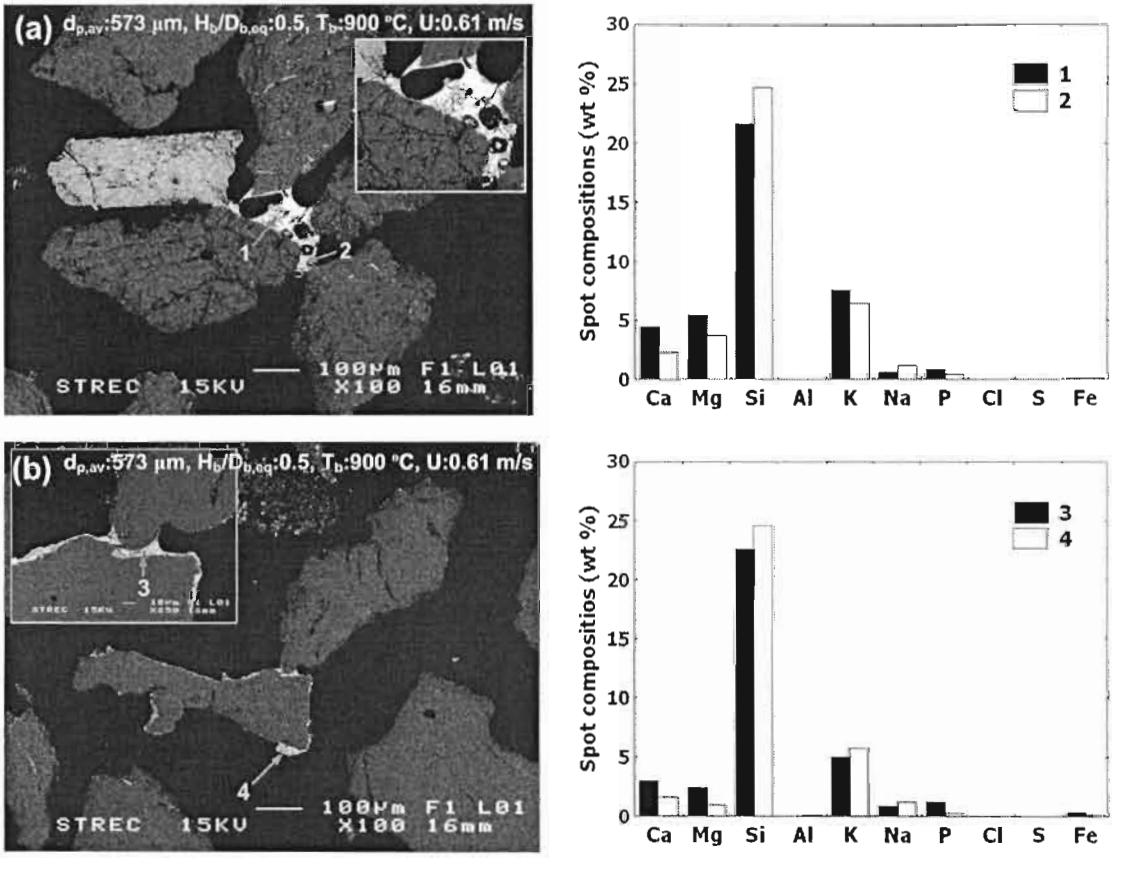

Figure 5.18 Typical SEM pictures and concomitant EDS elemental distributions of palm shell agglomerates from pilot scale FBC tests.

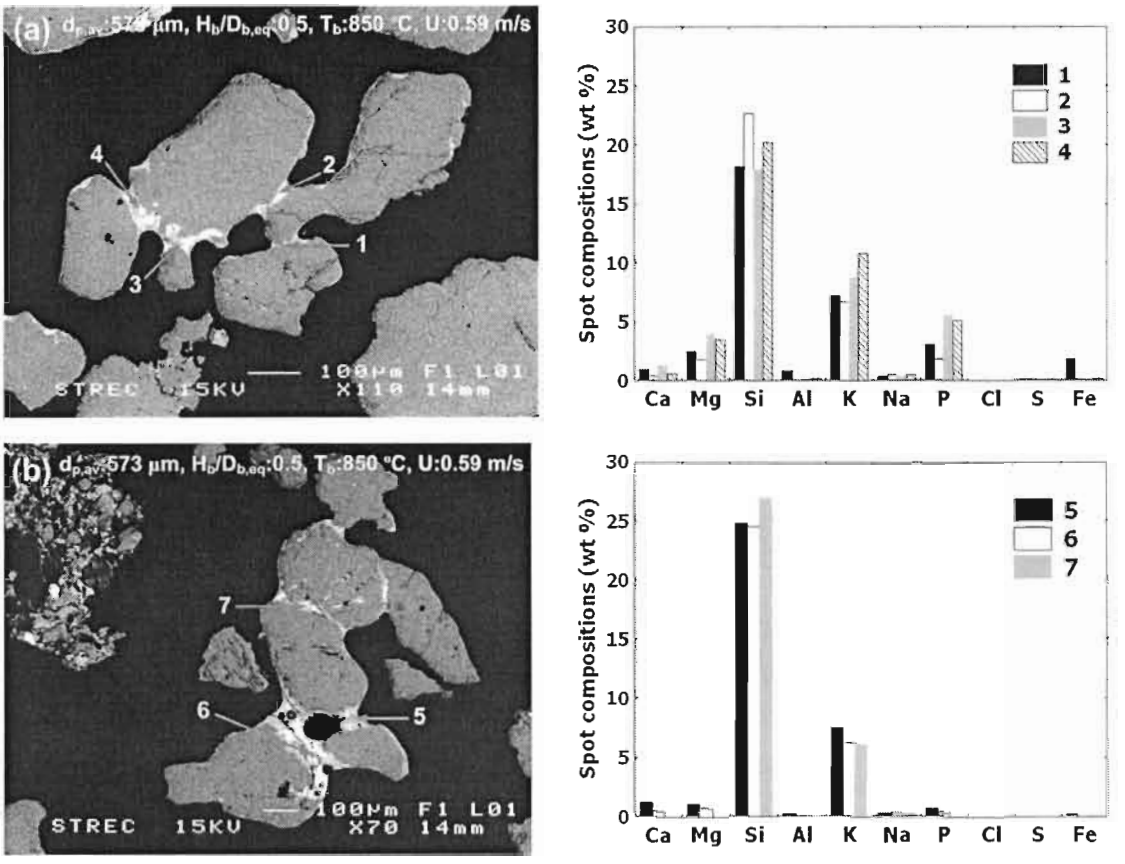

Figure 5.19 Typical SEM pictures and concomitant EDS elemental distributions of corncob agglomerates from pilot scale FBC tests.

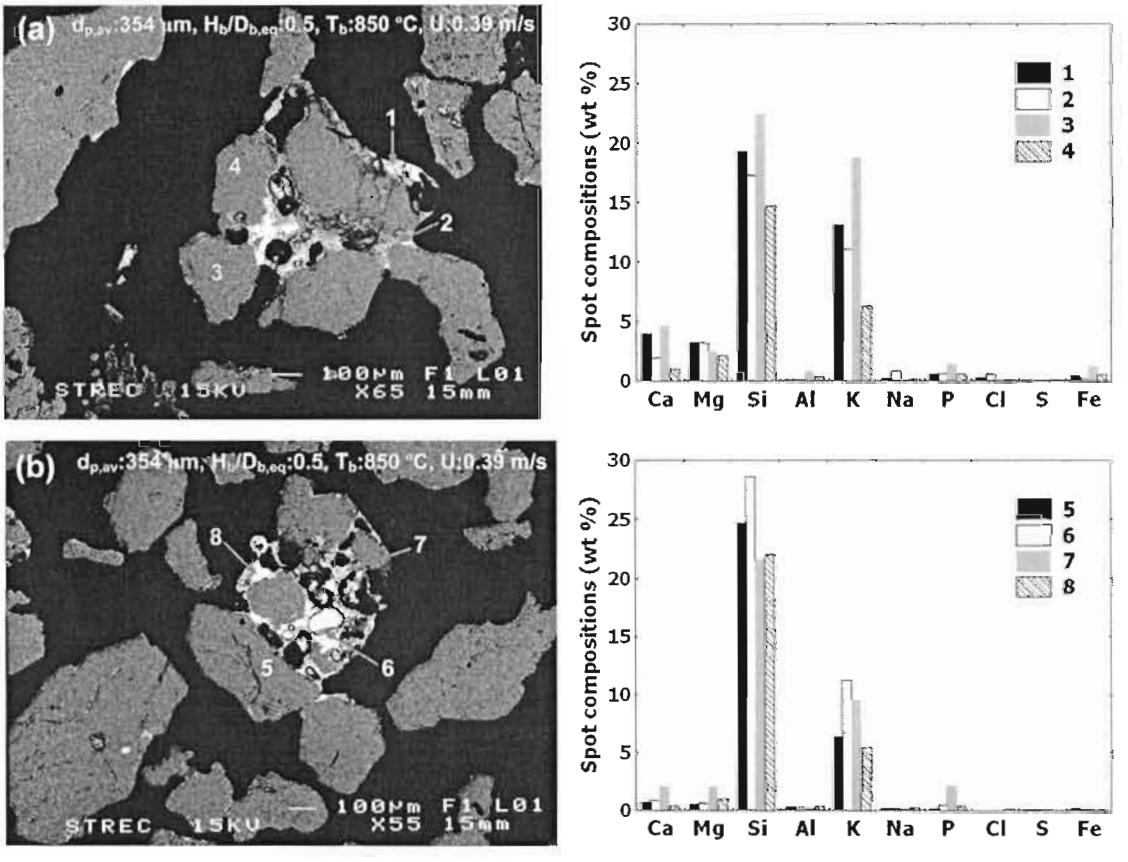

Figure 5.20 Typical SEM pictures and concomitant EDS elemental distributions of palm bunch agglomerates from pilot scale FBC tests.

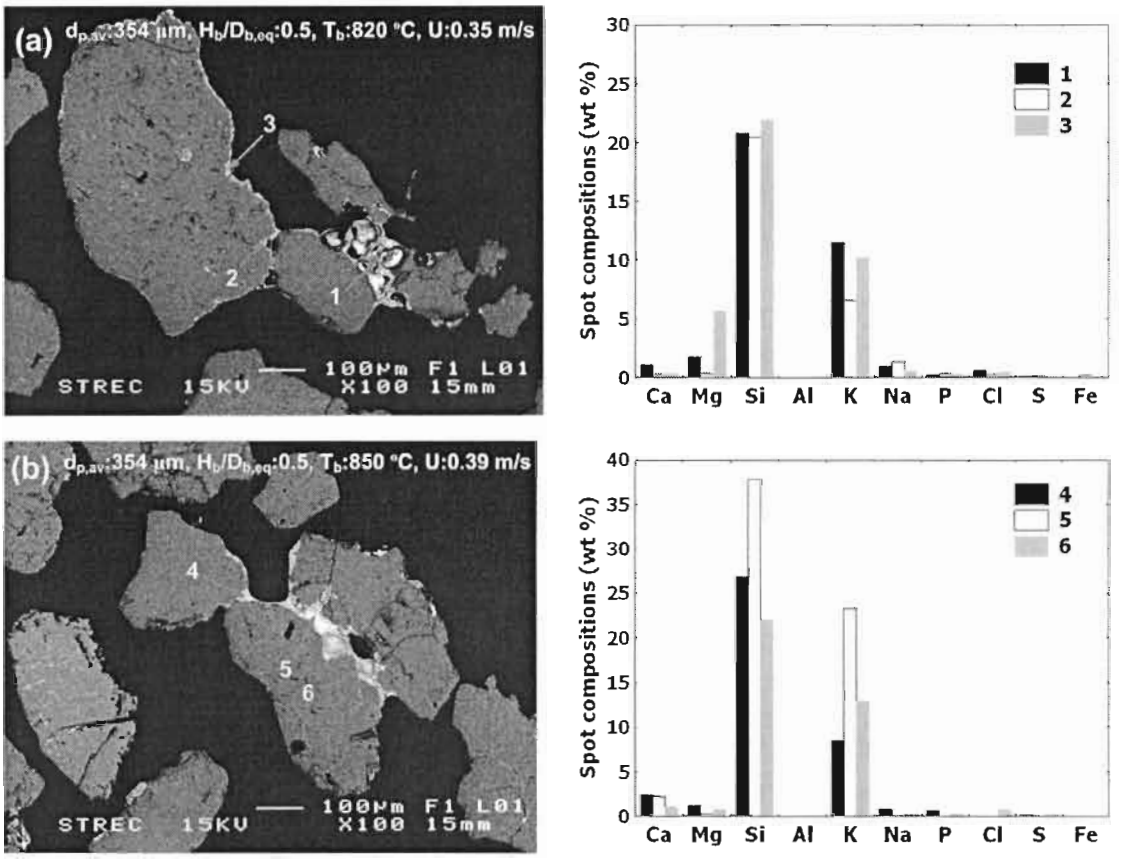

Figure 5.21 Typical SEM pictures and concomitant EDS elemental distributions of rice straw agglomerates from pilot scale FBC tests.

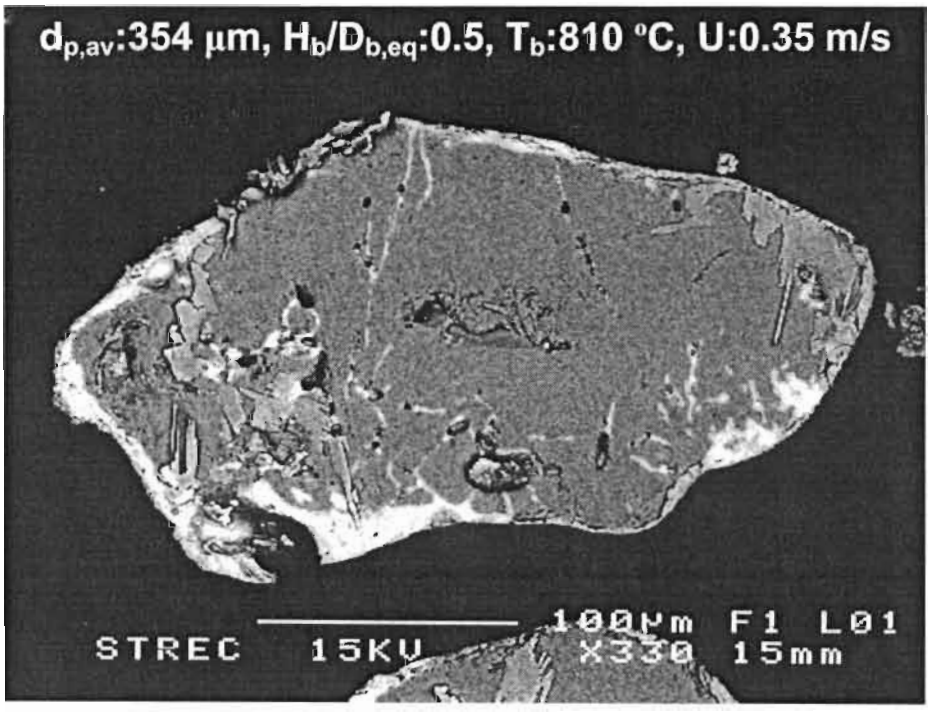

Figure 5.22 Illustration of the chemical attack inward quartz sand (Run No.4 of Table 5.7).

The features of agglomerate samples from pilot scale test were relatively similar to those from lab scale test. Agglomerates were formed likely by molten compounds as the neck and coating materials comprised of relatively rich Si and K; and Mg and Ca to a minor extent. They were likely the K-silicates. The relatively high P in corncob agglomerates was observed. S and Cl in very small fraction were also detected. Sand particles were adhered together by either bonding porous layer (Fig. 5.21b) or thin neck (Fig. 5.19a). The hollow structures located between bed particles (Fig. 5.20) or on the bed surface (Fig. 5.20a) were also observed. Non-homogenous coating and neck were common while relatively homogenous material was located between bed particles as thin layer neck. The diffusion and reaction propagating inward the quartz particle by gaseous potassium compounds or potassium containing aerosols, in existing cracks or from sand surface, was noticed typically as showed in Figure 5.22. This resulted in the presence of K silicates inside bed grains.

In the present work, the migration of ash forming constituents from fuel particle to bed particle was likely dominated by the collision. Condensation / aerosols deposition as parallel migration mechanisms showed an increasing degree, if K-gaseous and aerosol facilitators, namely Cl and S respectively, presented at relatively high content in biomass. It could be further concluded from the mentioned results that the bed agglomeration process was the reactor scale independent.

By the above SEM investigation, the mechanism which supposedly functions at relatively low temperature could be discerned in Figure 5.23.

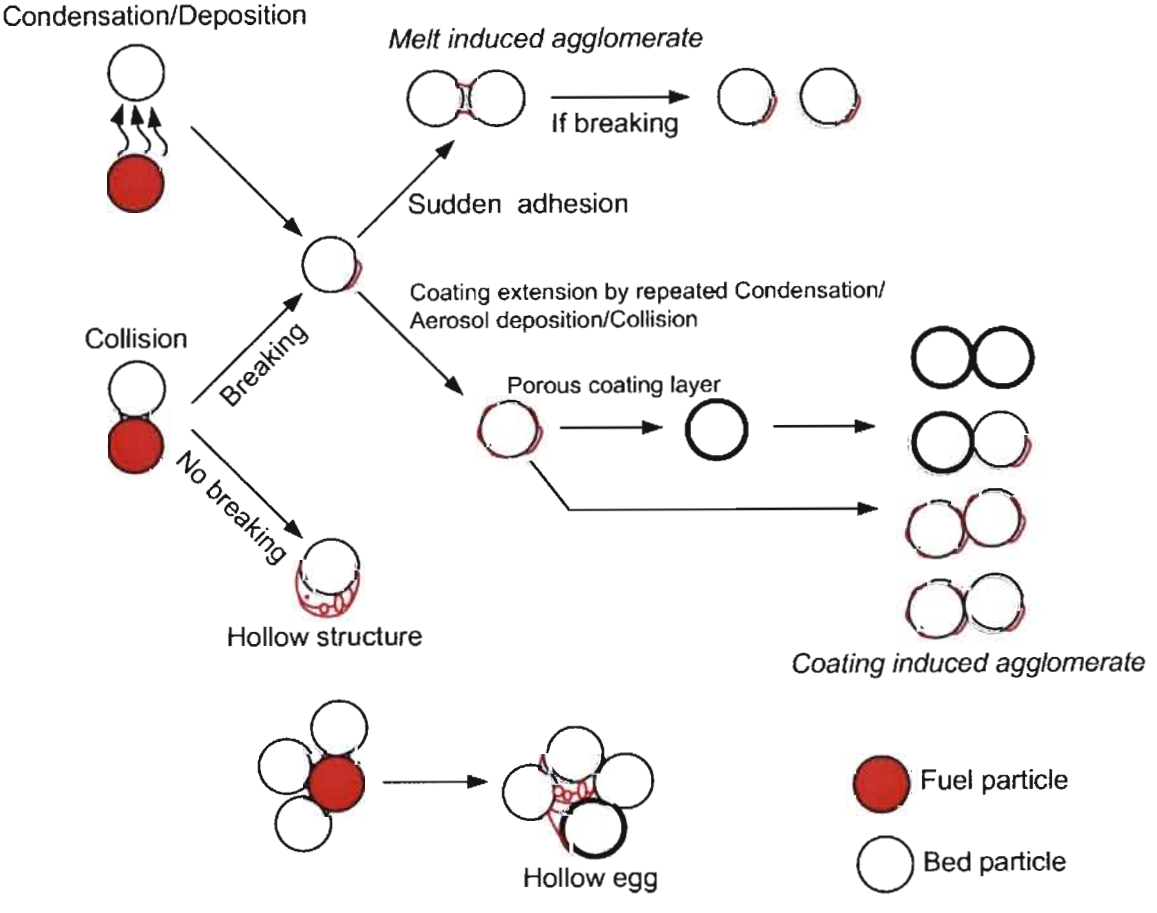

Figure 5.23 Suggested mechanism of the agglomerate formation

5.4 Thermodynamic behaviors of biomass ash under FBC conditions

In order to describe the presence of an individual ash forming element to the formation of fused material as coatings and necks, all EDS data including initial biomass ash for comparison were summarized to a set of plots showed in Figure 5.24.

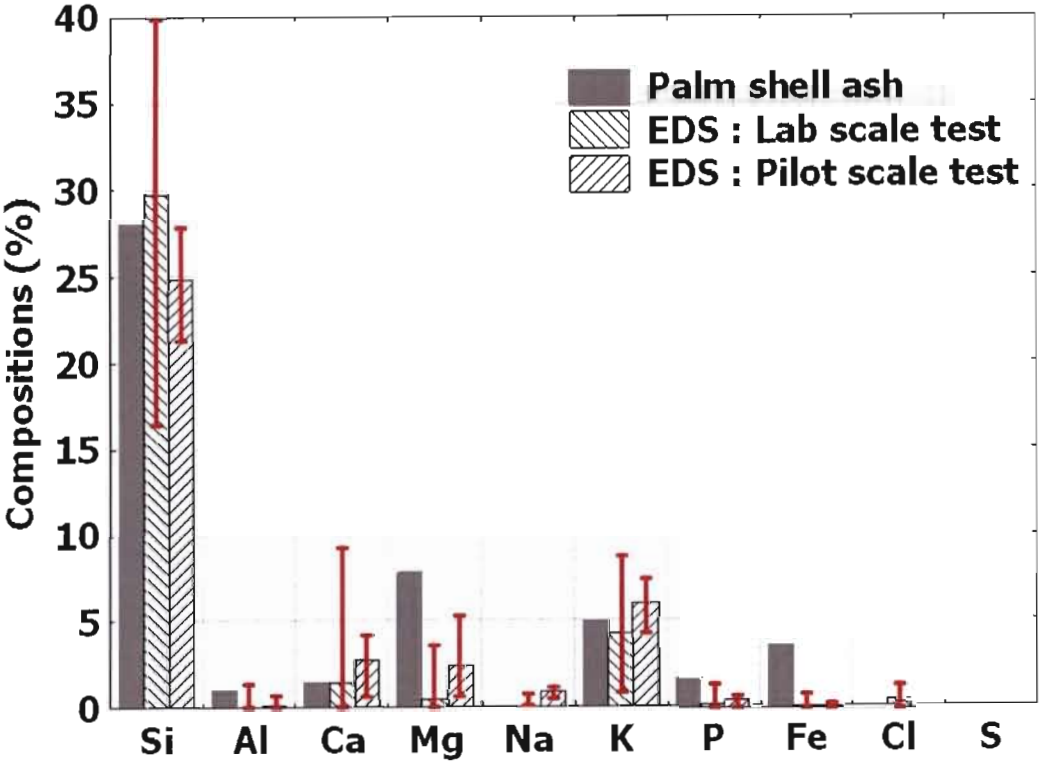

(a)

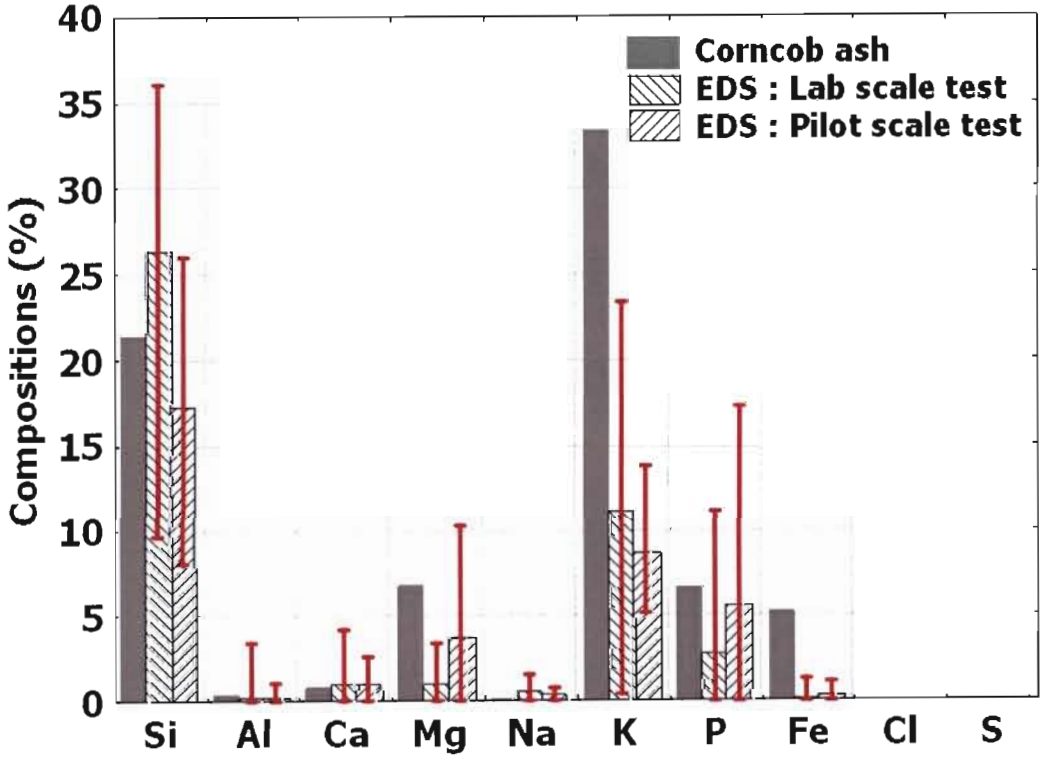

(b)

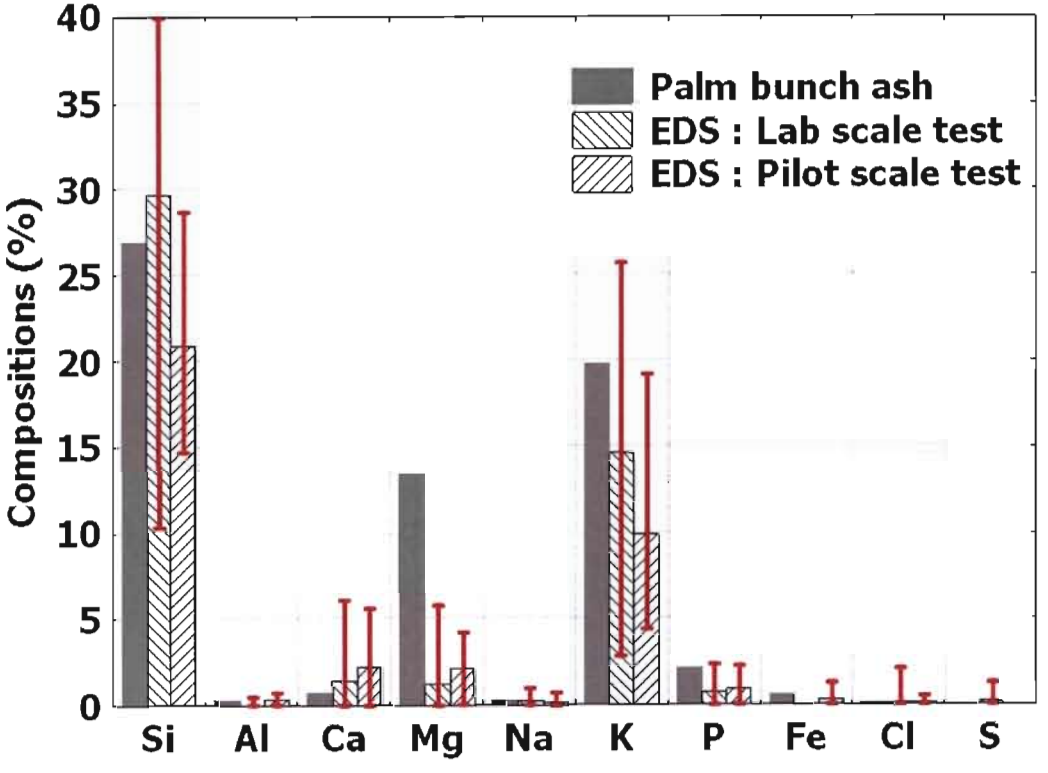

(c)

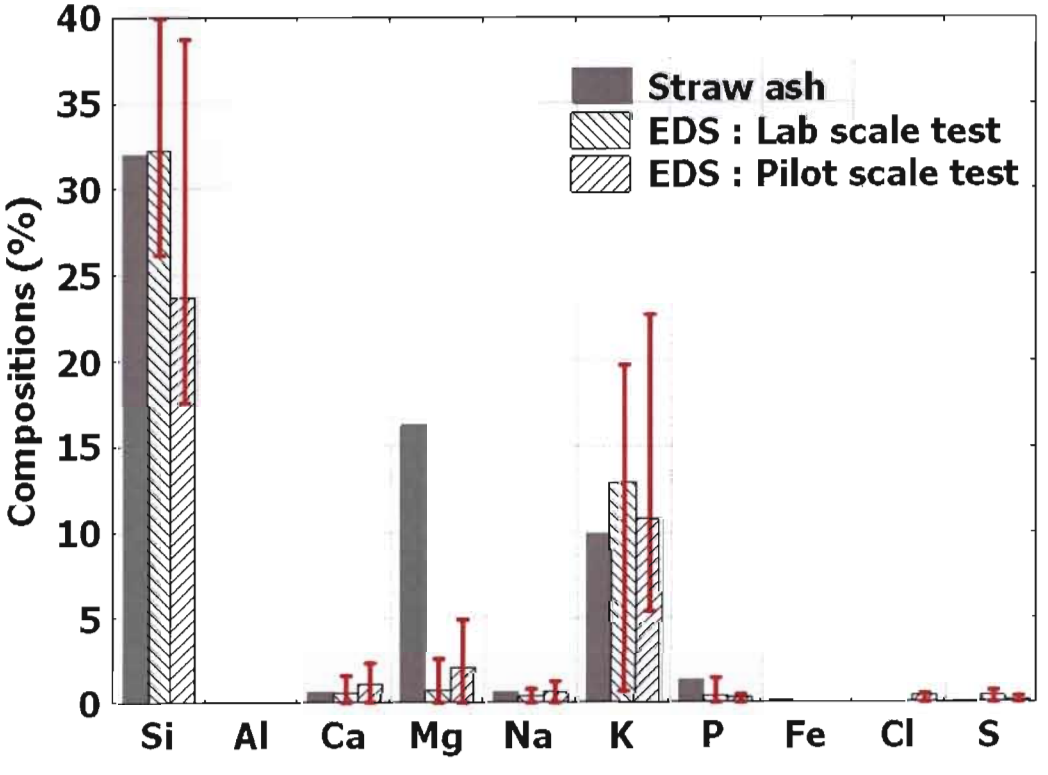

(d)

Figure 5.24 Distribution of elements in the initial biomass ash and EDS analysis of fused materials of agglomerates formed from burning (a) palm shell, (b) corncob, (c) palm bunch, and (d) rice straw in lab and pilot scale FBC.

In Figure 5.24, the distribution of elements in fused materials was widely, indicated by the vast ranges of error bars. The average compositions of fused materials were close to that of the biomass ash, confirming that the coating and neck were originated from fuel. Si and K were the two major elements; Si was proved to be the dominant element in fuel ashes and fused materials. The average P contents in agglomerates were relatively lower than those of fuel ashes. Na, Al, Fe, Cl and S content in fused materials were insignificant. It was further noticed in Figure 5.24 that despite its relatively large in fuel ash, Mg content in agglomerates was quite small; this indicates that Mg may not be included in the melt formation. On the other hand, Ca may be included in the fused material compositions due to its higher content in coating and necks of agglomerates against with the fuel ash.

In K and Si rich and Ca poor system like the chemistry of corncob, P species as $K_4P_2O_7$ (M.P.: 1109 °C), K_3PO_4 (M.P.: 1340 °C) or P-Si compounds (M.P. > 1150 °C) may be the major fine particle products [76]. This presumption of P was also corroborated by a result of a previous SEM/EDX study [177] which revealed that the major P was arrested in the deposited fine ash, instead of the molten ash. Mg as a free fine particle of high melting point oxide salt (MgO: M.P. 2852 °C) [53,178] is the major form in an oxygen rich environment at high temperature combustion. This is verifiable that Mg species may include to a lesser extent in the molten phase dominated by the significantly lower melting point K-silicates.

In the silica rich system as found in FBC with quartz bed particles, the onset of the bed agglomeration can be attributed to the melt of K-salts or K-silicates whereas Si in molten materials may be derived from the fuel itself or bed material [24,69]. K species mainly released during char combustion are mostly retained in the bed where they are transformed to K-silicates while S and Cl do not participate in final agglomeration process [69]. The present EDS results showed an agreement to these explanations. However, the insignificant fraction of Cl and S detected in agglomerates may be derived from the chloride and sulphate salts of alkali earth group in alkali lean system [61].

From the above chemical analyses, Si and K were the two major abundant elements. Possibly Ca was in part of the melt formation. To examine the thermodynamic behaviors of fused materials, all EDS data including fuel ash compositions were normalized and then plotted on the K_2O-CaO-SiO_2 ternary phase diagram [179] as illustrated in Figures 5.25 and 5.26, for lab scale and pilot scale samples, respectively.

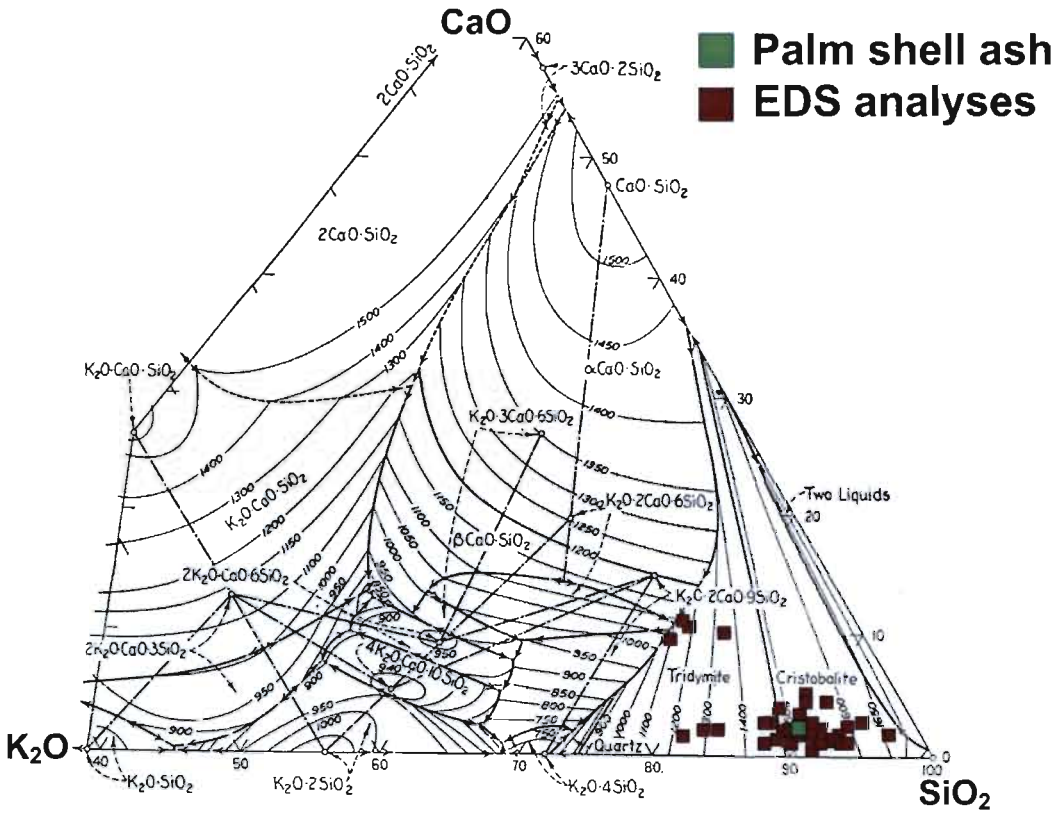
CaO
Palm shell ash
EDS analyses
3CaO·2SiO2
2CaO·SiO2
CaO·SiO2
αCaO·SiO2
βCaO·SiO2
K2O·CaO·SiO2
K2O·3CaO·6SiO2
K2O·2CaO·6SiO2
2K2O·CaO·6SiO2
2K2O·2CaO·9SiO2
2K2O·CaO·3SiO2
4K2O·CaO·10SiO2
Two Liquids
Tridymite
Cristobalite
Quartz
K2O·SiO2
K2O·2SiO2
K2O·4SiO2
K2O
SiO2

(a)

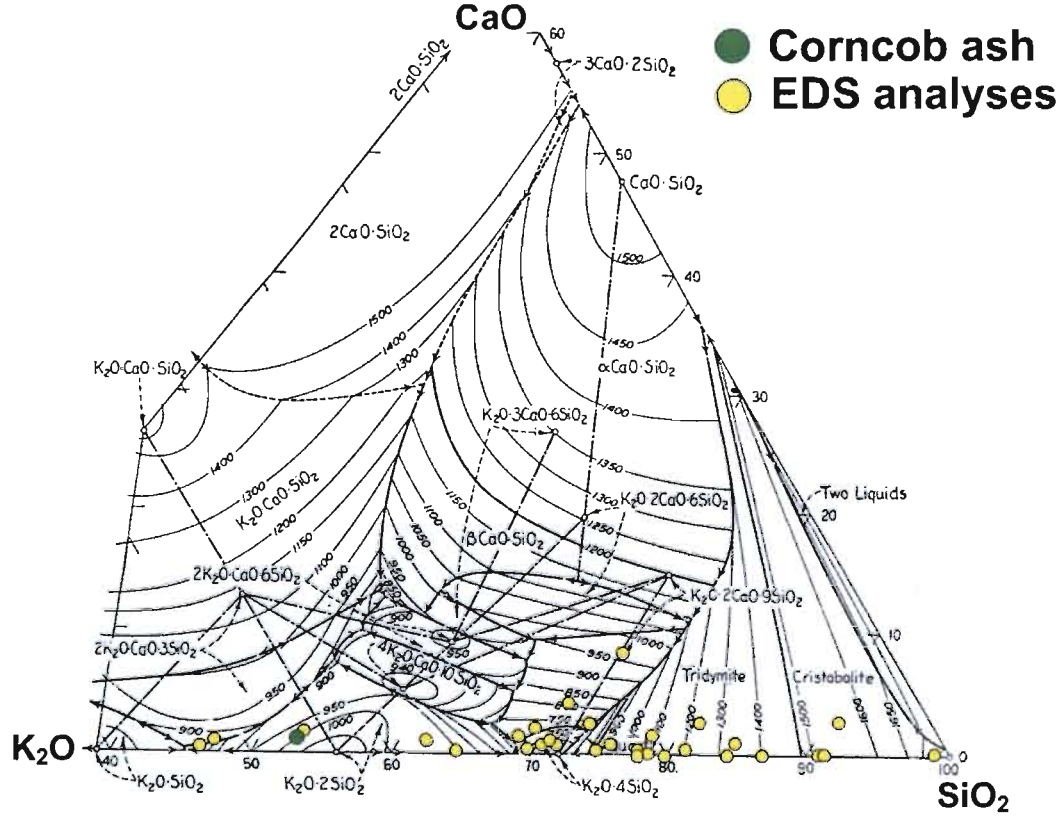
CaO
Corncob ash
EDS analyses
3CaO·2SiO2
2CaO·SiO2
CaO·SiO2
αCaO·SiO2
βCaO·SiO2
K2O·CaO·SiO2
K2O·3CaO·6SiO2
K2O·2CaO·6SiO2
2K2O·CaO·6SiO2
2K2O·2CaO·9SiO2
2K2O·CaO·3SiO2
4K2O·CaO·10SiO2
Two Liquids
Tridymite
Cristobalite
K2O·SiO2
K2O·2SiO2
K2O·4SiO2
K2O
SiO2

(b)

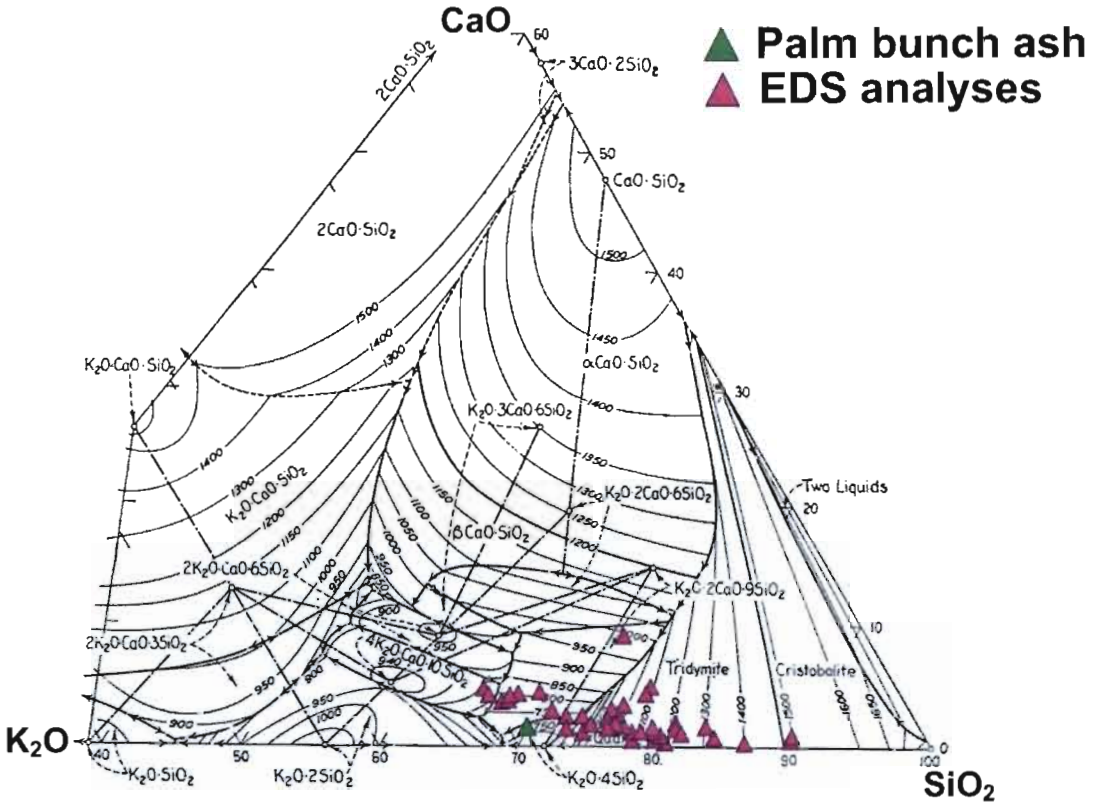

(c)

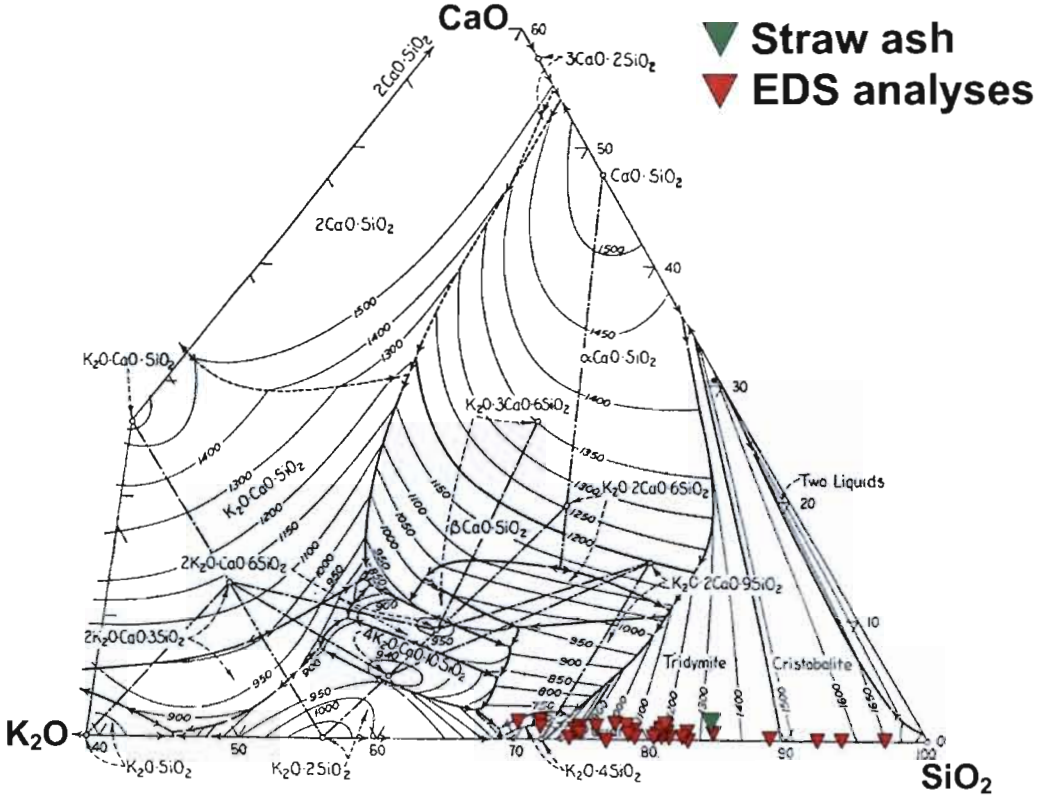

(d)

Figure 5.25 The simplified compositions of fused material from four biomass lab scale test and fuel ashes plotted in the K_2O-CaO-SiO_2 ternary phase diagram.

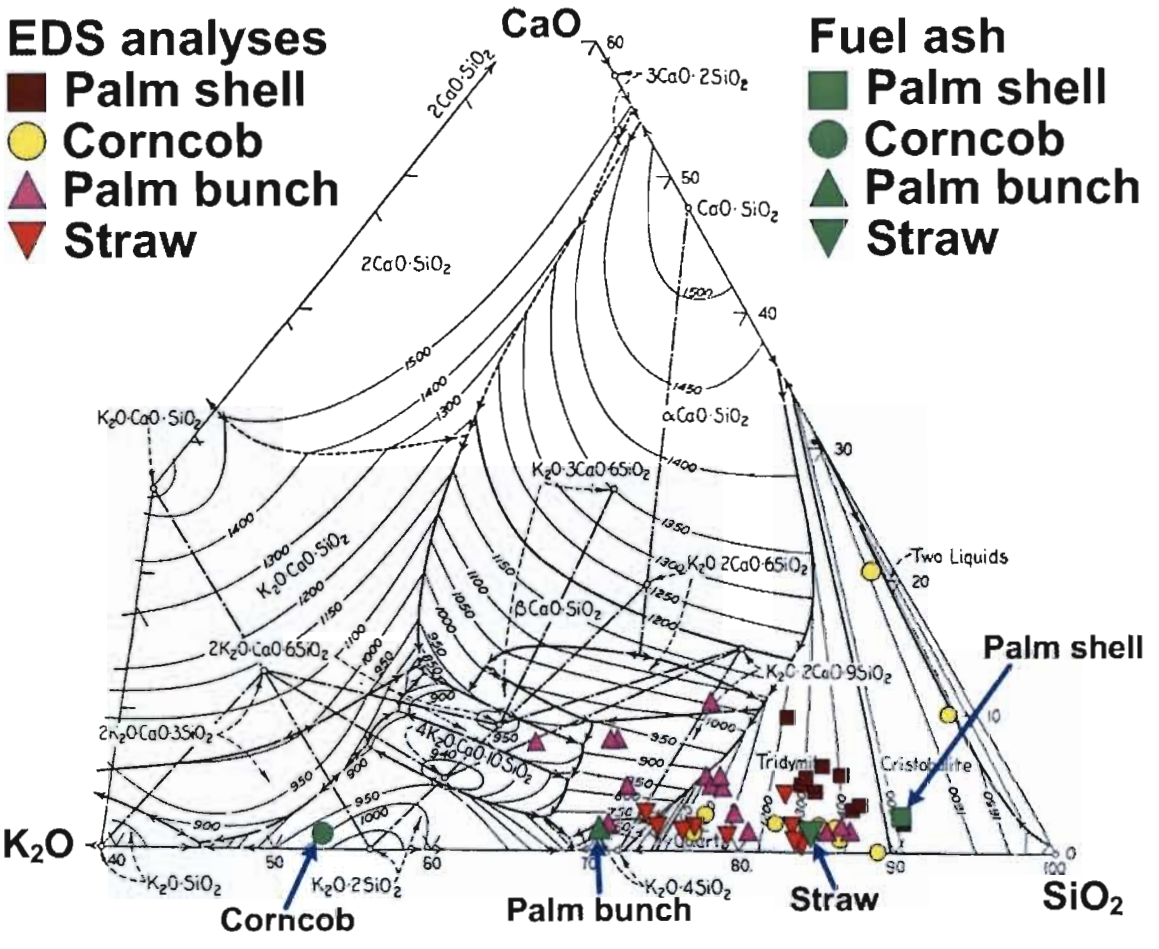

Figure 5.26 The simplified compositions of fused matters from pilot scale test and fuel ashes plotted in the K_2O-CaO-SiO_2 ternary phase diagram.

In Figure 5.25, they revealed that the compositions obtained from the lab scale agglomerate samples were mainly located to the SiO_2 rich and CaO poor region; especially those of palm shell agglomerates were mostly restricted to the SiO_2 rich corner and relatively close to the fuel ash composition (Fig. 5.25a). K_2O contents in agglomerates were widely distributed (palm shell: 5-15 %, corncob: 6-36 %, PEFB: 10-38% and rice straw: 15-29%). The compositions of fused materials in corncob, palm bunch and rice straw agglomerates were mainly located in the area where the eutectic with an initial melting temperature about 740 °C was nearby, while those of palm shell agglomerate were mainly in the zone of relatively higher liquidus temperature about 1200-1400 °C (*liquidus temperature is the minimum temperature at which all components of a mixture can be in a liquid state. Below the liquidus, the mixture will be partly or entirely solid*) [179]. The high K content can form the wide composition ranges of amorphous material and the wide distribution of EDS composition indicates to the poor elemental distribution of forming ash in fluidized bed.

The similar trends were also observed (Fig. 5.26) from the examination of pilot scale agglomerates. The simplified EDS compositions were so widely distributed but mainly located in the area, where the eutectic compositions with 740°C of an initial melting point were nearby. It is due to the fact that the fuel ash is the mixture of multi inorganic compositions giving the wide range of melting temperature. Previous works [106,128] had indicated that the chemical characteristics and thereby the melting of material at

coatings are significant for bed agglomeration process. If the coating has a high enough fraction of molten phase, it will cause bed agglomeration. The fraction of the melt needed for stickiness has been determined for silicate melts [92]. Therefore it was of interest in this study to determine the melting behavior of different fused material compositions. The fractions of the melt as a function of temperature at typical EDS compositions (in Figs. 5.14 to 5.21) were extracted from phase diagram by the well defined "Lever rule" and shown in Figures 5.27 and 5.28 for lab scale and pilot scale examination, respectively.

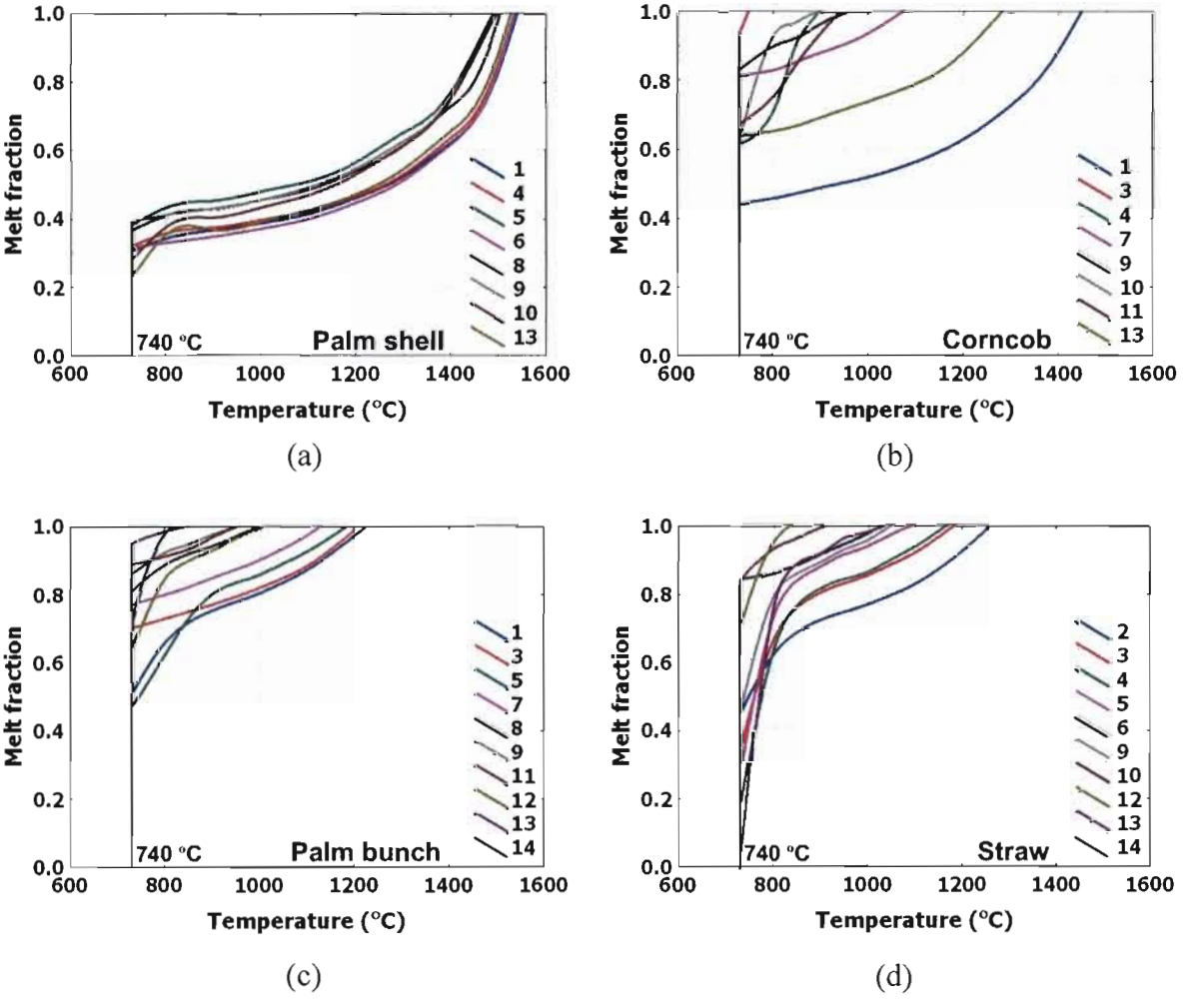

Figure 5.27 Typical melting behaviors at specific spot characteristics of fused material of agglomerates created from burning (a) palm shell, (b) corncob, (c) palm bunch, and (d) rice straw in a lab scale FBC (No. of lines correspond to EDS spots in Figure 5.14 to 5.17, respectively).

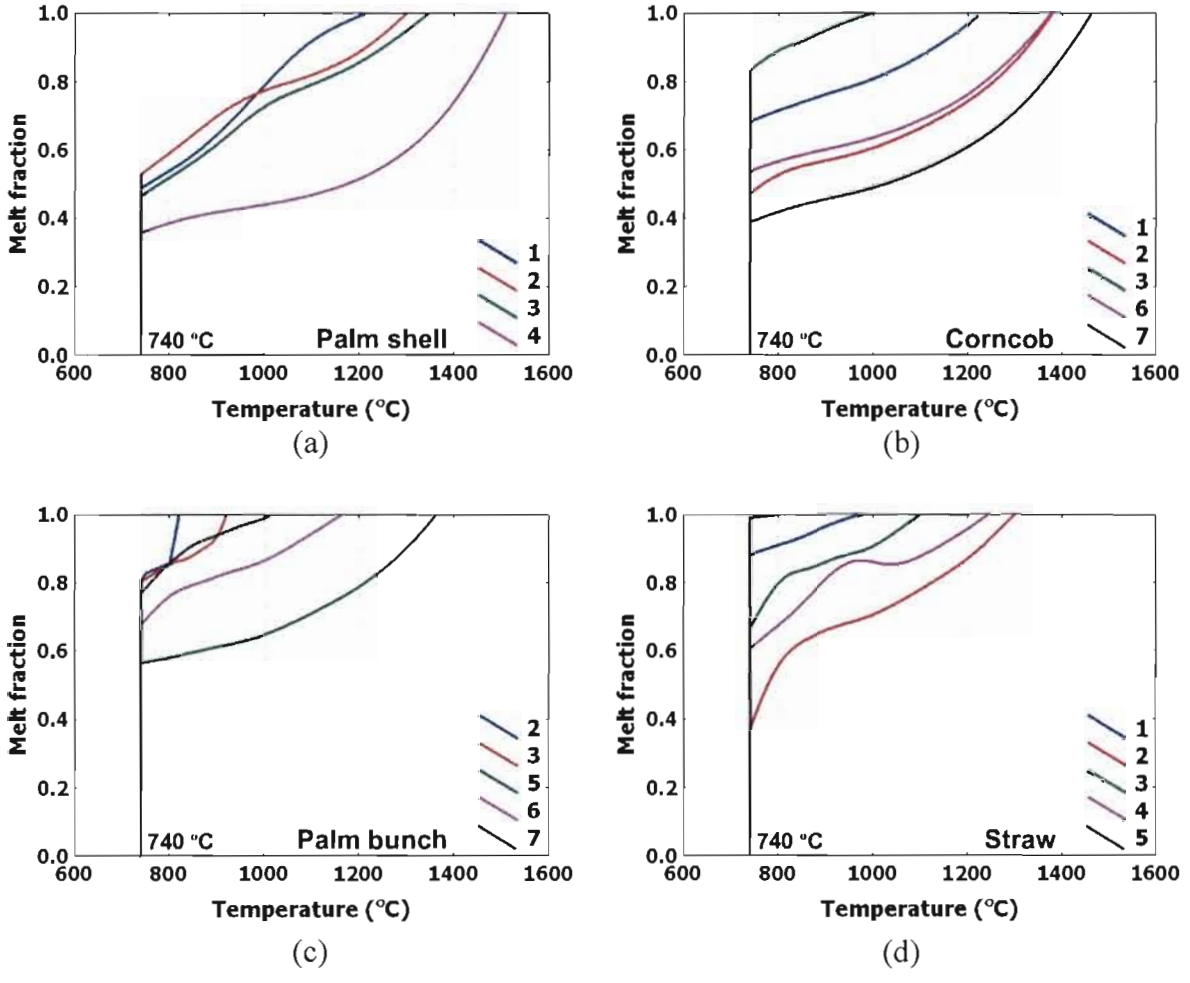

Figure 5.28 Typical melting behaviors at specific spot characteristics of fused material of agglomerates created from burning (a) palm shell, (b) corncob, (c) palm bunch, and (d) rice straw in a pilot scale FBC (No. of lines correspond to EDS spots in Figure 5.18 to 5.21, respectively).

It revealed from the results of lab scale test (Fig. 5.27) that the melting behaviors of the Ca lean system in this study were very sensitive to the amounts of K in the samples. All fused materials had an initial melting point about 740 °C. The melt profiles were relatively similar for corncob, palm bunch and rice straw agglomerates, even though that of rice straw agglomerates slightly differed at temperature of 740-840°C at which the relatively lower melt fraction had been estimated (Fig. 5.27d). Estimated fraction about 50-94 wt% of fused materials with relatively large potassium content, of corncob and palm bunch agglomerates, could melt at temperature as low as the initial melting temperature, while more than 50 wt% of fused materials in palm shell agglomerates would melt at temperature well above 1200 °C (Fig. 5.27a). Fused materials in corncob, palm bunch and rice straw agglomerates contained 60-95 wt% of melt fraction at low temperature as 800 °C, approximately.

The relatively similar trends were noticed in the estimation of melt fraction of pilot scale agglomerates illustrated in Figure 5.28. The higher fraction (40-90 wt%) of corncob, palm bunch and rice straw fused materials became to molten phase at an initial melting point, while palm shell fused materials were transformed to a liquid phase at relatively lower fraction (35-50 wt%). The aforementioned behaviors also confirmed the reactor scale independence in the bed agglomeration process.

The above results seemed to confirm that the partial molten phase formation in the released ash was responsible for the agglomeration, and it could be enhanced by the high surface temperature of burning char. The compositions of potassium silicate fused materials close to the eutectic mixture, caused by the high alkali content in fuel, yielded the greater melt fractions, at the same temperature range, giving the high bed agglomeration tendency. It should be noted that the fused materials in agglomerates analyzed above are the result of two competitive mechanisms as shown in Figure 5.23, and their influences are taken into inseparable consideration by the phase diagram analysis.

5.5 Mathematical model prediction and verification

The two mathematical models developed in Chapter 4 were verified by the present experimental results and the previous published experimental data.

5.5.1 A newly developed model

In this section, the prediction and verification of a newly proposed model was reported and discussed.

1. Model analysis

A present mathematical model mentioned in Chapter 4 was

$$\left(\frac{m'_{fuel}.t_{def}}{m_{bed}}\right) = B0*\left(\frac{\mu_l}{\mu_g}\right)^{B1}\left(\frac{U}{U_{mf}}\right)^{B2}\left(\frac{d_p}{D_b}\right)^{B3}\left(\frac{H_b}{D_b}\right)^{B4}\left(X_{melt}\%ash\right)^{B5} \tag{4.14}$$

The analytical results from MLR analysis, using the lab scale data in Table 5.5, described by the expression of Equation 4.14 were summarized in Table 5.8.

Table 5.8 Constants and contribution of independent dimensionless groups

Dimensionless term	Constant	β
	0.032 (B0)	-
Viscosity	0.360 (B1)	0.489
Fluidizing velocity	1.071 (B2)	0.188
Particle size	0.916 (B3)	0.121
Static bed height	-0.028 (B4)	-0.006
Ash melt fraction	-1.035 (B5)	-0.650

where beta coefficient (β) is the magnitude, the value between 0 to 1, indicates directly the intercomparable contribution; the higher Beta value, the higher influence. The negative implies the inverse form of the defined dimensionless term. The comparative results in Table 5.8 showed clearly that the characteristic of inorganic constituent in fuel and temperature which contributed to the development of the viscous ash melts were the major contribution to the bed agglomeration behaviors, while the bed conditions such as air velocity, bed particle size and static bed height showed minor. The velocity affected at relatively higher on the segregation in fluidized bed than the particle size, while the bed height showed a less significant effect. The velocity, particle size and melt fraction was quite in the linear relationship to t_{def}. The order of inverse melt quantity group (B5) was proved to 1, which corresponded to a model assumption, in Chapter 4.

This model analysis provided the firmly consistent description to the results of this present work and previously reviewed studies which clearly indicated the highly significant influences of the fuel ash chemistry and temperature and that the melt formation controlled the bed agglomeration.

The degree of mixing in fluidized bed relative to the breaking and collision is contributed mainly by the gas velocity [34,147,148]. The early mathematical models [109,166] proposed the half order of excess velocity ($U-U_{mf}$) to t_{def} by the regression analysis, while the above analysis indicated differently as the linear function (B2). Furthermore, approximately first order of bed particle size effect (B3) was presently revealed while the early works proposed variously (Lin et al [109] = -0.5 and Lin et al [166] = -0.25). The order of inverse melt quantity group (B5) was proved to 1, due to the direct mass calculation of ash feed. This was corresponding to the order of the inverse alkali feed rate group, relative to t_{def}, in the model formulated by Lin et al [166], while an early model [109] set this order to 0.5.

2. Model verification

The t_{def} prediction by a model of Equation 4.14 on the lab scale combustion data was showed in Figure 5.29. The predictive result followed the experimental data with a fairly good agreement, since they were the source of regression analysis. The error calculation ranged ±21%, showing satisfactory.

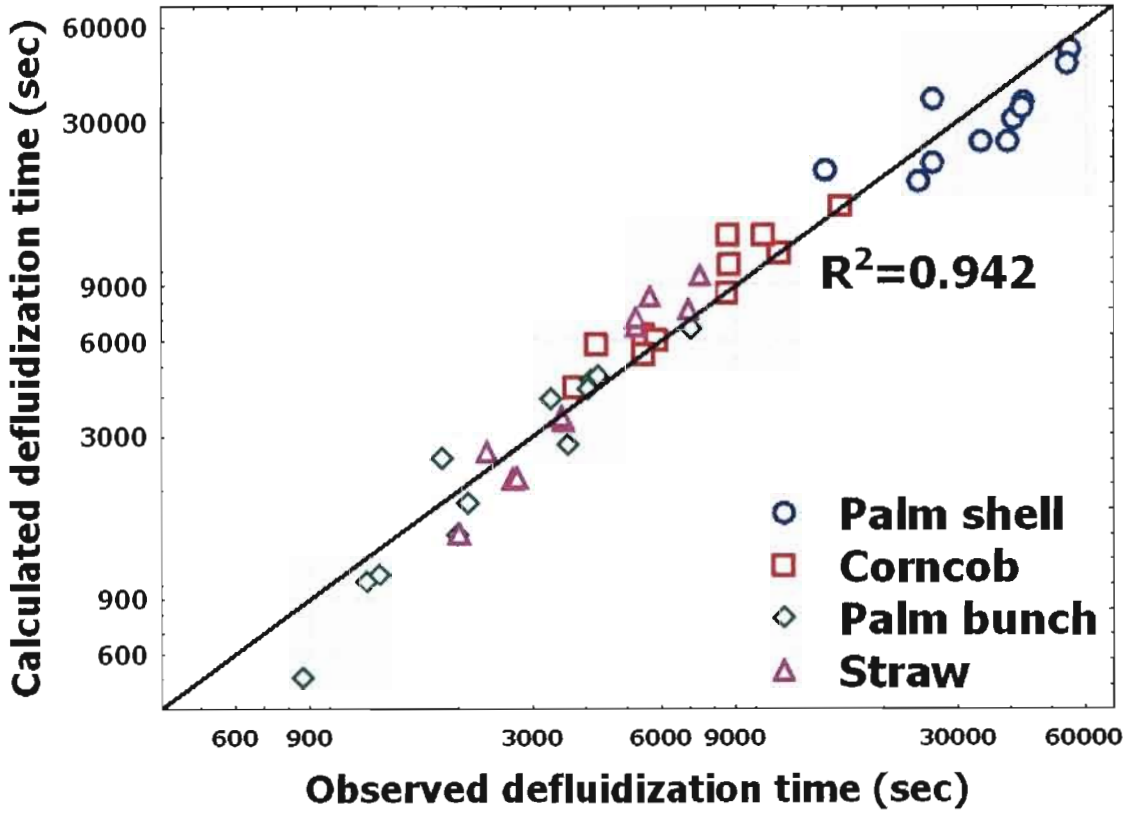

Figure 5.29 Comparison of calculated defluidization time with lab scale results.

To further verify the ensured accuracy of this model, the predictions of t_{def} from the conditions of pilot scale experiments of this study and previous bed agglomeration works performed experimentally with several kinds of biomass residues were carried out. Their predicted results with pilot scale and previously published data were illustrated in Figure 5.30a and 5.30b, respectively, and showed fairly well in consistence. In Figure 5.30b, the predictive results in the form of the dots with bands indicated the calculated average and reported range of straw feed rate in some conditions of wheat straw combustion [109,149]. The straw blends were the biomass mixture of rice straw and the defined commercial fuel (80% wood + 20% almond shell) [146].

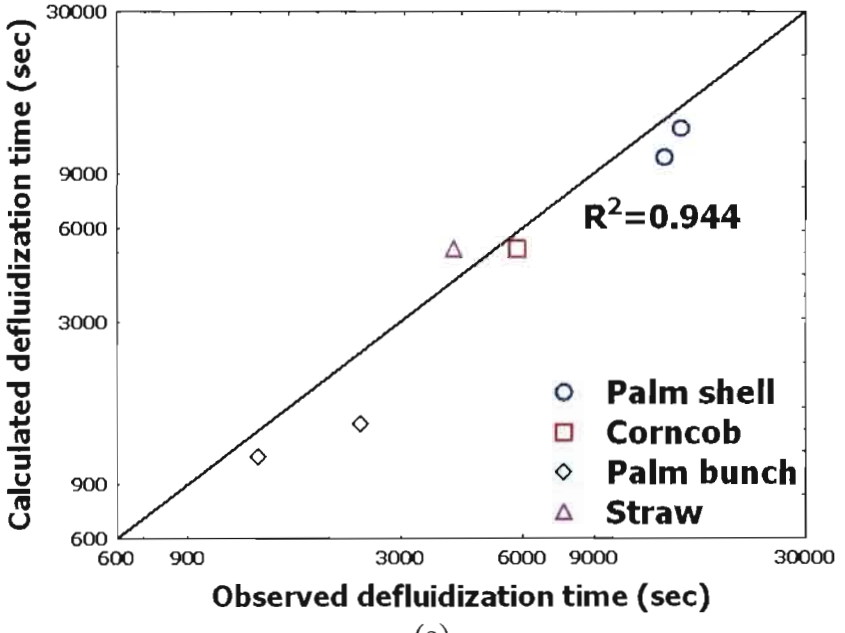

(a)

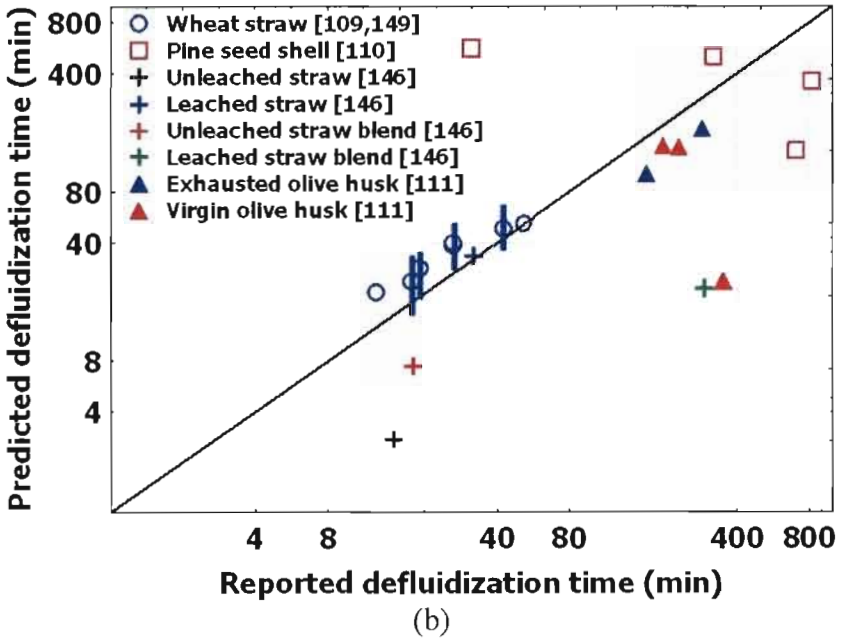

(b)

Figure 5.30 Verification of model with (a) the pilot scale results and (b) the previous published data.

5.5.2 A modified model

1. Model analysis

A model which was modified from the original model of Lin et al [109] to predict t_{def} was proposed as an optional model in Equation 4.25 viz;

$$t_{def} = C_{new}\left(\frac{m_{bed}}{m'_{fuel}\,X_{ash}X_{K.in.Ash}}\right)^{A}\left(\frac{U-U_{mf}}{d_p}\right)^{1/2}\exp\left(\frac{E_\mu}{2RT_b}\right) \quad (4.25)$$

A set of lab scale data were analyzed by using the linear regression technique to calculate C_{new}, A and E_μ of an individual biomass as following,

- A slope of the line plotted between t_{def} and inverse bed temperature in logarithm scales indicated the viscosity activation energy (E_μ).
- For each biomass at constant bed temperature, the logarithmic plot between t_{def} and the mass ratio group provided A constant, as the slope of the line.
- Finally, C_{new} was a slope calculated by plotting t_{def} in linear scale against with the group parameters on the right side of Equation 4.25 with corresponding A and E_μ, as the linear equation.

The regression results were summarized in Table 5.9, including the previously published data and prediction of original model (Eq. (4.23)) with lab scale data.

Table 5.9 Model parameters

Biomass	**A**	**C [Eq. (4.23)]**	**C_{new} [Eq. (4.25) at A=1]**	**E_μ/R (K)**
Palm shell	0.90	3.77×10^{-4}	1.04×10^{-3}	33,670
Corncob	1.12	1.81×10^{-3}	2.61×10^{-11}	27,340
Palm bunch	0.82	3.92×10^{-3}	2.25×10^{-8}	21,741
Rice straw	0.92	1.35×10^{-1}	7.52×10^{-8}	16,492
Wheat straw [109]	***0.5***	$\mathbf{1.11 \times 10^{-4}}$	$\boldsymbol{2.67 \times 10^{-10}}$	**29,000**

It was noticed that A, an order of the mass ratio group, were around 0.82 to 1.12 and close to 1, which was similar to B5 of Equation 4.14 in Table 5.8, while 0.5 was early set in an original model. Therefore, all A were set newly to 1 to determine C_{new} by the subsequent regression. Among the observed biomass, E_μ/R and C_{new} of palm shell showed the highest value. E_μ/R of the present biomass showed relatively similar order of magnitude to that of the wheat straw from a previous work [109].

2. Model verification

The C_{new} and E_μ/R in Table 5.9 obtained in this way were then applied to calculate t_{def} for comparison, and the t_{def} comparative results were then illustrated in Figure 5.31, including the prediction by original model.

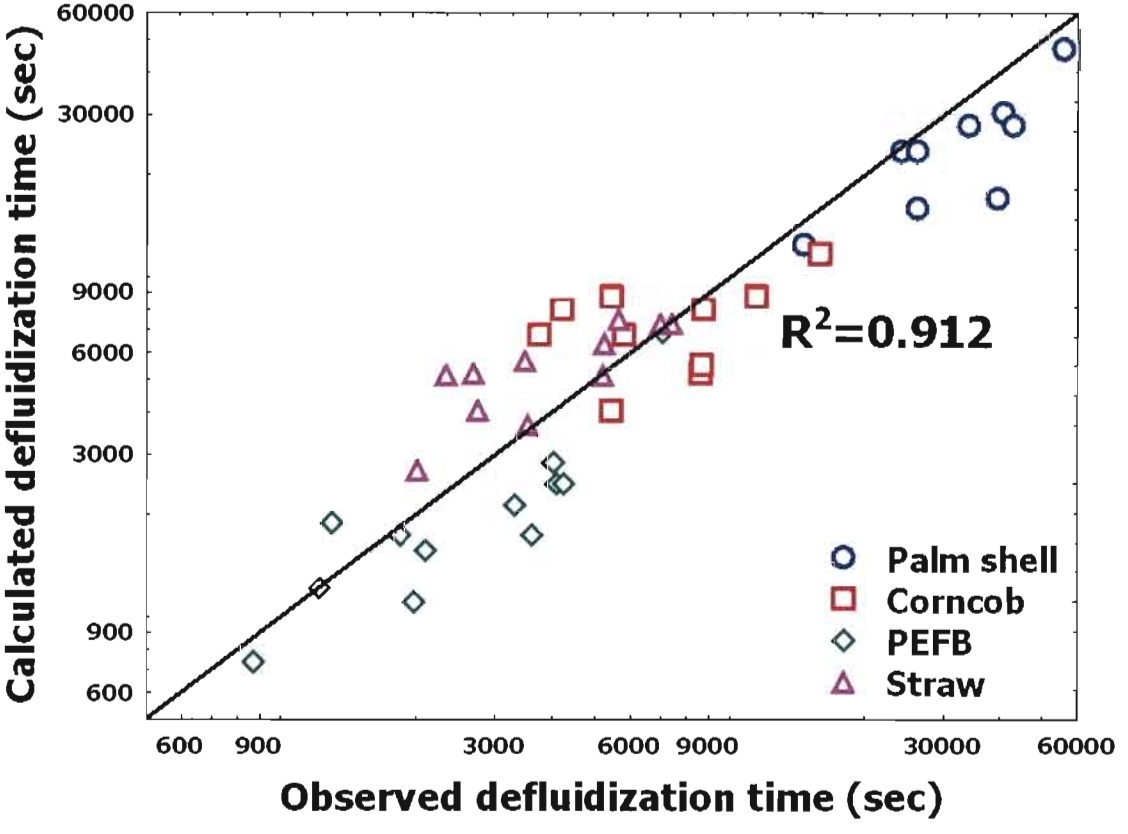
Calculated defluidization time (sec)
60000
30000
9000
6000
3000
900
600
600
900
3000
6000
9000
30000
60000
Observed defluidization time (sec)
R²=0.912
Palm shell
Corncob
PEFB
Straw

(a)

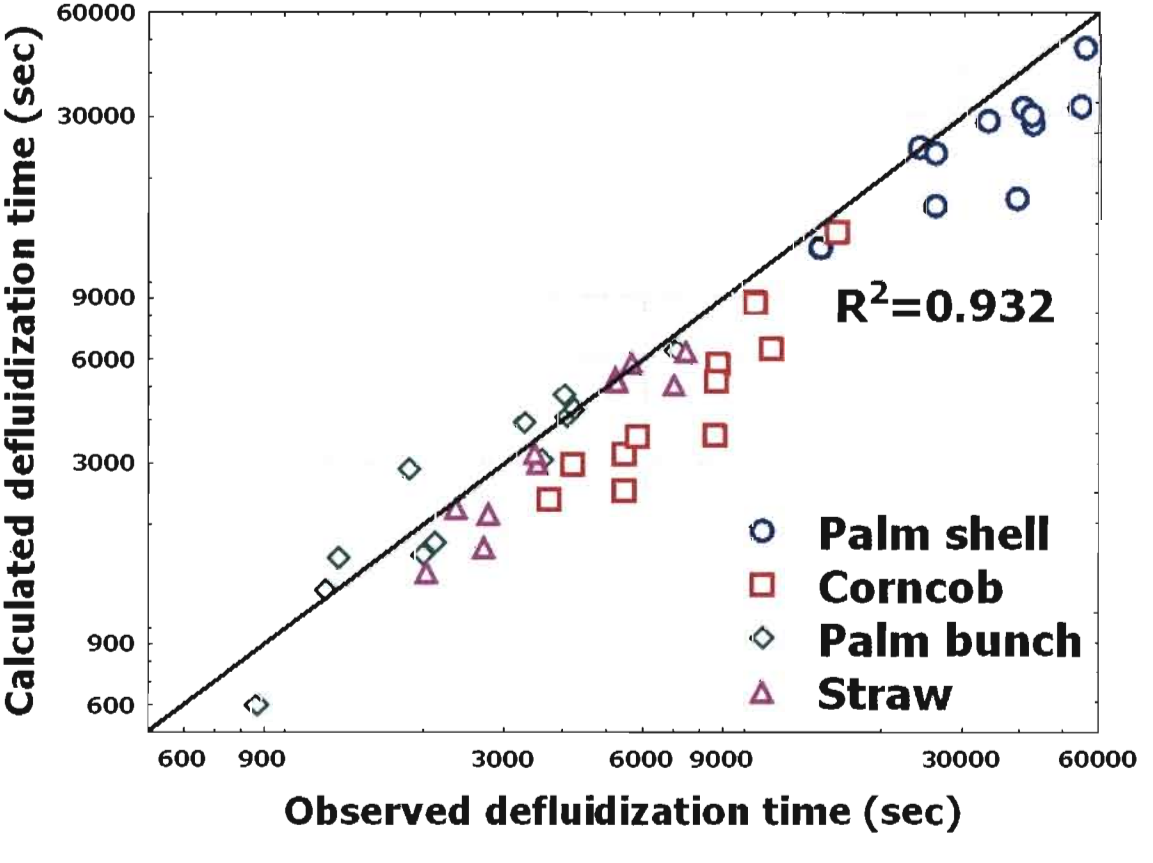
Calculated defluidization time (sec)
60000
30000
9000
6000
3000
900
600
600
900
3000
6000
9000
30000
60000
Observed defluidization time (sec)
R²=0.932
Palm shell
Corncob
Palm bunch
Straw

(b)

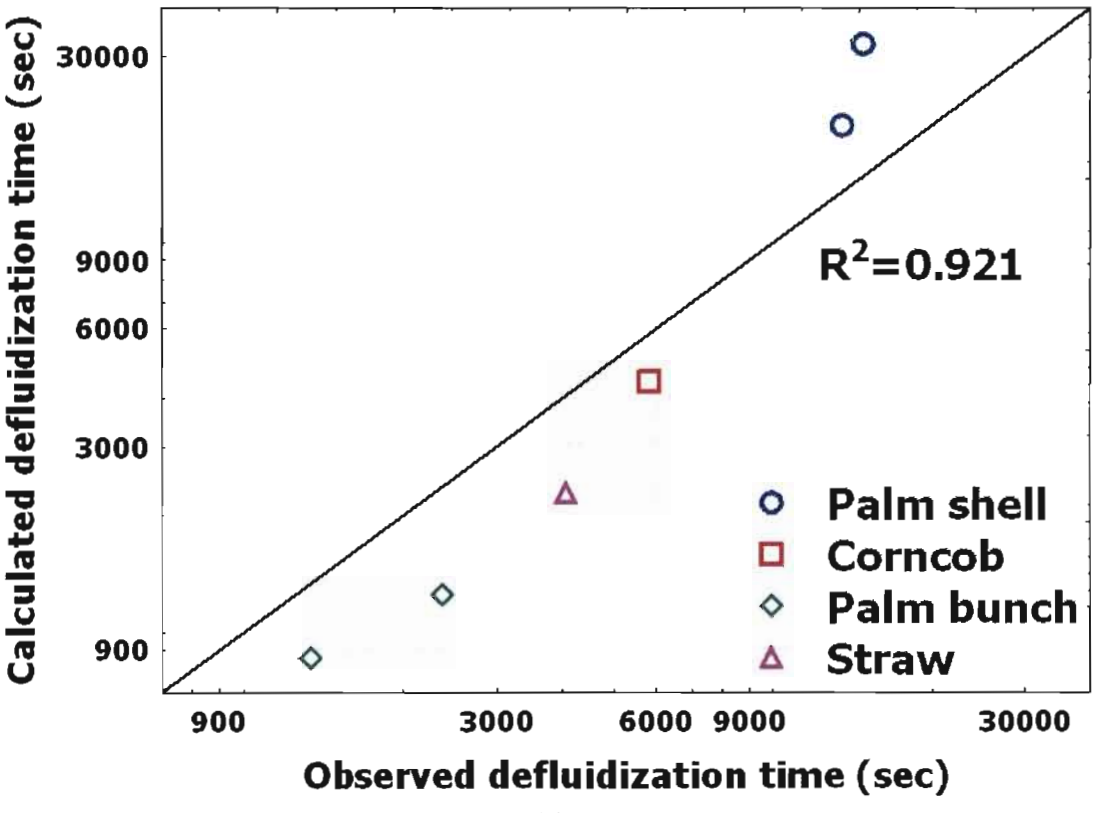

(c)

Figure 5.31 t_{def} comparisons with experimental data by; (a) Original model (Eq. (4.23)) with lab scale data, (b) Modified model (Eq. (4.25)) with lab scale data, (c) Modified model (Eq. (4.25)) with pilot scale data.

As illustrated in Figure 5.31a and 5.31b for lab scale prediction, it was noticed that a modified model provided slightly higher predictive accuracy with satisfactory agreement at ±32% of error. However, it seemed that this increasing model accuracy was insignificant since the original model (Eq. (4.23)) offered relatively high in the predictability at ±35% of error range. The fairly well consistence in time comparison of pilot scale data was obtained satisfactorily, as shown in Figure 5.31c.

As discussed in Chapter 4, the characteristics of C_{new} and E_{μ}/R were dependent on the ash compositions and possibly they were correlated mathematically with the variable terms, proposed in this work, which represent the fuel inorganic chemistry well known as Alkali Index (AI) and Base-to-Acid ratio ($R_{b/a}$) [112]. Early mentioned, they were defined as;

$$AI = \frac{kg(K_2O + Na_2O)}{GJ} \tag{2.6}$$

$$R_{b/a} = \frac{\%(Fe_2O_3 + CaO + MgO + K_2O + Na_2O)}{\%(SiO_2 + TiO_2 + Al_2O_3)} \tag{2.7}$$

The alkali index expresses the specific quantity of total alkali oxides in fuel (per unit mass of fuel) divided by heating value in GJ unit. HHV was selected in this study. Base-to-Acid ratio is defined as the ratio of basic oxide to acid oxide where the label for each compound makes reference to its weight concentration in the ash. Both indexes can be estimated by the fundamental fuel data of intensive laboratory characterization.

The MLR analysis further correlated C_{new} and E_{μ}/R of an individual biomass in Table 5.9 with AI and $R_{b/a}$ calculated from the corresponding ash data in Table 5.2 and 5.3. It provided the empirical correlations of AI and $R_{b/a}$ in Equation 5.1 and 5.2, respectively, and their prediction results with satisfactory agreement were illustrated in Figure 5.32.

$$C_{new} = 2.14x10^{-10} * (AI^{-1.55}) * (R_{b/a}^{-13.32}) \qquad (5.1)$$

$$E_{\mu}/R = 18543.47 * (AI^{-0.3}) * (R_{b/a}^{0.15}) \qquad (5.2)$$

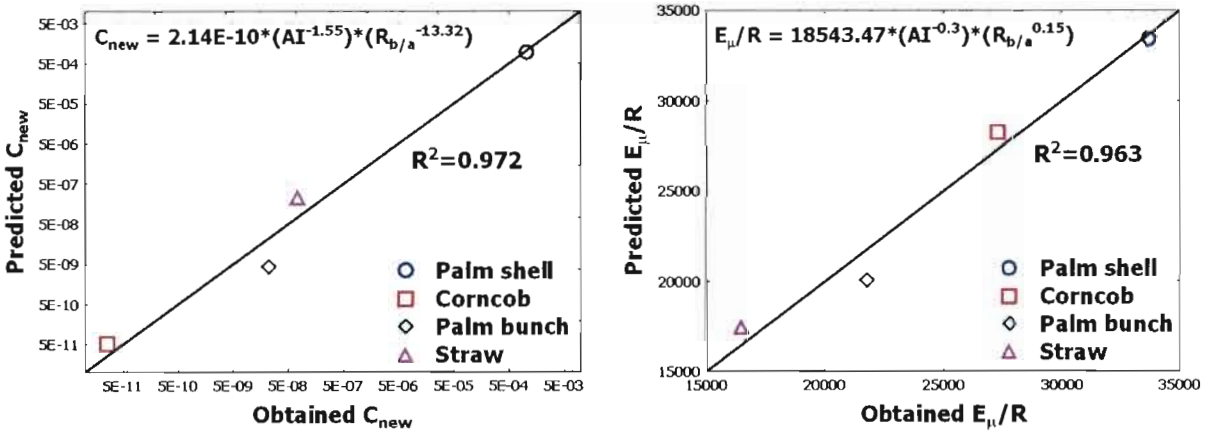

(a) (b)

Figure 5.32 Regression summaries of (a) C_{new} and (b) E_{μ}/R

When Equation 4.25, 5.1 and 5.2 at A=1 were employed to revise the verification of lab scale and pilot scale data, the obtained results were then reported in Figure 5.33 with fairly well agreement. This may be due to the using of a small number of biomass to perform the regression analysis in order to get C_{new} and E_{μ} equations, and their inaccuracy was included in the prediction.

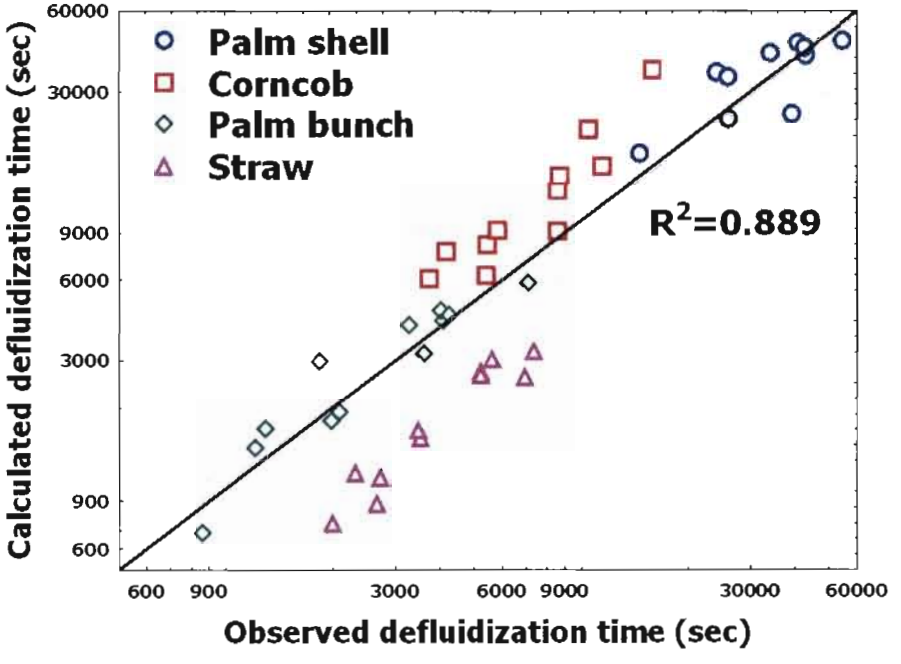

(a)

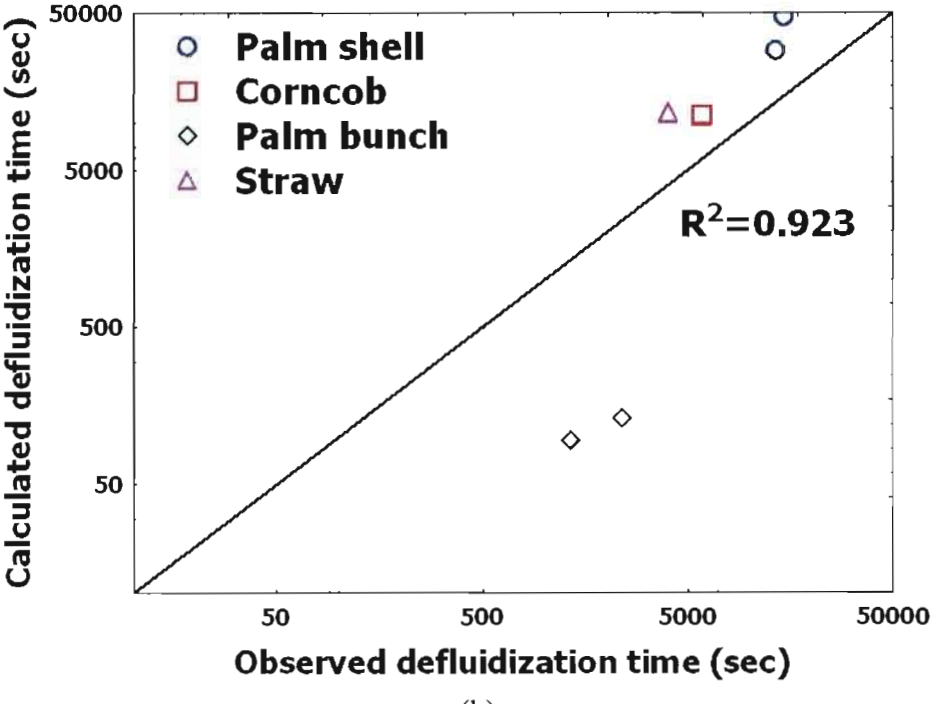

(b)

Figure 5.33 Revised t_{def} predictions to (a) lab scale data and (b) pilot scale data by Equation 4.25, 5.1 and 5.2.

In summary, the simple models in both newly proposed and modified from a previously published model were intentionally applied to describe the defluidization behaviors by bed agglomeration as dependence of the significant bed operating variable and biomass ash characteristics. The correlations newly set up by the dimensionless analysis and semi-empirical approach showed fairly well to good satisfactory agreement to the present experimental results. More experiments with the various types of biomass and operating conditions of FBC are therefore needed to improve these correlations.

CHAPTER 6 CONCLUSIONS

The following conclusions can be drawn from this present experimental research.

1. The defluidization caused by the agglomeration of bed particles affected directly to the bed hydrodynamic and could be observed by the abnormal decrease of bed pressure drop, more clearly than the inhomogeneous bed temperatures. It was developed steadily from partial to complete defluidization by the extension in the number and growth of agglomerates during combustion, resulting to the increase in bed voidage and the subsequent poor bed mixing.

2. Among the factors enhancing the bed agglomeration tendency, the increasing combustion (bed) temperature and bed particle size and the decreasing fluidizing air velocity showed significant effects, as previously suggested. Additionally, the increasing static bed height was also an effect. The relatively high potassium and chlorine contents increased the bed agglomeration problem. The order from high to low of bed agglomeration tendency of the biomass samples studied in this work were palm brunch, corncob, rice straw, and palm shell, respectively.

3. In this work, the presence of potassium in biomass caused likely the formation of potassium silicates as viscous liquid phase during combustion (above 750 °C) was the main reason for bed agglomeration. This was initiated by the high surface temperature of the burning biomass particles.

4. In this study, the migration of ash forming elements from relatively high surface temperature of char particle to lower surface temperature of bed particle was likely dominated by the collision. The gaseous condensation/aerosols deposition of ash species on the bed particle might have an increasing contribution on the migration if the K-gaseous/aerosol facilitators as chloride and sulfur presented in biomass at relatively high contents.

5. Chloride and sulfur did not participate in the final agglomeration process due to the formation of potassium silicates as the compounds of higher thermochemical stability. They were presumed to be included in the chloride and sulfate salts of alkali earth species.

6. The study of bed agglomeration process in this work, as previously reported in the literature, was the complex physical and chemical interactions between a number of ash forming elements and bed particle during thermal process and it was the reactor scale independent.

7. The model analyses provided the descriptions consistent with the experimental results of the present study and previous works on the bed agglomeration behaviors. The ash chemistry and the bed (combustion) temperature, as found in this study, were highly significant to bed agglomeration as the major contribution, while the bed operating parameters show the minor effect. The fluidizing air velocity dominated the contributions in the breaking and collision of agglomerates in fluidized bed, while the static bed height was less significant.

8. The fairly well to good predictability of the presently proposed mathematical models on the defluidization behavior, represented by the defluidization time, were obtained. ±21% and ±32% were the error ranges from the prediction with lab scale data by the newly developed model and the modified model, respectively. In addition, the modified model showed the slightly increase in the predictability, against with the original model.

CHAPTER 7 RECOMMENDATION

1. Since the study of bed agglomeration behaviors in this work was carried out with only four different biomass fuels at some specific operating conditions of FBC, more intensive works with various types of biomass and bed conditions are needed to investigate the further inorganic and bed agglomeration behaviors and to evidently verify the mechanism of bed agglomeration. In addition, the more experimental data being used, the more improvement in accuracy of the proposed models derived from the regression technique.

2. The initial steps of bed agglomeration process illustrated in Figure 5.23 were determined by two competitive processes: (1) condensation/deposition and (2) collision. The present experimental results revealed that these processes are dependent significantly on the chemistry of biomass. Presently, the degree of contributions in either relative or absolute of these processes are not investigated. The degree of contributions provides the further important information of the determining process of an individual biomass during bed agglomeration and the concept to develop the models with the enhanced accuracy of prediction. Additionally, the intensive study of the inorganic released behaviors which provide the important information on the ash-bed particle interaction is necessarily.

3. The further mathematical models, which predict the time dependent size distribution of any bed particle as a function of the controlled operating conditions and the fuel properties, is interested to develop in order to verify the pressure loss profile during bed defluidization. It is a theoretical model which may further predict the defluidization time.

4. The experimental verification in the plant/commercial scale fluidized bed boiler including the model verification can be the further works.

5. The future study in the mechanisms on the inorganic mitigation of bed agglomeration in FBC and the selection of appropriate additives for the observed biomass is recommended.

REFERENCES

1. United Nations Environments Programme {UNEP), **Global Trends in Sustainable Energy Investment 2007: Analysis of Trends and Issues in the Financing of Renewable Energy and Energy Efficiency in OECD and Developing Countries** [Online], Available : http://sefi.unep.org/fileadmin/media/sefi/docs/publications/SEFI_Investment_Report_2007.pdf [2010, March 16]

2. Renewable Energy Policy Network For the 21st Century (REN21), **Renewables 2010: Global Status Report** [Online], Available : http://www.ren21.net/REN21Activities/Publications/GlobalStatusReport/tabid/5434/Default.aspx [2011 , January 20]

3. Department of alternative energy development and efficiency, Ministry of Energy, **Thailand Energy Situation 2009** [Online], Available : http://www.dede.go.th/dede/images/stories/stat_dede/ThailandEnergySituation2009.pdf [2010, February 4]

4. Department of alternative energy development and efficiency, Ministry of Energy, **Thailand Alternative Energy Situation 2009** [Online], Available : http://www.dede.go.th/dede/images/stories/stat_dede/Thailand_Alter2009.pdf [2010, February 4]

5. WIKIPEDIA: The Free Encyclopedia, **Fossil fuel** [Online], Available : http://en.wikipedia.org/wiki/Fossil_fuel.html [2010, May 8]

6. Ladanai, S. and Vinterbäck, J., 2009, **Global Potential of Sustainable Biomass for Energy**, Report No. 013, Department of Energy and Technology, Swedish University of Agricultural Sciences

7. Sustainable Bioenergy Development in UEMOA Member Countries, **Chapter 5. Biomass Conversion Technologies** [Online], Available : http://www.globalproblems-globalsolutions-files.org/gpgs_files/pdf/UNF_Bioenergy/UNF_Bioenergy_5.pdf [2008, April 24]

8. Jenkins, B.M., Baxter, L.L., Miles Jr, T.R. and Miles, T.R., 1998, "Combustion properties of biomass", **Fuel Processing Technology**, Vol. 54, pp. 17-46.

9. Energy Press, **"PEA ENCOM International" - first subsidiary of Provincial Electricity Authority to penetrate both domestic and international energy businesses** [Online], Available : http://www.newswit.com/.nrg/2010-08-11/8cb748023252a86ea1f9261ae42424f3/ [2010, August 11]

10. Kwauk, M., 1992, **Fluidization: idealized and bubbles with application**, 1st ed., Science Press, Beijing, pp. 1-12.

11. Oka, S.N., 2004, **Fluidized bed combustion**, 1st ed., Marcel Dekker Inc, New York.

12. Werther, J., Saenger, M., Hartge, E.-U., Ogada, T and Siagi, Z., 2000, "Combustion of agricultural residues", **Progress in Energy and Combustion Science**, Vol. 26, pp. 1-27.

13. Benson, S.A. and Sondreal, E.S., 1999, "Ash-related issues during combustion and gasification", In **Impact of Mineral of Impurities in Solid fuel Combustion**, Gupta, R.P., Wall, T.F. and Baxter, L. (Ed.), Kluwer Academic Publisher, New York, pp. 1-21.

14. Goldberger, W.M., 1967, "Collection of fly ash in a self-agglomerating fluidized bed coal burner", **ASME Winter Annular Meeting and Energy Systems Exposition**, paper 67-WA/FU-3, 12-17 November, Pittsburgh, Pennsylvania.

15. Langston, B.G. and Stephens, F.M.J, 1960, "Self agglomerating fluidized bed conduction", **Journal of Metals**, Vol. 12, pp. 312-316.

16. Sadler, A.M., 1967, "High temperature fluidized bed process for the production of Portland cement", **AICHE Meeting**, New York.

17. Jacob, M., 2004, "An introduction to continuous fluidized-bed agglomeration and spray granulation", **Powder and Bulk Engineering**, Vol. 18, No. 4, pp. 23-61.

18. Gluckman, M.J., Yerushalmi, J. and Squires, A.M., 1976, "Defluidization characteristics of sticky or agglomerating beds", In **Fluidization Technology II**, Keairns, D.L. (Ed.), Hemisphere, Washington, pp. 395-422.

19. Benson, S.A., Karner, F.R., Goblirsch, G.M., and Brekke, D.W., 1982, "Bed agglomerates formed by atmospheric Fluidized-Bed combustion of A North Dakota lignite", Preprint Paper, **American Chemical Society**, Division of Fuel Chemistry, Vol. 27, pp. 174-181.

20. Manzoori, R.A. and Agarwal, P.K., 1994, "Agglomeration and defluidization under simulated circulating fluidized bed combustion conditions", **Fuel**, Vol. 73, No. 4, pp. 563-568.

21. Padban, N., Kiuru, S. and Hallgren, A.L., 1995, "Bed agglomeration on PFB biomass gasification", Preprint paper, **American. Chemical. Society**, Division of Fuel Chemistry, Vol. 40, pp. 743-747.

22. Öhman, M., Nordin, A., Lundholm, K., Bostrom, D., Hedman, H and Lundberg M., 2003, "Ash transformations during combustion of meat-, bonemeal, and RDF in a (bench-scale) fluidized bed combustor", **Energy and Fuels**, Vol. 17, No. 5, pp. 1153-1159.

23. Mann, M.D., Galbreath, K.C. and Kalmanovitch, D.P., 1992, "The role of ash chemistry and operating parameters on ash agglomeration and deposition in FBC systems", In **Inorganic Transformations and Deposition during Combustion**, Benson, S.A. (Ed.), ASME, New York.

24. Skrifvars, B.-J., Zevenhoven, M., Backman, R., Öhman, M. and Nordin, A., 2000, **Effect of Fuel quality on the bed agglomeration tendency in biomass fired fluidized bed boiler**, Report No. Värmeforsk B8-803. Thermal Engineering Research Association (Värmeforsk)

25. Vuthaluru, H.B. and Zhang, D.K., 1999, "Control methods for remediation of ash-related problems in fluidised-bed combustors", **Fuel Processing Technology**, Vol. 60, No. 2, pp. 145-156.

26. Vuthaluru, H.B., Linjewile, T.M., Zhang, D.K. and Manzoori, A.R., 1999, "Investigations into the control of agglomeration and defluidisation during fluidised-bed combustion of low-rank coals", **Fuel**, Vol. 78, No. 4, pp. 419-425.

27. Ghaly, A.E., Ergudenler, A. and Lafuger, E., 1993, "Agglomeration characterization of alumina sand-straw ash mixtures at elevated temperature", **Biomass and Bioenergy**, Vol. 5, No. 6, pp. 467-480.

28. Brus, E., Öhman, M., Nordin, A., Boström, D., Hedman, H. and Eklund, A., 2004, "Bed Agglomeration Characteristics of Biomass Fuels Using Blast-Furnace Slag as Bed Material", **Energy and Fuels**, Vol. 18, No. 4, pp. 1187-1193.

29. Livingston, W.R., 2007, **Biomass ash characteristics and behaviour in combustion, gasification and pyrolysis systems**, Report No: 34/07/005, Doosan Babcock Energy Limited.

30. Energy research Center of Netherlands (ECN), **PHYLLIS** [Online], Available : http://www.ecn.nl/phyllis/ [1998, March 12]

31. Bios Bioenergiesysteme GmbH, Graz, Austria, **Biobank** [Online], Available : http://www.ieabcc.nl/database/biobank.html/

32. Technical University of Vienna, Austria, **BIOBIB** [Online], Available : www.vt.tuwien.ac.at/biobib/biobib.html

33. U.S Department of Energy (USDOE), **Biomass Feedstock Composition and Property Database** [Online], Available : http://www.eere.energy.gov/biomass/feedstock_databases.html

34. Bryers, R.W., 1996, "Fireside slagging, fouling, and high-temperature corrosion of heat-transfer surface due to impurities in steam-raising fuels", **Progress in Energy and Combustion Science**, Vol. 22, No. 1, pp. 29-120.

35. Baxter, L.L., 1993, "Ash deposition during biomass and coal combustion: a mechanistic approach", **Biomass and Bioenergy**, Vol. 4, No. 2, pp. 85-102.

36. Marschner, H., 1995, **Mineral Nutrition of Higher Plants**, 2nd ed., Academic Press, New York, pp. 229-369.

37. WIKIPEDIA: The Free Encyclopedia, **Chlorophyll** [Online], Available : http://en.wikipedia.org/wiki/Chlorophyll [2011, May 25]

38. Wornat, M.J., Hurt, R.H., Yang, N.Y.C. and Headley, T.J., 1995, "A structural and compositional transformation of biomass chars during combustion", **Combustion and Flame**, Vol. 100, pp. 131-143.

39. Sultenfuss, J.H. and Doyle, W.J., 1999, "Functions of Phosphorus in Plants", **Better Crops with Plant Food**, Vol. 83, No.1, pp. 6-7.

40. WIKIPEDIA: The Free Encyclopedia, **Arginase** [Online], Available : http://en.wikipedia.org/wiki/Arginase [2011, June 17]

41. WIKIPEDIA: The Free Encyclopedia, **Phosphotransferase** [Online], Available : http://en.wikipedia.org/wiki/Phosphotransferase [2011, April 3]

42. WIKIPEDIA: The Free Encyclopedia, **Osmoregulation** [Online], Available : http://en.wikipedia.org/wiki/Osmoregulation [2011, July 25]

43. Korbee, R., Keil, J.H.A., Zevenhoven, M., Skrifvars, B.-J., Jensen, P.A and Frandsen, F.J., 2001, "Investigation of biomass inorganic matter by advanced fuel analysis and conversion experiments", **Power Production in the 21st Century: Impacts of Fuel and Operations**, 28 October - 2 November, Snow-bird, Utah.

44. Benson, S.A. and Holm, P.L., 1985, "Comparison of inorganic constituents in three low-rank coals", **Industrial Engineering Chemistry Production Research and Development**, Vol. 24, pp. 145-149.

45. Baxter L.L., 1994, **Task 2. Pollutant emission and deposit formation during combustion of biomass fuels**, Quarterly report to National Renewable Energy Laboratory, Sandia National Laboratories, Livermore, California.

46. Miles, T.R., Mile, T.R. Jr, Baxter, L.L., Bryers, R.W., Jinkins, B.M. and Oden, L.L., 1996, **Alkali deposits found in biomass power plants: A preliminary investigation of their extent and nature**, Final Report No. NREL/TP-433-8142 to National Renewable Energy Laboratory, Sandia National Laboratories, Livermore, California.

47. Zevenhoven-Onderwater, M., 2003, **Ash forming matter in biomass fuels**, Academic Dissertation, Faculty of Chemical Engineering, Abo academy, Finland.

48. Torres, W., Pansare, S.S. and Goodwin Jr, J.G., 2007, "Hot Gas Removal of Tars, Ammonia, and Hydrogen Sulfide from Biomass Gasification Gas", **Catalysis Reviews**, Vol. 49, pp. 407-456.

49. Nordin, A., 1994, "Chemical elements characteristics of biomass Fuels", **Biomass and Bioenergy**, Vol. 6, No. 5, pp. 339-347.

50. Skrifvars, B.-J., Hupa, M., Moilanen, A. and Lundqvist, R., 1996, "Characterization of biomass ashes", In **Applications of Advanced Technology to Ash-related Problems in Boilers**, Baxter, L. and DeSollar, R. (Ed.), Plenum Publishers, New York, pp. 383-398.

51. van der Drift, A. and Olsen, A., 1999, **Conversion of biomass {private} prediction and solution methods for ash agglomeration and related problems**, Report No. ECN-C-99-090, Energy research Center of Netherlands (ECN).

52. Vassilev, S., Baxter, D., Andersen, L. and Vassileva, C., 2010, "An overview of the chemical composition of biomass", **Fuel**, Vol. 89, pp. 913-933.

53. Misra, M.K., Ragland, K.W. and Baker, A.J., 1993, "Wood ash composition as a function of furnace temperature", **Biomass and Bioenergy**, Vol. 4, No. 2, pp. 103-116.

54. Bryer, R.W., 1994, **Analysis of a Suite of Biomass Samples**, Report FWC/FWDC/TR-94/03 to the alkali deposit investigation, Foster Wheeler Development Corporation, Livingston, New Jersey.

55. Olsson, J.G., Jaglid, U. and Pettersson, J.B.C., 1997, "Alkali metal emission during pyrolysis of biomass", **Energy and Fuels**, Vol. 11, pp. 779-784.

56. Davidsson, K.O., Stojkova, B.J. and Pettersson, J.B.C, 2002, "Alkali emission from birchwood particles during rapid pyrolysis", **Energy and Fuels**, Vol. 16, pp.1033-1039.

57. Dayton, D.C., French, R.J. and Milne, T.A., 1995, "Direct observation of alkali vapor release during biomass combustion and gasification. 1. Application of molecular Beam/Mass Spectrometry to switchgrass combustion", **Energy and Fuels**, Vol. 9, pp. 855-865.

58. Dayton, D.C., Jenkin, B.M., Turn, S.Q., Bakker, R.R., Williams, R.B., Belle-Oudry, D. and Hill, L.M., 1999, "Release of inorganic constituents from leached biomass during thermal conversion", **Energy and Fuels**, Vol. 13, pp. 860-870.

59. Bjorkman, E. and Stromberg B., 1997, "Release of chlorine from biomass at pyrolysis and gasification conditions", **Energy and Fuels**, Vol. 11, pp. 1026-1032.

60. Jensen, P.A., Frandsen, F.J., Johansen, K.D. and Sander, B., 2000, "Experimental investigation of the transformation and release to gas phase of potassium and chlorine during straw pyrolysis", **Energy and Fuels**, Vol. 14, pp. 1280-1285.

61. Okuno, T., Sonoyama, N., Hayashi, J.I., Li, C.Z., Sathe. C. and Chiba, T., 2005, "Primary release of alkali and alkaline earth metallic species during the pyrolysis of pulverized biomass", **Energy and Fuels**, Vol. 19, pp. 2164-2171.

62. Knudsen, J.N., Jensen, P.A., and Johansen, K.D., 2004, "Transformation and release to the gas phase of Cl, K, and S during combustion of annual Biomass", **Energy and Fuels**, Vol. 18, pp. 1385-1399.

63. Westberg, H.M., Bystorm, M. and Leckner B., 2003, "Distribution of potassium, chlorine and sulfur between solid and vapor phases during combustion of wood chips and coal", **Energy and Fuels**, Vol. 17, pp.18-28.

64. Knudsen, J.N., Jensen, P.A., Lin, W., Frandsen, F.J. and Johansen, K.D., 2004, "Sulfur transformations during thermal conversion of herbaceous biomass", **Energy and Fuels**, Vol. 18, pp. 810-819.

65. Glazer, M.P., Khan, N.A., de Jong, W., Spliethoff, H., Schurmann, H. and Monkhouse, P., 2005, "Alkali metals in circulating fluidized bed combustion of biomass and coal: measurements and chemical equilibrium analysis", **Energy and Fuels**, Vol. 19, pp. 1889-1897.

66. Iisa, K. and Lu, Y., 1999, "Sulfation of potassium chloride at combustion condition", **Energy and Fuels**, Vol. 13, pp. 1184-1190.

67. Knudsen, J.N., Jensen, P.A., Lin, W., and Johansen, K.D., 2005, "Secondary capture of chlorine and sulfur during thermal conversion of biomass", **Energy and Fuels**, Vol. 19, pp. 606-617.

68. French, R. and Milne, T.A., 1994, "Vapor phase release of alkali species in the combustion of biomass pyrolysis oils", **Biomass and Bioenergy**, Vol. 7, No.1-6, pp. 315-325.

69. Valmari, T., 2000, **Potassium behavior during combustion of wood in circulating fluidized bed power plants**, Dissertation, VTT Chemical Technology, Technical research center of FINLAND.

70. WIKIPEDIA: The Free Encyclopedia, **Potassium oxide** [Online], Available : http://en.wikipedia.org/wiki/Potassium_oxide [2011, July 7]

71. Arvelakis, S., Gehrmann, H., Beckmann, M. and Koukios, E.G., 2003, "Agglomeration problems during fluidized bed gasification of olive-oil residue: evaluation of fractionation and leaching as pre-treatments", **Fuel**, Vol. 82, pp. 1261-1270.

72. Visser, H.J.M., 2004, **The influence of fuel composition on agglomeration behavior in fluidized-bed combustion**, Report No. ECN-C-04-054, Energy research Center of Netherlands (ECN).

73. Nuutinen, L.H., Tiainen, M.S., Virtanen, M.E., Enestam, S.H. and Laitinen, R.S., 2004, "Coating layers on bed particles during biomass fuel combustion in fluidized-bed boilers", **Energy and Fuels**, Vol. 18, pp. 127-139.

74. Fryda, L., Panopoulos, K., Vourliotis, P., Pavlidou, E. and kakaras, R., 2006, "Experimental investigation of fluidized bed co-combustion of meat and bone meal with coals and olive bagasse", **Fuel**, Vol. 85, pp. 1685-1699.

75. Lundholm, K., Nordin, A., Öhman, M. and Bostrom, D., 2005, "Reduced bed agglomeration by co-combustion biomass with peat fuels in a fluidized bed", **Energy and Fuels**, Vol. 19, pp. 2273-2278.

76. Sorensen, L.H., Fjellerup, J. and Henriksen, U., 2003, **Method for reducing agglomeration, sintering and deposit formation in gasification and combustion of biomass**, US Patent No. 6615751.

77. Cohen, D., 2004, **Form and distribution of trace elements in biomass for power generation**, Research report No.48, Cooperative research centre for coal in sustainable development, Australian government's cooperative research centres program.

78. Bakisgan, C., Dumanli A.G. and Yurum, Y., 2009, "Trace elements in Turkish biomass fuels: Ashes of wheat straw, olive bagasse and hazelnut shell", **Fuel**, Vol. 88, pp. 1842-1851.

79. Font, O., Cordoba, P., Querol, X., Coca, P. and Garcia-Pena, F., 2011, "Co-Gasification of biomass: effect on the fate of trace elements", **2011 World of Coal Ash (WOCA) Conference**, 9-12 May, Denver, Colorado.

80. Paris, R., Desboeufs, K.V., Formenti, P., Nava, S. and Chou, C., 2010, "Chemical characterisation of iron in dust and biomass burning aerosols during AMMA-SOP0/DABEX: implication for iron solubility" **Atmospheric Chemistry and Physics**, Vol. 10, pp. 4273-4282.

81. Somppi, J.L., Kauppinen, E.I., Kurkela, J., Tapper, U., Öhman, M., Nordin, A. and Johanson, B., 1998, "Ultrafine ash particle formation during waste sludge incineration in fluidized bed reactors", **Combustion Science and Technology**, Vol.134, pp. 433-455.

82. Mann, D., Henderson, A.K., Swanson, M.L., Allan, S.E., 1996, **Development of methods to predict agglomeration and deposition in Fluidized-bed combustion systems (FBCS)**, Topical report DOE/MC/30098-5232 (DE96004497), U.S. Department of Energy.

83. Christensen, K.A., 1995, "**The formation of submicron particles from the combustion of straw**", Dissertation, Technical University of Denmark.

84. Somppi, J.L., Kurkela, J., Tapper, U., Kauppinen, E.I., Jokiniemi, J.K. and Johansson, B., 1998, "Ash deposition on bed-material particles during fluidized bed combustion of wood-based fuels", **The ABC '98 International conference on ash behavior control in energy conversion systems**, 18-19 March, Yokohama, pp. 110-118.

85. Brus, E., Öhman, M. and Nordin, A., 2005, "Mechanisms of Bed Agglomeration during Fluidized-bed Combustion of Biomass Fuels", **Energy and Fuels**, Vol. 19, pp. 825-832.

86. Kihara, T. and Ichimaru, S., 1978, **Intermolecular forces**, John Wiley & Sons, Chichester, U.K., pp. 1-5.

87. Seville, J.P.K., Willett, C.D. and Knight, P.C., 2000, "Interparticle forces in fluidization: a review", **Powder Technology**, Vol. 113, pp. 261-268.

88. Seville, J., Tüzün, U. and Clift, R., 1997, **Processing of particulate solids**, 1st ed., Blackie academic and professional, London, pp. 99-144.

89. Shaw, D.J., 1992, **Introduction to colloid and surface chemistry**, 4th ed., Butterworths-Heinemann, London, pp. 67-69.

90. Stachowiak, G.W. and Batchelor, A.W., 2001, **Engineering Tribology**, 2nd ed., Butterworth-Heinemann, Boston, pp. 130-133.

91. Senior, C.L. and Srinivasachar, S., 1995, "Viscosity of ash particles in combustion systems for prediction of particle sticking", **Energy and Fuels**, Vol. 9, pp. 277-283.

92. Skrifvars B.-J., Hupa M., Backman R. and Hiltunen M., 1994, "Sintering Mechanisms of FBC Ashes", **Fuel**, Vol. 73, No. 2, pp. 171-176.

93. Skrifvars, B.-J. Hupa, M. and Hiltunen M., 1992, "Sintering of ash during fluidized bed combustion", **Industrial and Engineering Chemistry Research**, Vol. 31, No. 4, pp. 1026–1030.

94. Skrifvars, B.-J., Backman, R. and Mikko, M., 1998, "Characterization of the sintering tendency of ten biomass ashes in FBC conditions by a laboratory test and by phase equilibrium calculation", **Fuel Processing Technology**, Vol. 56, pp. 55-67.

95. Skrifvars, B.-J. Hupa, M. and Anthony, E.J., 1998, "Mechanisms of bed material agglomeration in al petroleum coke-fired circulating fluidized bed boiler", **Journal of Energy Resources Technology**, Vol. 120, pp. 215-218.

96. Anthony, E.J., Iribarne, A.P., and Iribarne, J.V., 1995, "A new mechanism for FBC agglomeration and fouling when firing 100% petroleum coke", **Journal of Energy Resources Technology**, Vol. 119, pp. 55-61.

97. Tardos, G. and Pfeffer, R., 1995, "Chemical reaction induced agglomeration and defluidization of fluidized bed", **Powder Technology**, Vol. 85, pp. 29-35.

98. Frenkel, J., 1945, "Viscous flow of crystalline bodies under the action of surface tension", **Journal of Physics**, Vol. 9, No. 5, pp. 385-391.

99. Brus, E., 2004, **Bed agglomeration during combustion and gasification of biomass fuels mechanisms and measure prevention**, Licentiate Thesis, Energy Technology and thermal Process Chemistry, Umea University, Sweden.

100. Perkins, III D., Brekke, D.W. and Karner F.R., 1984, **Analysis of atmospheric fluidized-bed combustion agglomerates**, Final report DOE/FC/10120-1608, U.S. Department of Energy.

101. Manzoori, A.R. and Agarwal, P.K., 1992, "The fate of organically bound inorganic elements and sodium chloride during fluidized bed combustion of high sodium, high sulphur low rank coals", **Fuel**, Vol. 71, No. 5, pp. 513-522.

102. Manzoori, A.R. and Agarwal, P.K., 1993, "The role of inorganic matter in coal in the formation of agglomerates in circulating fluid bed combustors", **Fuel**, Vol. 72, No. 7, pp. 1069-1075.

103. Ergudenler, A. and Ghaly, A. E., 1993, "Agglomeration of alumina sand in a fluidized bed straw gasifier at elevated temperature", **Bioresource Technology**, Vol. 43, pp. 259-268.

104. Grubor, B., Oka, S., Ilić, M., Dakić, D. and Arsic, B.T., 1995, "Biomass FBC Combustion - Bed Agglomeration Problems", **The 13th International Conference on Fluidized Bed Combustion**, 7-10 May, Orlando, Florida, Vol. 1, pp. 515-522.

105. Bapat, D.W., Kulkarni, S.V. and Bhandarkar, V.P., 1997, "Design and operating experience on fluidized bed boiler burning biomass fuels with high alkali ash", **The 14th International Conference on Fluidized Bed Combustion**, 11-14 May, Vancouver, pp. 165-174.

106. Öhman, M., Nordin, A., Skrifvars, B.J., Backman, R. and Hupa, M., 2000, "Bed agglomeration characteristics during Fluidized bed combustion of biomass fuels", **Energy and Fuels**, Vol. 14, pp.169-178.

107. Öhman, M., 1998, "A new method for quantification of fluidized bed agglomeration tendencies: A sensitivities analysis", **Energy and Fuels**, Vol. 12, pp.90-94.

108. Atakul, H. and Ekinci, E., 1989, "Agglomeration of Turkish lignites in fluidized-bed combustion", **Journal of the Institute of Energy**, Vol. 62, pp. 56-61.

109. Lin, W., Johansen, K.D. and Frandsen, F., 2003, "Agglomeration in bio-fuel fired fluidized bed combustors", **Chemical Engineering Journal**, Vol. 96, pp. 171-185.

110. Chirone, R., Miccio, F. and Scala, F., 2006, "Mechanism and prediction of bed agglomeration during fluidized bed combustion of a biomass fuel: Effect of the reactor scale", **Chemical Engineering Journal**, Vol. 123, pp. 71-80.

111. Scala, F. and Chirone, R., 2006, "Characterization and early detection of bed agglomeration during the fluidized bed combustion of olive husk", **Energy and Fuels**, Vol. 20, pp. 120-132.

112. Vamvuka, D. and Zogrofos, D., 2004, "Predicting the behavior of ash from agricultural wastes during combustion", **Fuel**, Vol. 83, pp. 2051-2057.

113. Salour, D., Jenkins, B.M., Vafei, M. and Kayhanian, M., 1993, "Control of in-bed agglomeration by fuel blending in a pilot scale straw and wood fueled AFBC", **Biomass and Bioenergy**, Vol. 4, No. 2, pp. 117–133.

114. Osman, E.A., 1982, **A study of the effects of ash chemical composition and additives on fusion temperature in relation to slag formation during gasification of biomass**, Dissertation, University of California.

115. Zevenhoven-Onderwater, M., Backman, R., Skrifvars, B.J. and Hupa, M., 2001, "The ash chemistry in fluidised bed gasification of biomass fuels. Part I: predicting the chemistry of melting ashes and ash–bed material interaction", **Fuel**, Vol. 80, pp. 1489–1502.

116. Zevenhoven-Onderwater, M., Blomquist, J.P., Skrifvars, R., Beckman, R. and Hupa, M., 2000, "The prediction of behavior of ashes from five different solid fuels in fluidized bed combustion", **Fuel**, Vol. 79, pp. 1353-1361.

117. Huffman, G.P., Huggins, F.E. and Dunmyre, G.R., 1981, "Investigation of the high-temperature behaviour of coal-ash in reducing and oxidizing atmosphere", **Fuel**, Vol. 60, pp. 585-597.

118. Padban, N., Ye, Z. and Bjerle, I., "Alkali removal and bed material agglomeration studies applied to biomass gasification", In **Development in thermochemical biomass conversion**, Vol. 2, Bridgwater, A.V. (Ed.), Kluwer academic publishers, London, pp. 1031-1037.

119. Manzoori, A.R., 1990, **Role of inorganic matter in agglomeration and defluidization during the circulating fluidized-bed combustion conditions**, PhD Thesis, The University of Adelaide, Adelaide, Australia.

120. Al-Otoom, A.Y., Elliott, L. K., Wall, T.F. and Moghtaderi, B., 2000, "Measurement of the sintering kinetics of coal ash", **Energy and Fuels**, Vol. 14, pp. 994-1001.

121. Al-Otoom, A.Y., Ninimiya, Y., Moghtaderi, B. and Wall, T.F., 2003, "Coal ash buildup on ceramic filters in a hot gas filtration system", **Energy and Fuels**, Vol. 17, pp. 316-320.

122. Tangsathitkulchai, C. and Tangsathitkulchai, M., 2001, "Effect of bed materials and additives on the sintering of coal ashes relevant to agglomeration in fluidized bed combustion", **Fuel Processing Technology**, Vol. 72, No. 3, pp. 163-183.

123. Hansen, L.A., Frandsen, F.J., Sorensen, H.S., Rosenberg, P., Hjuler, K. and Johansen, K.D., 1999, "Ash fusion and deposit formation at straw fired boilers", In **Impact of mineral impurities in solid fuel combustion**, Gupta, R.P., Wall, T.F. and Baxter, L. (Ed.), Kluwer Academic Publisher, New York, pp. 341-356.

124. Arvelakis, S., Jensen, P.A. and Johansen, K.D., 2004, "Simultaneous thermal analysis (STA) on ash from High-Alkali biomass", **Energy and Fuels**, Vol. 18, pp. 1066-1076.

125. Moilanen, A., Nieminen, M., Sipila, K. and Kurkela, E., 1996, "Ash behavior in thermal fluidized-bed conversion processes of woody and herbaceous biomass", In Biomass for Energy and the Environment, **The 9th European Bioenergy Conference**, June, Copenhagen, Denmark, Pergamon/Elsevier Publishers, pp. 1227-1232.

126. Moilanen, A., Kurkela, E. and Luntama, J.L., 1999, "Ash behaviour in biomass fluidised-bed gasification" In **Impact of mineral of impurities in solid fuel combustion**, Gupta, R.P., Wall, T.F. and Baxter, L. (Ed.), Kluwer Academic Publisher, New York, pp. 555-567.

127. Conn, R.E., 1995, "Laboratory techniques for evaluating ash agglomeration potential in petroleum coke fired circulating fluidized bed combustor", **Fuel Processing Technology**, Vol. 44, pp. 95-103.

128. Skrifvars, B.J., Öhman, M., Nordin, A. and Hupa, M., 1999, "Predicting Bed Agglomeration Tendencies for Biomass Fuels Fired in FBC Boilers: A Comparison of Three Different Prediction Methods", **Energy and Fuels**, Vol. 13, pp.359-363.

129. Brown, R.C., Dawson, M.R. and Smeenk, J.L., 1996, **Bed material agglomeration during fluidized bed combustion**, Final Report DOE/PC/92530-T14, U.S. Department of Energy.

130. Schouten, J.C. and van den Bleek, C.M., 1998, "Monitoring the quality of fluidization using the short-term predictability of pressure fluctuation", **AICHE Journal**, Vol. 44, pp. 48-60.

131. van Ommen, J.R., Coppens. M.O. and van den Bleek, C.M., 2000, "Early warning of agglomeration in fluidized bed by attractor comparison", **AICHE Journal**, Vol. 46, pp. 2183-2197.

132. Korbee, R., Lensselink, J., van Ommen, J.R., Nijenhuis, J., van Gemert, M. and Haasnoot, K., 2004, **Early Agglomeration Recognition System – EARS From bench-scale testing to industrial prototype**, Report No. ECN-C-04-052, Energy research Center of Netherlands (ECN).

133. Goblirsch, G.M., Benson, S.A., Hajicek, D.R. and Cooper, J.L., 1982, "Sulfur Control and Bed Material Agglomeration Experience in Low-Rank Coal AFBC Testing", **The 7th International Conference on Fluidized-Bed Combustion**, 25-27 October, Philadelphia, Pennsylvania, pp. 1107-1120.

134. Svoboda, K., Cermak, Ji., Hartman, M. and Pohorely, M., 2000, "Possible ways of suppression of agglomeration of particles in fluidized bed combustion of selected waste biomass", **Energy Forum 2000**, 17-19 September, Varna, Bulgaria, pp. 1-6.

135. Silvennoinen, J., 2003, "A new method to inhibit bed agglomeration problems in fluidized bed boilers", **The 17th International Conference on Fluidized Bed Combustion**, ASME, New York.

136. Tsuo, Y and Wasson, E. (Kvaerner Power Inc.), 2004, "Utilization of waste fuels for power generation", **Southeastern and VA-Carolina Conference**, 17-18 February, Rock Hill, South Carolina.

137. Linjewile, T.M. and Manzoori, A.K., 1999, "Role of additives in controlling agglomeration and defluidisation during fluidised bed combustion of high-sodium, high-sulphur low-rank coal", In **Impact of mineral of impurities in solid fuel combustion**, Gupta, R.P., Wall, T.F. and Baxter, L. (Ed.), Kluwer Academic Publisher, New York, pp. 319-331.

138. Hallgren, A.L. and Oskarsson, J., 1998, "Minimization of sintering tendencies in fluidized-bed gasification of energy crop fuels", In **Biomass for Energy and Industry**, 10th European Biomass Conference, June, Würzburg, Germany, pp. 1700-1703.

139. Bhattacharya, S.P. and Harttig, M., 2003, "**Control of agglomeration and defluidization burning high alkali and high sulfur lignites in a small fluidized bed combustor - Effect of additive size and type and the role of calcium**", Energy and Fuels, Vol. 17, pp. 1014-1021.

140. Öhman, M. and Nordin, A., 2000, "The role of kaolin in prevention of bed agglomeration during fluidized bed combustion of biomass fuels", **Energy and Fuels**, Vol. 14, pp. 618-624.

141. Punjak, W.A., Uberoi, M. and Shadman, F., 1989, "Control of ash deposition through the high temperature adsorption of alkali vapors on solid sorbents", **Symposium on ash deposition: mineral matter deposition phenomena, formation and control**, 9-14 April, Dallas, Texas, pp. 399-435.

142. Turn, S.Q., Kinoshita, C.M., Ishimura, D.M., Zhou, J., Hiraki, T.T. and Masutani, S.M., 1998, "A review of sorbent materials for fixed bed alkali getter systems in biomass gasifier combined cycle power generation applications", **Journal of the Institute of Energy**, Vol. 71, pp. 163-177.

143. Daavitsainen, J.H.A., Nuutinen, L.H., Ollila, H.J., Tiainen, M.S. and Laitinen, R.S., 2001, "FB combustion of bark and sawdust in silica sand bed with dolomite addition: A case study", **The 16th International Conference on Fluidized Bed Combustion**, 13-16 May, Reno, Nevada, pp. 1314-1323.

144. Nordin, A. Öhman, M. Skrifvars, B-J. Hupa, M., 1996, "Agglomeration and defluidization in FBC of biomass fuels - Mechanisms and measures for prevention", In **Applications of advanced technology to ash-related problems in boilers**, Baxter, L. and DeSollar, R. (Ed.), Plenum Press, New York, pp. 353-366.

145. Arvelakis, S., Gehrmann, H., Beckmann, M. and Koukios, E.G., 2002, "Effect of leaching on the ash behavior of olive residue during fluidized bed combustion", Biomass and Bioenergy, Vol. 22, pp. 55-69.

146. Bakker, R.R., Jenkins, B.M. and Williams, R.B., 2002, "Fluidized bed combustion of Leached rice straw", **Energy and Fuels**, Vol. 16, pp. 356-365.

147. Reynolds, G.K., Fu, J.S., Cheong, Y.S., Hounslow, M.J. and Salman, A.D., 1993, "Breaking in a granulation: A review", **Powder technology**, Vol. 60, pp. 3969-3992.

148. Kunii, D. and Levenspiel, O., 1991, **Fluidization engineering**, 2nd ed., Butterworth-Heinemann, Boston.

149. Lin, W., Krusholm, G., Johansen, K.D., Musahl, E., Bank, L., 1997, "Agglomeration phenomena in fluidized bed combustion of straw", **The 14th International Conference on Fluidized Bed Combustion**, 11-14 May, Vancouver, pp. 831-838.

150. Basu, P. and Sarka, A., 1983, "Agglomeration of coal ash in fluidized beds", **Fuel**, Vol. 62, pp. 924-926

151. Steve Charlson, S. and Taylor, B., 1999, "Bubbling fluidized bed installation capitalizes on sludge", **TAPPI Engineering Conference**, 12-16 September, Anaheim, California, pp. 1-8.

152. Department of Alternative Energy Development and Efficiency (DEDE), Ministry of Energy, **Biomass potential in Thailand** [Online], Available : http://www.dede.go.th/dede/index.php?option=com_content&view=article&id=130:2010-05-07-08-10-57&catid=58&Itemid=68&lang=en [2010, April 21]

153. van de Wiel, H.J., 2003, **Determination of elements by ICP-AES and ICP-MS**, National Institute of Public Health and the Environment (RIVM), Bilthoven, Utrecht, Netherlands.

154. Siegell, J.H., 1984, "High-Temperature Defluidization", **Powder Technology**, Vol. 38, pp. 13-22.

155. Compo, P., Pfeffer, R. and Tardos, G. I., 1987, "Minimum sintering temperatures and defluidization characteristics of agglomerating particles", **Powder Technology**, Vol. 51, pp. 85-101.

156. Basu, P., 1982, "A study of agglomeration of coal-ash in fluidized beds", **Canadian journal of chemical engineering**, Vol. 60, pp. 791-795.

157. Liss, B., Blake, A., Squires, A.M. and Bryson, R., 1984, "Incipient defluidization of sinterable solids" In **Fluidization IV**, Kunii, D. et al. (Ed.), pp.249-256.

158. Seville, J.P.K., Silomon-Pflug, H. and Knight, P.C., 1998, "Modelling of sintering in high temperature gas fluidization", **Powder Technology**, Vol. 97, pp. 160–169.

159. Knight, P.C., Seville, J.P.K., Kamiya, H. and Hario, M., 2000, "Modelling of sintering of iron particles in high-temperature gas fluidization", **Chemical Engineering Science**, Vol. 55, pp. 4783–4787.

160. Tardos, G., Mazzone, D. and Pfeffer, R., 1985, "Destabilization of fluidized beds due to agglomeration Part I: theoretical model", **The Canadian journal of chemical engineering**, Vol. 63, pp. 377-383.

161. Tardos, G., Mazzone, D. and Pfeffer, R., 1985, "Destabilization of fluidized beds due to agglomeration Part II: experimental verification", **The Canadian journal of chemical engineering**, Vol. 63, pp. 384-389.

162. Moseley, J.L. and O'Brien, J.L, 1993, "A model for agglomeration in a fluidized bed", **Chemical Engineering Science**, Vol. 48, pp. 3043–3050.

163. Yang, Y., Arastoopour, H., Hariri, M.H. and Rehmat, A., 1993, "Agglomeration of polyolefin particles in a fluidized bed with a central jet. Part II-Theory", **Powder Technology**, Vol. 74, pp. 239-247.

164. Arena, U and Mastellone, M.L., 2001, "The phenomena of bed defluidiztion during the pyrolysis of a food-packaging plastic water", **Powder technology**, Vol. 120, pp. 127-133.

165. Ennis, B.J., Tardos, G. I. and Pfeffer, R., 1991, "A microlevel-based characterization of granulation phenomena", **Powder technology**, Vol. 65, pp. 257-272.

166. Lin, C.L., Wey, M.Y. and Lu, C.Y, 2006, "Prediction of defluidization time of alkali composition at various operating conditions during incineration", **Powder Technology**, Vol. 161, pp. 150-157.

167. Werther J, 1976, "Convective solids transport in large diameter gas fluidized beds", **Powder Technology**, Vol. 15, pp. 155-167.

168. Pitois O, Moucheront P and Chateau X, 2000, "Liquid bridge between two moving spheres: An experimental study of viscosity effects", **Journal of Colloid and Interface Science**, Vol. 231, pp. 26-31.

169. Barnocky, G. and Davis, R.H., 1988, "Elastohydrodynamic collision and rebound of spheres: Experimental verification", **Physical. Fluids**, Vol. 31, pp. 1324-1329.

170. Simons, S.J.R., 1996, "Modeling of agglomerating systems: from spheres to fractals", **Powder Technology**, Vol. 87, pp. 29–41.

171. Fox, R.W. and Mcdonald, A.T., 1994, **Introduction to fluid mechanics**, 4th ed., John Wiley&Sons Inc, New York.

172. Fluegel A, 2007, "Glass viscosity calculation based on a global statistical modeling approach", **Journal of Glass Science Technology. A**, Vol. 48, No. 1, pp. 13-30.

173. Mazurin, O.V., Streltsina, M.V. and Shvaikovskaya, T.P.S, 1983, **Handbook of glass data, Part A: Silica glass and binary silicate glasses**, Elsvier science publisher, New York.

174. Cullity, B.D. and Stock, S.R., 2001, **Elements of X-Ray Diffraction**, 3rd Ed., Prentice-Hall, New York, pp. 167-171.

175. Tamarin, A.I., 1964, "The origin of self-excited oscillations in fluidized bed", **International Chemical Engineering**, Vol. 4, pp. 50-54.

176. Svensson, A., Johnsson, F. and Leckner, B., 1993, "Fluid-dynamics of the bottom bed of circulating fluidized bed boilers", In **The 12th international conference on fluidized bed combustion**, Rubow, L.N. and Commonwealth, G. (Ed.), The American Society of Mechanical Engineers, pp. 887-897.

177. Scala, F and Chirone, R., 2008, "An SEM/EDX study of bed agglomerates formed during fluidized bed combustion of three biomass fuels", **Biomass and Bioenergy**, Vol. 32, pp. 252-266.

178. Ono, H., Nakahata, M.,Tsukihashi, F. and Sano, N., 1993, "Determination of Standard Gibbs Energies of Formation of MgO, SrO, and BaO", **Metallurgical Transactions**, Vol. 24B, pp. 487-492.

179. Levin, E.M, McMurdie, H.F. and Hall, F.P, 1956**, Phase diagrams for ceramists**, Vol. 1, American Ceramic Society, Columbus, New York.

180. Park, D., 1989, "Estimation of temperature difference between char particles and the fluidized bed in char combustion", **Fuel**, Vol. 68, pp. 1320-1324.

181. Crowe, C.T., 2005, **Multiphase flow handbook**, 1st ed., Taylor&Francis Group, New York, pp. 5-50-5-53.

APPENDIX A

Estimation of the ash melt fraction

X_{melt} in Equation 4.14 was estimated according to well known "Lever rule" on the ternary phase of the given elemental system. For instance, a system composed of three compounds A-B-C has the composition of A, B and C at point X as illustrated in Figure A.1. Point E in this figure is the ternary eutectic.

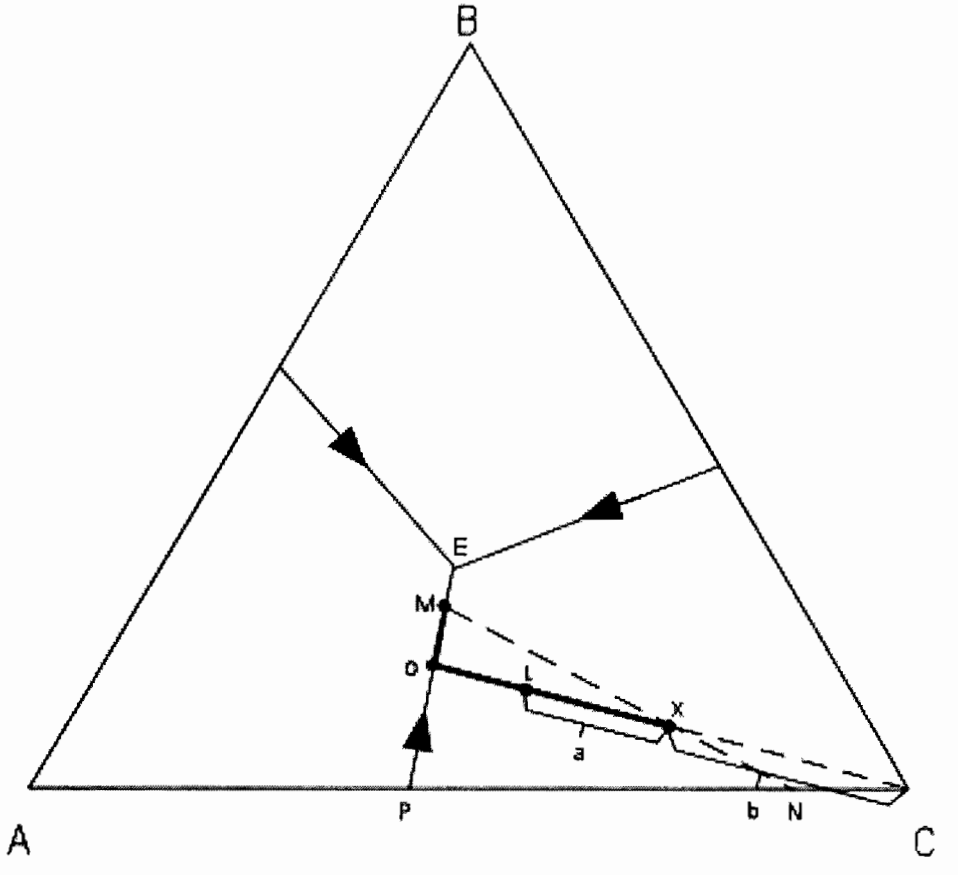

Figure A.1 Thermal behaviors of compounds in ternary phase diagram

Temperature referred to point X is called "liquidus temperature", at which the composition at X would be completely in liquid phase. At this point it would begin to precipitate crystals of C. As temperature is lowered, crystals of C would continue to precipitate, and the composition of the liquid would move along a straight line away from C. This is because C is precipitating and the liquid is becoming less in C and enriched in the components A + B.

As temperature decreased to point L which some amount of C has been precipitated, the relative portion of liquid phase and solid phase can be determined;

$$X_{liquid.at.L} = \frac{b}{a+b} \tag{A.1}$$

$$X_{soild.at.L} = \frac{a}{a+b} \tag{A.2}$$

With further cooling, the path of the liquid composition will intersect the boundary curve at point O. At the boundary curve, crystals of A will then precipitate. The liquid path will then follow the boundary curve towards point M. The bulk composition of the solid phase precipitated during this interval will be a mixture of A + C in the proportion shown by point P.

At point M, the bulk composition of the solid phases so far precipitated through the cooling history lies at point N (the extension of the straight line from M through the initial composition X). At this time the liquid and solid fraction will be given by the distances:

$$X_{liquid.at.M} = \frac{\overline{XN}}{\overline{MN}} \tag{A.3}$$

$$X_{solid.at.M} = \frac{\overline{XM}}{\overline{MN}} \tag{A.4}$$

With further cooling, the liquid composition will move to the ternary eutectic, Point E, at which crystals of B will precipitate. The temperature will remain constant until all of the liquid is used up. The final crystalline product will consist of crystals of A+B+C in the proportions given by the initial composition X.

APPENDIX B

Calculation of char surface temperature

The char surface temperature (T_{char}), an important parameter to estimate X_{melt}, is described by the energy balance at char surface between the heat generated by the combustion and the surface heat loss of char by fluidized bed. The main equations reported in a previous literature [180] are

$$T_{char} - T_b = \frac{\beta}{(1+\alpha)}(C_b q)\frac{D_{AB}}{k_g}\frac{Sh}{Nu} \quad \text{(B.1)}$$

where

$$\beta = \frac{1}{1 + k_m / k_c} \quad \text{(B.2)}$$

$$\alpha = \sigma\varepsilon(T_{char}^4 - T_b^4)/h(T_{char} - T_b) \quad \text{(B.3)}$$

where C_b is the oxygen concentration, 21 %Vol. can be assumable. q is the heat of combustion associated to the complete combustion of carbon content in biomass. Gas diffusivity (D_{AB}) and combustion rate constant (k_c) are determined by equation B.4 and B.5, respectively [180].

$$D_{AB} = 5.2x10^{-4} T_b^{1.5} / P \quad \text{(B.4)}$$

$$k_c = 595 T_{char} \exp(-149200 / RT_{char}) \quad \text{(B.5)}$$

Heat transfer coefficient (h) and mass transfer coefficient (k_m) included in Nusselt number (Nu) and Sherwood number (Sh), respectively, can be determined by the correlations [181].

$$(Nu - Nu_{i,large})/(Nu_l - Nu_{i,large}) = (d_{p,char} / d_p)^{2/3} \quad \text{(B.6)}$$

$$(Sh - Sh_{i,large})/(Sh_l - Sh_{i,large}) = (d_{p,char} / d_p)^{2/3} \quad \text{(B.7)}$$

where

$$Nu_{i,large} = 0.85 Ar^{0.19} + 0.006 Ar^{0.5} \Pr^{0.33} \quad \text{(B.8)}$$

$$Sh_{i,large} = 0.009 Ar^{0.5} Sc^{0.33} \quad \text{(B.9)}$$

$$Nu_l = 6 + 0.117 Ar^{0.39} \Pr^{0.33} \quad \text{(B.10)}$$

$$Sh_l = 2\varepsilon_{mf} + 0.117 Ar^{0.39} Sc^{0.33} \quad \text{(B.11)}$$

T_{char} at specific experimental conditions is calculated according to a diagram illustrated in Figure B.1 based on the **trial and error** methods.

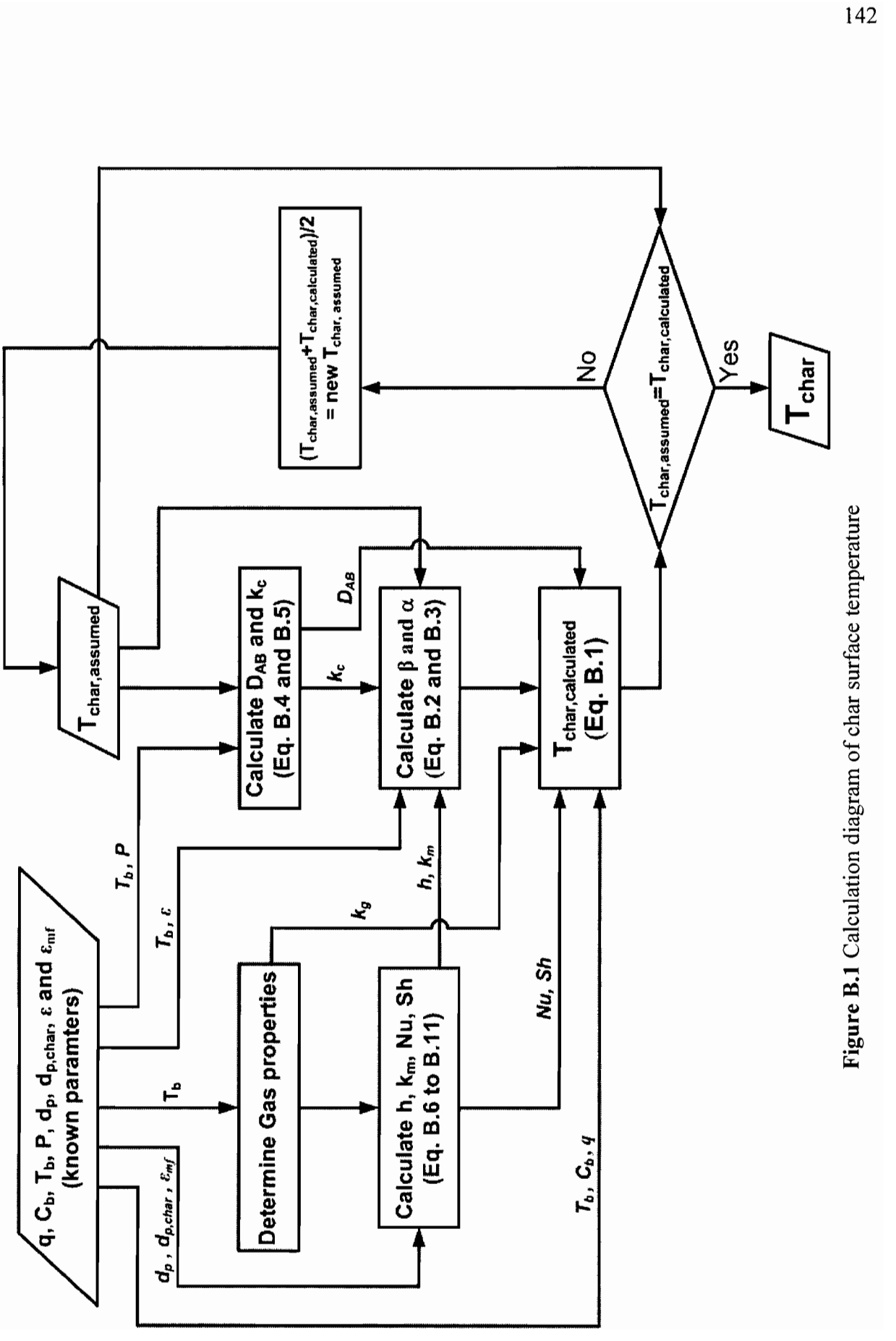

Figure B.1 Calculation diagram of char surface temperature

CURRICULUM VITAE

Name	Mr. Pawin Chaivatamaset
Home's address	65/29 Moo 4, Chaiyapurk Rd, Talingchan, Talingchan, Bangkok, Thailand.
Telephone number	+66 (2) 434-6445
E-mail address	ipawsath@yahoo.com ipawsath@hotmail.com
Date of birth	October 10, 1973
Nationality	Thai
Race	Thai
Religion	Buddhism

Educational Record

Bachelor's degree	Bachelor of Engineering (Chemical Engineering) Faculty of Engineering King Mongkut's Institute of Technology Thonburi Bangkok, Thailand, 1995.
Master's degree	Master of Engineering (Chemical Engineering) Faculty of Engineering King Mongkut's University of Technology Thonburi Bangkok, Thailand, 1999.
Doctoral degree	Doctor of Engineering (Chemical Engineering) Faculty of Engineering King Mongkut's University of Technology Thonburi Bangkok, Thailand, 2011.

Experiences

1997 – 1999	Researcher and Engineer Pilot Plant Development and Training Institute (PDTI) Combustion Research Laboratory Pilot Plant and Technical Department King Mongkut's University of Technology Thonburi 126, Pracha-utit Rd, Bangmod, Tung-Kru, Bangkok, Thailand.

Teaching Assistant
Department of Chemical Engineering
King Mongkut's University of Technology Thonburi
126, Pracha-utit Rd, Bangmod, Tung-Kru,
Bangkok, Thailand.

1997

- Technical Engineer, Perform the tapioca industrial waste water survey under Thai-Belgium Project.

1998 - 1999

- Technical Consultant, Fluidized bed combustion design, installation and performance test for coconut shell and fiber fuels under ASEAN-Australia Economic Cooperation Program (AAECP) Phase III at Ampol Food Processing co.,Ltd. 's factory
- Technical Consultant, The modified of combustion chamber of water tube boiler; Ampol Food Processing co.,Ltd. 's factory

1997 – 1999
(Researcher, Research assistant and Teaching assistant)

- Study on heat transfer mechanisms in Crater bed.
- Combustion of plastic waste in a fluidized-bed furnace.
- The Improvement of Fluidized Bed Garbage Furnace
- Combustion of Cassava Residue in a Fluidized Bed Furnace
- CHE 481: Chemical Engineering Laboratory I, CHE 482: Chemical Engineering Laboratory II, CHE 484: Chemical Engineering Project I and CHE 485 Chemical Engineering Project II.

1999 – 2003

Researcher and Engineer
Pilot Plant Development and Training Institute (PDTI)
Combustion research Laboratory
Pilot plant and Technical Department
King Mongkut's University of Technology Thonburi
126, Pracha-utit Rd, Bangmod, Tung-Kru,
Bangkok, Thailand.

Special Lecturer
Department of Chemical Engineering
King Mongkut's University of Technology Thonburi
126, Pracha-utit Rd, Bangmod, Tung-Kru,
Bangkok, Thailand.

1999 - 2000

- Technical Consultant, The improvement of 33 MWe Biomass Fluidized Bed Power Plant, Thai Power Supply Co. Ltd., Chachoengsao, Thailand.
- Technical Consultant, Perform in performance test of a Pilot scale Pneumatic Dryer for Tapioca Starch, Rayong Agricultural Research Center, Rayong, Thailand.
- Technical Consultant, Perform in Fluidized Bed Furnace Design for Retrofitting a 20 ton/hr Biomass-fired Stroker-type Steam Boiler, Thai Power Supply Co. Ltd., Chachoengsao, Thailand.

1999 - 2005

- Technical consultant, Fluidized bed combustion for coconut shell and fibre fuels under ASEAN-Australia Economic Cooperation Program (AAECP) Phase III; Ampol Food Processing co.,Ltd.

1999 – 2005
(Researcher, Research assistant and Teaching assistant)

- Hydrodynamics and Heat Transfer Characteristics of Crater Bed
- Development of Crater Bed Combustor for Solid Fuel Powder
- Hydrodynamic and Heat Transfer Characteristics of the Multi-pipe Crater Bed
- Heat Transfer Characteristics of Swirling Flow LPG Cooking Stove
- Catalytic Combustion of Soot from Diesel Engine
- Combustion of Diesel Soot on Copper Catalytic Filter
- Teaching assistant, CHE 481: Chemical Engineering Laboratory I, CHE 482: Chemical Engineering Laboratory II, CHE 484: Chemical Engineering Project I and CHE 485 Chemical Engineering Project II.

2003 – Present

Researcher and Part-time Engineer
Pilot Plant Development and Training Institute (PDTI)
Combustion research Laboratory
Technical and Engineering Department
King Mongkut's University of Technology Thonburi
126, Pracha-utit Rd, Bangmod, Tung-Kru,
Bangkok, Thailand.

Teaching Assistant
Department of Chemical Engineering
King Mongkut's University of Technology Thonburi
126, Pracha-utit Rd, Bangmod, Tung-Kru,
Bangkok, Thailand.

2004

- Technical Engineer, Design of Hot Oil Boiler for 11.6 MWth Wood Furnace, North Eastern Starch (1987) Co.,Ltd., Nakornrajchasrima, Thailand.

2006

- Technical Engineer, Perform in Improvement of Activated Carbon Furnace in rural area of Bang saphan, Prachuapkhirikhan, Thailand.

2008

- Technical Engineer, Participate in consultancy team, Air Emission Evaluation from Power Plant Stacks of EGAT, Electricity Generating Authority of Thailand.

2003 – Present
(Researcher, Research assistant and Teaching assistant)

- Researcher, Study on Bed agglomeration in Biomass-fired fluidized bed combustor.
- Teaching assistant, CHE 481: Chemical Engineering Laboratory I, CHE 482: Chemical Engineering Laboratory II, CHE 484: Chemical Engineering Project I and CHE 485 Chemical Engineering Project II.

Workshop and Training Programs

1995 Combustion of Solid Treatment of Product, Faculty of Engineering, King Mongkut's Institute of Technology North Bangkok, Thailand

1997 Energy Gain from Loss, National Energy Policy office, Thailand. Industrial Natural Gas Utilization Training, PTT and KMITT, Century Park Hotel, Bangkok, Thailand.

2000 Workshop on AAECP III: Energy Production from Biomass Residues Supplemented by Fossil, KMUTT, Century Park Hotel, Bangkok, Thailand.

Lists of Publication and Presentation

1. Tia, S., Chaivatamasat, P., Jumnongpon, V., and Manomaiwong, S., "Biogas Combustion in a Crater Bed", **Proc. of 2nd ASEAN Renewable Energy Conf.**, Phuket, Thailand, Nov. 5-7 (1997).
2. Tia, S., Chaivatamasat, P., Jumnongpon, V., and Manomaiwong, S., 1998, "Biogas Combustion in a Crater Bed", **RERIC International Energy Journal**, Vol. 20, No. 1, June, pp. 1-8.
3. Chaivatamaset, P. and Tia, S., "Heat Transfer in a Crater Bed", **Applied Thermal Engineering**, Vol. 27, No. 17-18, 2007, pp. 2767-2778.
4. Chaivatamaset, P., Sricharoon, P. and Tia, S., 2011, "Bed agglomeration characteristics of palm shell and corncob combustion in fluidized bed", **Applied Thermal Engineering**, Vol. 31, 2916-2927.

2004

- Technical Engineer, Design of Hot Oil Boiler for 11.6 MWth Wood Furnace, North Eastern Starch (1987) Co.,Ltd., Nakornrajchasrima, Thailand.

2006

- Technical Engineer, Perform in Improvement of Activated Carbon Furnace in rural area of Bang saphan, Prachuapkhirikhan, Thailand.

2008

- Technical Engineer, Participate in consultancy team, Air Emission Evaluation from Power Plant Stacks of EGAT, Electricity Generating Authority of Thailand.

2003 – Present
(Researcher, Research assistant and Teaching assistant)

- Researcher, Study on Bed agglomeration in Biomass-fired fluidized bed combustor.
- Teaching assistant, CHE 481: Chemical Engineering Laboratory I, CHE 482: Chemical Engineering Laboratory II, CHE 484: Chemical Engineering Project I and CHE 485 Chemical Engineering Project II.

Workshop and Training Programs

1995 Combustion of Solid Treatment of Product, Faculty of Engineering, King Mongkut's Institute of Technology North Bangkok, Thailand

1997 Energy Gain from Loss, National Energy Policy office, Thailand. Industrial Natural Gas Utilization Training, PTT and KMITT, Century Park Hotel, Bangkok, Thailand.

2000 Workshop on AAECP III: Energy Production from Biomass Residues Supplemented by Fossil, KMUTT, Century Park Hotel, Bangkok, Thailand.

Lists of Publication and Presentation

1. Tia, S., Chaivatamasat, P., Jumnongpon, V., and Manomaiwong, S., "Biogas Combustion in a Crater Bed", **Proc. of 2nd ASEAN Renewable Energy Conf.**, Phuket, Thailand, Nov. 5-7 (1997).
2. Tia, S., Chaivatamasat, P., Jumnongpon, V., and Manomaiwong, S., 1998, "Biogas Combustion in a Crater Bed", **RERIC International Energy Journal**, Vol. 20, No. 1, June, pp. 1-8.
3. Chaivatamaset, P. and Tia, S., "Heat Transfer in a Crater Bed", **Applied Thermal Engineering**, Vol. 27, No. 17-18, 2007, pp. 2767-2778.
4. Chaivatamaset, P., Sricharoon, P. and Tia, S., 2011, "Bed agglomeration characteristics of palm shell and corncob combustion in fluidized bed", **Applied Thermal Engineering**, Vol. 31, 2916-2927.

- 5 มี.ค. 2555

King Mongkut's University of Technology Thonburi
Agreement on Intellectual Property Rights Transfer for Postgraduate Students

Date...23...March...2012.....

Name.....Pawin.....Middle Name.....
Surname/Family Name.....Chaivatamaset.....
Student Number.....54500001..... who is a student of King's Mongkut's University of Technology Thonburi (KMUTT) in ○ Graduate Diploma ○ Master Degree
⊘ Doctoral Degree
Program.....Doctoral degree.....Field of Study.....Chemical Engineering.....
Faculty/School.....Faculty of Engineering.....
Home Address....65/29.....Soi Chaiyapruk 27.....Chaiyapruk Rd.....Talingchan.....
..... Talingchan.....Bangkok.....
Postal code.....10170.....Country.....Thailand.....

I, as 'Transferer', hereby transfer the ownership of my thesis copyright to King's Mongkut's University of Technology Thonburi who has appointed (Dean's name).....
....Assoc..Prof..Booncharoen..Sirinaovakul.....Dean of Faculty of....Engineering....to be 'Transferee' of copyright ownership under the 'Agreement' as follows.

1. I am the author of the thesis entitled.... A study of bed agglomeration in biomass-fired fluidized bed combustor....under the supervision of....Assoc. Prof. Suvit Tia...who is my supervisor, and/or....Asst..Prof..Panchan Sricharoon..and..Prof..Bernd Bilitewski....who is/are my co-supervisor(s), in accordance with the Thai Copyright Act B.E. 2537. The thesis is a part of the curriculum of KMUTT.
2. I hereby transfer the copyright ownership of all my works in the thesis to KMUTT throughout the copyright protection period in accordance with the Thai Copyright Act B.E. 2537, effective on the approval date of thesis proposal consented by KMUTT.
3. To have the thesis distributed in any form of media, I shall in each and every case stipulate the thesis as the work of KMUTT
4. For my own distribution of thesis or the reproduction, adjustment, or distribution of thesis by the third party in accordance with the Thai Copyright Act B.E. 2537 with remuneration in return, I am subject to obtain a prior written permission from KMUTT.
5. To use any information from my thesis to make an invention or create any intellectual property works within ten (10) years from the date of signing this Agreement, I am subject to obtain prior written permission from KMUTT, and KMUTT is entitled to have intellectual property rights on such inventions or intellectual property works, including entitling to take royalty from licensing together with the distribution of any benefit deriving partly or wholly from the works in the future, conforming with the Regulation of King Mongkut's Institute of Technology Thonburi Re the Administration of Benefits deriving from Intellectual Property B.E. 2538.
6. If the benefits arise from my thesis or my intellectual property works owned by KMUTT, I shall be entitled to gain the benefits according to the allocation rate stated in the Regulation of King Mongkut's Institute of Technology Thonburi Re the Administration of Benefits deriving from Intellectual Property B.E. 2538.

Signature Pawin Chaivatamaset Transferor

(.....Pawin..Chaivatamaset.....)

Student

Signature ..... Transferee

(...Assoc..Prof..Piyabutr..Wanichpongpan...)

Associate Dean for Academic Affairs (Action for Dean)

Signature ..... Witness

(..Assoc..Prof..Anawat..Sungpet..)

Signature ..... Witness

(.....Assoc..Prof..Suvit..Tia.....)